
[All ETDs from UAB](#)

[UAB Theses & Dissertations](#)

2011

Assessment of Mitochondrial Stressors on Cellular Bioenergetics

Blake Reid Zelickson
University of Alabama at Birmingham

Follow this and additional works at: <https://digitalcommons.library.uab.edu/etd-collection>

Recommended Citation

Zelickson, Blake Reid, "Assessment of Mitochondrial Stressors on Cellular Bioenergetics" (2011). *All ETDs from UAB*. 3433.

<https://digitalcommons.library.uab.edu/etd-collection/3433>

This content has been accepted for inclusion by an authorized administrator of the UAB Digital Commons, and is provided as a free open access item. All inquiries regarding this item or the UAB Digital Commons should be directed to the [UAB Libraries Office of Scholarly Communication](#).

ASSESSMENT OF MITOCHONDRIAL STRESSORS ON CELLULAR
BIOENERGETICS

by

BLAKE R. ZELICKSON

VICTOR M. DARLEY-USMAR, COMMITTEE CHAIR

JOHN C. CHATHAM

YABING CHEN

LOUIS J. DELL'ITALIA

AIMEE LANDAR

C. ROGER WHITE

A DISSERTATION

Submitted to the graduate faculty of The University of Alabama at Birmingham,
in partial fulfillment of the requirements for the degree of
Doctor of Philosophy

BIRMINGHAM, ALABAMA

2011

ASSESSMENT OF MITOCHONDRIAL STRESSORS ON
CELLULAR BIOENERGETICS

BLAKE R. ZELICKSON

MOLECULAR AND CELLULAR PATHOLOGY

ABSTRACT

The mitochondrion plays a central role in the maintenance of bioenergetic function through the production of ATP and essential metabolites. The development of mitochondrial bioenergetic defects is a hallmark of important pathologies such as cardiovascular and liver diseases. It is well established that a decrease in mitochondrial function, typically of 20-40%, is associated with the progression of these pathologies. Causal relationships have been more difficult to establish because of the challenge of assessing mitochondrial function in a cellular setting. Specifically, it is known that mitochondria function at less than their maximal respiratory capacity and the remainder, known as reserve or spare capacity, is thought to be utilized for increased work or combating oxidative stress. The following questions have been addressed in this dissertation: 1) Does reserve capacity change under conditions of diminished oxygen availability?, 2) Do the variations in mitochondrial phenotype caused by differences in the mitochondrial DNA sequence amongst different populations modify the response to a pathological stress?, and 3) Does the metabolism of alcohol in the liver interact with the mitochondria to change reserve capacity and the response to nitric oxide and hypoxia? In testing these concepts, we have used *in vivo* models of alcoholic liver disease and cardiac volume overload and an *ex vivo* model of vascular ischemia/reperfusion. Taken together, our da-

ta support the concept that mitochondrial bioenergetics are a key determinant of the response of a wide variety of cells to pathological stressors.

Keywords: Mitochondrial Function, Extracellular Flux, 4-Hydroxynonenal, Nitric Oxide, Hypoxia, Reserve Capacity

DEDICATION

This dissertation is dedicated to my parents, Jeff & Kelley Zelikson, and my grandparents, Meyer & Joan Zelikson and Harvey & Dotty Golden.

ACKNOWLEDGEMENTS

The completion of this dissertation and the research within would not have been possible without the help of several people throughout my tenure in graduate school. First and foremost, I would like to thank my mentor, Victor Darley-USmar. In the four and a half years I spent in your lab, you helped me to grow not only as a scientist, but also as a person. You always took the time to figure out the best way to push me to succeed, and I am truly grateful for all of the support, encouragement, patience, and even the “bollockings” you have given me over the years. I can only hope to one day be as good of a mentor to someone else as you have been to me.

To my “lab family,” both past and present, thank you so much for everything that you’ve done for me over the years. To Michelle Johnson, my “lab mom,” your proficiency in all things science is always impressive and beyond compare. You always seem to know how to do every possible kind of assay, as well as the secrets of how to make them work. But more importantly, you were always willing to take the time out of your absurdly busy day to share your expertise with me. To Gloria Benavides, my “lab wife,” I have thoroughly enjoyed working and traveling with you over the past few years. We made an excellent team, and I can’t think of anyone with whom I would have rather spent all those countless hours running up to eight Seahorse experiments per day. You helped me to become more patient, understanding, and an all-around better person, and for that I

will always be grateful. To Ashlee Higdon, my “lab sister,” you have been my partner-in-crime for the past four and a half years. You taught me all the basics of bench-work and were always willing to discuss my data and give me advice, even when it meant that you would have to stay late as a result. We have been through a lot together, and I will definitely miss all of our chats and life-coaching sessions. To Sam Giordano, my “little lab sister,” I enjoyed acting as your pseudo-mentor while you were rotating through our lab, and maybe even a little bit afterwards as well. To Balu Chacko, I have really enjoyed all of our scientific discussions. You know so much about so many different things, and always seem to have a new and interesting perspective about what different results could mean. To Brad Hill, I loved working with you during your short time at UAB. I learned so much about how to be successful in science from you, and your never-ending energy and enthusiasm continue to amaze me. To Joo Yeun Oh, the Korean ninja, you were a constant source of entertainment in the lab. In addition, you are probably one of the most selfless and giving people I have ever met, and I will always be in awe of all that you do. To Mi Jung Chang, never in my entire life have I witnessed anyone do as much work as you managed to do on a daily basis. I will miss working with you and your help with my Korean, even if I only know two phrases. To Sarah Owusu, I really enjoyed working with you for the year that you were here. We have so much in common, and it was really great to have a partner in the avoidance of all things unkosher. Thanks also to Colin Reily, Philip Kramer, Elena Ulasova, Yaozu Ye, Brian Dranka, and Jessica Perez for helping to make it so that I never dreaded going to work, even when I knew it would be a really long day. I have enjoyed working with you all.

To Lou Dell'Italia, I have loved working with you for the past couple of years. You have more enthusiasm for science than I have ever seen before, which inspires me to be more enthusiastic and interested as well. I have always been impressed by how you manage to juggle being a clinician and a researcher, and I hope to be able to achieve even a percentage of the success that you have in your career. I would also like to thank several members of the Dell'Italia lab for all of their support throughout all of our collaborations. To Doug Gladden, thanks for always being willing to isolate myocytes whenever they were needed, even if you sometimes decided that they didn't need to be counted. Working with you has been interesting and fun to say the least, and I will miss all of our random conversations and your unique perspective on things. To Eddie Bradley, rarely have I seen such impressive skills as I have witnessed observing you perform various surgeries or procedures on mice and rats. To Pam Powell, thanks for always being willing to perform immunohistochemistry for me, even when I came to you with ideas that could have potentially kept you busy for months at a time.

To Aimee Landar, thank you for always being willing to share your expertise with me whenever I needed it. I don't know anyone who can troubleshoot a Western blot as well as you can. Thank you also to the members of the Landar lab, both past and present, for all of their support over the years. To Stephanie Wall, I have enjoyed interacting with you whenever I got the chance. Trying to get you to be just a little bit less nice was always a great source of entertainment for me. To Fen Zhou, thank you so much for ordering antibodies for me so quickly when I decided last minute that I needed to probe for just one more thing. Thanks also to Anne Diers and Praveen Vayalil, my fellow investigators into bioenergetics in hypoxia.

To Samantha Gromko, thank you so much for all that you have done for me over the years. Between scheduling meetings, getting reimbursements, figuring out what exactly the training grant would pay for, and helping me track down Victor, you made my time in graduate school go so much more smoothly than it ever could have without you. To Nicole Newton, you were always an incredibly valuable source of information. Thank you so much for always having answers to my one million questions, particularly as I was preparing to graduate. To Rakesh Patel, thank you for all of your advice over the years. You always knew what my best course of action was, and probably helped me avoid a lot of grief in the process. To my committee, John Chatham, Yabing Chen, Lou Dell'Italia, Aimee Landar, and Roger White, thank you so much for your ideas regarding my research and for always pushing me to look for additional explanations for my data.

Last, but certainly not least, I would like to thank my family for everything that they have done for me throughout my entire life. To my parents, thank you so much for always supporting and believing in me, even when it was not deserved. You are the smartest and hardest working people I know, and I can only hope to live up to the example that you have set for me. To my grandparents, thank you for all the faith you have had in me. You make me strive to succeed in everything that I do in the hopes that I can one day deserve how proud you always are of me. To my brothers, aunts, uncles, and cousins, thank you as well for your encouragement over the years. I could never have made it this far without your constant support.

“Truly great friends are hard to find, difficult to leave, and impossible to forget.”

–G. Randolph

TABLE OF CONTENTS

	<i>Page</i>
ABSTRACT.....	ii
DEDICATION.....	iv
ACKNOWLEDGEMENTS.....	v
LIST OF TABLES.....	xiv
LIST OF FIGURES.....	xv
LIST OF ABBREVIATIONS.....	xx
CHAPTER	
1 INTRODUCTION.....	1
Role of the Mitochondrion in Physiology.....	6
Bioenergetics.....	6
Mitochondrial ROS Production.....	9
Importance of mtDNA Haplotype.....	14
Role of the Mitochondrion in Pathology.....	18
Bioenergetic Dysfunction.....	18
Diseases Associated with Mitochondrial Dysfunction.....	24
Alcoholic Liver Disease.....	24
Ischemia/Reperfusion in the Vasculature.....	27
Cardiac Volume Overload.....	30
Summary.....	32

2	EFFECT OF CHRONIC ALCOHOL CONSUMPTION ON HEPATIC MITOCHODRIAL FUNCTION IN RESPONSE TO HYPOXIA: ROLE OF NITRIC OXIDE	34
	Introduction.....	34
	Role of Nitric Oxide in Alcohol-Induced Hepatotoxicity.....	34
	Chronic Alcohol Consumption Causes Mitochondrial Dysfuncion.....	35
	Materials and Methods.....	39
	Materials	39
	Alcohol Feeding.....	39
	Hepatocyte Preparations	39
	Mitochondrial Enzyme Activity Assays	41
	Immunoblot Analysis.....	41
	Mitochondrial Bioenergetics.....	42
	Hypoxia Exposure.....	45
	Immunohistochemistry	46
	Statistics	48
	Results.....	48
	Hepatocyte Density for Measurement of Mitochondrial Bioenergetics.....	48
	Alcohol Induces Characteristics of Liver Toxicity in Hepatocytes.....	50
	Hepatocytes Exhibit Bioenergetic Defect in Response to Alcohol Exposure	50
	Chronic Alcohol Increases Hepatocyte Sensitivity to Nitric Oxide	54
	Alcohol Exacerbates Bioenergetic Alterations Induced by Hypoxia and Nitric Oxide.....	57
	Alcohol-Induced Hypoxia in the Liver in iNOS-Dependent	59
	Discussion.....	66
3	HYPOXIA/REOXYGENATION ALTERS THE RESPONSE OF CELLULAR BIOENERGETICS TO 4-HYDROXYNONENAL IN ENDOTHELIAL CELLS	73
	Introduction.....	73

	Bioenergetic Alterations Associated with Ischemia/Reperfusion: Effects of Reactive Lipid Species	76
	Materials and Methods.....	77
	Materials	77
	Cell Culture.....	77
	Measurement of Oxygen Consumption in Endothelial Cells	77
	Mitochondrial Function Assay.....	78
	Exposure to Hypoxia and Reoxygenation.....	80
	Immunoblot Analysis.....	82
	Statistics	82
	Results.....	83
	Oxygen Dependence of Endothelial Cell Mitochondrial Function	83
	Reactive Lipid-Induced Alterations to Endothelial Cell Bioenergetics.....	87
	Oxygen-Dependence of Endothelial Cell Bioenergetic Alterations Induced by HNE.....	93
	Exacerbation of Reoxygenation-Induced Loss of Mitochondrial Function by HNE	97
	Discussion	102
4	MITOCHONDRIAL HAPLOTYPE DETERMINES SUSCEPTIBILITY TO CARDIOMYOCYTE DYSFUNCTION RESULTING FROM CARDIAC VOLUME OVERLOAD	105
	Introduction.....	105
	Effects of Acute Volume Overload on the Cardiomyocyte Mitochondrion.....	105
	Elucidating Role of mtDNA Haplotype on Susceptibility to Volume Overload.....	108
	Materials and Methods.....	111
	Reagents.....	111
	Generation of Mitochondria:Nuclear Exchange (MNX) Mice	111
	Aortocaval Fistula Surgery	113
	Cardiomyocyte Isolation.....	115

	Mitochondrial Enzyme Activities.....	115
	Immunoblot Analysis.....	116
	Cellular Bioenergetics.....	116
	Echocardiography and Hemodynamic Measurements.....	117
	Immunohistochemistry	120
	Transmission Electron Microscopy	120
	Statistics	122
	Results.....	122
	Comparison of C57BL/6 and C3H/HeN Mitochondrial Phenotypes	122
	Bioenergetic Response of C57BL/6 and C3H/HeN Mice to Volume Overload	125
	Morphometry and Left Ventricular Function of Mice after Volume Overload	128
	Volume Overload-Induced Alterations in Bioenergetic Function	131
	Alterations in Desmin Organization in Cardiomyocytes after Volume Overload	134
	Effect of Volume Overload on Mitochondrial Morphology.....	136
	Discussion	139
5	DISCUSSION.....	146
	Introduction.....	146
	Reserve Capacity and the Cellular Response to Pathological Stresses.....	147
	Alcohol-Induces Loss of Mitochondrial Function.....	148
	Role of Nitric Oxide in Alcohol-Dependent Hepatotoxicity	149
	Alcohol Consumption Alters Hepatocellular Response to Hypoxia.....	149
	Hypoxic Signaling as a Mediator of Alcohol-Induced Bioenergetic Alterations	152
	Effect of Hypoxia/Reoxygenation on Bioenergetic Function.....	153
	Endothelial Cell Mitochondrial Function is Altered in Hypoxia.....	153
	Reoxygenation Induces Progressive Loss of	

Mitochondrial Function	157
Oxygen-Dependent Effects of HNE on Mitochondrial Function	158
Susceptibility to Bioenergetic Alterations is Mediated by mtDNA Haplotype	159
Bioenergetic Responses to Volume Overload in C57BL/6 and C3H/HeN Mice	161
Effect of mtDNA on Changes in Morphometry and Function by Volume Overload.....	162
Volume Overload-Induced Alterations in Mitochondrial Function in MNX Mice.....	162
Loss of Desmin Mediates Bioenergetic Alterations Induced by Volume Overload.....	163
Volume Overload-Induced Changes in Cardiomyocyte Morphology.....	164
Relating Mouse mtDNA Haplotypes to Human mtDNA Haplogroups.....	165
Conclusions.....	168
LIST OF REFERENCES	170
APPENDIX: IACUC APPROVAL FORMS.....	215

LIST OF TABLES

<i>Table</i>		<i>Page</i>
4-1	Mouse Strains Utilized for Studies of Susceptibility to Volume Overload.....	113
4-2	Acute Hemodynamic and Echocardiography Data	129

LIST OF FIGURES

<i>Figure</i>		<i>Page</i>
1-1	The pathophysiologies of many diseases are mediated by the development of mitochondrial dysfunction	3
1-2	Mitochondrial oxidative phosphorylation.....	7
1-3	Mechanisms of ROS formation in the mitochondria	10
1-4	Reverse electron transport.....	12
1-5	Mitochondrial DNA map	15
1-6	Model of human migration based on mtDNA haplogroups.....	17
1-7	Death rate from cardiovascular diseases between Caucasians and African Americans	19
1-8	Effects of mitochondrial ROS.....	21
1-9	Reserve capacity protects tissue from bioenergetic dysfunction in response to increased workload or stress	23
1-10	Chronic alcohol consumption induces hepatocellular mitochondrial dysfunction.....	26
1-11	Ischemia/reperfusion causes damage to the endothelium and underlying tissue	28
1-12	Increased xanthine oxidase activity leads to mitochondrial dysfunction in the volume overloaded heart.....	31

<i>Figure</i>	<i>Page</i>
2-1 Chronic alcohol consumption induces mitochondrial dysfunction mediated by nitric oxide and hypoxia.....	36
2-2 Hypoxia inducible factor-1 α signaling pathway is activated in hypoxia.....	38
2-3 Alcohol feeding schedule for rats and mice.....	40
2-4 XF24 analyzer technology	43
2-5 Measurement of bioenergetic parameters of isolated primary hepatocytes using an XF24 analyzer.....	44
2-6 Measuring mitochondrial function in hypoxia.....	47
2-7 Cell density-dependent changes in hepatocyte respiration following chronic alcohol consumption	49
2-8 Effect of alcohol consumption on mitochondrial protein levels and activity.....	51
2-9 Alcohol consumption causes diminished mitochondrial function.....	52
2-10 Chronic alcohol consumption alters mitochondrial function in primary hepatocytes	53
2-11 Alcohol sensitizes hepatocytes to nitric oxide-induced inhibition of mitochondrial function	55
2-12 Chronic alcohol consumption sensitizes hepatocytes to nitric oxide-induced mitochondrial dysfunction.....	56
2-13 Alcohol toxicity increases hepatocyte susceptibility to nitric oxide-induced inhibition of respiration in hypoxia.....	58
2-14 Chronic alcohol consumption alters hepatocyte response to decreasing oxygen concentration and nitric oxide.....	60

<i>Table</i>	<i>Page</i>
2-15 Chronic alcohol consumption alters bioenergetic response to decreasing oxygen concentration and nitric oxide.....	61
2-16 Chronic alcohol consumption causes induction of cytochrome P450 2E1 in wild type and iNOS ^{-/-} mice.....	63
2-17 Lack of iNOS prevents hepatic steatosis in alcohol-fed animals.....	64
2-18 iNOS-derived nitric oxide is required for chronic alcohol-induced liver hypoxia	65
2-19 iNOS expression is required for chronic alcohol-induced stabilization of HIF-1 α in the liver	67
3-1 Ischemia causes bioenergetic and cellular dysfunction	75
3-2 Measurement of parameters of mitochondrial function in endothelial cells using an XF24 analyzer	79
3-3 An XF24 analyzer in a hypoxia chamber was used for hypoxia and reoxygenation protocols.....	81
3-4 Oxygen consumption of endothelial cells in room air	84
3-5 Effect of hypoxia on oxygen consumption of endothelial cells.....	85
3-6 Hypoxia causes loss of oxygen consumption of endothelial cells.....	86
3-7 Hypoxia/reoxygenation alters oxygen consumption in endothelial cells	88
3-8 Structures of 4-hydroxynonenal and nonanal	89
3-9 HNE alters mitochondrial function in intact endothelial cells.....	90
3-10 Effect of HNE on mitochondrial function in endothelial cells	92

<i>Figure</i>	<i>Page</i>
3-11 Bioenergetic response of endothelial cells to HNE exposure in hypoxia.....	95
3-12 Effects of HNE exposure in hypoxia on mitochondrial function	96
3-13 Protein-HNE adduct formation after exposure to HNE in both hypoxia and room air	98
3-14 HNE exacerbates reoxygenation injury in endothelial cells.....	99
3-15 Mitochondrial damage in endothelial cells induced by changing oxygen concentrations and HNE exposure	101
4-1 The disease progression of volume overload leading to the development of heart failure	106
4-2 Differences in mtDNA haplotype between different strains of mice	110
4-3 Generation of mitochondria:nuclear exchange (MNX) mice	112
4-4 Induction of left ventricular volume overload by surgically creating an aortocaval fistula	114
4-5 Measurement of mitochondrial function of cardiomyocytes using an XF24 analyzer.....	118
4-6 Oligomycin does not decrease cardiomyocyte oxygen consumption.....	119
4-7 Using echocardiography to measure cardiac function <i>in vivo</i>	121
4-8 Comparison of mitochondrial protein levels and activity from cardiomyocytes isolated from C57BL/6 and C3H/HeN mice	124
4-9 Cardiomyocytes isolated from C57BL/6 and C3H/HeN mice exhibit differences in mitochondrial function.....	126
4-10 Cardiomyocytes isolated from C57BL/6 and C3H/HeN mice exhibit different bioenergetic responses to volume overload	127

<i>Figure</i>	<i>Page</i>
4-11 Changes in left ventricular dimension and volume in response to volume overload	130
4-12 Changes in mitochondrial parameters of oxygen consumption of cardiomyocytes in response to volume overload.....	132
4-13 Volume overload alters desmin expression in left ventricular myocytes in C57BL/6 mice.....	135
4-14 Transmission electron microscopy of left ventricle in mice subjected to volume overload	137
4-15 Further magnification of transmission electron microscopy of left ventricle in mice subjected to volume overload	138
5-1 Peroxynitrite formation is a likely mediator of bioenergetic dysfunction in alcohol-induced hepatotoxicity	150
5-2 Regulation of cytochrome <i>c</i> oxidase activity in different systems	155
5-3 Kinetics of cytochrome <i>c</i> oxidase activity in different systems	156
5-4 Reperfusion exacerbates bioenergetic and cellular dysfunction.....	160
5-5 mtDNA single nucleotide polymorphisms between C57BL/6 and C3H/HeN mouse haplotypes and between L and H human haplogroups.....	167

LIST OF ABBREVIATIONS

NO	nitric oxide
°C	degrees Celsius
µg	microgram
µL	microliter
µm	micrometer
µM	micromolar
³¹ P-NMR	phosphorus-31 nuclear magnetic resonance
A	antimycin A
A+R	antimycin A + rotenone
ACF	aortocaval fistula
ADP	adenosine diphosphate
Ala	alanine
ALD	alcoholic liver disease
ALDH2	aldehyde dehydrogenase 2
AMCM	adult mouse cardiomyocyte
AMP	adenosine monophosphate
AMPK	AMP-activated protein kinase
ANOVA	analysis of variance
ANT	adenine nucleotide transporter

Arg	arginine
Asp	aspartic acid
ATP	adenosine triphosphate
BAEC	bovine aortic endothelial cell
BSA	bovine serum albumin
Ca ²⁺	calcium
CcOX	cytochrome <i>c</i> oxidase
CcOX-III	cytochrome <i>c</i> oxidase subunit III
CcOX-IV	cytochrome <i>c</i> oxidase subunit IV
CO ₂	carbon dioxide
CoA	coenzyme A
CoQ	coenzyme Q
CPT-1	carnitine palmitoyltransferase-1
CS	citrate synthase
Cu	copper
Cu/ZnSOD	copper/zinc superoxide dismutase (SOD1)
CVD	cardiovascular disease
CYP2E1	cytochrome P450 2E1
d	day
DAPI	4',6-Diamidino-2-phenylindole dihydrochloride
DetaNO	Deta NONOate
DMEM	Dulbecco's modified Eagle's medium
DNA	deoxyribonucleic acid

DTNB	5,5'-dithiobis-(2-nitrobenzoic acid)
e ⁻	electron
EC50	half maximal effective concentration
EDD	end-diastolic dimension
ER	endoplasmic reticulum
EtOH	alcohol
F	FCCP
FAD	flavin adenine dinucleotide
FBS	fetal bovine serum
FCCP	carbonyl cyanide 4-(trifluoromethoxy)phenylhydrazone
Fe/S	iron/sulfur cluster
FMN	flavin mononucleotide
FS	fractional shortening
g	gram
GBS	glycerine-buffered saline
H&E	hematoxylin and eosin
H ⁺	protons
H ₂ O	water
H ₂ O ₂	hydrogen peroxide
HEPES	4-(2-hydroxyethyl)piperazine-1-ethanesulfonic acid, N-(2-hydroxyethyl)piperazine-N'-(2-ethanesulfonic acid)
Hg	mercury
HIF-1	hypoxia inducible factor-1
HIF-1 α	hypoxia inducible factor-1 α

HNE	4-hydroxynonenal
hr	hour
HRE	hypoxia response element
HRP	horseradish peroxidase
HX	hypoxanthine
i.m.	intramuscular
i.p.	intraperitoneal
i.v.	intravenous
IL-1 β	interleukin-1 β
Ile	isoleucine
iNOS	inducible nitric oxide synthase
J _{max}	maximum flux
K	thousand
KCl	potassium chloride
kDa	kilodalton
kg	kilogram
KH ₂ PO ₄	potassium phosphate monobasic
K _m	Michaelis constant
L	liter
LPO	lipid peroxidation
LV	left ventricle
M	molar
MAP	mean arterial pressure

Met	methionine
mg	milligram
min	minute
mL	milliliter
mm	millimeter
mM	millimolar
MMP	matrix metalloproteinase
Mn	manganese
MnSOD	manganese superoxide dismutase (SOD2)
MNX	mitochondria:nuclear exchange
mPTP	mitochondrial permeability transition pore
MR	mitral regurgitation
mtDNA	mitochondrial DNA
mt-tRNA ^{Arg}	mitochondrial tRNA for arginine
n	number of replicates
NaCl	sodium chloride
NAD ⁺	nicotinamide adenine dinucleotide (oxidized)
NADH	nicotinamide adenine dinucleotide (reduced)
NADPH	nicotinamide adenine dinucleotide phosphate (reduced)
NaHCO ₃	sodium bicarbonate
NDIII	NADH dehydrogenase subunit III
nDNA	nuclear DNA
ng	nanogram

nm	nanometer
NOX	NADPH oxidase
NRVM	neonatal rat ventricular myocytes
O	oligomycin
O ₂	oxygen
O ₂ ^{•-}	superoxide
OCR	oxygen consumption rate
ONOO ⁻	peroxynitrite
OSCP	oligomycin sensitivity-conferring protein
p	probability
P ₅₀	concentration of 50% saturation
PBS	phosphate-buffered saline
pH	power of hydrogen
PHD	prolyl hydroxylase domain
PMN	polymorphonuclear cell
pmol	picomole
PO	propylene oxide
prtn	protein
PVDF	polyvinylidene difluoride
PWT	posterior wall thickness
Q	ubiquinone
QH	semiquinone
QH ₂	ubiquinol

RET	reverse electron transport
RLS	reactive lipid species
RNS	reactive nitrogen species
ROS	reactive oxygen species
rRNA	ribosomal ribonucleic acid
RWT	relative wall thickness
SDS-PAGE	sodium dodecyl sulfate-polyacrylamide gel electrophoresis
SEM	standard error of the mean
SNP	single nucleotide polymorphism
SOD1	superoxide dismutase 1 (Cu/ZnSOD)
SOD2	superoxide dismutase 2 (MnSOD)
TBS	Tris-buffered saline
Thr	threonine
Tlr4	Toll-like receptor-4
TNB	2-nitro-5-thiobenzoic acid
TNF- α	tumor necrosis factor- α
tRNA	transfer ribonucleic acid
Txn	transcription
Tyr	tyrosine
U	units
Ub	ubiquitin
UCP	uncoupling protein
Val	valine

VC Fr	velocity of circumferential shortening
VDAC	voltage-dependent anion channel
V_{\max}	maximum rate
VO	volume overload
wk	week
XF	extracellular flux
XO	xanthine oxidase
Zn	zinc

CHAPTER 1

INTRODUCTION

The mitochondrion has long been established as the central intracellular organelle responsible for key metabolic functions which contribute to normal physiology and the control of cell death pathways [1, 2]. For example, mitochondria play a critical role in maintenance of calcium homeostasis [3-6], thermogenesis [7-9], redox signaling [10], and the induction of apoptosis [11-13]. These activities clearly extend the role of the mitochondrion well beyond its most well-known function as the “powerhouse” of the cell [14, 15]. Understanding the molecular mechanisms of these pathways in a cellular setting is important because changes to mitochondrial function have been noted in a broad range of pathological conditions, as will be discussed in detail.

Mitochondria within different tissues have in common the same maternally-inherited mitochondrial DNA (mtDNA) and possess the same proteins and enzymatic pathways; however, the relative expression of the various mitochondrial proteins and pathways are different in distinct cell types due to the specific metabolic needs of the cell [14]. For example, the preferred source of substrates for energy production in the heart is through fatty acid oxidation [16, 17]; therefore, cardiomyocytes have high expression levels of carnitine palmitoyltransferase-1 (CPT-1), which is the enzyme responsible for the transport of long chain fatty acids into the mitochondria where they can then undergo β -oxidation [18].

In addition to the unique mitochondrial composition within individual tissues, it has recently become apparent that mtDNA can also be altered, resulting in different responses to pathological conditions [19-22]. Mutations in mtDNA are known to mediate the development of many diseases, through both inherited and spontaneous mutations. These mutations can lead to pathology by altering the structure, interactions, and function of the mitochondrial-encoded subunits of the electron transport chain complexes, thus altering the mitochondrial production of ATP and reactive oxygen and nitrogen species (ROS/RNS) [23]. In addition, the combination of decreased bioenergetic efficiency coupled with the increased energy demand associated with many pathologies leads to cellular dysfunction and death; this occurs through the induction of apoptosis by the mitochondrial release of cytochrome *c* or complete mitochondrial failure to make ATP leading to necrosis (termed necroapoptosis) [24-26].

Understanding the relationship between variations in mtDNA, mitochondrial function, cellular bioenergetics and the response to the stress of a developing disease is the goal of this dissertation. To achieve this we have used an integrated approach using animal and cell models of diverse pathologies associated with mitochondrial dysfunction in which we measure endpoints directly related to the pathology and cellular bioenergetic function (**Figure 1-1**). The disease models investigated herein are alcoholic liver disease (ALD), vascular ischemia/reperfusion, and cardiac volume overload. While the etiologies of these pathologies are different, they were chosen because they all cause cellular and organ dysfunction which is mediated by the decreased capacity for mitochondrial bioenergetics [27-31].

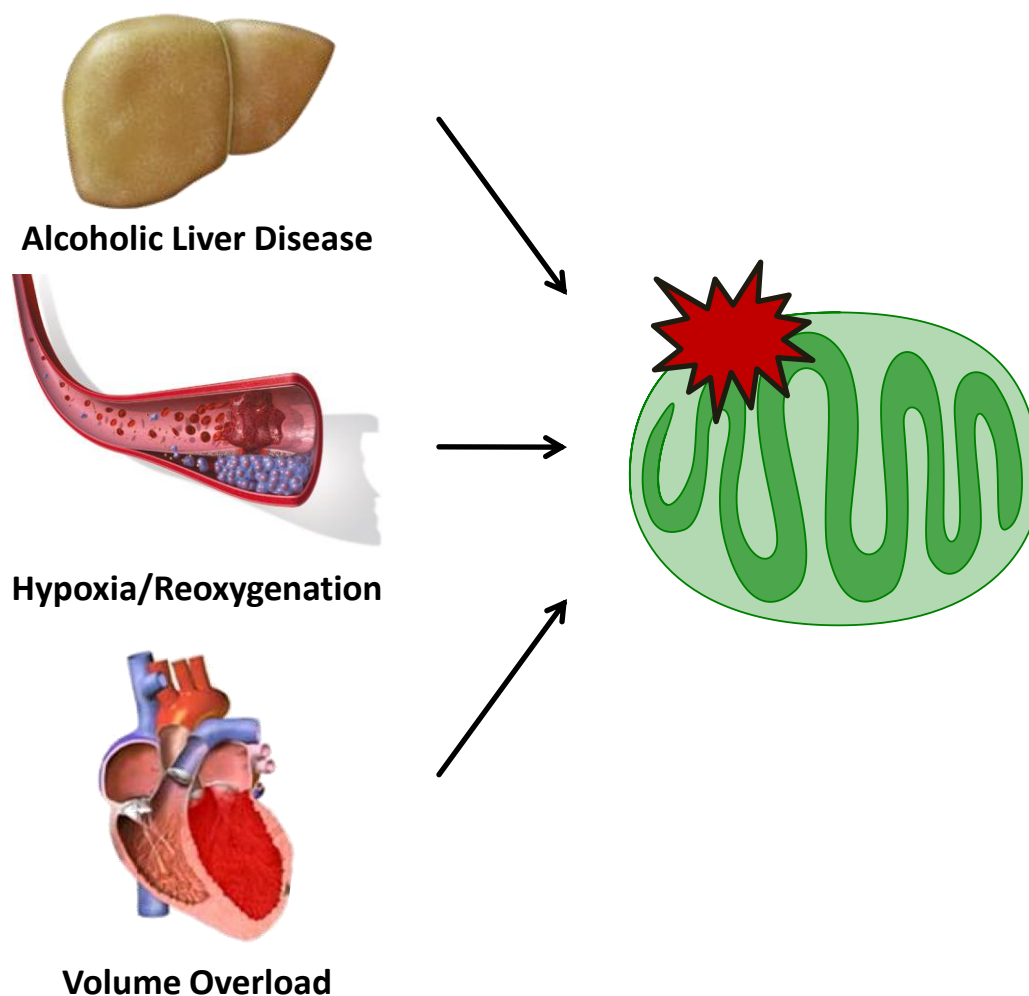


Figure 1-1. The pathophysiologies of many diseases are mediated by the development of mitochondrial dysfunction. Alcoholic liver disease, hypoxia/reoxygenation, and volume overload were selected as the focus of this dissertation because they all cause progressive organ damage and dysfunction mediated by the loss of cellular and mitochondrial bioenergetic function. Herein we describe the effects of these three pathologies on the bioenergetics of intact primary cells to further understand the mechanisms of pathological progression of these diseases.

A well understood example is ALD, which is caused by chronic alcohol (EtOH) consumption leading to the development of mitochondrial bioenergetic dysfunction through EtOH metabolism-induced increases in ROS production, increased reductive stress, and mtDNA damage [28-30, 32]. This causes depressed ATP synthesis and hepatocellular bioenergetic dysfunction, leading to the further progression of ALD [28, 32]. Moreover, ALD also causes hypoxia and the increased production of nitric oxide (NO) in the liver, which both individually and in combination can inhibit mitochondrial function [33-36].

Ischemia/reperfusion also leads to bioenergetic dysfunction, albeit through a different mechanism. During ischemia, the concentration of oxygen (O₂) available for mitochondrial respiration and ATP production is greatly diminished, resulting in decreased energy capacity of the cell [37]. Furthermore, ischemia is also known to cause increased mitochondrial ROS production [31]. The reperfusion of hypoxic tissue causes an even greater production of ROS, which leads to increased lipid peroxidation, mtDNA damage, and protein oxidation, all of which induce mitochondrial dysfunction [31, 38]. Furthermore, mitochondrial calcium overload which is associated with long periods of ischemia followed by reperfusion can cause damage through the induction of ROS production and the opening of the mitochondrial permeability transition pore, leading to programmed cell death [39-42]. While the consequences of ischemia/reperfusion injury have been investigated in several organ systems such as the heart, liver, and kidneys, the effects on the bioenergetic function of vascular tissue are not as well understood. Ischemia/reperfusion injury to vascular endothelial cells has recently been shown to increase ROS production

and alter cell signaling; furthermore, long exposure to ischemia can lead to endothelial dysfunction [43-45].

The final disease model examined in this dissertation is cardiac volume overload, which is mediated by bioenergetic dysfunction through a mechanism involving changes in mitochondrial signaling, increased ROS and RNS, and adaptive changes to heart function and cellular metabolism [46, 47]. Volume overload causes stretching of the cardiomyocytes leading to disruption of the cytoskeleton and increased ROS production, both of which diminish mitochondrial bioenergetic function [27, 48-50]. Moreover, the increased ventricular preload associated with volume overload leads to increased cardiomyocyte ATP demand [46, 47]. This, coupled with decreased mitochondrial function, causes cardiomyocyte bioenergetic and cellular dysfunction, leading to heart failure [27, 46, 51]. Furthermore, individuals from various ethnic backgrounds with distinct mtDNA sequences exhibit different susceptibilities to heart failure and other cardiovascular diseases [52, 53]. Therefore the effect of mtDNA sequence, which influences mitochondrial bioenergetic efficiency and ROS production, on the susceptibility to volume overload-induced bioenergetic dysfunction is discussed in this dissertation [54-60].

Understanding the unique role of the mitochondrion in different organ systems, and how chronic EtOH consumption, ischemia/reperfusion, and volume overload alter that role, is critical to the development of potential therapies to protect mitochondrial bioenergetics and thus prevent cellular dysfunction. This dissertation contains a series of studies which elucidate the effects of these pathologies on mitochondrial function in intact primary cells, yielding a more complete understanding of the development of mitochondrial and cellular dysfunction during disease progression.

ROLE OF THE MITOCHONDRION IN PHYSIOLOGY

Bioenergetics

The mitochondrion plays an important role in cellular metabolism and bioenergetics by being the predominant site of ATP production [1, 14, 15, 61]. This occurs by the oxidation of reducing equivalents produced by the citric acid cycle coupled with the phosphorylation of ADP to yield ATP in a process collectively known as oxidative phosphorylation. The mitochondrion does this by taking in substrates such as pyruvate, which is formed from glycolysis in the cytosol, and fatty acids. Pyruvate is then converted into acetyl CoA by the mitochondrial pyruvate dehydrogenase complex while fatty acids are imported into the mitochondria by the carnitine shuttle, where they undergo a series of β -oxidation producing an acetyl CoA molecule for every two carbons in the fatty acid chain [17, 62]. The acetyl CoA produced by these pathways is then used as a substrate for the citric acid cycle, where it is cycled through several intermediate reactions by eight mitochondrial enzymes which are coupled to the production of electron donors such as NADH, succinate, and malate [62, 63]. These electron donors are then used by the mitochondrial electron transport chain to produce ATP.

Mitochondrial oxidative phosphorylation occurs through the coupling of the electron transport chain, which is a series of four major enzyme complexes (Complexes I through IV), ubiquinone (Q), and cytochrome *c*, with ATP synthase (or Complex V) in the inner membrane of the mitochondria; together these five complexes are responsible for the majority of cellular ATP production [64, 65] (**Figure 1-2**). Complexes I and II oxidize electron donors produced by the citric acid cycle, using the electrons to reduce Q to ubiquinol (QH₂) within the mitochondrial inner membrane [66-68]. The QH₂ is then

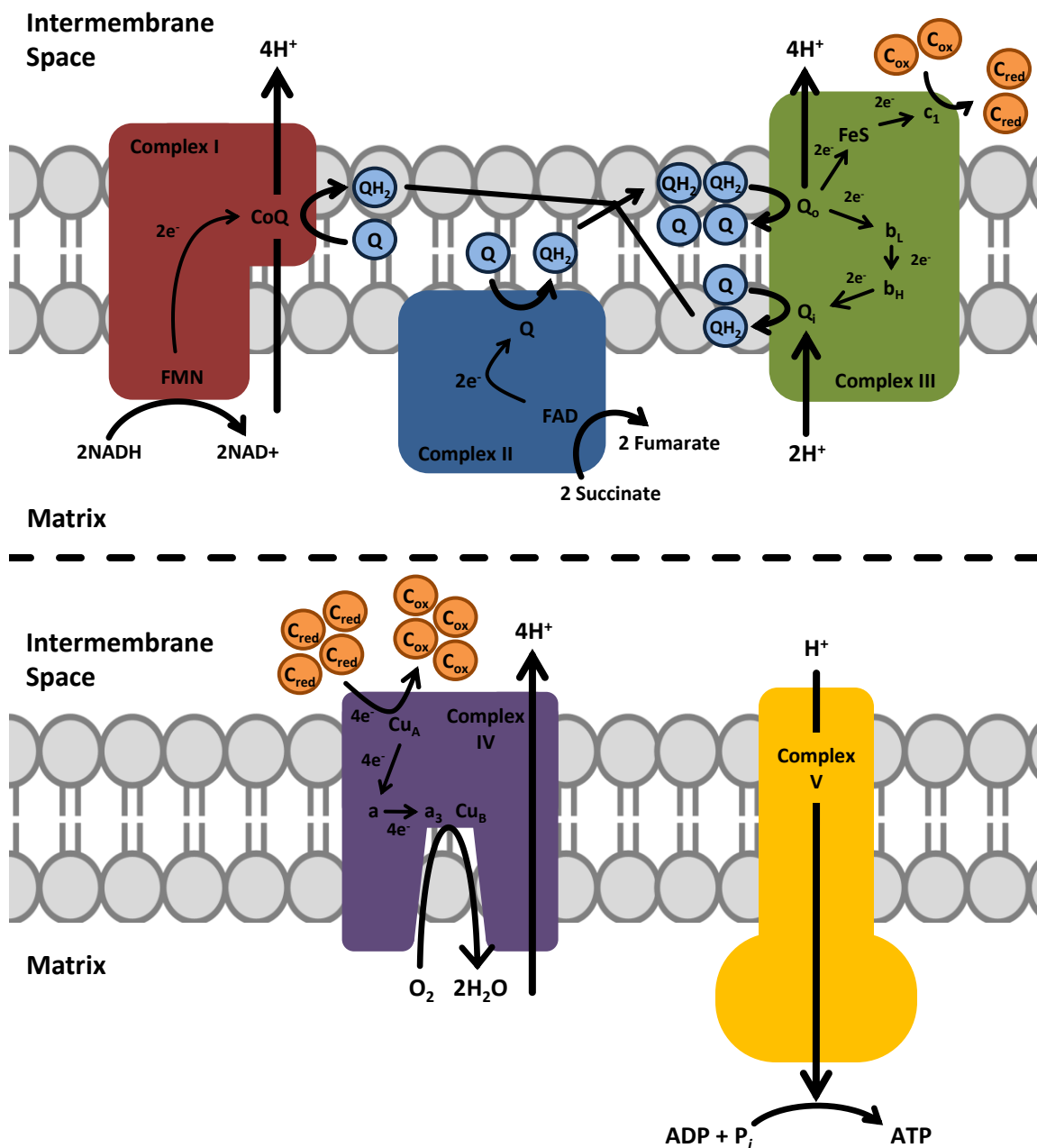


Figure 1-2. Mitochondrial oxidative phosphorylation. Complex I oxidizes NADH and shuttles the electrons (e^-) to the CoQ site, where they are used to reduce ubiquinol (Q) to ubiquinone (QH_2). Complex II can oxidize succinate at the FAD site and transfer the e^- to the Q site to reduce Q to QH_2 . The QH_2 produced by either Complex I or II can then feed into Complex III to participate in the Q cycle leading to the reduction of cytochrome c . Reduced cytochrome c is then reoxidized by Complex IV, which uses the e^- to reduce O_2 to H_2O . This electron transfer is coupled to the pumping of protons (H^+) from the matrix to the intermembrane space to produce an electrochemical gradient. This gradient is then used by Complex V to drive the phosphorylation of ADP to produce ATP.

reoxidized by the Q cycle in Complex III, transferring the electrons to cytochrome *c* [69]. Complex IV uses the electrons from reduced cytochrome *c* as the substrate to perform the complete, four-electron reduction of O₂ to H₂O [70-72]. Moreover, the transport of electrons through Complexes I, III, and IV to convert O₂ to H₂O are coupled to the pumping of protons from the mitochondrial matrix across the inner membrane into the intermembrane space, thus establishing an electrochemical proton gradient [73, 74]. This gradient is then used by Complex V, or ATP synthase, to provide energy for the phosphorylation of ADP in the matrix [75].

In addition, the activities of these enzymes are also capable of regulating non-mitochondrial bioenergetics. Low ATP to ADP and AMP ratios can activate AMP-activated protein kinase (AMPK), which when activated stimulates fatty acid oxidation, glucose uptake, cholesterol synthesis, insulin release, and lipogenesis [76-80]. Moreover, the export of ATP from mitochondria is controlled by the adenine nucleotide transporter (ANT), thus regulating the supply of ATP to the cytosol and other organelles [81-83]. Many cell types also have a mitochondrial isoform of creatine kinase, which is located in the intermembrane space and participates in energy buffering and transport through the activity of the creatine shuttle [84-86].

Preserving mitochondrial bioenergetics under stress is necessary for supplying sufficient energy for the maintenance of cellular function. The effects of cellular and mitochondrial stress induced by ALD, ischemia/reperfusion, and volume overload, all of which are implicated with increased production of mitochondrial ROS, on mitochondrial bioenergetics are a major focus of this dissertation.

Mitochondrial ROS Production

The importance of reactive oxygen and nitrogen species (ROS/RNS) in physiology and their interactions with mitochondria are well established [87]. Originally ROS/RNS were considered to be simply destructive and cytotoxic, but more recently it has become clear that they have several beneficial effects through their ability to activate specific cell signaling pathways [88, 89]. ROS have been shown, at low levels, to induce cell proliferation and control the synthesis of endogenous antioxidant enzymes. Mitochondria are both a source and target for ROS and play a key role in redox cell signaling [90-93]. Under pathological conditions, increased levels of mitochondrial ROS formation can lead to the oxidative damage of DNA, lipids and proteins; this can impair bioenergetic function, and in some cases initiate programmed cell death or apoptosis.

Mitochondria can generate ROS from a number of different redox centers in several metabolic pathways [94]. The basic principle for ROS generation from these sites is shown in **Figure 1-3A**. Electrons are transferred to a redox center which then acts as an intermediate carrier to another redox active member of the metabolic pathway [95]. The more reduced the redox center is, the greater the potential production of ROS. While there are several mitochondrial enzymes which are known to produce ROS, the primary contributors are Complexes I and III [96].

Complex I (NADH:ubiquinone oxidoreductase) consists of 45 subunits with a combined mass of close to 1MDa [67, 68]. Complex I accepts two electrons from NADH, which is produced by the citric acid cycle, via a flavin mononucleotide (FMN) and transfers them through a chain of seven iron-sulfur centers to the CoQ reduction site [67, 68]. There the electrons are transferred to ubiquinone (Q), reducing it to ubiquinol

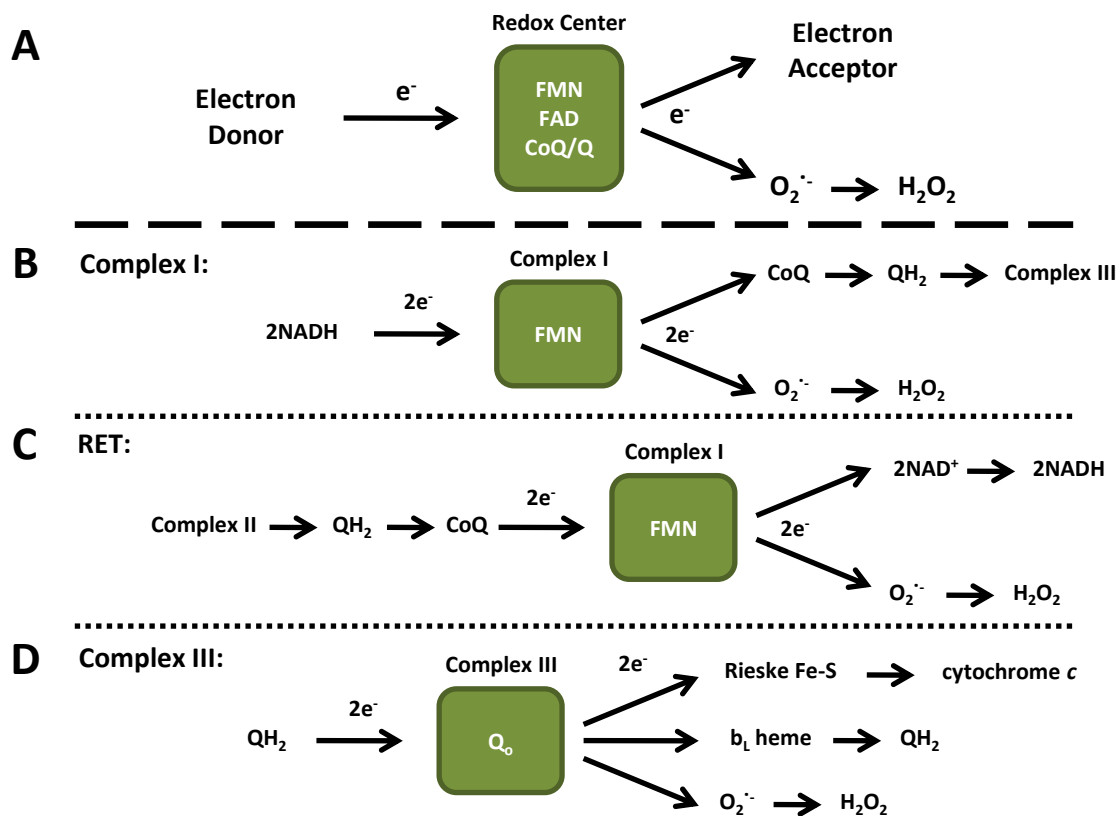


Figure 1-3. Mechanisms of ROS formation in the mitochondria. The sites of ROS production within the mitochondria all follow a similar mechanism. An electron donor donates an electron to a redox center, which then reduces the electron acceptor. However, electrons can also be transferred from the redox center to reduce oxygen into superoxide (A). Complex I oxidizes NADH through the FMN site, and can transfer the electrons to either the CoQ site to make ubiquinol (QH_2) or, if the CoQ site is inhibited, to O_2 to make superoxide (B). In reverse electron transport (RET), QH_2 produced by Complex II can be transferred back into Complex I through the CoQ site to the FMN, which can then either reduce NAD^+ back to NADH or it can reduce O_2 to form superoxide (C). Complex III uses QH_2 produced predominantly by Complex I and II as the electron donor, transferring the electrons to the Rieske Fe-S and then on to cytochrome c1 and finally cytochrome c. Complex III also transfers electrons to the b_L heme, which participates in the Q cycle. However, when the Q cycle is inhibited, by antimycin A for example, the electrons can leak out of the Q_o site to reduce O_2 to make superoxide (D).

(QH₂). One mechanism by which Complex I produces ROS is by the reaction of O₂ with the fully reduced FMN forming O₂^{••} on the matrix side of the complex [97]. The rate of O₂^{••} production at the FMN can be increased by inhibiting the CoQ site using the small molecule inhibitor rotenone [98]. Similarly, this production of O₂^{••} at the FMN is dependent on the NADH/NAD⁺ ratio, which determines the proportion of FMN that is fully reduced. Under physiological conditions, O₂^{••} generation from Complex I is sensitive to the redox state of the respiratory chain [99, 100] (**Figure 1-3B**).

An additional mechanism through which Complex I can produce ROS is called reverse electron transport (RET) [101-104] (**Figure 1-3C**). This occurs when the mitochondria are utilizing succinate as a substrate through Complex II [97, 105]. Under conditions of low electron flux (when ADP levels are low), the larger pool of reduced QH₂ is sufficient to reduce Complex I at the CoQ site [106]. This reverses the normal flow of electrons back through the complex to reduce the FMN site, and as a result reducing NAD⁺ to form NADH, while also reducing O₂ to form O₂^{••} [101, 103, 104, 107] (**Figure 1-4**). RET results in the generation of O₂^{••} in the matrix and can be inhibited with rotenone treatment [108]. Interestingly, RET generates the highest rate of O₂^{••} formation detected thus far in the mitochondrion [108-110]. Whether RET plays a physiological role in cell signaling through ROS production is not clear.

Complex III is approximately 240kDa and is made up of 11 subunits, three heme groups, and the Rieske iron-sulfur (Fe-S) center [69]. It functions by oxidizing QH₂ in the inner membrane and transferring the electrons to reduce cytochrome *c* in the intermembrane space [69]. The rates of O₂^{••} production from Complex III are relatively low during RET compared to that of Complex I [111]. However, the further inhibition of

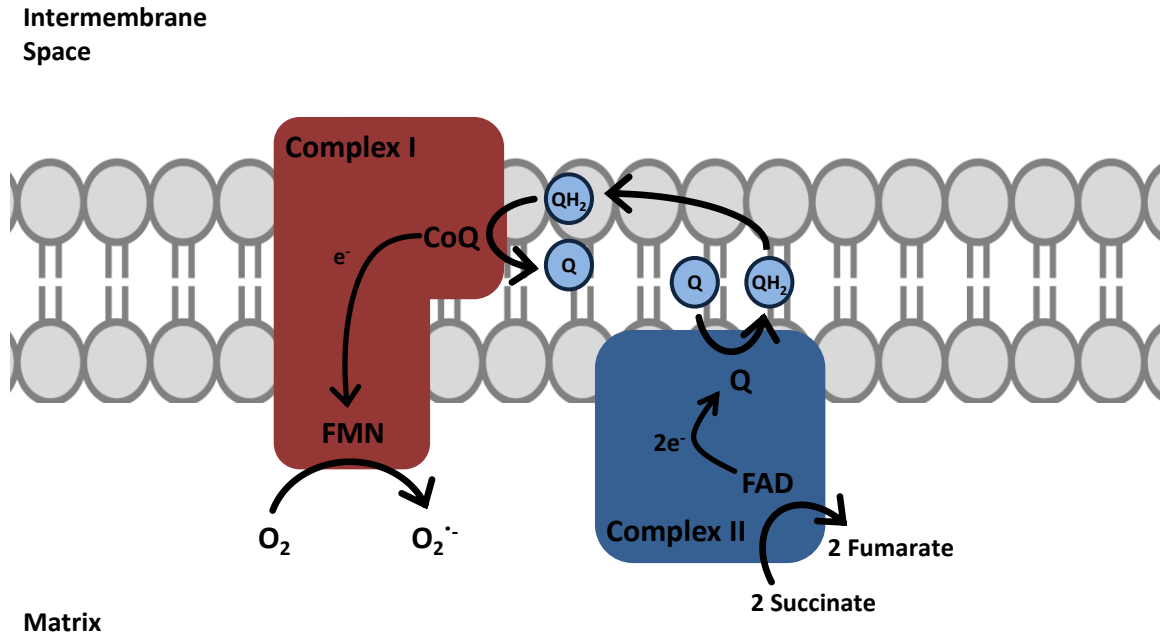


Figure 1-4. Reverse electron transport. Reverse electron transport occurs when there is a high membrane potential and high levels of ubiquinol (QH_2) produced by Complex II. The QH_2 can be oxidized to ubiquinone (Q) by the CoQ site in Complex I, sending electrons (e^-) back down to the FMN site, which can then transfer the electrons to O_2 , reducing it to form superoxide ($\text{O}_2^{\cdot-}$).

Complex III with the Q_o site inhibitor myxothiazol attenuates most of this O₂^{•-} production, suggesting that Complex III does produce some O₂^{•-} during RET, albeit a small amount [103, 108]. Alternatively, when the Q_i site is inhibited using antimycin A, Complex III produces increased amounts of O₂^{•-} [98, 104, 112-115], which are released to both sides of the inner membrane [102, 107, 116, 117]. This formation of O₂^{•-} is due to the reaction of O₂ with the QH bound to the Q_o site. This O₂^{•-} formation due to antimycin A can be abrogated by treatment with myxothiazol, which inhibits the Q_o site, suggesting that QH bound to the Q_o site is the main site of O₂^{•-} production [98, 104, 112-115] (**Figure 1-3D**). There are several other mitochondrial enzymes which are able to produce low levels of ROS, including Complex II, α -ketoglutarate dehydrogenase, and glycerol-3-phosphate dehydrogenase [96].

The mitochondrion also has several ways through which it can control the levels of ROS it produces [87]. Superoxide can be converted to hydrogen peroxide by the enzyme superoxide dismutase [118, 119]. The superoxide dismutase located in the mitochondrial matrix contains a Mn prosthetic group and is known as SOD2 or MnSOD [118]. The superoxide dismutase located in the cytosol contains Cu/Zn prosthetic groups and is known as Cu/Zn SOD or SOD1, and may also be present in the mitochondrial inter-membrane space [120, 121]. SOD2 provides a major mechanism by which the mitochondrion can control the levels of ROS, through its ability to catalyze the dismutation of superoxide (O₂^{•-}) to hydrogen peroxide, which can be further metabolized to H₂O by catalase, peroxiredoxin, thioredoxin, or glutathione peroxidase [122, 123]. In addition, these systems can also help to remove other peroxides, such as those that have formed on lipids and proteins.

Mitochondria also control ROS production through the ability of uncoupling proteins (UCP) which increase proton leak, thereby decreasing mitochondrial membrane potential and the redox state of sites of $O_2^{\cdot -}$ formation [104, 124-134]. UCP3 has also been suggested to lower mitochondrial levels of lipid peroxidation by causing fatty acid efflux from the matrix when fatty acid levels are in excess [135-137].

Although much is already known about the production and function of these reactive species, many aspects of how ROS are formed by and interact with the mitochondrion are still unclear, particularly *in vivo*. Moreover, the production of ROS is known to be increased in response to ALD [30], vascular ischemia/reperfusion [31], and cardiac volume overload [27], and could exacerbate the damage to the mitochondria. This dissertation focuses on elucidating a greater understanding of how these reactive species affect mitochondrial and cellular bioenergetic function in these pathologies.

Importance of mtDNA Haplotype

An important target of damage induced by mitochondrial ROS which is implicated in the development of mitochondrial dysfunction and disease is mtDNA. Each mitochondrion contains multiple copies of their own genome, independent of nuclear DNA, which exists as a circular DNA molecule of approximately 16,000 base pairs and codes for 37 genes (**Figure 1-5**) [138]. These genes encode for the large and small subunits of rRNA, 22 tRNAs, and 13 proteins [19, 20]. Importantly, all 13 of the mtDNA encoded proteins are subunits of the electron transport chain complexes [138]. Differences in the mtDNA which encodes for these protein subunits have been shown to change the structure, folding, and/or activities of the complexes in which they reside [20, 139]. It has

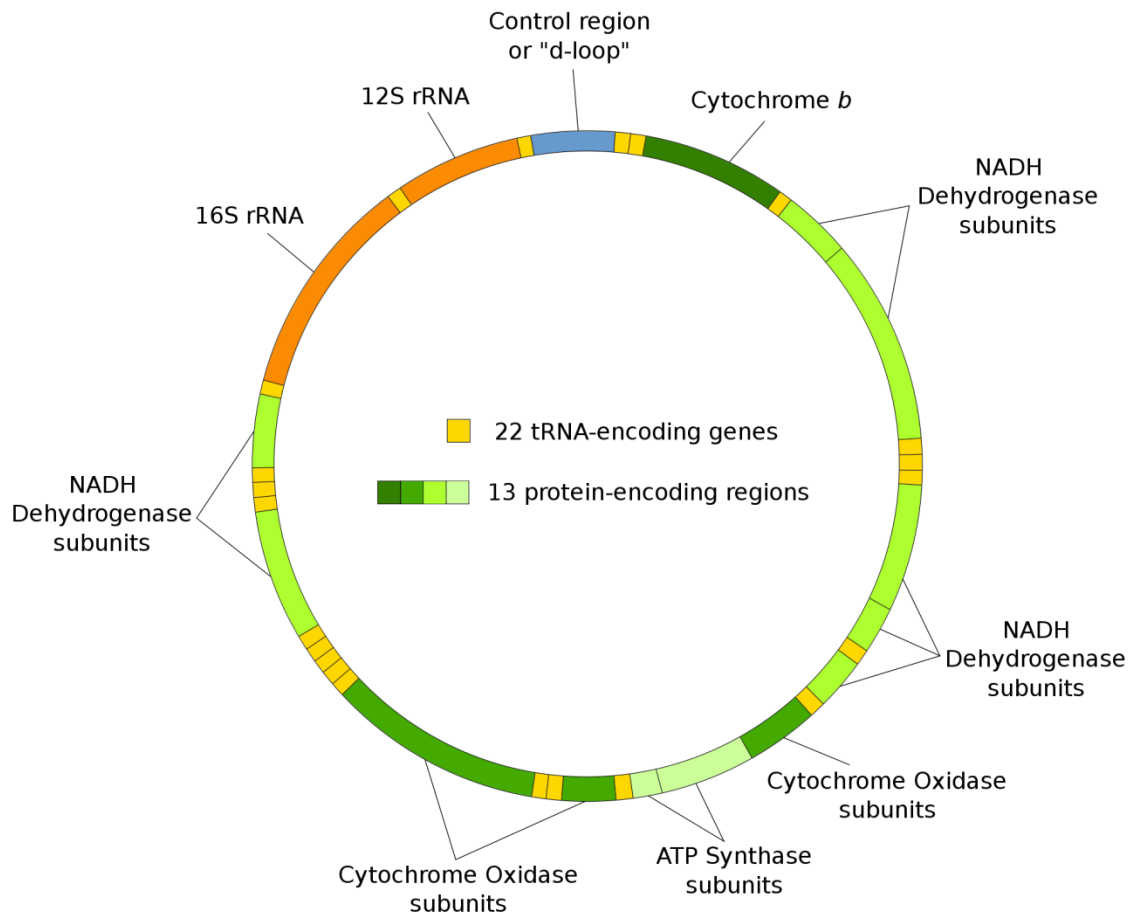


Figure 1-5. Mitochondrial DNA map. The mitochondrial DNA (mtDNA) encodes for 37 different genes: 2 rRNAs, 22 tRNAs, and 13 peptides. The 2 rRNAs make up the large and small subunits of the mitochondrial ribosomes. The 22 tRNAs are responsible for transferring amino acids to a growing peptide at the ribosome during mitochondrial protein synthesis. The 13 peptides which are encoded by mtDNA make up 7 subunits of Complex I, 1 subunit of Complex III, 3 subunits of Complex IV, and 2 subunits of Complex V. Figure obtained from Wikipedia.

been suggested that different mtDNA haplotypes have been selected for during the evolution of certain populations of humans and animals. Some of these haplotypes have subtle differences in their mtDNA sequences, which have been shown to alter their mitochondrial bioenergetics, resulting in the better adaptation for their specific environments [140-142].

Through the sequencing of mtDNA from different populations from around the world, humans can be grouped into several different mitochondrial haplogroups [143-145] (**Figure 1-6**). These mtDNA haplogroups were likely selected for evolutionarily based on environmental factors as populations migrated into different environments [140, 142]. For example, as humans moved further north where temperatures were lower, mtDNA mutations that allowed for greater mitochondrial heat production at the expense of decreased bioenergetic efficiency were probably more favorable. In contrast, populations of people who originated in Africa where temperatures are high selected for mtDNA mutations resulting in increased bioenergetic efficiency with less heat generation [140, 142].

Along with altering mitochondrial efficiency and heat production, different mtDNA mutations also affect the rate of mitochondrial ROS production. Northern European populations associated with increased heat production and decreased mitochondrial efficiency also have lower levels of ROS production, while African populations associated with lower levels of heat production and increased mitochondrial efficiency have higher levels of ROS production [140]. These different levels of mitochondrial ROS production, along with different bioenergetic efficiencies, likely play a role in the susceptibility of different populations to several diseases, particularly those characterized by

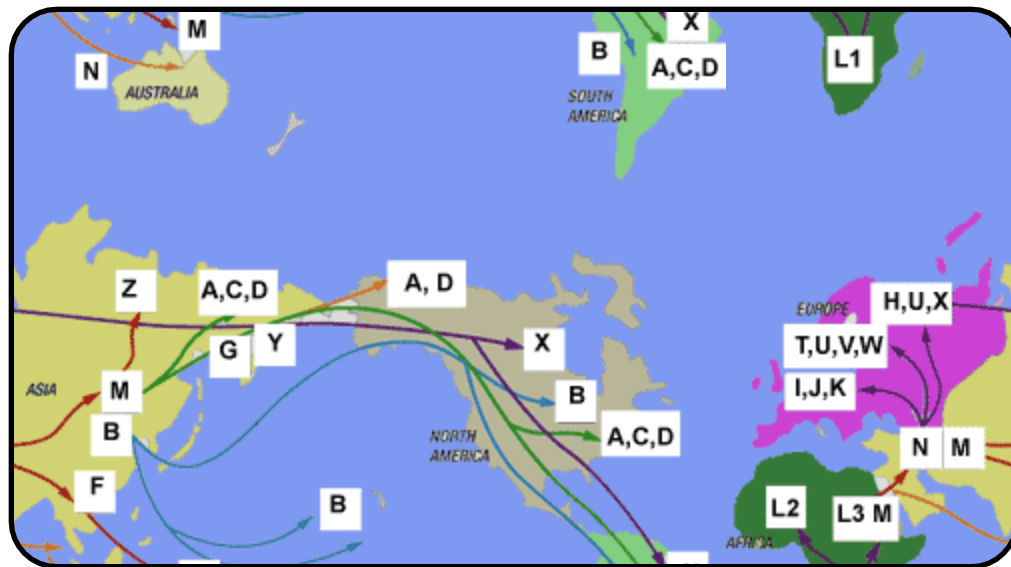


Figure 1-6. Model of human migration based on mtDNA haplogroups.

The migration pattern of human populations out of Africa and around the world has been traced based on the evolution of different haplotypes of maternally-inherited mtDNA. The letters represent different mtDNA haplotypes amongst populations from around the world. Haplotypes of interest in the dissertation are the H and L haplotypes, which contain 17 mtDNA nonsynonymous mutations: 4 in Complex I, 1 in Complex III, 1 in Complex IV, 1 in Complex V, 2 in tRNA for Asp and Ile, 4 in 12S rRNA, and 3 in 16S rRNA. Figure obtained from Wikipedia [143].

alterations in mitochondrial function such as heart failure. For example, it has been shown that a higher percent of people of African descent suffer from various forms of cardiovascular diseases than people of European descent, which supports the theory that increased ROS production due to the African mtDNA haplotype plays a role in increased disease susceptibility [52, 53] (**Figure 1-7**).

In this dissertation, the effect of mtDNA haplotype on mitochondrial bioenergetics and the susceptibility to disease were examined using the model of cardiac volume overload in mice with different mtDNA haplotypes. The utilization of this mouse model allows for the investigation into the role of distinct mtDNA haplotypes, each with unique bioenergetic efficiencies and rates of ROS production, in the development of mitochondrial and cellular bioenergetic dysfunction.

ROLE OF THE MITOCHONDRION IN PATHOLOGY

Bioenergetic Dysfunction

An increasing number of diseases have been shown to be characterized by alterations in mitochondrial function [19, 21, 22, 138, 146]. Some of these diseases, such as Leber's hereditary optic neuropathy and Kearns-Sayre syndrome, have been linked to mutations in specific mtDNA genes [147, 148]; others, such as Friedreich's ataxia, have been linked to nuclear encoded mitochondrial genes [149-151]. There are also numerous diseases whose etiologies and pathophysiologies directly involve the development of mitochondrial dysfunction. A few examples of these include diabetes mellitus [152, 153], cardiovascular diseases [23, 154-157], fatty liver diseases [28-30, 158-161], and neurodegenerative diseases [162-164]. The major unifying link between these different pa-

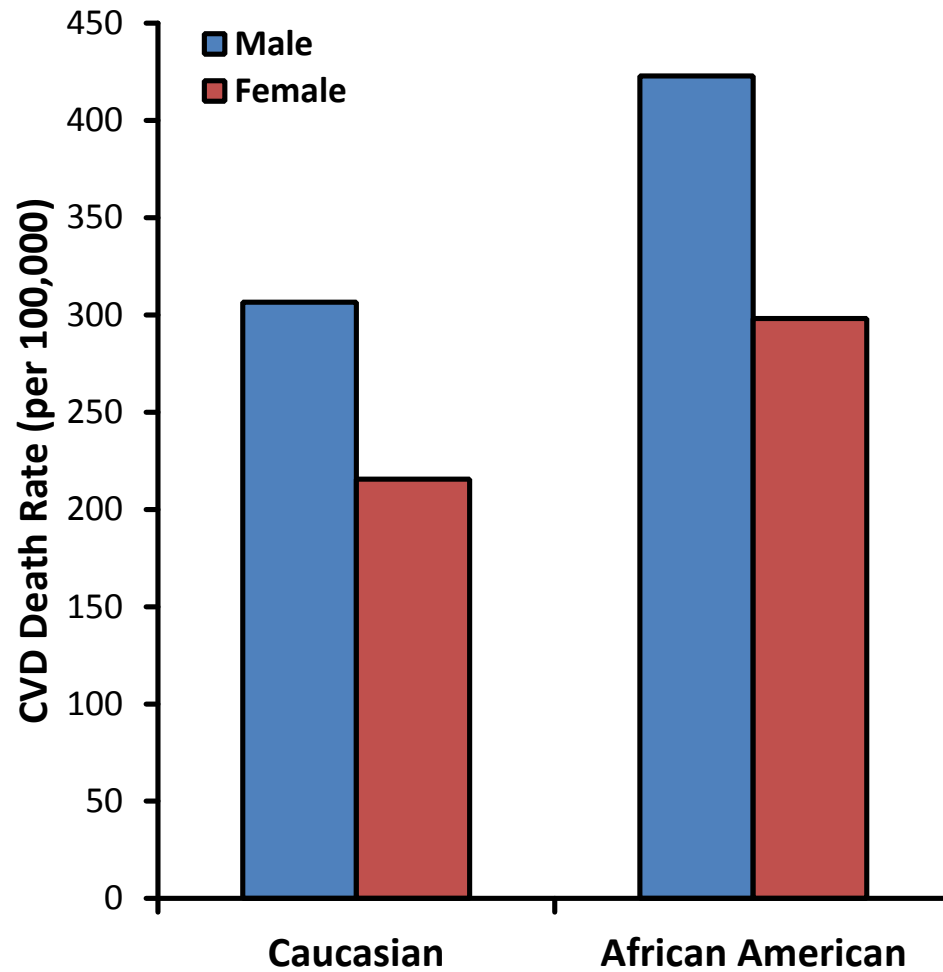


Figure 1-7. Death rate from cardiovascular diseases between Caucasians and African Americans. Both male and female African Americans are known to suffer from a higher rate of morbidity and mortality from cardiovascular diseases than Caucasians [48, 49].

thologies is cellular damage which causes increases in oxidative stress, and the mitochondrion is a major source and target of oxidative stress.

Oxidative stress is known to cause mitochondrial dysfunction through the oxidative damage to mitochondrial proteins, lipids, and DNA [23, 87, 96] (**Figure 1-8**). Studies have shown that ROS can cause sustained mtDNA damage, thus altering mitochondrial transcript levels and protein synthesis [22, 23]. Moreover, ROS have been shown to mediate the formation of oxidative post-translational modifications of mitochondrial proteins, resulting in their altered function and inactivation [157, 160, 165]. For example, the citric acid cycle enzyme aconitase is known to exhibit decreased activity following exposure to ROS, and as such aconitase activity is often used as a marker of mitochondrial oxidative stress [166-170]. Furthermore, the adenine nucleotide transporter has been shown to be inactivated in response to oxidative stress [171, 172].

Oxidative damage to the mitochondrion results in the decreased ability of the cell to generate energy [23, 160, 173]. When the loss of mitochondrial bioenergetic function is great enough that the cells can no longer meet their energy requirements, the cells become dysfunctional and can induce apoptosis mediated by the mitochondrial release of cytochrome *c* [11, 24, 174, 175]. This loss of cellular function mediated by the development of mitochondrial dysfunction plays a key role in the progression of diseases associated with high levels of oxidative and cellular stress and is a major focus of this dissertation.

The study of mitochondrial function has traditionally been achieved by isolating the mitochondria from a tissue and measuring their respiration and specific enzymatic activities [176]. While these types of studies have led to significant advances in the un-

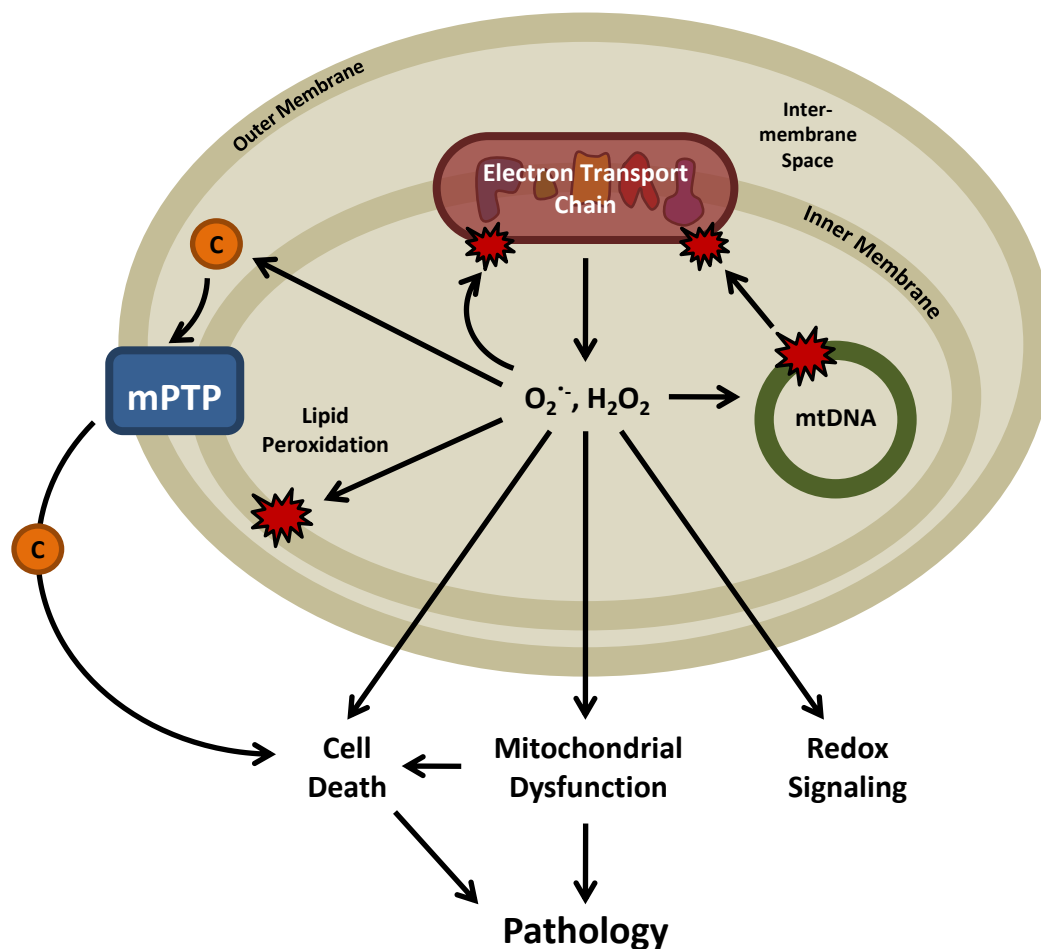


Figure 1-8. Effects of mitochondrial ROS. Mitochondrial ROS production can alter the function through a variety of pathways. Lower levels of ROS can act through several redox signaling mechanisms, while higher levels can directly damage mitochondrial proteins, leading to the further production of ROS. ROS can also damage mtDNA and induce lipid peroxidation in the membrane, and can also cause mitochondrial permeability transition pore (mPTP) opening, which leads to cytochrome *c* release and apoptosis induction.

derstanding of the role of mitochondrial function in disease progression, there are still many drawbacks to using this approach. Isolated mitochondria are lacking their cellular environment and endogenous substrates, which negates any cellular regulation and also makes it very difficult to mimic pathological conditions. Because of this, we have utilized recent advances in the study of cellular bioenergetics to study the effects of different pathologies on mitochondrial function within their cellular environment [176-178].

The ability to measure mitochondrial bioenergetics within intact, adherent cells allows for the measurement of the cells' basal respiration rate, which cannot be measured using isolated mitochondria [178]. This ability allows for the determination of the effects of different pathologies on basal mitochondrial function in different tissues. Moreover, when compared to the cells' maximal respiration rate, the reserve respiratory capacity of the cells can also be calculated [179, 180]. This fundamental parameter of mitochondrial function represents the cells' mitochondrial function which they are not using under basal conditions, but can call upon under conditions of increased stress or ATP demand [179, 180] (**Figure 1-9**). Previous studies using ^{31}P -NMR have shown that cardiac cells possess a reserve capacity for ATP production which is depleted under conditions of stress, such as pressure overload-induced heart failure [179, 181-184]. Importantly, pathological conditions which result in diminished mitochondrial function cause a decrease in the reserve capacity, which renders the tissue more susceptible to dysfunction in response to an additional stress. The effects of ALD, hypoxia/reoxygenation, and volume overload on mitochondrial bioenergetic function and reserve capacity are a central focus of this dissertation.

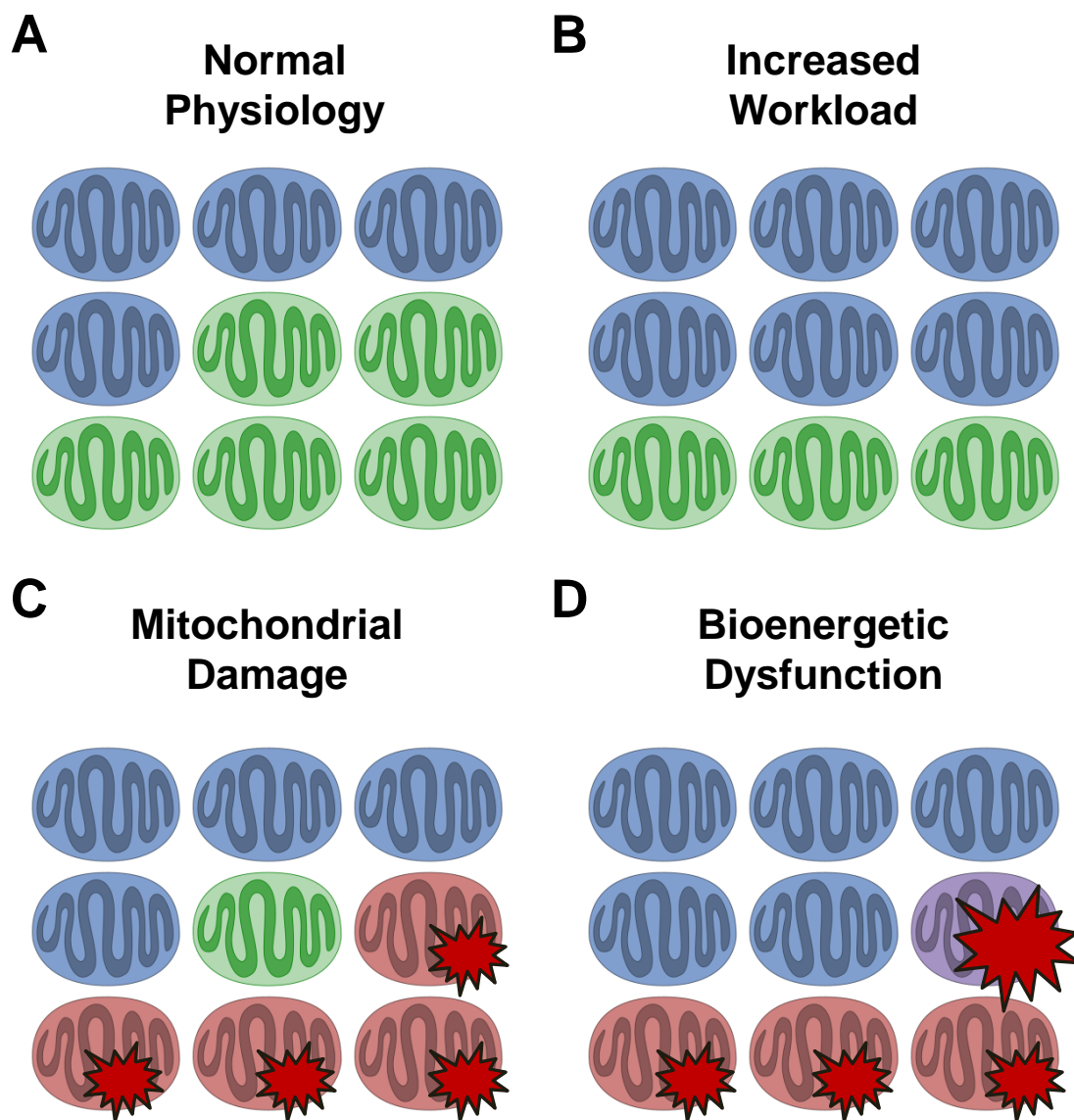


Figure 1-9. Reserve capacity protects tissue from bioenergetic dysfunction in response to increased workload or stress. (A) Under normal physiology, most cell types inherently possess a bioenergetic reserve capacity, which is mitochondrial function which is not being used and is available to the cell under conditions of increased ATP demand. (B) Cells with increased ATP demand can utilize the reserve mitochondrial function available to the cell. (C) Mitochondrial damage decreases the total mitochondrial function available to the cell, thus decreasing the reserve capacity. (D) Bioenergetic dysfunction occurs because there is not enough available mitochondrial function to meet the cells energetic requirements. Blue mitochondria = mitochondrial function being used. Green mitochondria = reserve capacity (spare mitochondrial function available to the cell). Red mitochondria = dysfunctional mitochondria. Purple mitochondria = deficit of mitochondrial function due to lack of reserve capacity.

DISEASES ASSOCIATED WITH MITOCHONDRIAL DYSFUNCTION

Elucidating the relationship between mitochondrial dysfunction and the response to the stresses associated with developing pathologies is the aim of this dissertation. To accomplish this, we used animal and cell models of diverse pathologies associated with mitochondrial dysfunction in which we measure endpoints directly related to the pathology and cellular bioenergetic function. The disease models investigated herein are ALD, vascular ischemia/reperfusion, and cardiac volume overload. While the development of these pathologies occurs via different mechanisms, they were chosen because they all cause cellular and organ dysfunction which is mediated by diminished mitochondrial bioenergetics.

Alcoholic Liver Disease

Alcoholic liver disease (ALD) affects over 2,000,000 people in the United States alone, and can lead to cirrhosis and hepatocellular carcinoma [185, 186]. The early stages of ALD are characterized by liver hypoxia, oxidative and nitrative stress, as well as alterations in the mitochondrial function of the hepatocytes, rendering the cells more susceptible to bioenergetic dysfunction by secondary stresses [28-30, 33, 34, 160, 161, 187, 188]. ALD-induced mitochondrial dysfunction has been shown by measuring the respiration of isolated liver mitochondria [28, 33, 34] and the products of mitochondrial bioenergetics from isolated hepatocytes [161, 187, 188]. However, the effect of chronic EtOH consumption on the bioenergetic responses of primary hepatocytes to stresses associated with ALD remains unclear.

Chronic EtOH consumption has been shown to cause an increase in inducible nitric oxide synthase (iNOS) levels, which leads to the increased production of NO and nitritative stress [33, 34, 36]. It is known that NO inhibits mitochondrial respiration, particularly at the low O_2 concentrations experienced in hypoxia [189-191]; furthermore, nitritative stress is also known to diminish mitochondrial function even in normoxic conditions [180, 192-194]. Chronic EtOH toxicity is known to cause hypoxia in the liver [33, 34, 161, 187, 188], which is able to alter mitochondrial function via cell signaling and the availability of O_2 as a substrate for cytochrome *c* oxidase (CcOX) [195-201]. We have shown that NO treatment diminishes the maximal respiration of the mitochondria in intact cells, rendering them more susceptible to toxicity induced by secondary stresses [180] (**Figure 1-10**). Furthermore, the effect of NO on mitochondrial function in intact primary hepatocytes under hypoxia has not been shown. Therefore, it is important to understand both the individual and combined effects of hypoxia and NO on the already impaired mitochondrial bioenergetics of hepatocytes in ALD. Understanding the role of the increased production of NO in the liver hypoxia which develops as a result of ALD could be of critical importance, as hypoxia is well known to alter mitochondrial function.

In this dissertation, the effects of chronic EtOH consumption, NO , and hypoxia on mitochondrial function in intact primary hepatocytes were determined. Moreover, the effect of iNOS on the development of hypoxia in response to chronic EtOH consumption is discussed herein. Understanding the effects of these pathological features of chronic EtOH consumption on the development of mitochondrial dysfunction leading to hepatotoxicity and ALD are critical to gaining further insight into how cellular bioenergetics are altered by pathologies.

Ischemia/Reperfusion in the Vasculature

Much like ALD, albeit through different mechanisms, ischemia/reperfusion causes mitochondrial bioenergetic dysfunction mediated by increases in reductive stress and mitochondrial ROS formation which damage mitochondrial proteins, lipids, and DNA. While hypoxia and reoxygenation are known to alter mitochondrial function, the effects of altering O₂ concentration over time on the bioenergetics of intact cells are not as well understood. Moreover, many of the studies which have elucidated the effects of hypoxia and reoxygenation have been using isolated mitochondria and have been focused on the effects on the extra-vascular tissue, while few studies have focused on the effects of hypoxia and reoxygenation on the endothelium within the vessel. Understanding the alterations in mitochondrial function induced during hypoxia and reoxygenation are of great importance in the vasculature because maintaining proper endothelial function is crucial in the reperfusion that is needed following an occlusion. Loss of endothelial function after ischemia/reperfusion injury can lead to the no-reflow phenomenon, in which the obstruction is cleared but there is failure of the blood to reperfuse the ischemic tissue, further contributing to tissue damage [202, 203].

Exposure of the vasculature to hypoxia and reoxygenation occurs *in vivo* during ischemia/reperfusion when a thrombus prevents blood flow from reaching downstream tissues followed by removal of the clot and the restoration of blood flow and O₂ (**Figure 1-11**). Both hypoxia and the reoxygenation that follows are known to cause increased ROS production from both xanthine oxidase and mitochondria [31, 204]. While both states result in increased oxidative stress, reoxygenation causes a much greater increase

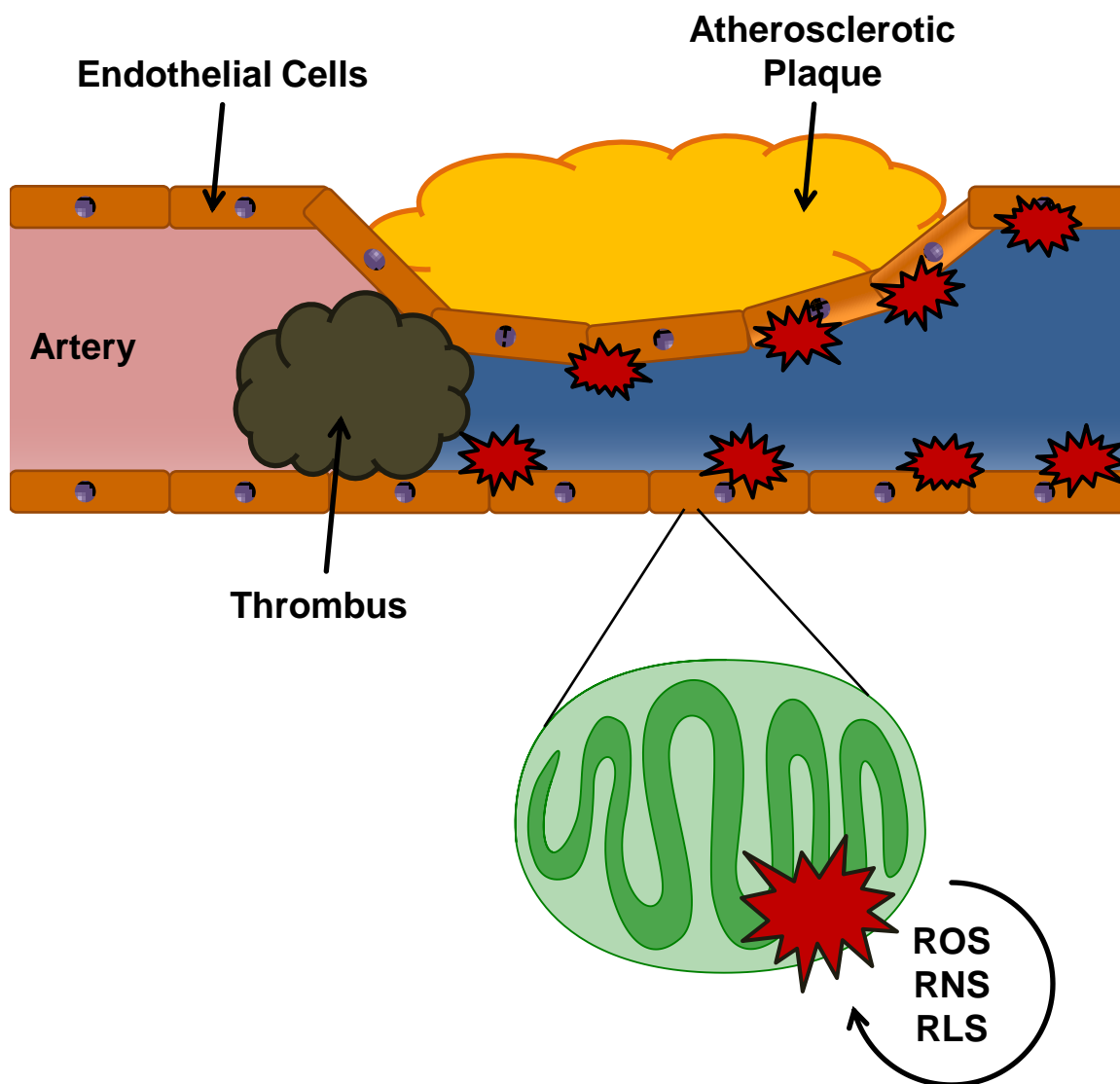


Figure 1-11. Ischemia/reperfusion causes damage to the endothelium and underlying tissue. Ischemia in the vasculature caused by thrombus formation renders the downstream endothelium and tissue to become hypoxic due to the lack of blood flow, inhibiting mitochondrial bioenergetics and inducing reactive oxygen, nitrogen, and lipid species (ROS, RLS, and RNS) formation. When the clot is cleared via thrombolysis, the vessel is reperfused. Reperfusion is known to cause large increases in oxidative stress, resulting in further damage to mitochondrial bioenergetics.

in ROS [38, 205]. This increase in ROS production has been shown to modulate redox signaling, damage mtDNA, induce lipid peroxidation, and denature proteins [205-207].

Cells exposed to low O_2 are also known to exhibit diminished mitochondrial bioenergetics [195, 196, 208]. Complex IV and MnSOD have decreased enzymatic activities under low O_2 concentrations. The decrease in Complex IV activity results in the increased formation of ROS due to the leak of electrons from the earlier complexes in the electron transport chain. In addition, the decrease in MnSOD activity also contributes to increased ROS damage due to the loss of the ability to convert $O_2^{\cdot -}$ into H_2O_2 , which can then be converted to O_2 and H_2O by catalase. These increases in ROS produced during hypoxia damage the complexes of the electron transport chain [209-211]; furthermore, when the cells are reoxygenated, the damage to the electron transport chain caused during hypoxia causes a large increase in ROS formation, which leads to further damage and often dysfunction [38, 212-214]. It has been shown that increasing times of hypoxic exposure causes greater amounts of oxidative damage to the mitochondria and increasing cytotoxicity upon reoxygenation, due in part by the loss of mitochondrial function and the subsequent induction of apoptosis [215].

Elucidating the bioenergetic response of the endothelium to decreasing O_2 concentrations is critical to understanding how mitochondria regulate their respiration in hypoxia. Furthermore, determining the mitochondrial response to reoxygenation following hypoxia allows for greater understanding on the effects of reperfusion injury on endothelial bioenergetics. Therefore, the effects of hypoxia and reoxygenation on endothelial cell bioenergetics are a major focus of this dissertation.

Cardiac Volume Overload

Mitochondrial dysfunction is implicated in both the initiation and progression of most cardiovascular diseases, such as ischemia/reperfusion and volume overload [23]. Cardiovascular disease is the leading cause of death in the United States, resulting in over 800,000 deaths per year; moreover, approximately 7% of these deaths are attributed to heart failure [52, 53]. A major cause of heart failure is volume overload due to mitral valve regurgitation (MR) [216]. In patients with acute MR, the left ventricle (LV) develops volume overload because with every contraction it now has to pump out not only the volume of blood that goes into the aorta, but also the blood that leaks back into the left atrium. This increase in stroke volume causes the progressive increase in LV volume, resulting in LV dysfunction and heart failure [48, 217].

Volume overload (VO) is associated with an increased workload on the myocardium, resulting in a greater utilization of ATP and yielding increased levels of AMP and ADP [27, 46, 47, 218]. These are degraded through purine catabolism to form xanthine and hypoxanthine, which act as substrates for xanthine oxidase to produce ROS [219, 220] (**Figure 1-12**). Importantly, xanthine oxidase has been shown to have increased activity in models of volume overload, along with increased levels of ROS production [221, 222]. These ROS damage cellular proteins, particularly those in the mitochondria which are known to be a major target of ROS [87]. This in turn can cause mitochondrial dysfunction, which manifests as a decrease in ATP production along with an increase in the production of mitochondrial ROS. The mitochondrial damage and resulting increase in ROS production form a feed-forward loop causing even more bioenergetic dysfunction

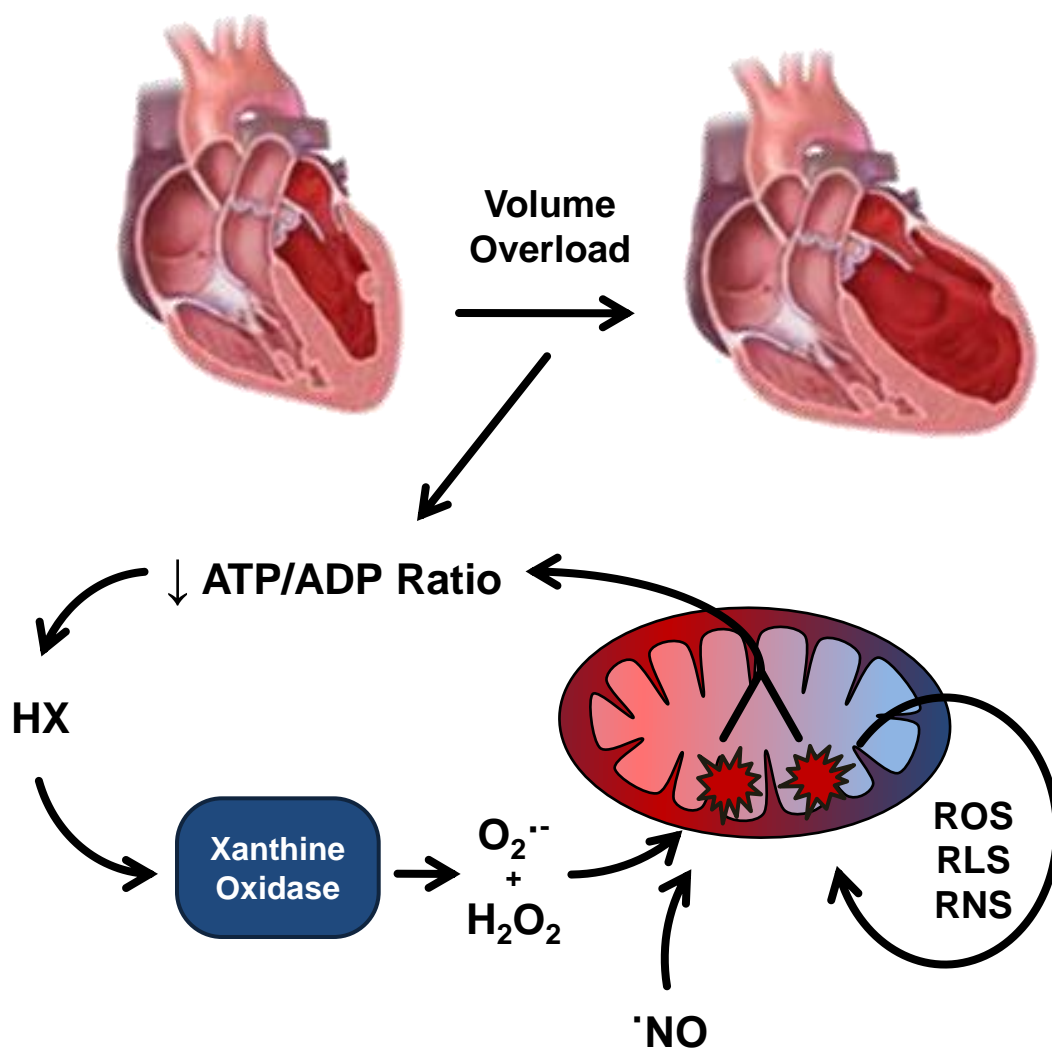


Figure 1-12. Increased xanthine oxidase activity leads to mitochondrial dysfunction in the volume overloaded heart. Volume overload in the heart leads to increased usage of ATP for energy, resulting in increased levels of ADP and AMP. ADP and AMP are then degraded into hypoxanthine (HX) via purine catabolism. Xanthine oxidase then uses HX as a substrate to form superoxide ($O_2^{\cdot-}$) and hydrogen peroxide (H_2O_2), which then damages the mitochondria, leading to bioenergetic dysfunction. This results in increased electron leak to form more ROS and decreased ATP production. The increase in ROS and decrease in ATP production feed back into the cycle causing further mitochondrial damage, thereby increasing left ventricle systolic dysfunction.

over time, which eventually leads to myocyte dysfunction when the energy demand of the cells can no longer be met [27, 221].

Volume overload has also been shown to cause the disruption of the myocyte cytoskeleton, which is mediated by the activation of matrix metalloproteinases (MMPs) [223, 224]. The MMPs have been suggested to become activated by ROS produced by xanthine oxidase and the mitochondria [225]. Because the cytoskeleton is known to play a role in the regulation of mitochondrial function and cellular bioenergetics [49, 226-228], the disruption of the cytoskeleton seen in volume overload may also play a role in the bioenergetic dysfunction that is characteristic of volume overload.

Furthermore, because people and animals with distinct mtDNA haplotypes have been shown to have different susceptibilities to cardiovascular diseases and discrete bioenergetic efficiencies and rates of ROS production [52, 53, 140-142], we decided to study the effect of mtDNA haplotype on the susceptibility to volume overload-induced cardiomyocyte dysfunction. To accomplish this, volume overload was induced in two strains of mice with different mtDNA haplotypes. Therefore, the effects of mtDNA haplotype on acute volume overload-induced cytoskeletal disorganization and mitochondrial bioenergetics are a major focus of this dissertation.

SUMMARY

The mitochondrion is a key player in redox signaling, the regulation of apoptosis, and the bioenergetic function of the cell, and as such has been a major subject of research for many years. The majority of this research has been done using mitochondria isolated from the tissue of interest, which removes them from their cellular environment, com-

plete with endogenous substrates and signaling, and makes it extremely difficult to mimic pathological conditions. The research discussed in this dissertation utilizes recent advances in technology which allow for the measurement of mitochondrial bioenergetics within their cellular environment, yielding new insights into how mitochondria function both in response to endogenous substrates and signaling and also in response to various pathological conditions.

This dissertation examines the bioenergetic response to three different pathological conditions which are all mediated by the common etiology of alterations in mitochondrial function. We hypothesized that ALD, hypoxia/reoxygenation, and volume overload all induce changes in cellular bioenergetics in the tissue of interest, leaving the tissue more susceptible to damage and dysfunction in response to a secondary stress. The effects of ALD, along with the associated confounding factors of hypoxia and increased NO production, on hepatocellular bioenergetics are discussed in Chapter 2. Chapter 3 then examines the effects of hypoxia and reoxygenation on mitochondrial bioenergetic function within the endothelium. Following this, the role of volume overload on the alteration of cardiomyocyte bioenergetics and the potential mediators of mtDNA haplotype and cytoskeletal disruption are investigated in Chapter 4. Finally, a discussion of the role of disease in the alterations of mitochondrial function in intact tissue and the potential future directions of these projects are included in Chapter 5.

CHAPTER 2

EFFECT OF CHRONIC ALCOHOL CONSUMPTION ON HEPATIC MITOCHONDRIAL FUNCTION IN RESPONSE TO HYPOXIA: ROLE OF NITRIC OXIDE

INTRODUCTION

Role of Nitric Oxide in Alcohol-Induced Hepatotoxicity

It has recently been recognized that NO is capable of regulating several aspects of mitochondrial function, including respiration and mitochondrial biogenesis [154, 189-192, 194, 201, 229-234]. These new insights are also leading to a deeper understanding of the cross talk between NO signaling pathways and major regulatory and metabolic pathways in the cell. Among these are the findings that mitochondrial biogenesis can be regulated by the soluble guanylate cyclase pathway and that NO can modulate the response to hypoxia, depending on its concentration, through both mitochondrial-dependent and independent pathways [234-236].

A role for the NO -CcOX pathway in regulating O_2 gradients has been proposed based upon both theoretical modeling and the observation that NO is a more effective inhibitor of the most actively respiring mitochondria [237]. This suggests that under normal conditions the binding of NO to CcOX limits O_2 consumption in the most actively respiring tissues, and so extends O_2 gradients in organs such as the heart or liver [238, 239]. However, under conditions associated with inflammation, increased ROS will decrease the available NO to modify CcOX and will stress mitochondrial function through

the oxidation, nitration, and inactivation of mitochondrial proteins. We have recently shown that amelioration of mitochondrial oxidant stress with a mitochondrial antioxidant, probably through the scavenging of peroxynitrite, can inhibit HIF-1 α activation in response to chronic EtOH consumption [240]. Moreover, in response to hypoxic stress associated with EtOH-dependent hepatotoxicity, evidence suggests that mitochondria become more sensitive to inhibition by \cdot NO. This will further contribute to tissue hypoxia and oxidative stress through increasing production of superoxide within the respiratory chain [241, 242].

Chronic Alcohol Consumption Causes Mitochondrial Dysfunction

Previous studies have shown that chronic EtOH consumption causes marked bioenergetic defects in both perivenous and periportal hepatocytes (**Figure 2-1**). Upon exposure to hypoxic conditions, which occurs in EtOH-induced hepatotoxicity, these defects become more pronounced, and is associated with decreased aerobic and anaerobic ATP production [161, 187, 188]. These findings support the concept that the mitochondrial bioenergetic reserve has been depleted. Recently we have shown that cellular bioenergetic reserve capacity is required to protect cells against oxidative stress and is diminished by exposure to \cdot NO [180]. We hypothesized that alterations in the bioenergetic reserve capacity of the hepatocytes in response to chronic EtOH consumption plays a major role in determining their susceptibility to hypoxia. This is important since inducible nitric oxide synthase (iNOS) is known to be induced in response to EtOH consumption, and mitochondria isolated from EtOH-treated animals are more susceptible to \cdot NO-dependent inhibition of respiration [242, 243]. Given that induction of iNOS is also as-

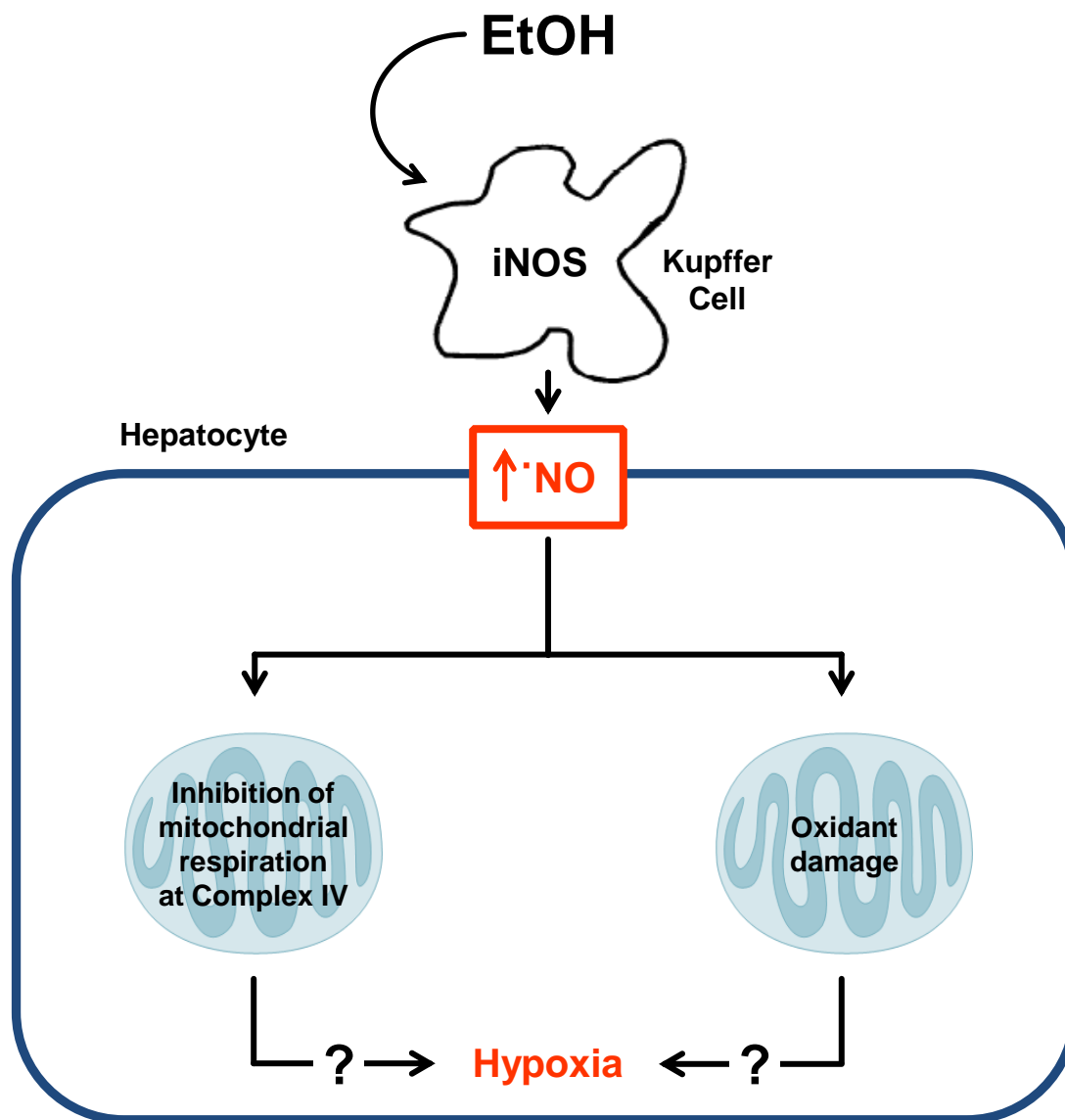


Figure 2-1. Chronic alcohol consumption induces mitochondrial dysfunction mediated by nitric oxide and hypoxia. The development of ALD is mediated by the induction of iNOS. This leads to increased levels of $\cdot\text{NO}$, resulting in oxidative and nitrative stress and the inhibition of mitochondrial function. The increased production of $\cdot\text{NO}$ also causes hypoxia in the liver, leading to further inhibition of mitochondrial function and oxidative/nitrative stress. Together these factors cause the loss of hepatocyte bioenergetics and function, leading to the progression of ALD.

sociated with protein nitration, we reasoned that $\cdot\text{NO}$ would exacerbate the effects of hypoxia on hepatocytes from EtOH-exposed animals.

In support of this concept, using a model of chronic EtOH feeding in mice, we and others have shown that EtOH-dependent hepatotoxicity is suppressed in $\text{iNOS}^{-/-}$ animals [36, 243]. These data support the proposed link between increased $\cdot\text{NO}$ formation from iNOS during chronic EtOH intoxication, enhanced sensitivity of mitochondrial respiration to $\cdot\text{NO}$, and hypoxia. The control of inter and intracellular O_2 gradients is essential for the normal functioning of cells within a complex organ such as the liver. The adaptive response to hypoxia is orchestrated through hypoxia-inducible factor 1 (HIF-1) which is a heterodimer composed of alpha and beta subunits [244]. At normal O_2 tension the enzyme prolyl hydroxylase (PHD), which requires O_2 as a cosubstrate, catalyzes the hydroxylation of critical proline residues in HIF-1 α , and this ultimately targets the protein to the proteasome for degradation [245]. Where, the O_2 tension is low, decreased hydroxylation of proline residues in the HIF-1 α subunit stabilizes the protein and enables it to translocate to the nucleus, where it causes enhanced transcription of various genes, which protect the cell against hypoxia (**Figure 2-2**). Several genes have been identified which contain a hypoxia responsive element (HRE) within their promoter including those involved in iron metabolism and iNOS [197, 246]. A number of studies have been directed towards understanding the effects of $\cdot\text{NO}$ on hypoxia. However, the response of HIF-1 α to iNOS induction in an *in vivo* model of EtOH-dependent hepatotoxicity and the impact of $\cdot\text{NO}$ on reserve capacity has not been examined. These concepts were tested in a model of chronic EtOH induced hepatotoxicity using primary hepatocytes isolated from Sprague-Dawley rats and liver sections from C57BL/6 and $\text{iNOS}^{-/-}$ mice [36, 243].

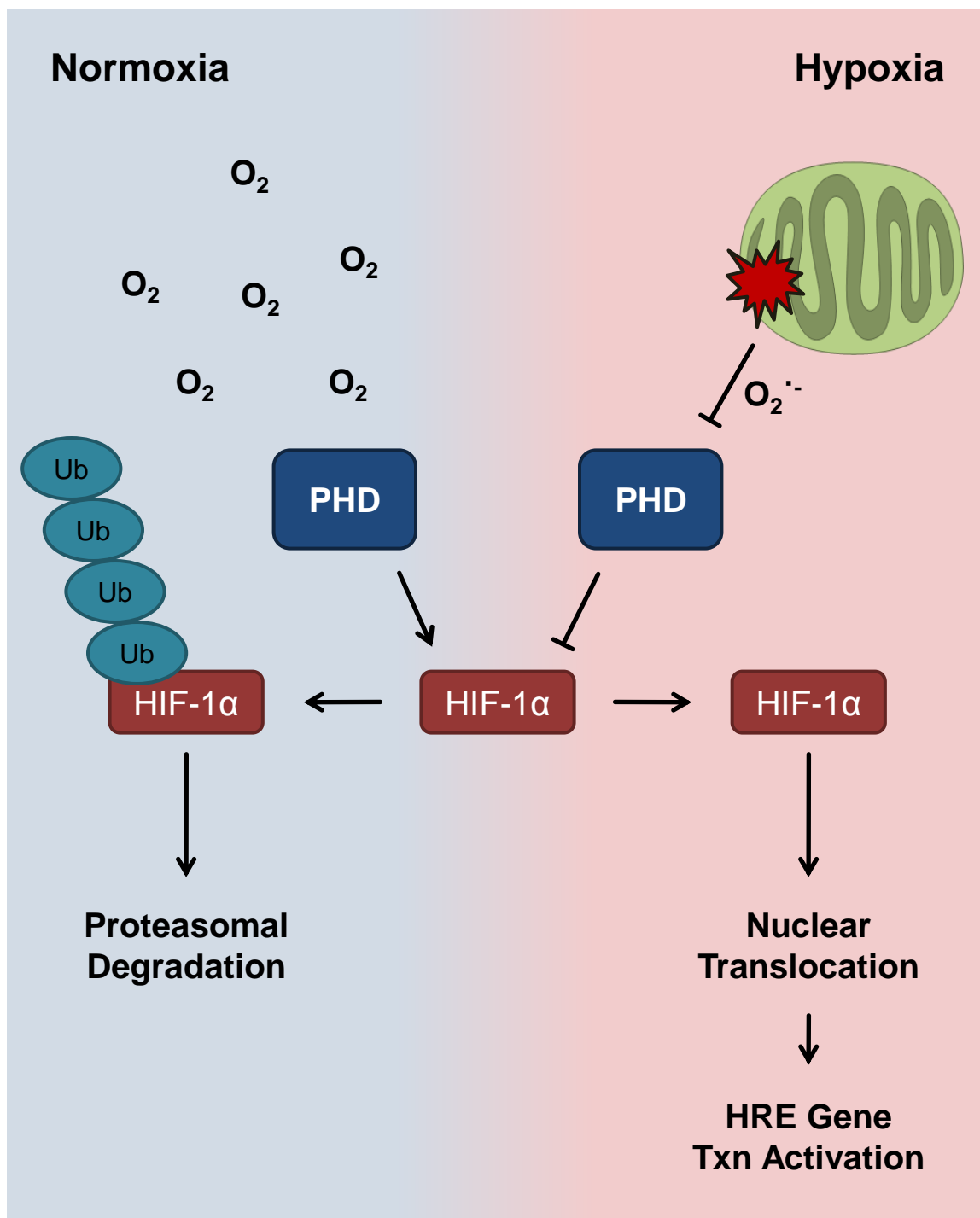


Figure 2-2. Hypoxia inducible factor-1 α signaling pathway is activated in hypoxia. Under normoxic conditions, prolyl hydroxylase domains (PHD) are active and can hydroxylate critical proline residues on HIF-1 α , targeting it for ubiquitination and proteasomal degradation. In hypoxic conditions, PHD activity is inhibited by the lack of O_2 as a substrate and mitochondrial ROS, resulting in HIF-1 α stabilization. This leads to HIF-1 α translocation to the nucleus where it acts as a transcription factor by activating the transcription of hypoxia response element (HRE) genes.

MATERIALS AND METHODS

Materials

All chemicals were purchased from Sigma-Aldrich (St.-Louis, MO) unless stated otherwise and were of the highest grade available.

Alcohol Feeding

Male Sprague-Dawley rats or wild type (C57BL/6) and *iNOS*^{-/-} (B6.129P2-NOS2^{tm/lau}) mice were fed according to the Lieber-DeCarli liquid diet protocol for 5-6 weeks as described previously [243, 247] (**Figure 2-3**). EtOH consumption was uniform throughout the study period and there was no difference in EtOH consumption between wild type and *iNOS*^{-/-} mice or rats with and without EtOH consumption (data not shown). All animals were handled in accordance to the recommendations in “The Guide for the Care and Use of Laboratory Animals” approved by the Institutional Animal Care and Use Committee at the University of Alabama at Birmingham.

Hepatocyte Preparations

Rat primary hepatocytes were isolated as previously described by the digitonin-collagenase procedure [187, 248]. Rats were anesthetized with xylazine:ketamine (10:100 mg/kg, i.m.). The liver was cannulated via the portal vein and superior vena cava and was flushed with GBS, followed by perfusion with 7 mM digitonin and then 250 mL of 0.5 mg/mL collagenase to isolate the hepatocytes. The cells were resuspended in DMEM supplemented with 20 mM HEPES and 10 mM sodium bicarbonate at a cell den-

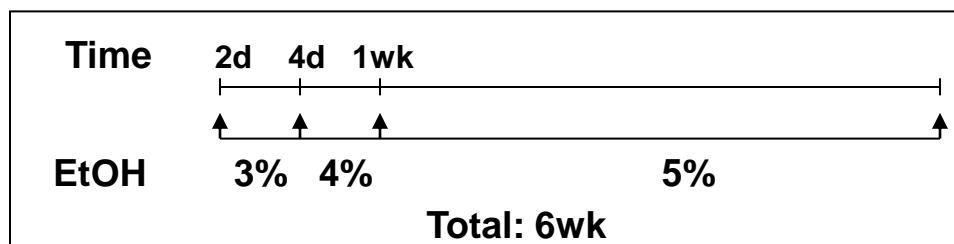
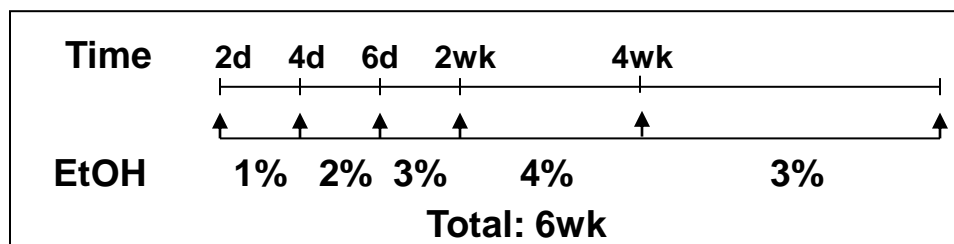
A**Rats****B****Mice**

Figure 2-3. Alcohol feeding schedule for rats and mice. (A) Twelve rats were divided into two groups (control and EtOH) and were pair fed either the control or EtOH diet, with progressive increase in EtOH content at the time points shown. (B) C57BL/6 and *iNOS*^{-/-} mice were divided into control and EtOH groups (n=4 per group) and were pair-fed control or EtOH diets for 6 weeks. The EtOH content in the liquid diet for the EtOH groups was progressively increased at the time points shown. After 4 wk, the EtOH content was lowered from 4% to 3% because the mice were not eating enough of the food and were losing weight.

sity of approximately 1.5×10^7 cells/mL. The viability of the isolated hepatocytes was assessed, and was typically $93 \pm 1\%$ from both control and EtOH-fed rats.

Mitochondrial Enzyme Activity Assays

Citrate synthase and CcOX were measured in primary hepatocytes isolated from both control and EtOH-fed rats and lysed in PBS containing 0.2% lauryl maltoside, as previously described [242, 249, 250]. Briefly, CcOX activity was measured by using a spectrophotometer to monitor the oxidation of cytochrome *c* over time by the hepatocyte lysates at 550 nm [249]. Citrate synthase activity was measured by monitoring the conversion of oxaloacetate and acetyl-CoA into citrate and CoA. CoA formation was detected by adding DTNB (5,5'-dithiobis-(2-nitrobenzoic acid)), which is converted to TNB (2-nitro-5-thiobezoic acid) by CoA and can be measured spectrophotometrically at 412 nm.

Immunoblot Analysis

For cytochrome P-450 2E1 (CYP2E1) detection, whole liver homogenates were separated by SDS/PAGE and immunoblotted against CYP2E1 using an anti-CYP2E1 antibody (AB 1252; Millipore, Billerica, MA) and β -actin using an anti- β -actin antibody (4970; Cell Signaling, Beverly, MA) followed by HRP-conjugated donkey anti-rabbit secondary antibody (NA934V; GE Healthcare Amersham, Piscataway, NJ). Mitochondrial proteins were immunoblotted for CcOX subunit IV (CcOX-IV) using anti-CcOX-IV antibody (A21348; Invitrogen, Carlsbad, CA) and voltage-dependent anion channel (VDAC/porin) using an anti-porin antibody (459500; Invitrogen), followed by an HRP-

conjugated sheep anti-mouse secondary antibody (NA931V; GE Healthcare Amersham). The intensities of protein bands were quantified using AlphaEaseFC software (Alpha Innotech, Santa Clara, CA). Images were selected for analysis prior to saturation of the signal.

Mitochondrial Bioenergetics

To determine the effects of EtOH consumption on hepatocyte bioenergetics, the XF24 analyzer (Seahorse Bioscience, Billerica, MA) was used to measure O₂ consumption in intact, primary hepatocytes [177, 178, 251]. The XF24 analyzer works by using a disposable cartridge (FluxPak, Seahorse Bioscience) with fluorescent probes on the end which is lowered onto V7 plate (Seahorse Bioscience) to make a temporary microchamber (**Figure 2-4A**). This allows for the measurement of O₂ consumption by the cells, which is used to calculate the oxygen consumption rate (OCR) (**Figure 2-4B**). Importantly, the cartridge is then raised back up allowing the system to return to baseline, which prevents the cells from becoming hypoxic or anoxic and thus allowing for repeated measurements over long periods of time and in response to various treatments.

Primary hepatocytes were attached to V7 plates coated with collagen. The cells were allowed to adhere overnight, after which time the culture media was changed to unbuffered DMEM (pH 7.4) supplemented with 5.5 mM D-glucose, 1 mM sodium pyruvate, and 4 mM L-glutamine (Invitrogen) for the XF24 assays.

Parameters of mitochondrial function were measured utilizing the ability of the XF24 to inject four different compounds into the wells during an assay as described previously [179, 180, 250, 252] (**Figure 2-5**). Briefly, the basal O₂ consumption of the he-

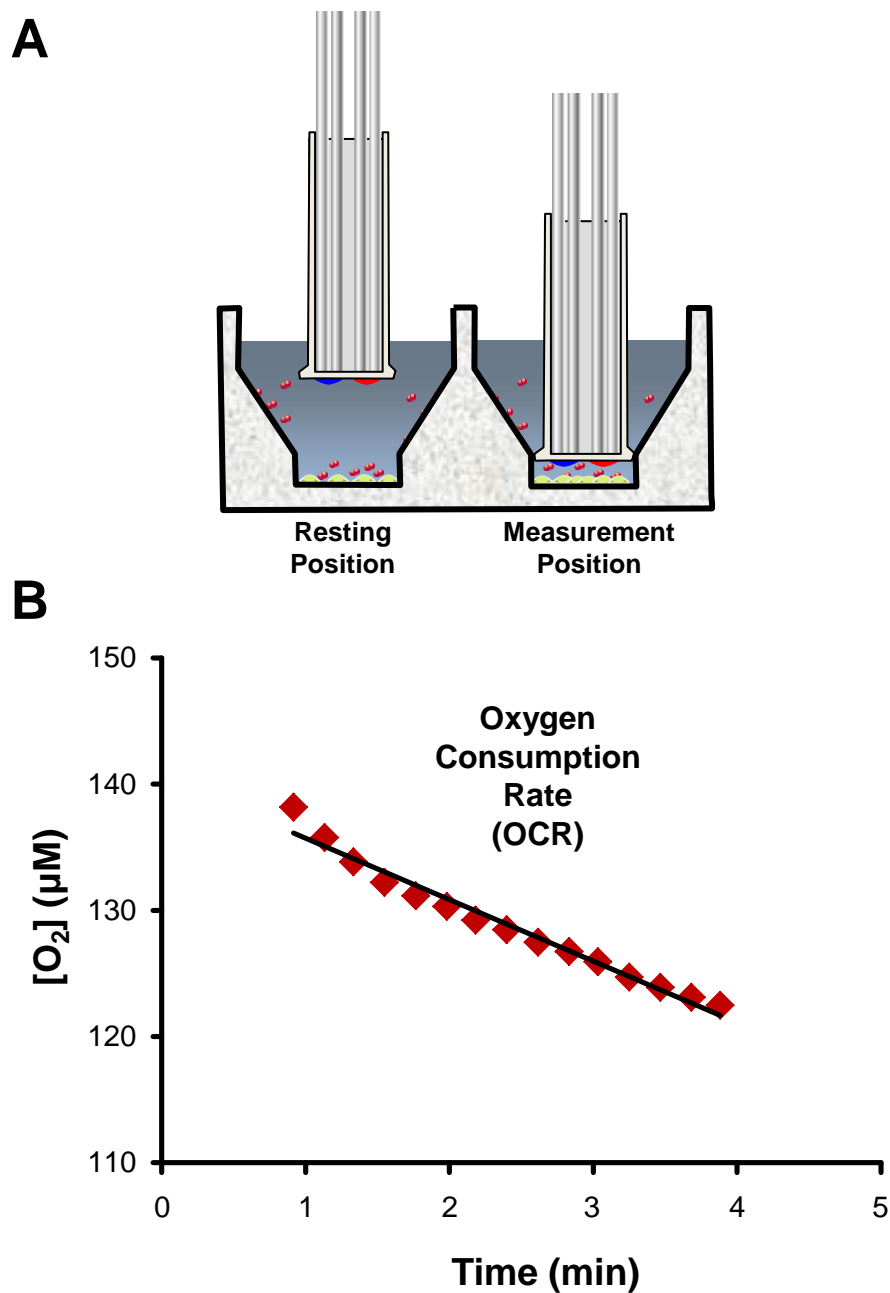


Figure 2-4. XF24 analyzer technology. The XF24 analyzer (Seahorse Bioscience) utilizes 24 probe heads to analyze cells in culture. Panel A shows a schematic depiction of the measurement chamber utilized in this technique. The first well shows the optics in the resting position. For measurements, the cartridge is lowered in all wells to create a transient 7 μL chamber. The red dot at the tips of the sensor probes is representative of the fluorescent sensor quenched by oxygen to allow for measurement of this parameter. Monitoring these concentrations over time allows for the calculation of the oxygen consumption rate (OCR) (B).

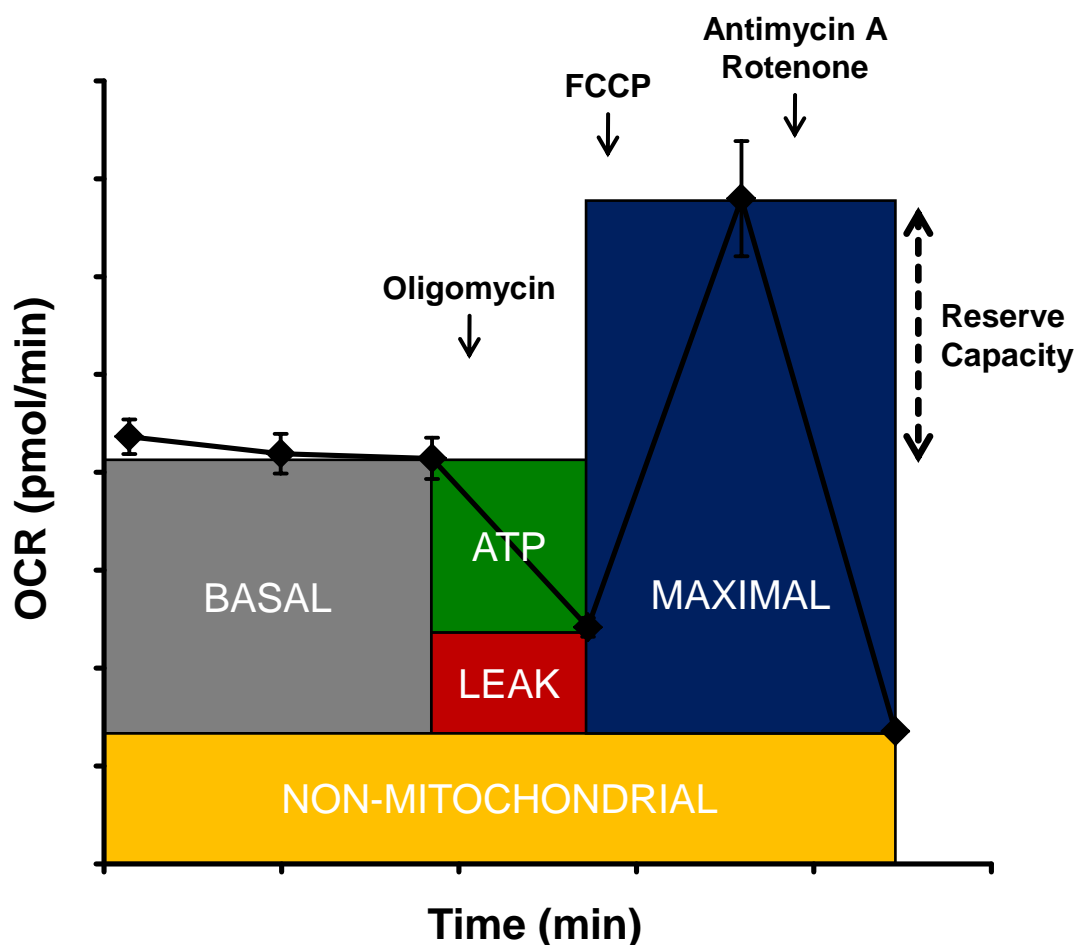


Figure 2-5. Measurement of bioenergetic parameters of isolated primary hepatocytes using an XF24 analyzer. After three basal OCR measurements, oligomycin (1 $\mu\text{g/mL}$), FCCP (0.3 μM) and antimycin A (10 μM) plus rotenone (1 μM) were injected sequentially with OCR measurements recorded after each injection. ATP-linked oxygen consumption (ATP) and the OCR due to proton leak (LEAK) can be calculated using the basal and the oligomycin-insensitive rate. FCCP, a proton ionophore, is then used to determine the maximal respiratory capacity. Lastly, injection of antimycin A plus rotenone allows for the measurement of non-mitochondrial oxygen consumption. The reserve capacity is calculated by subtracting the maximal from the basal OCR.

patocytes was determined by measuring the oxygen consumption rate (OCR) of the cells over time prior to any treatment. The cells were then treated with oligomycin (1 $\mu\text{g}/\text{mL}$), resulting in a decrease in OCR which is attributed to ATP-linked respiration. The remaining mitochondrial O_2 consumption following oligomycin treatment is ascribed to proton leak. Next, carbonyl cyanide-p-trifluoromethoxyphenylhydrazone (FCCP, 0.3 μM) was injected to stimulate the maximal OCR of the cells. The maximal OCR also allows for the calculation of the reserve capacity, which is the difference between the maximal and basal OCR and represents the cells reserve mitochondrial function that is available to be utilized during an increased work load or stress [179, 180]. Finally, antimycin A (10 μM) and rotenone (1 μM) were injected simultaneously to completely inhibit the mitochondrial electron transport chain, thus yielding the non-mitochondrial OCR of the hepatocytes.

The concentrations of the compounds used in these experiments were determined by titrating the amount to yield their optimal effects (data not shown). The OCR was expressed as pmoles of O_2 consumed per minute (pmol/min), as pmol/min normalized to total protein in each well using the DC Protein Assay (BioRad, Hercules, CA), or as the percent change from the baseline reading in each well, which was the last OCR measurement prior to the first injection.

Hypoxia Exposure

To measure the effect of changing O_2 tension on primary hepatocytes, an XF24 analyzer (Seahorse Bioscience) was placed in a sealed glove box (Plas-Labs, Lansing, MI) which was equilibrated to 1% O_2 (11.5 μM O_2) via repeated cycles of vacuuming out

the air in the chamber and replacing it with argon (**Figure 2-6A**). Primary hepatocytes were seeded in V7 culture plates and were changed into unbuffered DMEM equilibrated to room air 1 hr prior to starting the XF assay (as described above). The OCR of the hepatocytes was then measured over time as the O₂ tension of the media decreased as it equilibrated to the 1% O₂ atmosphere in the glove box (**Figure 2-6B**).

Immunohistochemistry

To detect tissue hypoxia, pimonidazole was injected via tail vein (i.v.) after 5 weeks of EtOH consumption. Briefly, restrained mice were administered pimonidazole (120 mg/kg) in saline (1 ml/kg) and after 60 min were anesthetized with ketamine:xylazine (60:10 mg/kg i.p). Brief anesthesia immediately prior to sacrifice does not significantly affect pimonidazole adduct accumulation in liver [253]. Blood and unbound pimonidazole were cleared from the circulation by perfusing oxygenated buffer into the heart with a 22-gauge needle. Livers were harvested and a portion of the tissue was fixed in 10% buffered formalin for immunofluorescence studies. Paraffin blocks containing liver tissue were then sectioned at 5 μm thickness. Sections were deparaffinized with xylene and rehydrated by washing with a graded series of EtOH concentrations. Hydrated sections were briefly treated with 0.01% protease (pronase E), and blocked for 5 min with serum-free protein block at room temperature. Sections were then incubated with hydroxyprobe-1 (mouse anti-pimonidazole, 1:50 dilution) for 40 min at room temperature. Sections were then blocked again for 10 min with 5% BSA in PBS. The sections were then washed with PBS, and then incubated with for 1 hr with the secondary antibody. The secondary antibody was AlexaFluor® 350 conjugated goat anti-mouse (Invitrogen).

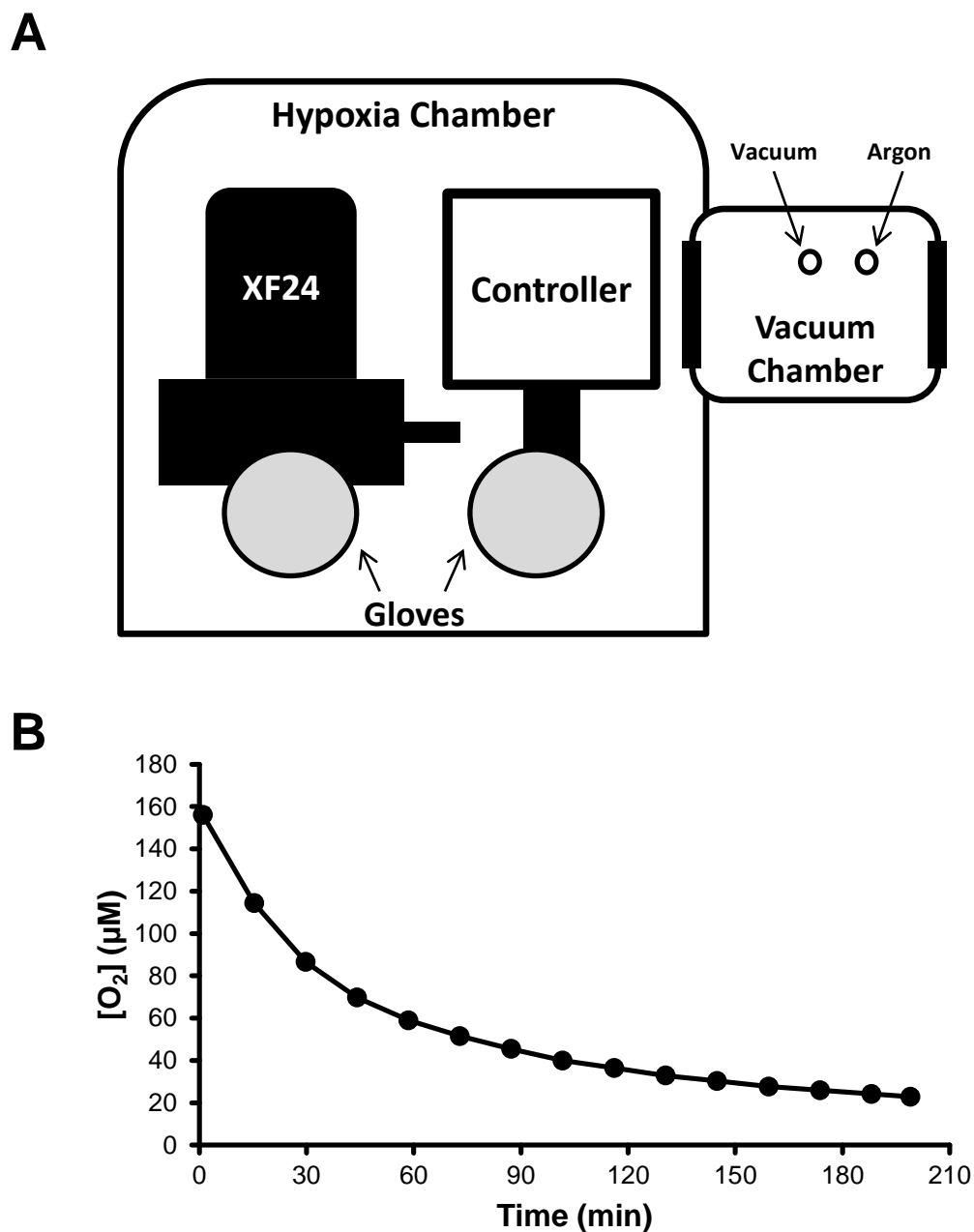


Figure 2-6. Measuring mitochondrial function in hypoxia. (A) A XF24 analyzer was placed in a sealed glove box. The atmosphere in the glove box was then lowered to 1% O₂ by alternating flushing with argon gas and then vacuuming the air out of the chamber. The 1% O₂ was maintained for the length of all experiments with hypoxia as a condition. For all experiments performed in hypoxia, a control experiment was run simultaneously in an additional XF24 analyzer in room air. (B) Changes in O₂ concentration in room air-equilibrated media above attached hepatocytes over time following exposure to 1% atmospheric O₂.

Sections were washed several times with PBS prior to counterstaining the nuclei with Oregon Green® 488 conjugated goat anti-rabbit antibody (Invitrogen) for 10 min. Sections were washed again in PBS and images analyzed using a Leica fluorescent microscope with IPLAB Spectrum (Scanalytics, Rockville, MD). The intensity of fluorescence was quantified by using SIMPLEPCI software (Compix, Irvine, CA).

HIF-1 α levels were assessed using formalin fixed, paraffin embedded sections, which were deparaffinized through a graded series of EtOH. Antigen unmasking was performed by incubating the sections with 0.1 M sodium citrate (pH 6.0). All sections were rinsed with TBS (0.1 M, pH 7.2), incubated for 1 hr with 10% goat serum, followed by overnight incubation at 4°C in a humidified chamber with anti-HIF-1 α (NB 100-105) antibody (Novus Biologicals, Littleton, CO) at a dilution of 1:50. Sections were then blocked again and developed with secondary antibody as described above.

Statistics

All experiments were performed 3-6 times, and data are presented as mean \pm SEM. The experiment was performed with six pair-fed controls and EtOH-containing diets for rats or wild type and iNOS^{-/-} mice. Statistical significance was determined using student's *T*-test, with $p < 0.05$ taken as significantly different.

RESULTS

Hepatocyte Density for Measurement of Mitochondrial Bioenergetics

Primary hepatocytes were attached to V7 culture plates coated with collagen. The cell seeding density was optimized for both control (**Figure 2-7A**) and EtOH hepatocytes

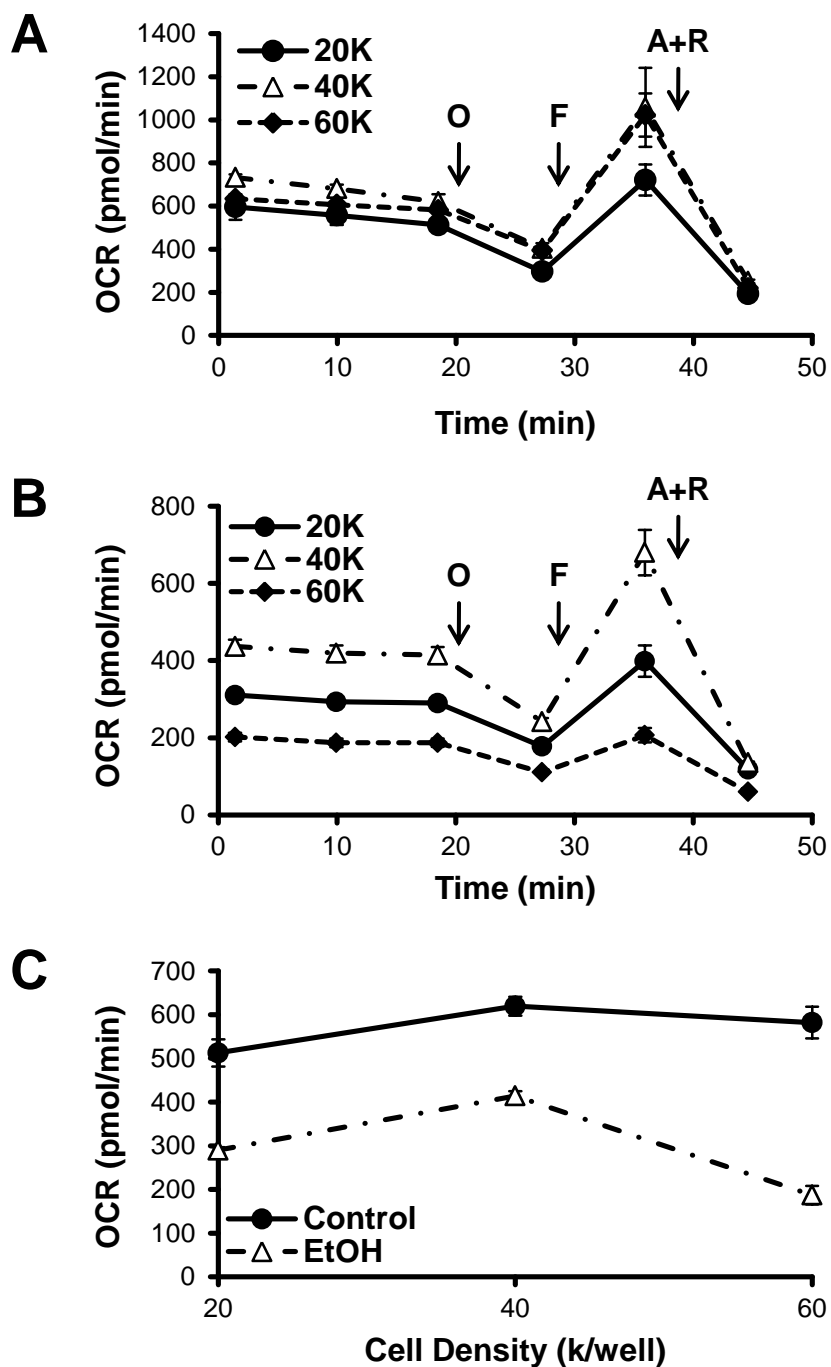


Figure 2-7. Cell density-dependent changes in hepatocyte respiration following chronic alcohol consumption. (A) The OCR of primary hepatocytes isolated from control rats was measured at varying seeding densities (20,000, 40,000, or 60,000 cells/well) followed by sequential injections of oligomycin (O), FCCP (F), and antimycin A plus rotenone (A+R). (B) Effect of different seeding densities (20,000, 40,000, or 60,000 cells/well) of hepatocytes from EtOH-fed rats on mitochondrial function as examined in panel A. (C) Basal OCR of control and EtOH-fed rats as a function of cell densities. Results are mean \pm SEM. $n=5$ for each group.

(**Figure 2-7B**). The density chosen was 20,000 cells/well for the control hepatocytes and 40,000 cells/well chosen for EtOH hepatocytes because they expressed the most similar basal OCR values (**Figure 2-7C**) and total protein within each well (data not shown).

Alcohol Induces Characteristics of Liver Toxicity in Hepatocytes

The activity and levels of key mitochondrial enzymes were determined from primary hepatocytes isolated from control and EtOH-fed rats. As reported previously, EtOH consumption causes a decrease in CcOX activity and protein subunits whereas the levels of citrate synthase activity are unchanged (**Figure 2-8**). Protein levels of the outer mitochondrial membrane protein VDAC was not modified by EtOH consumption (**Figure 2-8C,D**). It has been well established that the induction of CYP2E1 occurs in response to chronic EtOH consumption, and was found to be elevated in hepatocytes isolated from the EtOH-fed group (**Figure 2-8C,D**).

Hepatocytes Exhibit Bioenergetic Defect in Response to Alcohol Exposure

In order to determine if chronic EtOH consumption causes alterations in hepatocyte cellular bioenergetics, mitochondrial function was measured using the XF24 analyzer (**Figure 2-9**). Chronic EtOH consumption had no effect on basal OCR, ATP-linked OCR or proton leak of the hepatocytes (**Figure 2-10A,B**). The proton ionophore FCCP (0.3 μM) was then injected to stimulate the maximal OCR of the cells. Interestingly, the hepatocytes isolated from EtOH-fed rats exhibited a significantly diminished maximal OCR, (**Figure 2-10C**). The amount of mitochondrial function available for the hepatocytes to use under conditions of increased energy demand and/or stress is termed the cel-

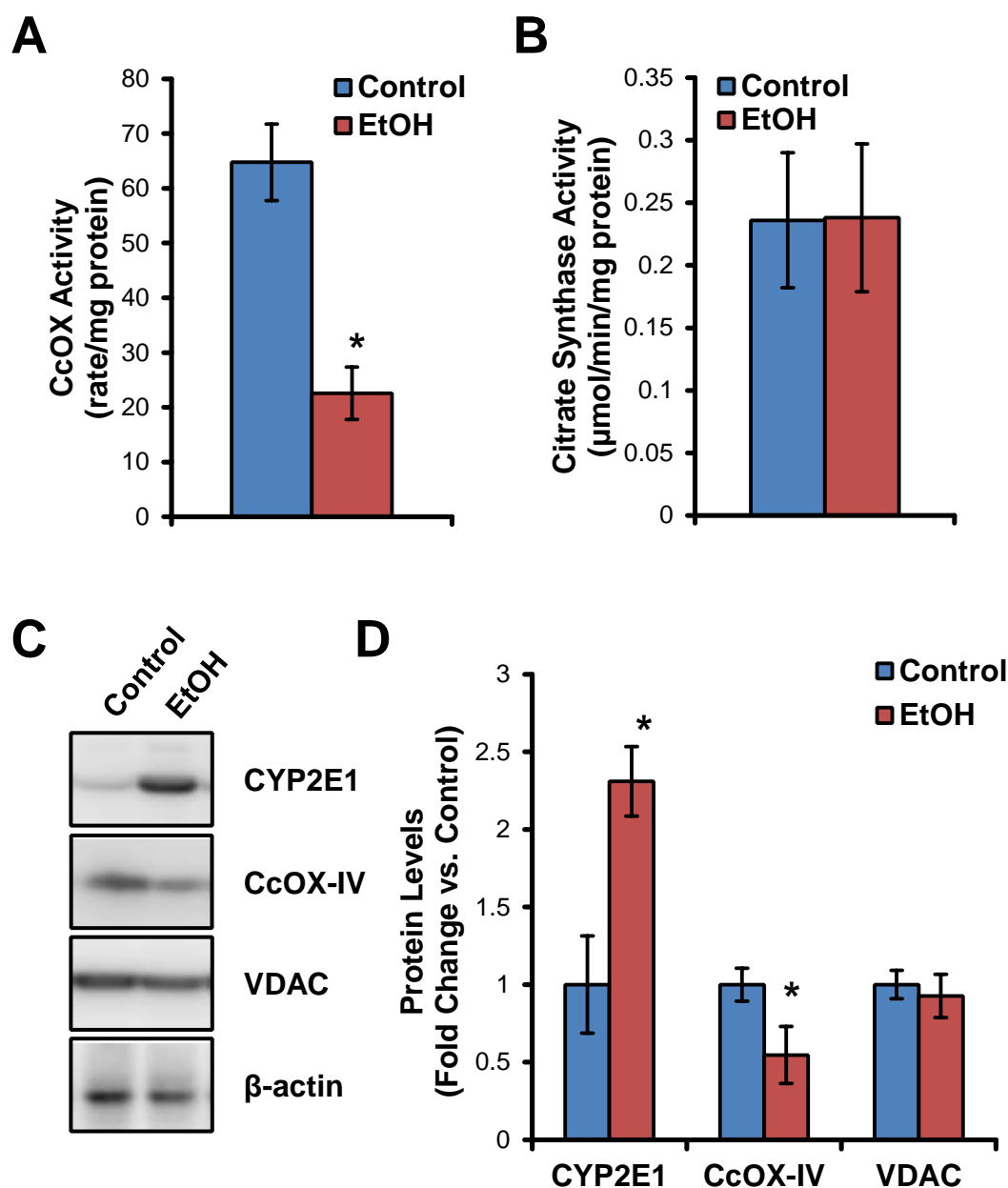


Figure 2-8. Effect of alcohol consumption on mitochondrial protein levels and activity. (A) Cytochrome *c* oxidase (CcOX) activity in isolated hepatocytes from control and EtOH-fed rats. (B) Citrate synthase activity in isolated hepatocytes from control and EtOH-fed rats. (C) Protein levels of CYP2E1, cytochrome *c* oxidase subunit IV (CcOX-IV), VDAC, and β -actin from primary hepatocytes isolated from control and EtOH-fed rats, along with the quantification of the densitometry for the different proteins normalized to total protein and expressed as the fold change vs. control (D). Data are mean \pm SEM. $n \geq 6$ for each group. * $p \leq 0.05$ compared to control. Data obtained by M.S. Johnson.

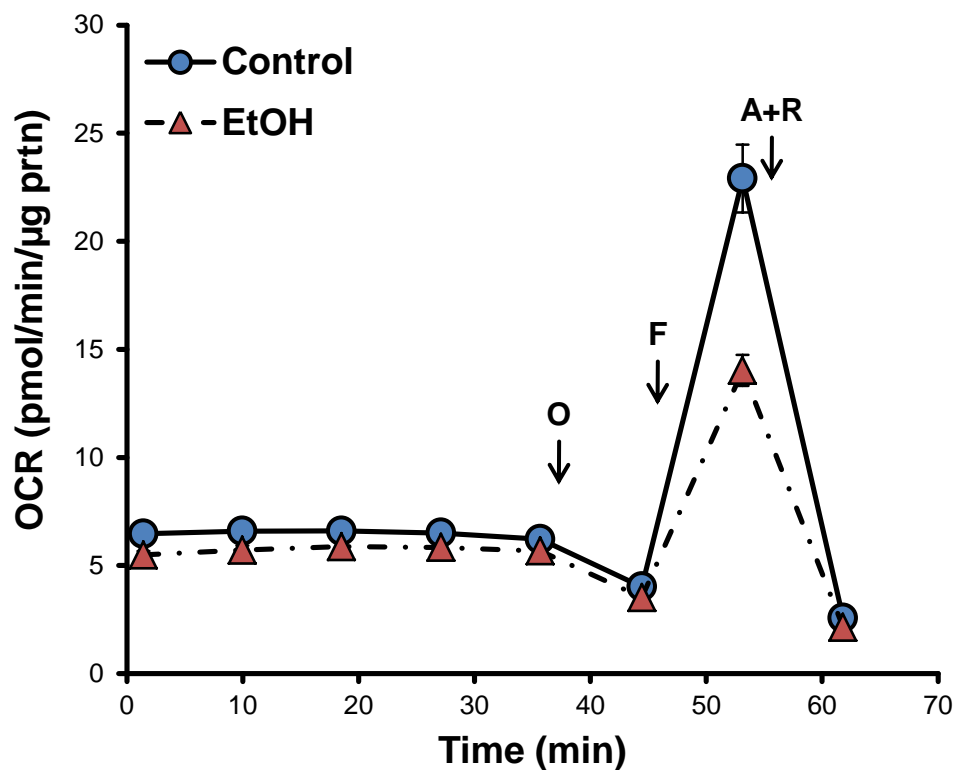


Figure 2-9. Alcohol consumption diminishes mitochondrial function.

Primary hepatocytes were isolated from rats fed control and EtOH containing diets for 6 wk, seeded at 40 000 cells/well and allowed to attach overnight prior to OCR measurements. OCR traces from control and EtOH hepatocytes with serial injections of oligomycin (O), FCCP (F), and antimycin A plus rotenone (A+R) to determine parameters of mitochondrial function. Results are mean \pm SEM. n=5 per group.

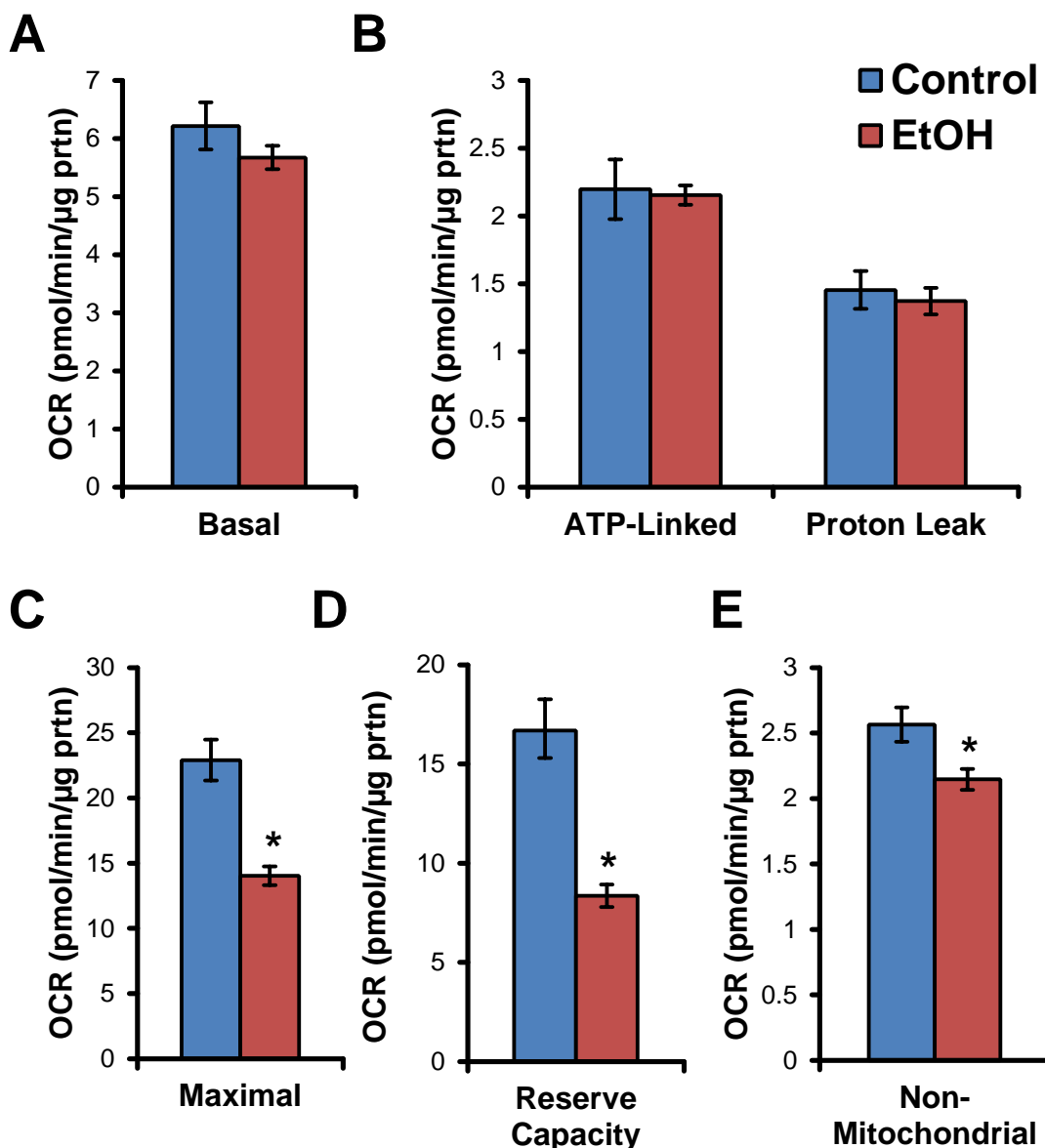


Figure 2-10. Chronic alcohol consumption alters mitochondrial function in primary hepatocytes. Parameters of mitochondrial function were calculated from the OCR traces in Figure 2-9. (A) Basal OCR of hepatocytes measured prior to any injection. (B) ATP-linked respiration was calculated from the decrease in OCR following oligomycin injection, with the remainder being attributed to proton leak. (C) Maximal OCR was measured following FCCP injection. (D) The reserve capacity was calculated from the difference between the maximal and basal OCR. (E) The non-mitochondrial OCR of the hepatocytes was determined by injecting antimycin A and rotenone simultaneously to fully inhibit the mitochondrial electron transport chain. Results are mean \pm SEM. $n=5$ per group. * $p<0.05$ compared to control.

lular bioenergetic reserve capacity [179, 180]. The hepatocytes isolated from EtOH-fed animals exhibited a 50% decrease in their available reserve capacity as compared to the control hepatocytes (**Figure 2-10D**). Hepatocytes were then exposed to antimycin A (10 μ M) and rotenone (1 μ M) to fully inhibit the mitochondrial electron transport chain. This caused a large decrease in the OCR of the hepatocytes, with all remaining O₂ consumption attributed to non-mitochondrial sources. The hepatocytes isolated from EtOH-fed rats displayed a small but significant decrease in non-mitochondrial OCR (**Figure 2-10E**).

Chronic Alcohol Increases Hepatocyte Sensitivity to Nitric Oxide

The effect of $\dot{\text{N}}\text{O}$ on the mitochondrial function of primary hepatocytes isolated from control and EtOH-fed rats was assessed using the $\dot{\text{N}}\text{O}$ donor DetaNONOate (DetaNO), which releases $\dot{\text{N}}\text{O}$ at a low rate similar to that reported for iNOS [254]. As shown in **Figure 2-11**, control and EtOH-exposed hepatocytes were exposed to 500 μ M DetaNO for 4 hr while monitoring the OCR, followed by the evaluation of mitochondrial function. As shown in **Figure 2-10**, EtOH consumption did not change basal OCR and conversely decreased the maximal respiration. However, hepatocytes from EtOH-fed rats treated with DetaNO exhibited a progressive decrease in the basal OCR after approximately 2 hr exposure to the $\dot{\text{N}}\text{O}$ donor, resulting in a 40% inhibition after 4 hr (**Figure 2-12A**). Following oligomycin injection, the EtOH-exposed hepatocytes treated with DetaNO also showed a significant decrease in their ATP-linked OCR and proton leak (**Figure 2-12B**), while EtOH consumption alone had no effect.

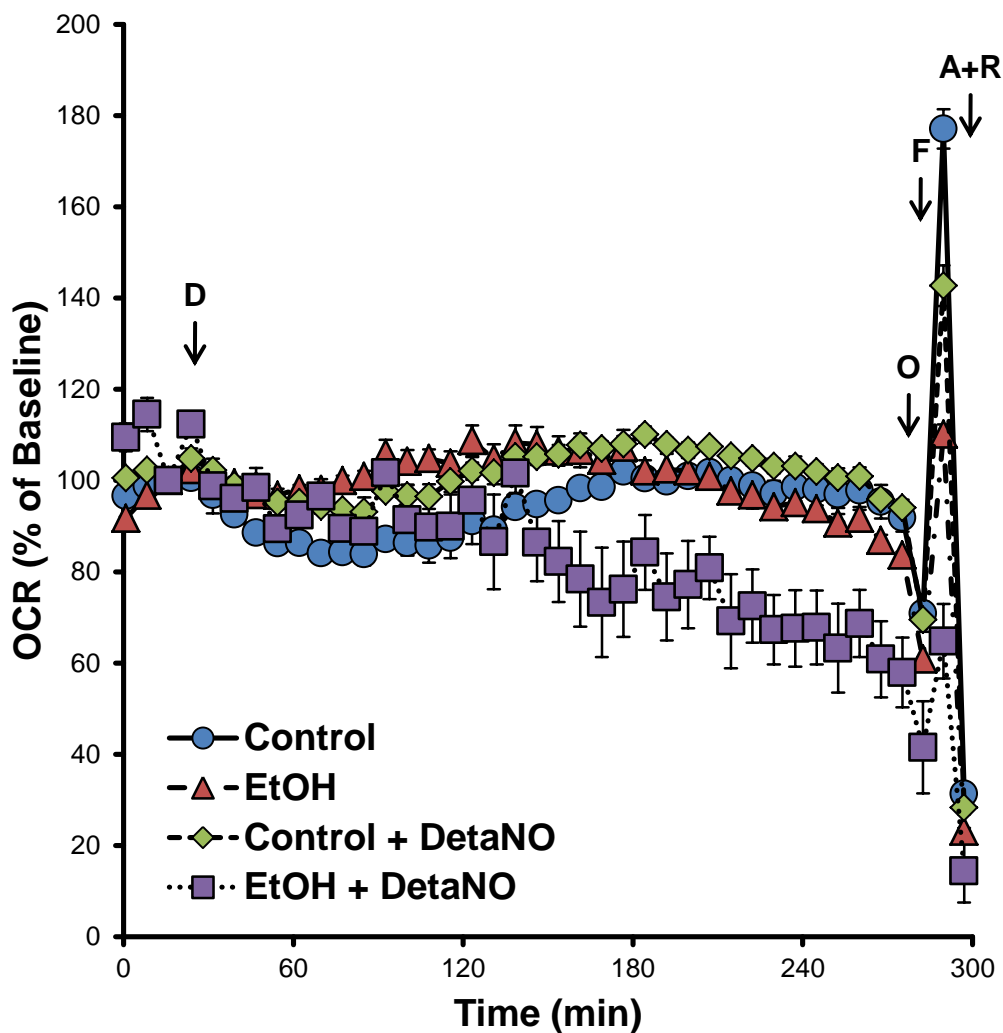


Figure 2-11. Alcohol sensitizes hepatocytes to nitric oxide-induced inhibition of mitochondrial function. The effect of nitric oxide on hepatocytes isolated from control and EtOH-fed rats was determined by treating with DetaNO (D, 500 μ M) for 4 hr followed by serial injections of oligomycin (O), FCCP (F), and antimycin A plus rotenone (A+R) to measure parameters of mitochondrial function. Results are mean \pm SEM. $n=5$ per group.

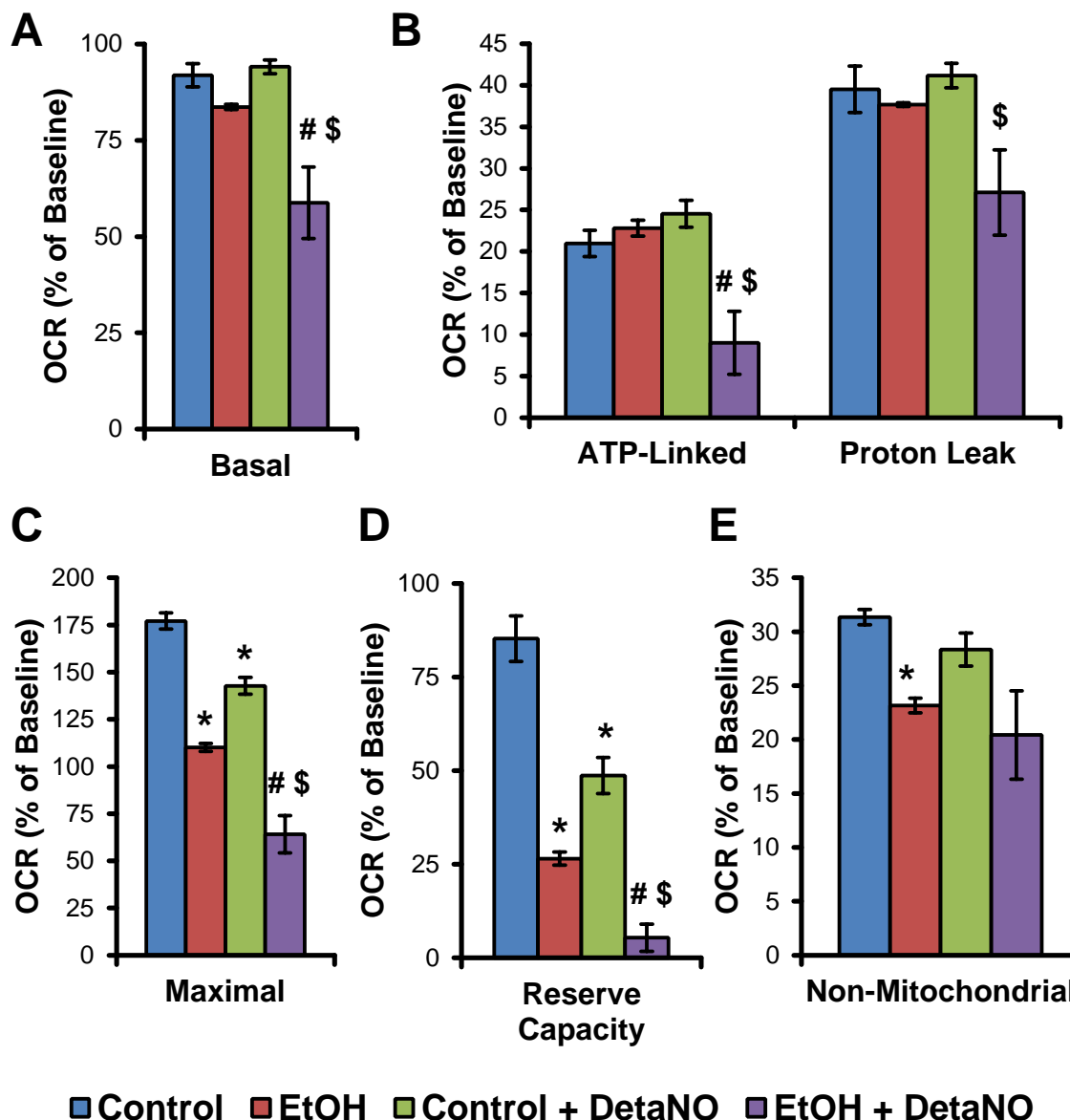


Figure 2-12. Chronic alcohol consumption sensitizes hepatocytes to nitric oxide-induced mitochondrial dysfunction. Parameters of mitochondrial oxygen consumption were calculated from the OCR traces shown in Figure 2-11. (A) Basal OCR of hepatocytes is measured prior to oligomycin injection. (B) ATP-linked respiration is equal to the oligomycin-induced decrease in OCR., with the remaining OCR following oligomycin injection is due to proton leak. (C) Maximal OCR was measured following FCCP injection. (D) The reserve capacity was calculated from the difference between the maximal and basal OCR. (E) The non-mitochondrial OCR was determined by injecting antimycin A and rotenone simultaneously to fully inhibit the electron transport chain. Results are mean \pm SEM. $n=5$ per group. * $p<0.005$ compared to Control. # $p<0.05$ compared to EtOH. \$ $p<0.05$ compared to Control + DetaNO.

The maximal OCR of primary hepatocytes isolated from control and EtOH-fed rats was assessed using FCCP treatment, and was dramatically suppressed by the combined exposure to $\dot{\text{N}}\text{O}$ and EtOH (**Figure 2-12C**). The reserve capacity decreased following DetaNO and EtOH exposure alone; however, the combined DetaNO/EtOH exposure to hepatocytes resulted in a cumulative decrease in reserve capacity (**Figure 2-12D**). Chronic EtOH consumption again resulted in a slight although significant decrease in non-mitochondrial OCR, but DetaNO had no additional effect (**Figure 2-12E**).

Alcohol Exacerbates Bioenergetic Alterations Induced by Hypoxia and Nitric Oxide

The effect of hypoxia on the mitochondrial bioenergetics of primary hepatocytes was determined next. To achieve this, cells were plated with media equilibrated to room air into an XF24 analyzer placed in a sealed chamber with an atmosphere of 1% O_2 . The O_2 levels in the cell culture plate were then allowed to reach equilibrium with the atmosphere in the hypoxia chamber. The O_2 concentration was measured every 8 min in the media in individual wells containing cells and decreased exponentially over 2-3 hrs as the media reached equilibrium with the atmosphere in the hypoxia chamber as shown previously in **Figure 2-6B**. After approximately 160 min, the O_2 concentration was essentially stable at 20 μM . Over the same time course, the basal OCR of control hepatocytes was measured and remained unchanged for the first 60 min corresponding to an O_2 concentration of approximately 60 μM , after which it began to decrease progressively (**Figure 2-13A**). In contrast, hepatocytes from EtOH-fed animals showed less of a dependence on decreasing O_2 concentrations (**Figure 2-13B**). To determine the effect of $\dot{\text{N}}\text{O}$ on the OCR of control hepatocytes in hypoxia, 250 μM – 1 mM DetaNO was added to

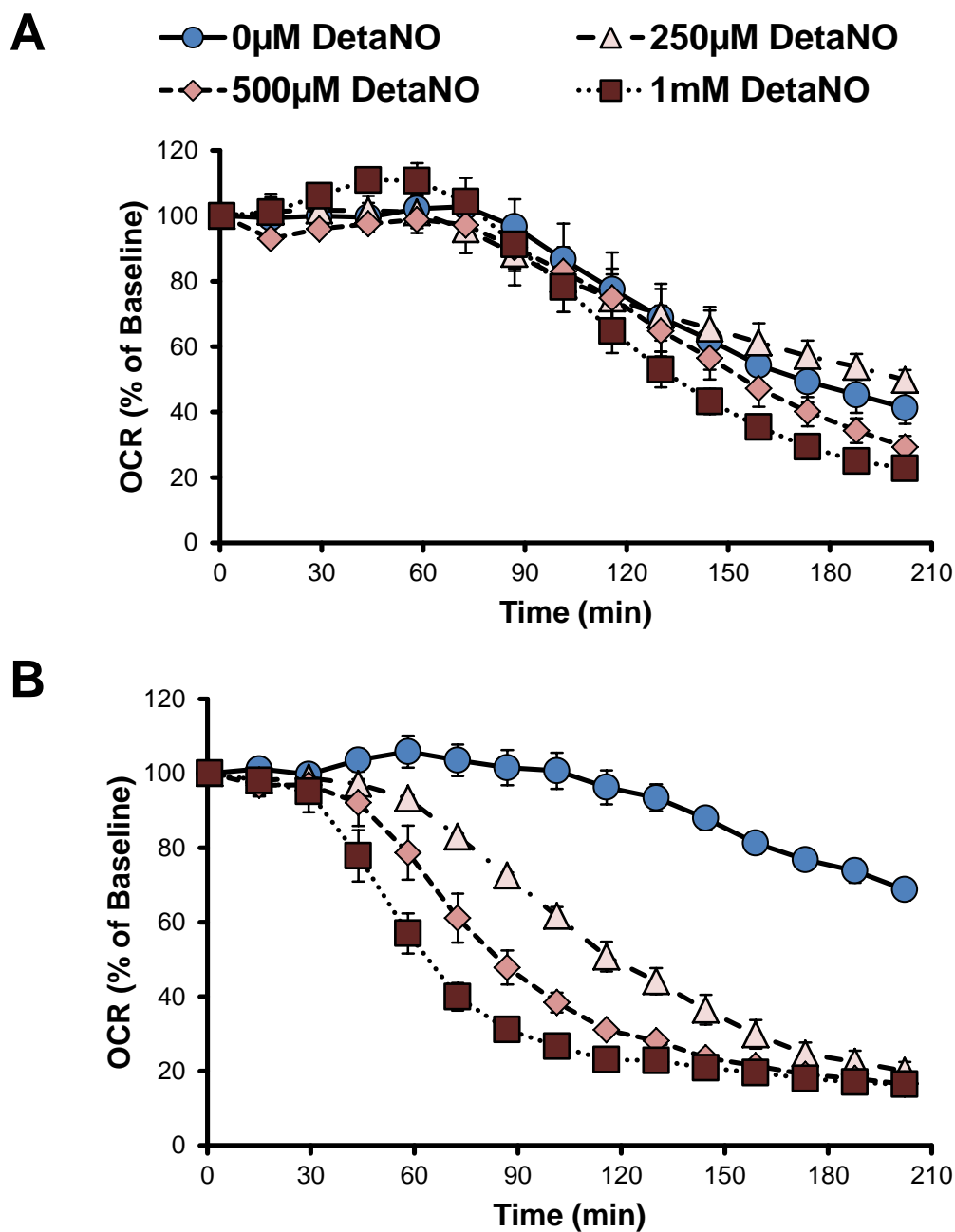


Figure 2-13. Alcohol toxicity increases hepatocyte susceptibility to nitric oxide-induced inhibition of respiration in hypoxia. The effect of 0-1000 μ M DetaNO (added immediately prior to the start of the assay) on the OCR of hepatocytes from (A) control rats and (B) EtOH-fed rats over time as O_2 concentration equilibrates from room air to 1% O_2 in the hypoxia chamber as seen in Figure 2-6B. Results are mean \pm SEM. $n=5$ per group.

the cells immediately prior to the beginning of the assay. The control hepatocytes were essentially resistant to exposure to $\dot{\text{N}}\text{O}$ under hypoxic conditions with only the highest levels of DetaNO modestly decreasing OCR after 2 hr. In contrast, hepatocytes isolated from EtOH-fed rats were much more sensitive to $\dot{\text{N}}\text{O}$ -induced inhibition of OCR at low O_2 tensions than the control hepatocytes.

The changes in OCR in control and EtOH hepatocytes were then plotted as a function of the O_2 measured in the media at the time of the OCR measurement. As shown in **Figure 2-14A**, $\dot{\text{N}}\text{O}$ caused a right shift of the O_2 dependency in control cells and showed no clear dependency on DetaNO concentration. Hepatocytes isolated from EtOH-fed animals showed a dose-dependent shift in inhibition of OCR by DetaNO under low O_2 conditions (**Figure 2-14B**). Taken together, this data shows that the O_2 dependency for OCR in the hepatocytes from the EtOH treated animals is left shifted compared to controls, but the respiration is much more sensitive to inhibition by $\dot{\text{N}}\text{O}$. While increasing concentrations of DetaNO caused a slight increase in the IC_{50} for the dependence of OCR on O_2 in control hepatocytes, the IC_{50} of EtOH-fed hepatocytes was significantly higher in response to increasing concentrations of DetaNO (**Figure 2-15**).

Alcohol-Induced Hypoxia in the Liver is iNOS-Dependent

Since $\dot{\text{N}}\text{O}$ is able to significantly inhibit O_2 consumption in primary hepatocytes isolated from EtOH-fed rats, we then determined the effects of endogenous $\dot{\text{N}}\text{O}$ production on the hypoxia induced by chronic EtOH consumption. In order to manipulate $\dot{\text{N}}\text{O}$ levels using a molecular approach, we next used $\text{iNOS}^{-/-}$ mice on a C57BL/6 background.

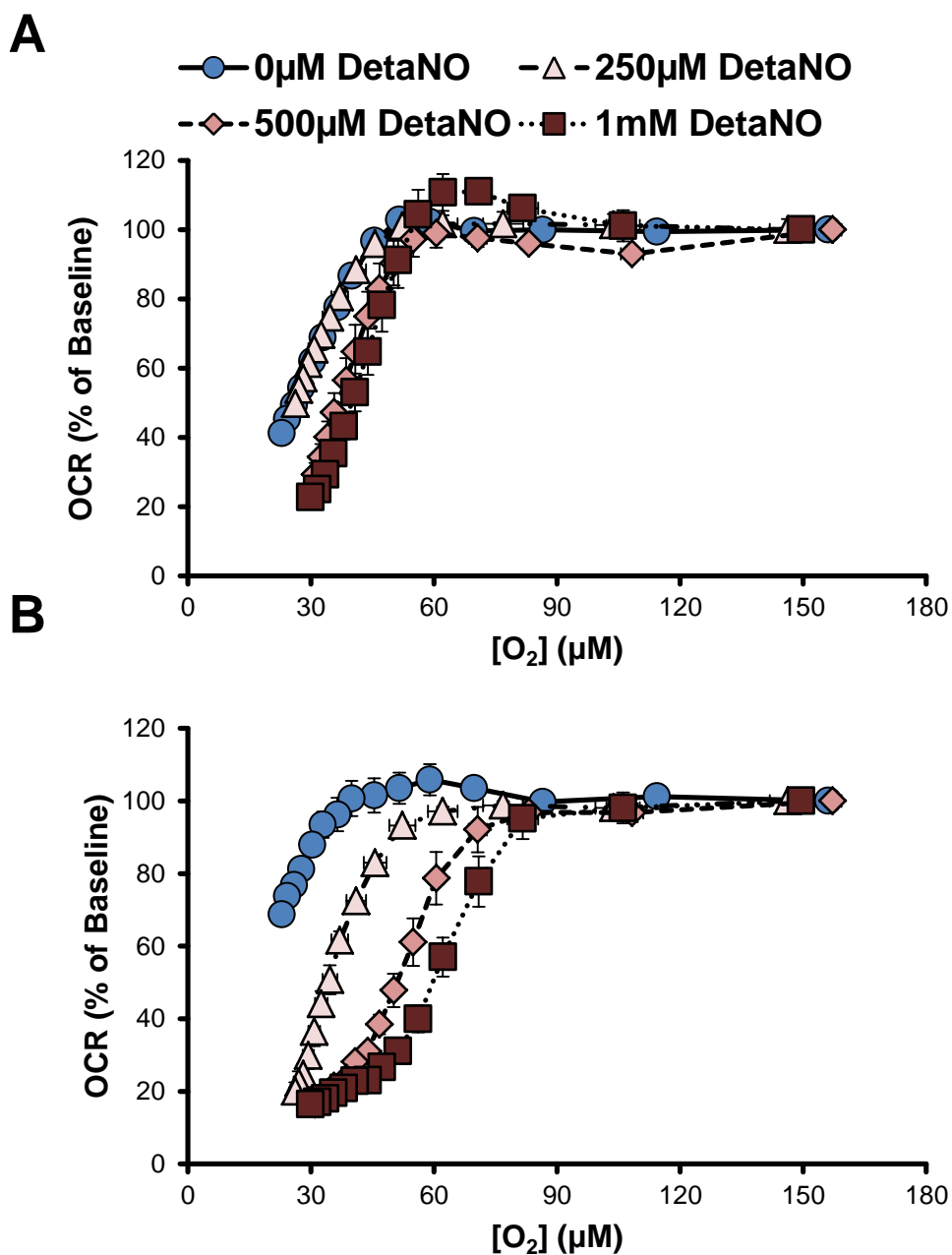


Figure 2-14. Chronic alcohol consumption alters hepatocyte response to decreasing oxygen concentration and nitric oxide. (A) The change in OCR of control hepatocytes treated with DetaNO plotted as a function of the decreasing O_2 concentration of the media as seen in Figure 2-13A. (B) The change in OCR of hepatocytes isolated from EtOH-fed rats pretreated with 0-1000 μM DetaNO is plotted as a function of the O_2 concentration of the media as it becomes hypoxic, as seen in Figure 2-13B. Results are mean \pm SEM. $n=5$ per group.

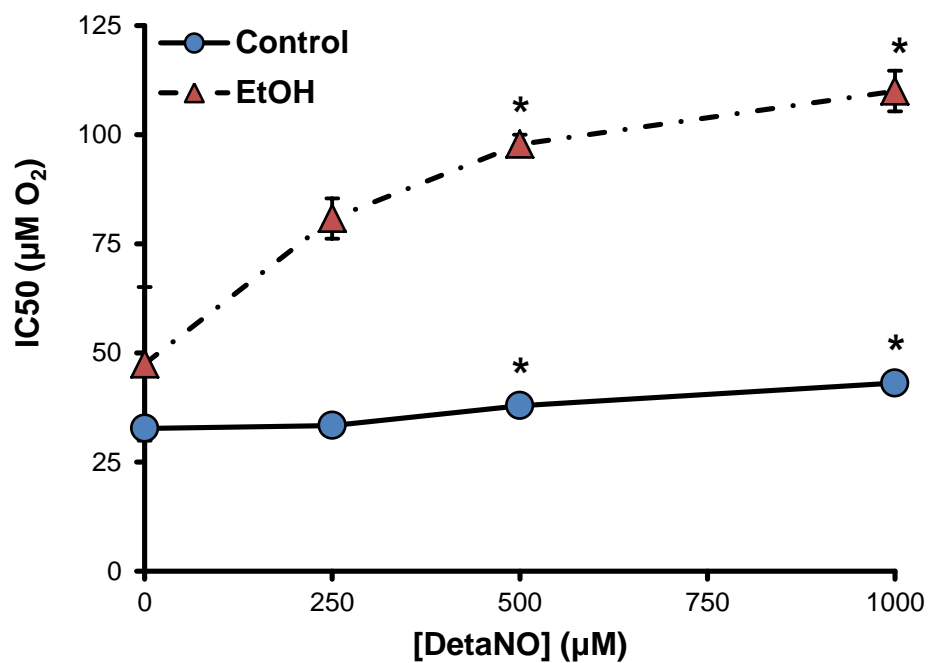


Figure 2-15. Chronic alcohol consumption alters bioenergetic response to decreasing oxygen concentration and nitric oxide. The IC₅₀ of the curves from Figure 2-14 were calculated by fitting the data to a sigmoidal curve. Results are mean \pm SEM. n=5 per group. *p<0.05 compared to respective vehicle-treated group.

EtOH is metabolized predominantly by the enzymes CYP2E1 and alcohol dehydrogenase; acetaldehyde, the main product of EtOH metabolism, is then metabolized by aldehyde dehydrogenase 2 (ALDH2) [255, 256]. To validate our model, we examined the effect of chronic EtOH consumption on CYP2E1 and ALDH2 expression in *iNOS*^{-/-} and wild type mice to rule out any potential alterations in the expression of these enzymes. CYP2E1 expression was significantly increased after EtOH feeding in wild-type and *iNOS*^{-/-} mice (**Figure 2-16A**). ALDH2 protein was equal between control and EtOH groups and genotypes (**Figure 2-16B**). Chronic EtOH consumption is also associated with the development of liver steatosis [158, 240, 257-259], which also occurred in these experiments with C57BL/6 mice (**Figure 2-17**). Furthermore, the lack of *iNOS* was able to attenuate the development of steatosis [34].

Using the hypoxia marker pimonidazole, which is reductively activated at low O₂ concentrations and reacts with protein thiols [253], we were able to use immunohistochemistry to visualize the O₂ gradients in liver sections isolated from control and EtOH-fed wild type and *iNOS*^{-/-} mice. In normal, healthy liver, the most hypoxic region is zone 3, or the peri-central zone. A significant increase in pimonidazole binding was seen in the zone 3 region in liver of EtOH-fed wild-type mice, which extended into the mid-zonal and peri-portal regions compared to controls (**Figure 2-18A**). These data are indicative of the development of peri-portal and peri-central hypoxia due to chronic EtOH consumption. In contrast, livers from EtOH-fed *iNOS*^{-/-} mice exhibited a significant decrease in pimonidazole binding (i.e., less zonal hypoxia) in the peri-portal regions, and when staining was present it was localized in the peri-central region of the liver lobule. Livers from control-fed wild type and *iNOS*^{-/-} mice showed minimal pimonidazole stain-

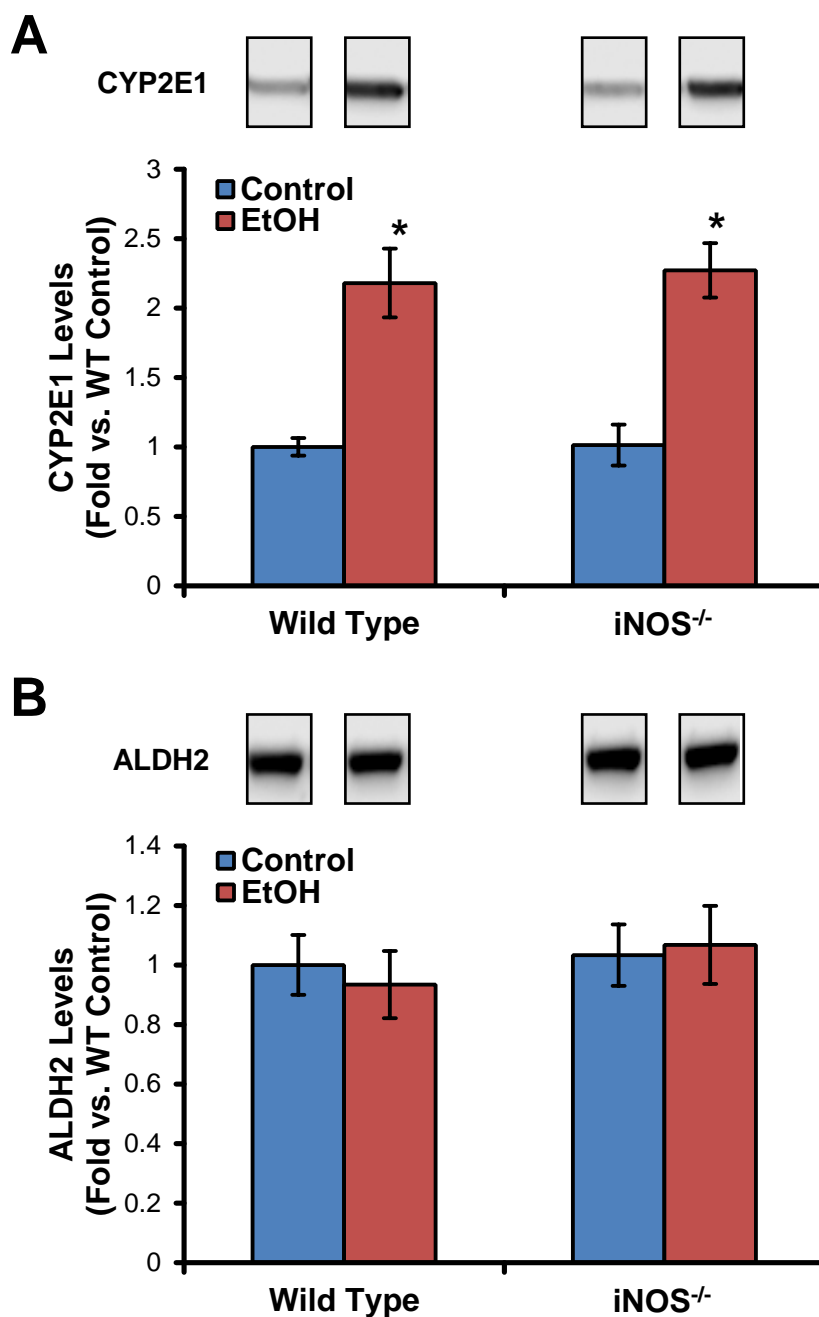


Figure 2-16. Chronic alcohol consumption causes induction of cytochrome P450 2E1 in wild type and iNOS^{-/-} mice. (A) Liver homogenates (25 μ g protein) from control and EtOH-fed wild type and iNOS^{-/-} mice were used for analysis of CYP2E1 (A) and ALDH2 (B) expression by SDS/PAGE followed by Western blotting. The densitometry of the band was quantified using the AlphaEaseFC software. Results are mean \pm SEM. n=6 per group. *p<0.0005 compared to the respective control mice. Data obtained by M.J. Chang.

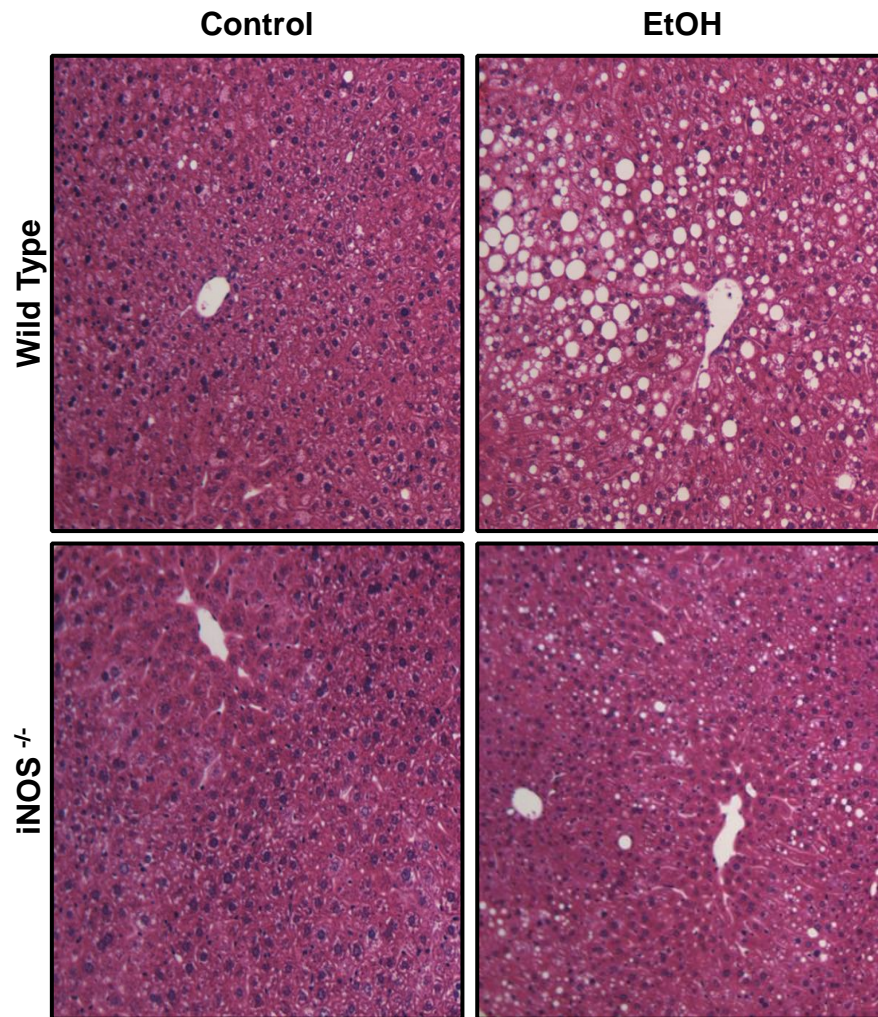


Figure 2-17. Lack of iNOS prevents hepatic steatosis in alcohol-fed animals. Hepatic steatosis was assessed using H&E stained liver sections. Images are representative from each group and quantification results are mean \pm SEM. n=6 per group. Data obtained by A. Venkatraman.

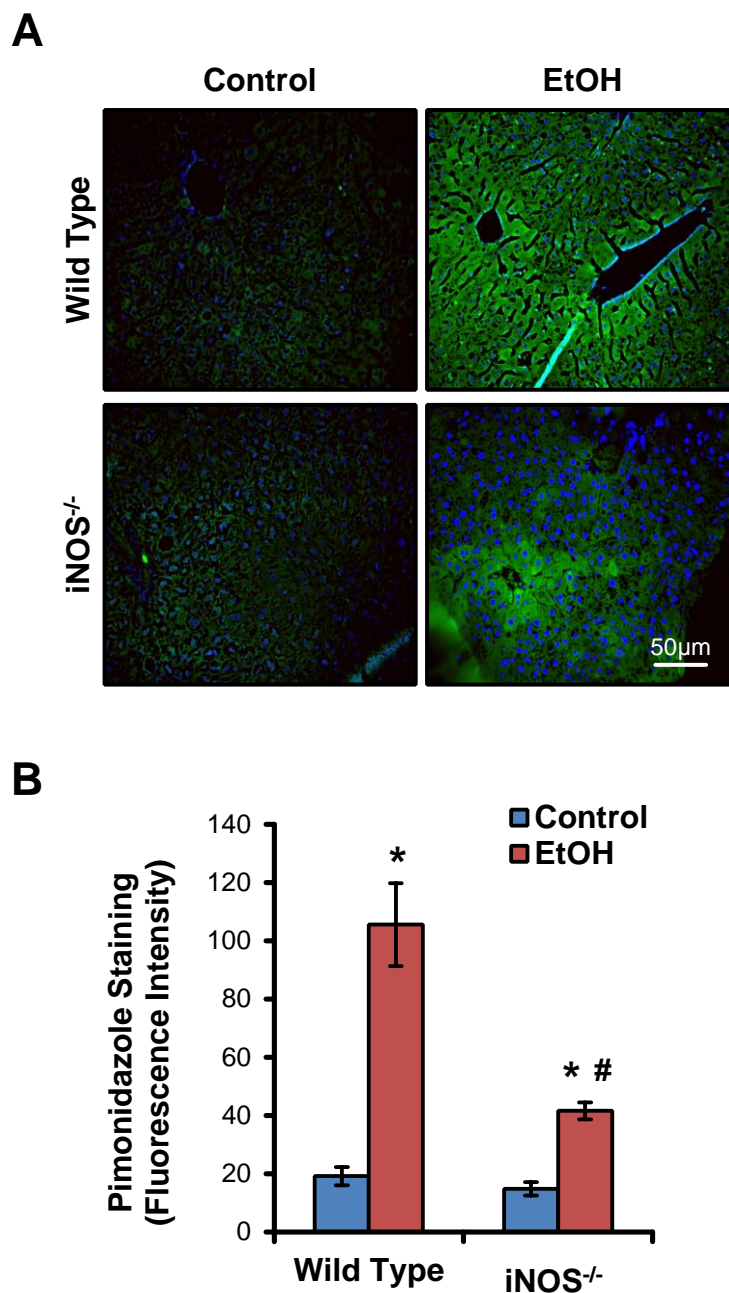


Figure 2-18. iNOS-derived nitric oxide is required for chronic alcohol-induced liver hypoxia. (A) Pimonidazole staining of formalin fixed liver sections from wild type and iNOS^{-/-} mice with and without alcohol (EtOH) feeding was performed to assess liver hypoxia. (B) Quantification of the pimonidazole staining intensity from (A). Images are representative from each group and quantification results are mean \pm SEM. n=6 per group. *p<0.05 compared to respective controls. #p<0.05 compared to EtOH-fed wild type mice. Data obtained by A. Venkatraman.

ing, indicating that there is a lower level of hypoxia in the absence of chronic EtOH exposure. Sections incubated with pre-immune sera or without the primary antibody for pimonidazole adducts showed low background staining similar to that seen of in control livers (data not shown). Quantitative analysis of images showed a 5.5 fold increase in pimonidazole staining in wild type animals on the EtOH diet compared to their pair-fed controls, whereas the lack of iNOS expression attenuated the EtOH-dependent pimonidazole staining by 60% as compared to wild type animal consuming EtOH (**Figure 2-18B**).

Given that HIF-1 α stabilization has also been shown to be modulated by NO [260], we also used immunohistochemistry to examine HIF-1 α in liver from iNOS^{-/-} and wild type mice fed the control and EtOH diets. Consistent with pimonidazole staining, there was increased HIF-1 α staining in the liver peri-central region from EtOH-fed wild type mice as compared to pair-fed controls (**Figure 2-19A**). Interestingly, there was a significant decrease in HIF-1 α staining in the liver peri-central region from EtOH-fed iNOS^{-/-} mice as compared to EtOH-fed wild type mice. These results implicate a role of iNOS in the response to chronic EtOH consumption and the development of tissue hypoxia *in vivo*. Both controls had negligible background staining. **Figure 2-19B** depicts the quantitative analysis of HIF-1 α levels in liver of all treatment groups.

DISCUSSION

The development of mitochondrial dysfunction is an important feature of the pathophysiology of EtOH-induced hepatotoxicity. It has been shown that EtOH toxicity causes alterations in the mitochondrial proteome, resulting in decreased levels of the complexes required for oxidative phosphorylation [159]. This has been shown to cause

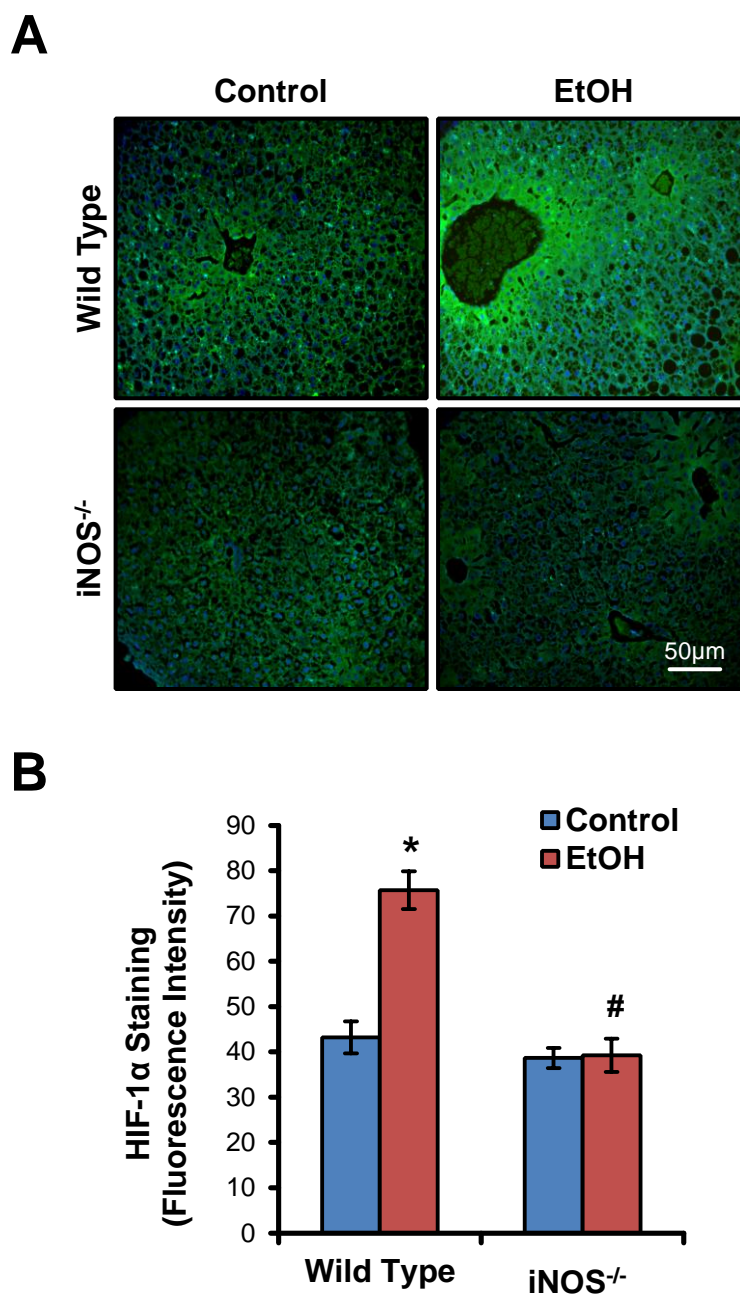


Figure 2-19. iNOS expression is required for chronic alcohol-induced stabilization of HIF-1 α in the liver. Fluorescence microscopy was used to detect HIF-1 α stabilization in liver sections from control and alcohol (EtOH)-fed wild type and iNOS^{-/-} mice (A). The quantification of the immunofluorescence is shown in (B). Images are representative from each group and quantification results are mean \pm SEM. n=6 per group. *p<0.05 compared to respective controls. #p<0.05 compared to EtOH-fed wild type mice. Data obtained by A. Venkatraman.

bioenergetic defects, with diminished glycogen utilization and ATP production [161, 187, 188]. It has also been shown that chronic EtOH consumption causes mitochondrial dysfunction using isolated liver mitochondria [160, 243]; however, the effects of EtOH toxicity on different parameters of mitochondrial function and the impact of $\dot{\text{N}}\text{O}$ in intact hepatocytes remain unclear.

We found that hepatocytes isolated from EtOH-exposed rats do not have different levels of basal mitochondrial function; however, these hepatocytes did exhibit a significant decrease in their maximal OCR and reserve capacity (**Figure 2-10**). Given that the basal OCR is not affected by EtOH consumption suggests that in the absence of an additional stressor, such as $\dot{\text{N}}\text{O}$, the bioenergetic needs of the cell can be met. Since chronic EtOH consumption is associated with increased ROS/RNS from a number of different sources within the cell, this finding leads to the hypothesis that hepatocytes from EtOH-fed animals are less tolerant to secondary stresses.

Importantly, increased iNOS leads to the increased production of $\dot{\text{N}}\text{O}$, which can inhibit mitochondrial respiration reversibly at CcOX and irreversibly when combined with ROS at other respiratory complexes [36, 180, 237, 239, 241, 243, 261]. We found that the inhibition of mitochondrial function by chronic EtOH consumption was further exacerbated by exposure to $\dot{\text{N}}\text{O}$ (**Figure 2-11**). The combination of these stressors decrease total available mitochondrial function to the point that only negligible reserve capacity remains (**Figure 2-12C,D**), and the addition of a secondary stress such as $\dot{\text{N}}\text{O}$ to hepatocytes from the EtOH group resulted in a significant decrease in the basal OCR as compared to control and pair-fed control hepatocytes (**Figure 2-12A**). In addition to the combination of the stresses of chronic EtOH and $\dot{\text{N}}\text{O}$ causing the loss of mitochondrial

function that was seen, the formation of peroxynitrite and subsequent mitochondrial damage likely also mediated the effect [36, 262-265]. This data emphasizes the concept that reserve capacity serves as a protective buffer for available mitochondrial function, enabling the cells to maintain the bioenergetic function necessary to maintain overall cellular function even after being exposed to a stressor.

The loss of reserve capacity of EtOH-exposed hepatocytes upon treatment with $\dot{\text{N}}\text{O}$ becomes more apparent when the hepatocytes were subjected to low O_2 concentrations as would occur *in vivo* (**Figure 2-13**). Chronic EtOH consumption is known to cause liver hypoxia, particularly in zone 3 of the liver [258]. While control hepatocytes were mostly resistant to the effects of $\dot{\text{N}}\text{O}$ under decreasing O_2 tensions, the EtOH-exposed hepatocytes displayed a significant inhibition of mitochondrial function by $\dot{\text{N}}\text{O}$ under hypoxia. This is due to the hepatocytes isolated from EtOH-fed animals having reduced reserve capacity as compared to control animals (**Figure 2-10D**), which is then further diminished by exposure to $\dot{\text{N}}\text{O}$ (**Figure 2-12D**). These data suggest that the available functional CcOX in EtOH hepatocytes is diminished, thus leading to $\dot{\text{N}}\text{O}$ becoming a stronger competitor with O_2 for binding with CcOX. Moreover, as the O_2 concentration decreases, the ability of $\dot{\text{N}}\text{O}$ to outcompete O_2 from binding CcOX increases, resulting in an increase in the $\dot{\text{N}}\text{O}$ -induced inhibition of respiration as the hepatocytes became hypoxic. This supports previous findings which have shown that isolated mitochondria from EtOH-fed animals are more sensitive to inhibition by $\dot{\text{N}}\text{O}$ than those from control animals [242], and that $\dot{\text{N}}\text{O}$ is a more robust inhibitor of respiration during hypoxic stress [239].

Cells respond to low O₂ availability by initiating a series of adaptive responses through transcriptional activation and stabilization of hypoxia inducible factor 1 α (HIF-1 α) [199]. Accumulation of HIF-1 α is an important step in the activation of HIF1 during hypoxia. Regulation of HIF-1 α by \cdot NO is an additional mechanism by which \cdot NO might modulate cellular responses to hypoxia [233]. The modulation of the hypoxic response by \cdot NO is believed to have wide pathophysiological significance [266]. The susceptibility of the centrilobular region of the liver to low O₂ tensions is predominantly due to an O₂ gradient between the portal blood and hepatic venous blood *in vivo* [267]. Since it is well established that EtOH consumption causes hypoxia and increased expression of iNOS in zone 3 of the liver lobule *in vivo* [35, 243], and here we have shown that \cdot NO inhibits mitochondrial function in EtOH-exposed hepatocytes, we used iNOS^{-/-} mice to test the role of \cdot NO in the formation of hypoxia in the liver following chronic EtOH consumption. In agreement with earlier studies, chronic EtOH consumption significantly increased the binding of the hypoxia marker pimonidazole in liver tissue, predominantly in the O₂-poor (zone 3) region of the liver lobule (**Figure 2-18**) [35]. In addition, we demonstrate that chronic EtOH consumption can lead to HIF-1 α expression in the O₂ deprived region of the liver lobule (**Figure 2-19**).

EtOH metabolism increases O₂ utilization by hepatocytes, thereby reducing the O₂ availability for other important cellular functions, and this in turn leads to hypoxia. This phenomenon is most predominant in the zone 3 region of the liver lobule, which normally is exposed to lower O₂ concentrations as compared to zones 1 and 2. The tendency of hypoxia to occur in zone 3, taken together with increased oxidative (4-hydroxynonenal protein adduct formation) and nitrative stress (increased iNOS and nitro-

tyrosine staining) in this zone [36, 243], may account for the increased severity of EtOH-induced hepatotoxicity in this region of the liver lobule. Interestingly, the absence of iNOS prevented the accumulation of HIF-1 α and pimonidazole staining in mice on the EtOH diet (**Figure 2-18,19**). The disruption of O₂ gradients observed in the wild type mice after EtOH consumption was also restored in iNOS^{-/-} mice, revealing a major role for iNOS in regulating responses to hypoxia. In addition, we and others have also demonstrated that ablation of iNOS blunted the various hepatotoxic effects of EtOH consumption [36, 243].

How does depletion of iNOS cause restoration of the O₂ gradient? There could be several possibilities. It is becoming increasingly evident that chronic EtOH administration increases peroxynitrite mediated hepatotoxicity by enhancing concomitant production of \cdot NO (from iNOS) and superoxide [265]. Another possibility is the involvement of mitochondria in the development of hypoxia within the tissue. Studies using pharmacological inhibitors of the respiratory chain, as well as cells lacking mtDNA and electron transport chain activity, suggest that HIF-1 α activity is dependent on mitochondrial function [198, 268-270]. This may partly explain the \cdot NO-dependent expression of HIF-1 α in wild type mice on an EtOH diet and the reversal of the induction in iNOS^{-/-} mice. It is possible that these effects of \cdot NO are mediated through the mitochondrion as a consequence of inhibiting respiration at CcOX. This response may be exacerbated by changes in the \cdot NO-dependent control of respiration which occurs in response to stress. For example, we have demonstrated that mice on an EtOH diet have increased sensitivity to inhibition of mitochondrial respiration by \cdot NO, an effect reversed in mice lacking iNOS [243]. This finding was also evident in the isolated hepatocytes (Figure 5) which suggests

that the combined effects of increased $\dot{V}NO$ and ROS in the intact liver would lead to areas of non-functioning mitochondria and hypoxia.

Taken together, these data provide evidence for the role on $\dot{V}NO$ as an important regulator of mitochondrial respiration at CcOX in EtOH-induced hepatotoxicity. We have shown that the addition of $\dot{V}NO$ to hepatocytes isolated from rats consuming EtOH have diminished basal OCR, ATP-linked OCR, increased proton leak and decrease in reserve capacity, or the ability to withstand mitochondrial stressors. We have also shown that under conditions of hypoxic stress, the addition of $\dot{V}NO$ to EtOH hepatocytes resulted in an increased susceptibility to decreases in OCR under low O_2 tensions. Lastly, we have shown that the removal of iNOS in a mouse model of EtOH exposures leads to decreased hypoxia and hypoxic markers in the liver.

CHAPTER 3

HYPOXIA/REOXYGENATION ALTERS THE RESPONSE OF CELLULAR BIOENERGETICS TO 4-HYDROXYNONENAL IN ENDOTHELIAL CELLS

INTRODUCTION

The pathophysiology of ischemia and reperfusion is a central mediator in the morbidity and mortality accompanying many diverse pathological conditions. Myocardial infarction, stroke, atherosclerosis, circulatory shock, and organ transplantation are all associated with the development of pathology which is often initiated by ischemia/reperfusion injury [271, 272]. While ischemia/reperfusion is often studied in combination, both ischemia and reperfusion elicit cell damage through separate yet related mechanisms [31].

Ischemic tissue can quickly develop bioenergetics dysfunction, due to the lack of O₂ and nutrients which are necessary for cellular energy production. Moreover, ischemia is known to cause the electron transport chain to become more reduced due to the lack of available O₂ to accept the electrons, thereby promoting the leaking of electrons to form ROS [31, 37, 198, 209-211, 268-270, 273-282]. Xanthine oxidase and NADPH oxidase have also been implicated in the increased formation of ROS associated with ischemia [220, 283, 284]. This increase in hypoxia-induced mitochondrial ROS induce oxidative damage to proteins, lipids, and mtDNA; however, they also play a role in cell signaling, in part through the stabilization of HIF-1 α , leading to the induction of genes under the

control of the hypoxia response element (HRE) [198, 268, 269, 280, 285, 286]. Furthermore, during ischemia there is an increased dependence on glycolysis for energy production, which causes lactic acid accumulation which results in a more acidic intracellular pH [271, 287]. The development of cytosolic acidosis initiates the release of Ca^{2+} from the endoplasmic reticulum, leading to calcium overload [40, 42, 288-291].

Upon prolonged ischemic periods, the mitochondria lose their membrane potential due to the hindrance of the electron transport chain [287, 292]. This causes ATP synthase to reverse directions, using ATP hydrolysis to in an attempt to maintain the membrane potential [287]. Furthermore, prolonged hypoxia has been shown to decrease Mn-superoxide dismutase (SOD) activity and CcOX expression, both of which lead to further oxidative stress [195, 196, 208]. The loss of ATP, in combination with increased levels of Ca^{2+} and ROS leads to cellular dysfunction and, if the ischemia persists, cell death (**Figure 3-1**) [26, 207, 292-297].

Reperfusion, while necessary for the maintenance of viability and function, causes further damage to the ischemic tissue [271]. The reintroduction of O_2 and nutrients is associated with the rapid and abundant formation of ROS [31, 38, 212-214, 287, 298-301]. Several mechanisms have been implicated with this increase in oxidative stress. Xanthine oxidase has been shown to produce large quantities of ROS during reperfusion [31, 38, 215], as has NADPH oxidase, through a Ca^{2+} overload-dependent mechanism [41, 291, 302, 303]. Another important source of reperfusion-induced ROS is the mitochondria, due in part to the abundance of reducing equivalents, the damage incurred during ischemia, and the decreased activity of MnSOD [195, 299, 304-308]. An external source of oxidative damage caused by reperfusion is the inflammatory response mediated

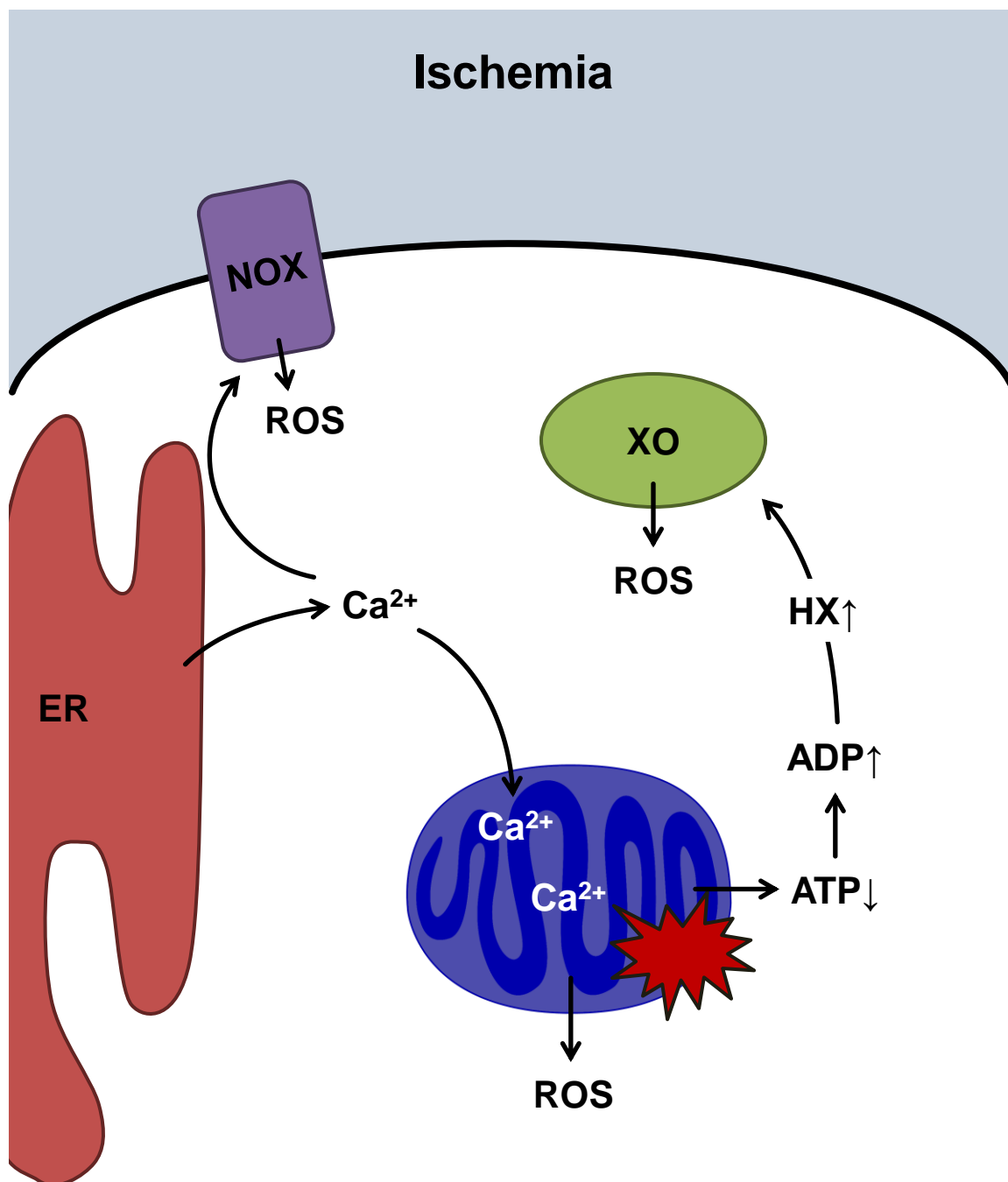


Figure 3-1. Ischemia causes bioenergetic and cellular dysfunction. Ischemia causes damage by inhibiting mitochondrial function and stimulating mitochondrial ROS formation. Glycolysis is increased, causing cellular acidosis, which stimulates the release of calcium (Ca^{2+}) from the endoplasmic reticulum (ER). This results in cytosolic and mitochondrial Ca^{2+} overload, as well as the activation of NADPH oxidase (NOX). Xanthine oxidase (XO) is also activated in ischemia, producing high levels of ROS. Furthermore, the loss of mitochondrial function in ischemia leads to increased ADP levels, which is broken down through purine catabolism to hypoxanthine (HX), which is the substrate for XO to produce more ROS.

by the recruitment of polymorphonuclear cells due to the tissue damage caused by the ischemia and reperfusion [31, 271, 272, 309-311]. All of these sources of ROS lead to the exacerbation of mitochondrial damage and bioenergetic dysfunction, inducing apoptotic and necrotic cell death [24-26, 39, 293, 297, 312-315].

Many studies have elucidated the effects of ischemia and reperfusion on cellular bioenergetics and mitochondrial function in various tissues; however, the development of mitochondrial dysfunction in the endothelium over time during the exposure to hypoxia is not as clear. Understanding the effect of ischemia and reperfusion on the mitochondrial bioenergetics in the endothelial cells is of critical importance, because the loss of endothelial function can hinder the reperfusion of ischemic tissues [202, 203, 271, 272, 309, 310, 316, 317]. The focus of this chapter is to examine the alterations to mitochondrial bioenergetic function in intact endothelial cells over time in response to hypoxia and reoxygenation to further understand the mechanisms of pathogenesis of ischemia and reperfusion.

Bioenergetic Alterations Associated with Ischemia/Reperfusion: Effects of Reactive Lipid Species

The oxidative stress caused by both ischemia and reperfusion induce high levels of lipid peroxidation, which leads to formation of reactive, electrophilic lipids which are capable of adducting to proteins and altering their structure and function [31, 318-321]. A major product of lipid peroxidation which has been shown to be produced in large quantities in ischemia/reperfusion is 4-hydroxynonenal (HNE) [322-326]. Importantly, the modification of mitochondrial proteins by HNE is well known to modulate bioener-

getic function [179, 327-332]; however, the effect of HNE on mitochondrial function in hypoxia is not clear, and is a focus of this chapter.

MATERIALS AND METHODS

Materials

All reagents were purchased from Sigma (St. Louis, MO) and were of the highest grade offered, unless otherwise stated. V7 microplates and FluxPaks for running XF24 assays were purchased from Seahorse Bioscience (Billerica, MA).

Cell Culture

Bovine aortic endothelial cells (BAEC) were harvested from descending thoracic aortas and maintained at 37°C with 5% CO₂ in DMEM growth medium (Mediatech, Manassas, VA) supplemented with 5.5mM D-glucose (Sigma), 4 mM L-glutamine, 1 mM sodium pyruvate, 3.7 g/L sodium bicarbonate, 100 U/mL penicillin, and 100 ng/mL streptomycin (Invitrogen, Carlsbad, CA, USA), and 10% fetal bovine serum (Atlanta Biologicals, Atlanta, GA, USA).

Measurement of Oxygen Consumption in Endothelial Cells

An XF24 analyzer (Seahorse Bioscience, Billerica, MA) was used to measure the oxygen consumption rates (OCR) of adherent BAEC [177, 178, 333]. The XF24 does this using specialized microplates and disposable assay cartridges which use fluorescent probes to measure the concentration of O₂ in the media. We have found that the mitochondrial function of BAEC decreases with passage number; therefore, only BAEC between pas-

sages 5-8 were used [180]. BAEC were seeded into V7 microplates (Seahorse Bioscience) at 40,000 cells/well and were allowed to adhere and grow for 24 hr. One hr prior to the beginning of the XF24 assays, the growth media was changed to unbuffered DMEM (supplemented with 5.5 mM D-glucose, 4 mM L-glutamine, and 1 mM sodium pyruvate, with the pH adjusted to 7.4 at 37°C). The OCR of the BAEC was measured over time and in response to treatments or changing O₂ concentrations.

Mitochondrial Function Assay

In order to assess various parameters of mitochondrial function in BAEC, we used a previously described protocol utilizing sequential injections of oligomycin, FCCP, and antimycin A [179, 180, 250, 252, 330] (**Figure 3-2**). The injection of oligomycin results in a decrease in the OCR below basal, which represents the ATP-linked OCR. Next, FCCP is injected, causing an increase in OCR to the maximal point of which the cells are capable. This represents the maximal OCR. Moreover, the difference between the maximal OCR and the basal OCR is the reserve capacity, which represents the amount of mitochondrial function that the cells are capable of utilizing in response to stress or increased ATP demand. Finally, antimycin A is injected to inhibit the electron transport chain at Complex III. This causes a major decrease in the OCR of the cells, with the remaining OCR representing non-mitochondrial OCR. In addition, the difference between the oligomycin-sensitive OCR and the antimycin A-sensitive OCR represents the proton leak of the cells. The concentrations of oligomycin, FCCP, and antimycin A necessary to give maximal effects were determined, and these concentrations were used for all experiments [180]. For the calculation of these parameters of O₂ consumption, the OCR for

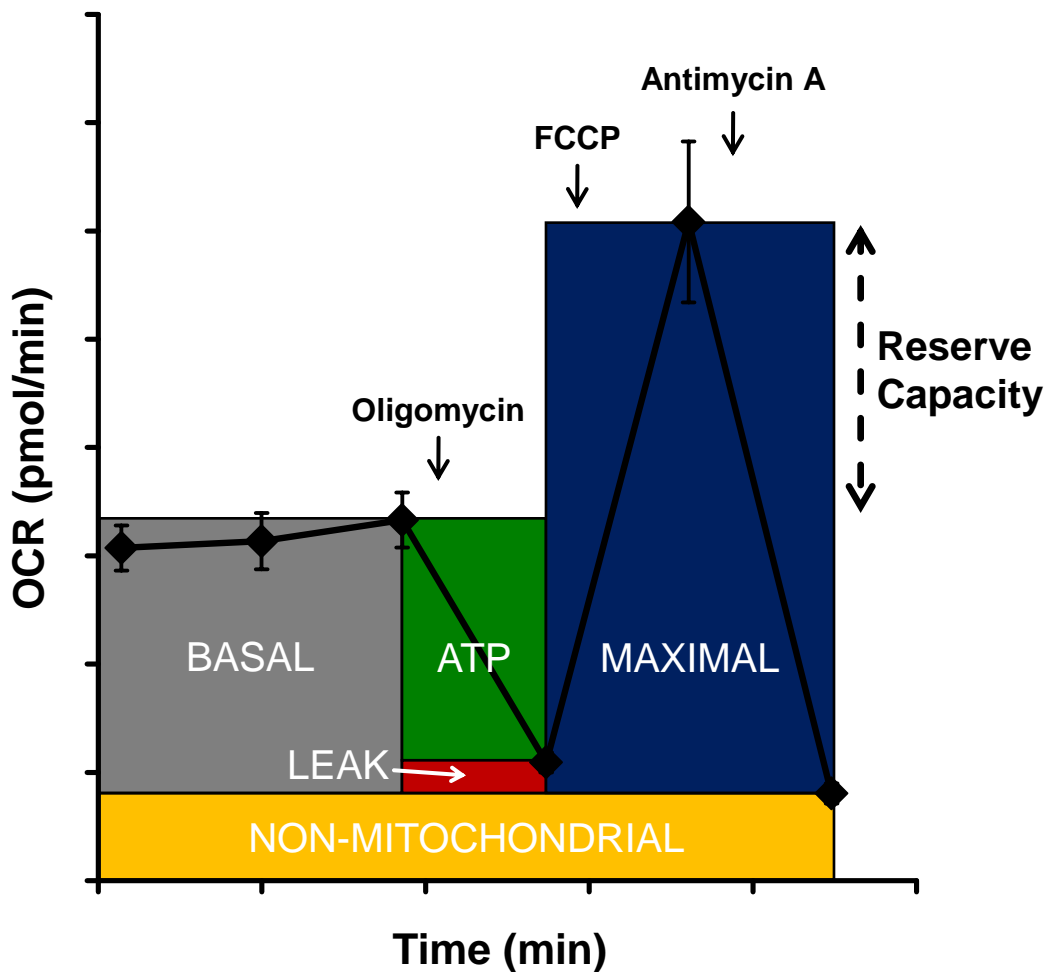


Figure 3-2. Measurement of parameters of mitochondrial function in endothelial cells using an XF24 analyzer. After three basal OCR measurements, oligomycin (1 $\mu\text{g}/\text{mL}$), FCCP (1 μM) and antimycin A (10 μM) were injected sequentially with OCR measurements recorded after each injection. ATP-linked oxygen consumption (ATP) and the OCR due to proton leak (LEAK) can be calculated using the basal and the oligomycin-insensitive rate. FCCP, a proton ionophore, is then used to determine the maximal respiratory capacity. Lastly, injection of antimycin A allows for the measurement of non-mitochondrial oxygen consumption. The reserve capacity is calculated by subtracting the maximal from the basal OCR.

each well were normalized to the total protein in that well using the DC Protein Assay (BioRad, Hercules, CA)

Exposure to Hypoxia and Reoxygenation

In order to determine the effects of decreasing the O₂ concentration on the OCR of BAEC, an XF24 analyzer was placed in a sealed glove box (PLAS labs, Lansing, MI) which was equilibrated to 1% O₂ ± 0.2% by vacuuming the air out of the chamber and refilling it with argon gas (**Figure 3-3A**). This cycle was repeated until the O₂ reached 1%, which was determined using an O₂ sensor. A second XF24 was maintained in room air (20.9% O₂), in which parallel plates were run as a control. Hypoxia experiments were performed by using cells and media which were equilibrated to room air and monitoring the changes in OCR and O₂ concentration over time (**Figure 3-3B**). In order to perform the reoxygenation studies, the cells were allowed to become hypoxic for the indicated amount of time, followed by re-equilibrating the glove box to room air by opening the chamber and flushing with room air using a fan. For these studies, the KSV algorithm (developed by Seahorse Bioscience) was used to calculate the OCR of the cells. While this algorithm is known to underestimate the OCR of cells in room air, it allows for the more sensitive measurement of the OCR of cells in hypoxia [333]. Because the fluorescence of the O₂ sensor is exquisitely sensitive to changes in temperature, XF24 assays are typically preceded by an equilibration period to verify that the temperature of the media is stable at precisely 37.0°C. For XF24 assays in hypoxia, the equilibration period was removed in order to monitor the initial decreases in O₂ concentration. With the slight variations in temperature due to the lack of equilibration, the O₂ sensor is still able to ac-

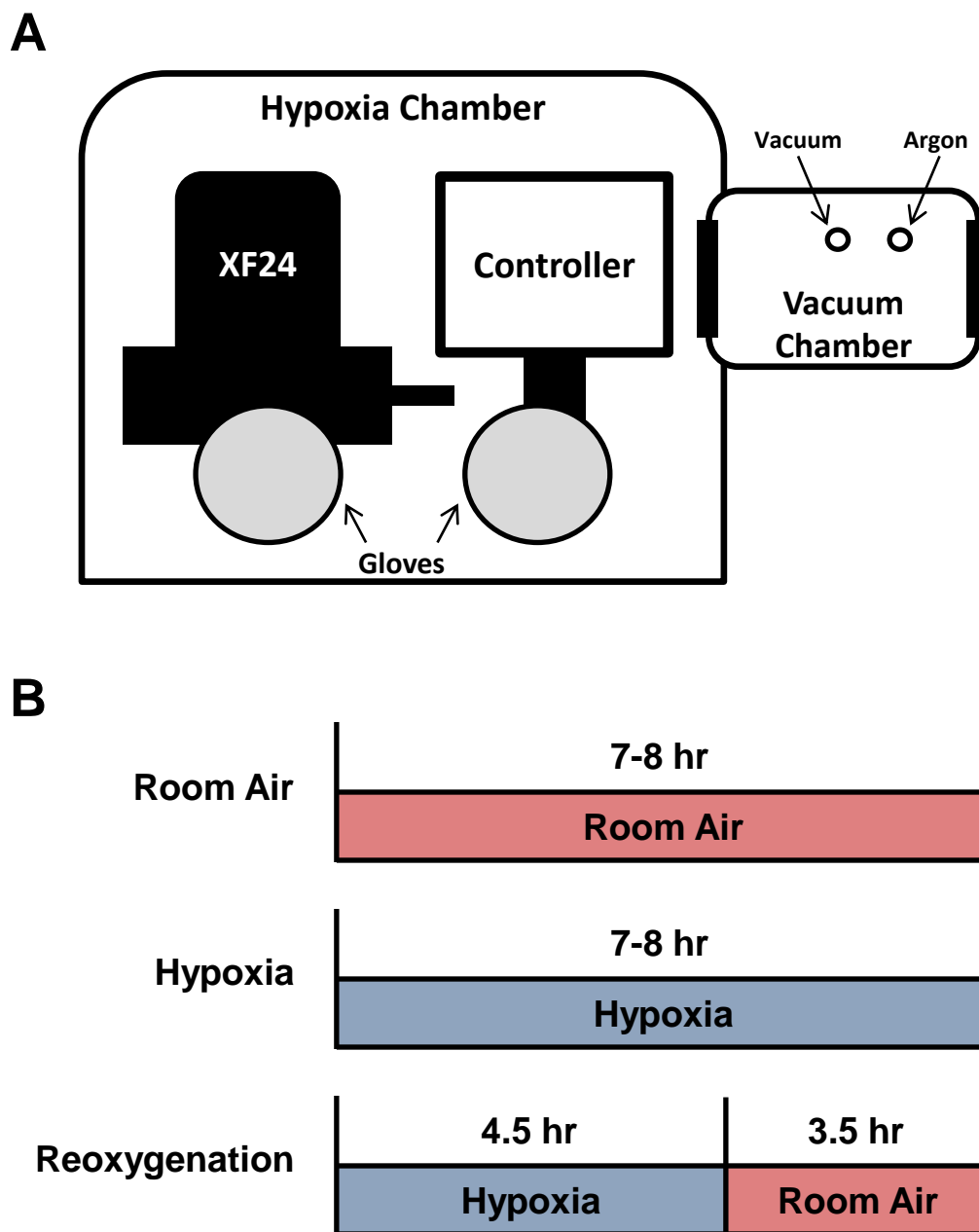


Figure 3-3. An XF24 analyzer in a hypoxia chamber was used for hypoxia and reoxygenation protocols. (A) XF24 analyzer was placed in a sealed glove box. The atmosphere in the glove box was then lowered to 1% O₂ by alternating flushing with argon gas and then vacuuming the air out of the chamber. The 1% O₂ was maintained for the length of all experiments with hypoxia as a condition. For reoxygenation experiments the chamber was opened, thus allowing the XF24 to re-equilibrate to room air. (B) The protocols of room air and hypoxia exposures for room air, hypoxia, and reoxygenation experiments.

curately measure the O₂ concentration at the beginning of the assay; however, with the variability in temperature, the sensor lacks the precision necessary to measure the change in O₂ concentration over time. Therefore, the first three OCR measurements of every hypoxia experiment were discarded to allow for the stabilization of the temperature of the media.

Immunoblot Analysis

Immediately following the conclusion of an XF assay, the BAEC were lysed in the V7 well using Laemmli sample buffer. The entire contents of each well were then separated by SDS/PAGE and Western blot, and were probed for protein-HNE adducts using a protein-HNE antibody (provided by Dr. Aruni Bhatnagar, U. of Louisville) followed by the HRP-conjugated anti-rabbit secondary antibody (Cell Signaling, Danvers, MA). The staining intensities for the entire lanes were quantified prior to saturation using AlphaEaseFC software (Alpha Innotech, Santa Clara, CA).

Statistics

Mitochondrial function measurements and Western blot densitometries were compared using a student's *T*-test. A $p < 0.05$ between groups was considered statistically significant. For OCR traces generated during XF24 assays, statistics were omitted for the sake of visual clarity.

RESULTS

Oxygen-Dependence of Endothelial Cell Mitochondrial Function

The mitochondrial function of BAEC in room air-equilibrated media was determined by using the XF24 analyzer to measure their OCR over time. Throughout the 7 hr assay, the O₂ concentration remained constant at approximately 220 μM (**Figure 3-4A**). The OCR of the BAEC also remained essentially unchanged for the duration of the assay (**Figure 3-4B**).

Next, the effect of decreasing the availability of O₂ to the endothelial cells on mitochondrial function was examined by monitoring the OCR of BAEC during the exposure to the progressive loss of O₂. BAEC were placed in XF media equilibrated to room air (20.9% O₂) prior to being placed in an XF24 analyzer maintained under a 1% O₂ atmosphere. The decreasing concentration of O₂ in the media above the cells was monitored over time as it equilibrated with the 1% O₂ atmosphere in the hypoxia chamber. This was achieved by measuring the O₂ concentration in the media above the cells every 8 min, and it was found to decrease exponentially (**Figure 3-5A**). After approximately 360 min, the O₂ concentration was essentially stable at 16 μM. Over the same time course, the basal OCR was measured for the endothelial cells and remained unchanged for 180 min, corresponding to an O₂ concentration of approximately 35 μM, after which it decreased progressively (**Figure 3-5B**).

Using the data shown in **Figure 3-5**, the relationship between OCR and O₂ concentration was determined (**Figure 3-6**). This analysis allowed for the determination that the OCR of the BAEC was insensitive to changes in O₂ concentrations of 35 μM and above. Once the concentration of O₂ decreased below 35 μM, the BAEC exhibited a

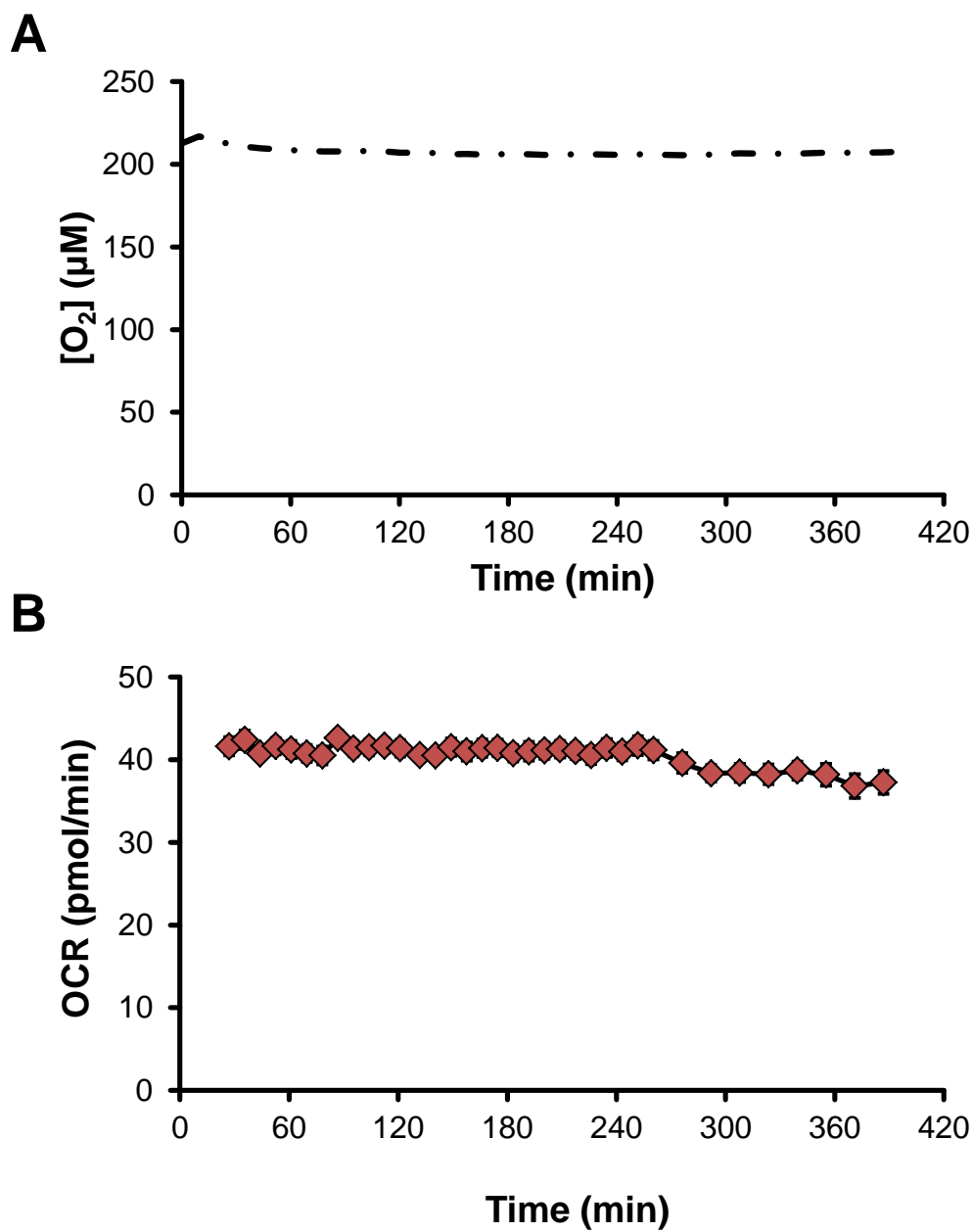


Figure 3-4. Oxygen consumption of endothelial cells in room air. (A) The O_2 concentration of media was monitored in an XF24 analyzer in room air. (B) BAEC seeded at 40,000 cells/well in V7 microplates and their OCR was measured over time. Results are mean \pm SEM. $n=5$ per group.

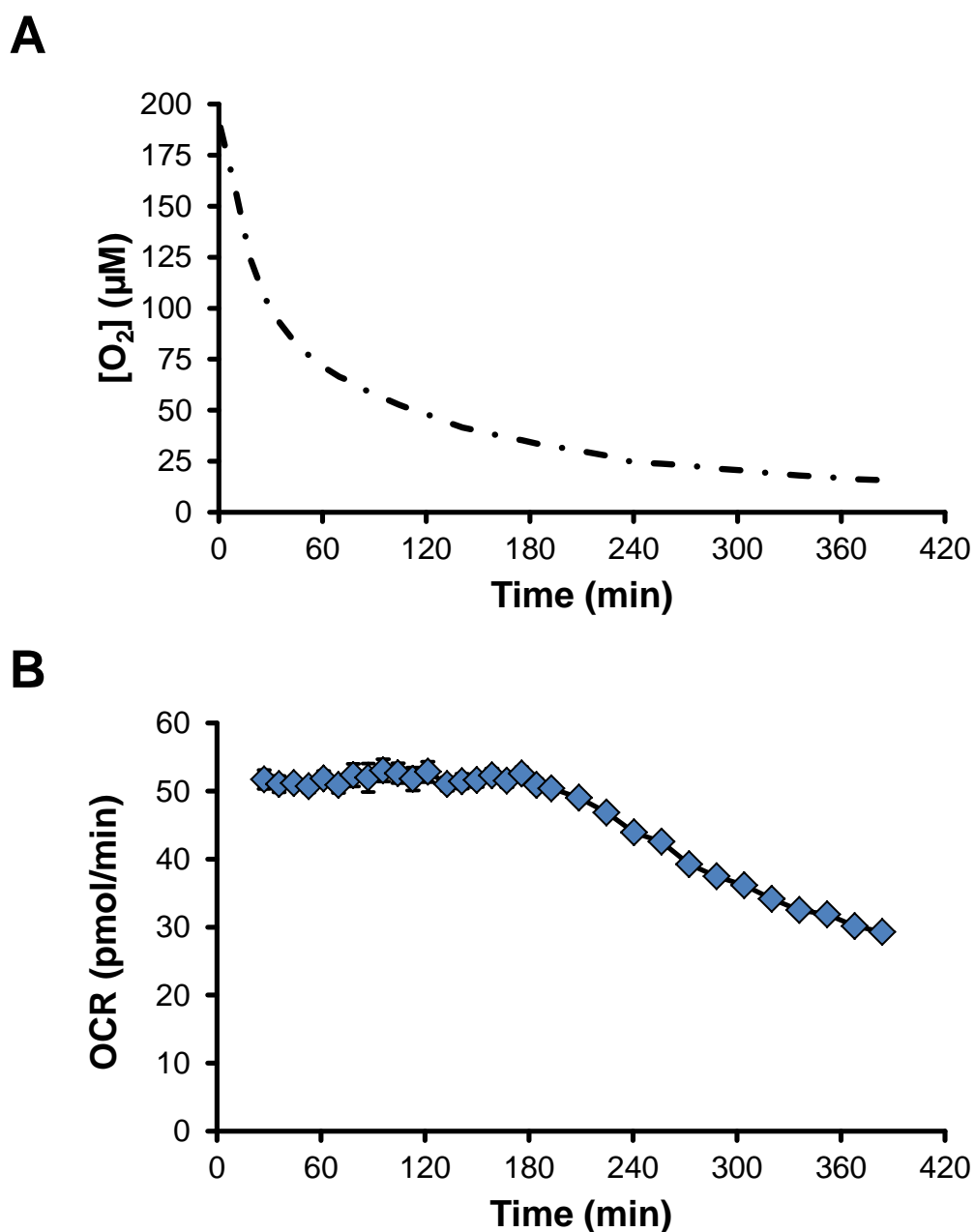


Figure 3-5. Effect of hypoxia on oxygen consumption of endothelial cells. (A) Media alone equilibrated to room air (20.9% O₂) was placed in an XF24 analyzer in a sealed glove box equilibrated to 1% O₂. The change in O₂ concentration of the media over time was measured. (B) BAEC seeded at 40,000 cells/well in a V7 microplate equilibrated to room air were placed into the XF24 in 1% O₂. The change in oxygen consumption rate (OCR) of the cells was measured over time as the O₂ concentration of the media equilibrated to 1% O₂. Results are mean ± SEM. n≥4 per group.

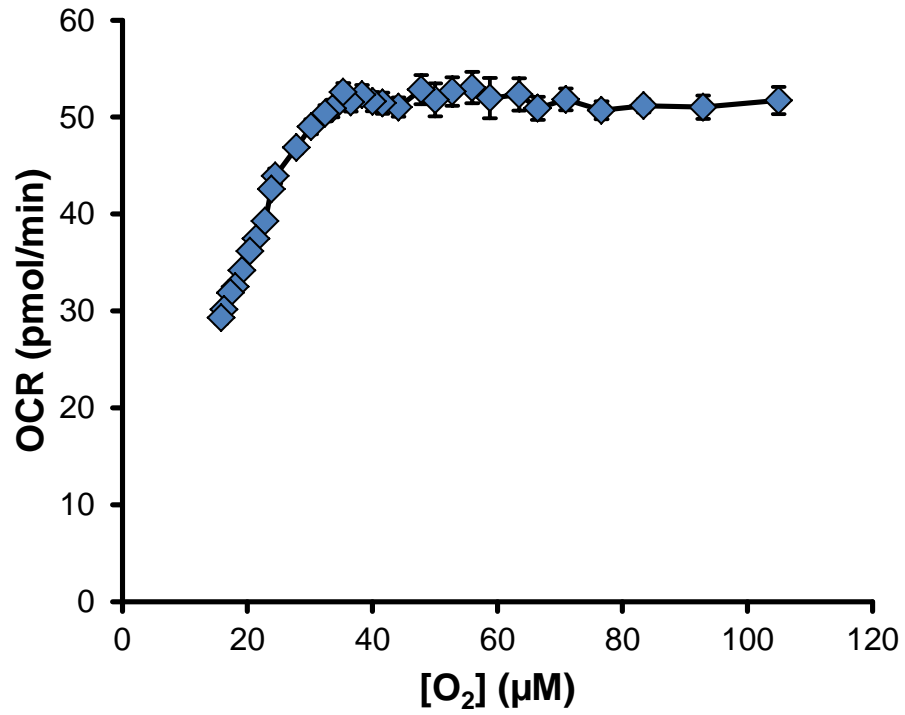


Figure 3-6. Hypoxia causes loss of oxygen consumption of endothelial cells. The change in OCR of BAEC (as seen in Figure 3-5B) was plotted as a function of the changing O₂ concentration of the media over time (as seen in Figure 3-5A). Results are mean \pm SEM. $n \geq 4$ per group.

progressive loss of mitochondrial respiration. These data conformed to saturation kinetics, with an apparent J_{\max} of 55 pmoles O_2 /min and an apparent P_{50} of 9.27 μM O_2 .

In order to determine the effect hypoxia followed by reoxygenation has on the mitochondrial function of the endothelial cells, BAEC were exposed to approximately 4.5 hr of hypoxia followed by 3.5 hr of reoxygenation in the XF24. As seen in **Figure 3-7A**, the O_2 concentration of the media decreased exponentially while equilibrating to 1% O_2 ; the media then exhibited a rapid increase in O_2 concentration when the chamber was re-equilibrated to room air (20.9% O_2). The OCR of the BAEC remained stable as the O_2 concentration of the media decreased (as seen before in **Figure 3-5**). However, when reoxygenated prior to the point at which the O_2 became limiting, the BAEC exhibited a progressive decrease in their OCR (**Figure 3-7B**). This decrease in OCR is consistent with the development of mitochondrial dysfunction, since the majority of this OCR in endothelial cells is attributed to the mitochondria O_2 consumption and is inhibitable by antimycin A.

Reactive Lipid-Induced Alterations to Endothelial Cell Bioenergetics

Ischemia/reperfusion and other vascular pathologies are associated with increased levels of lipid peroxidation, which leads to the production of reactive lipid species such as 4-hydroxy-2-nonenal (HNE) [31, 37, 298, 299, 318, 323, 324, 334, 335] (**Figure 3-8**). In order to determine the effect of HNE on endothelial cell mitochondrial bioenergetics in room air, BAEC were treated with HNE (20 μM) and the resulting alterations in the OCR were monitored over 4.5 hr (**Figure 3-9A**). In addition, the endothelial cells were also exposed to nonanal (20 μM), which is a non-reactive analog of HNE. Treatment with

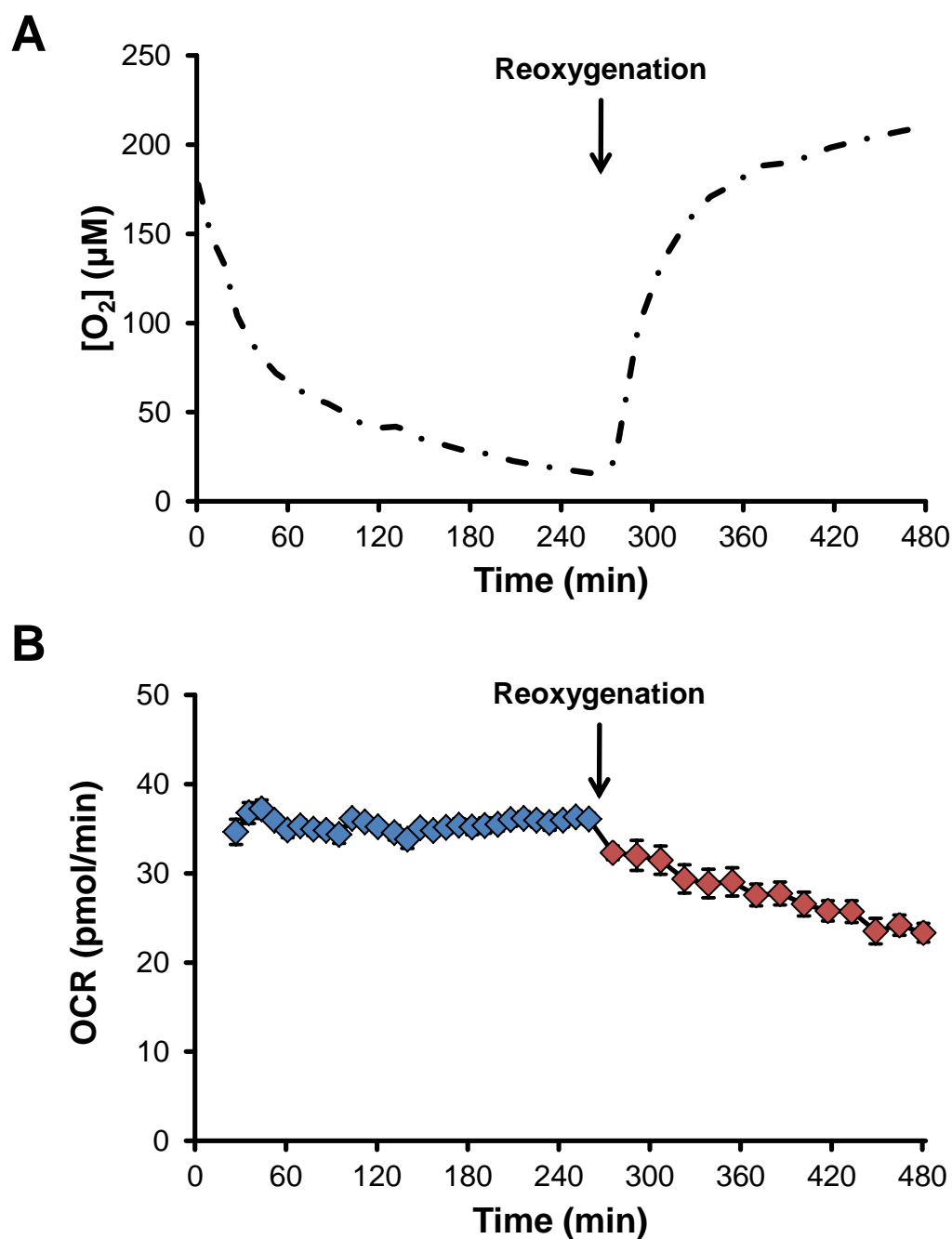
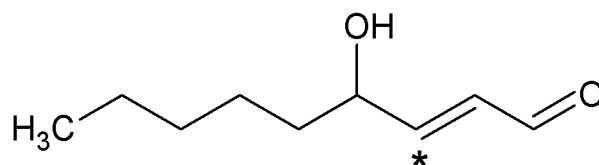
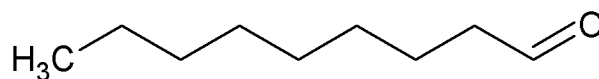


Figure 3-7. Hypoxia/reoxygenation alters oxygen consumption in endothelial cells. (A) Media alone equilibrated to room air (20.9% O_2) was placed in an XF24 analyzer in a sealed glove box equilibrated to 1% O_2 . The change in O_2 concentration of the media was monitored during the 4.5 hr exposure to hypoxia, followed by reoxygenation to room air. (B) The OCR of BAEC was monitored during the exposure to hypoxia and reoxygenation as described in (A). Results are mean \pm SEM. $n \geq 4$ per group.



4-Hydroxynonenal



Nonanal

Figure 3-8. Structures of 4-hydroxynonenal and nonanal. The structure of two lipids used in this chapter are shown. HNE has a single electrophilic carbon denoted by the asterisk due to the α,β -unsaturated carbonyl. Nonanal is a non-electrophilic 9-carbon lipid used as a structural control for HNE.

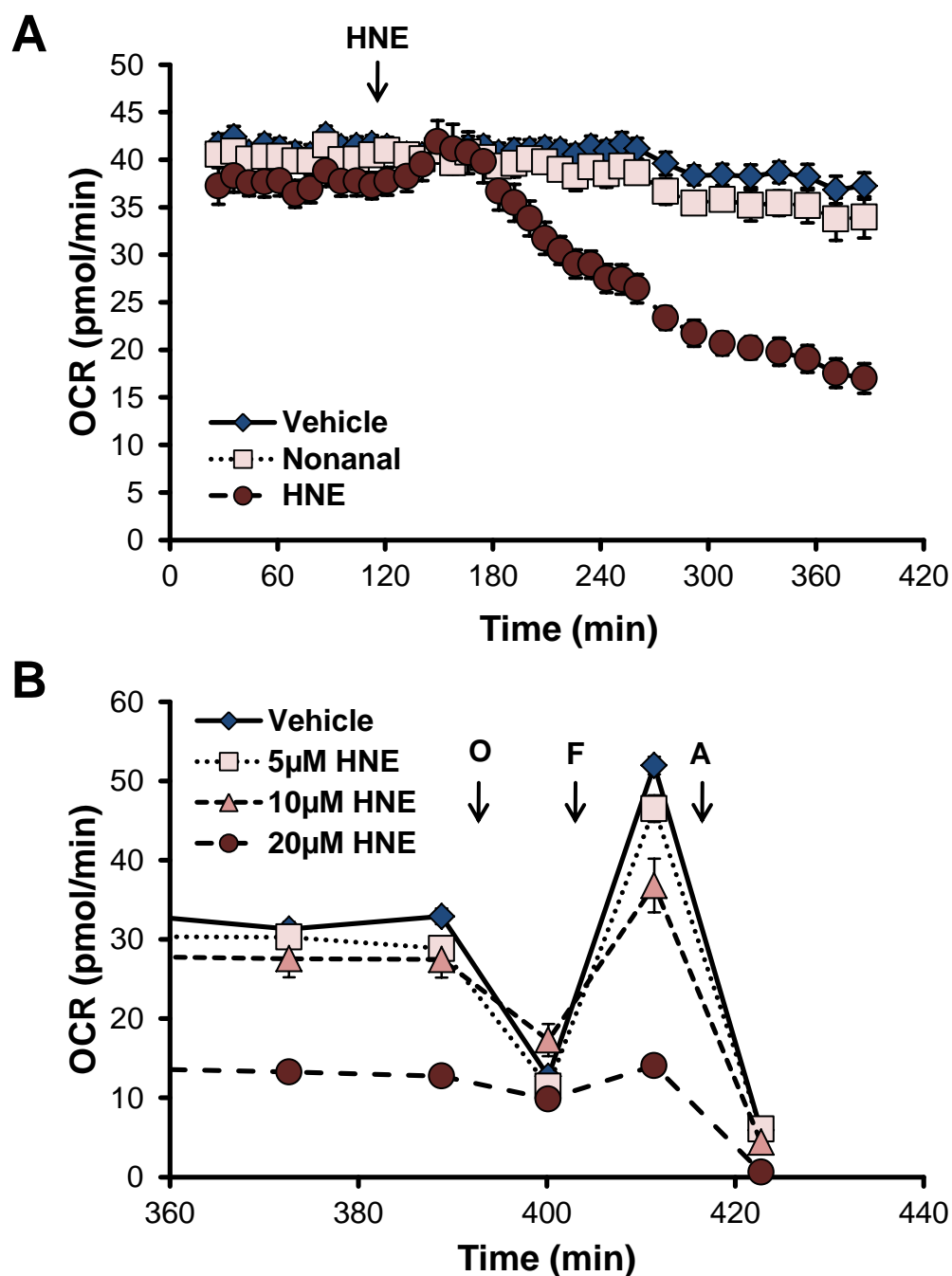


Figure 3-9. HNE alters mitochondrial function in intact endothelial cells. BAEC plated at 40,000 cells/well were placed in an XF24 analyzer to measure the OCR of the cells over time. (A) The cells were then treated with HNE (20 μ M) or nonanal (20 μ M), the unreactive analog of HNE, and OCR was monitored for 4 hr. (B) BAEC treated with HNE (5-20 μ M) for 4h followed by serial injections of oligomycin (O, 1 μ g/mL), FCCP (F, 1 μ M), and antimycin A (A, 10 μ M) to measure parameters of mitochondrial function. The graph is zoomed in to show the resulting OCR from the injections of these compounds. Results are mean \pm SEM. $n \geq 3$ per group.

nonanal or the vehicle control did not have any effect on the OCR of the BAEC; however, 20 μM HNE elicited a significant loss of mitochondrial function, as seen by the progressive decrease in the OCR. The lack of a nonanal-induced effect on OCR suggests that the loss of mitochondrial function in response to HNE exposure is due to its reactivity with proteins.

Next, alterations in the OCR of the endothelial cells were measured following the exposure to different concentrations of HNE (5-20 μM) for 4.5 hr, followed by the measurement of several parameters of mitochondrial function (as described in **Figure 3-2**). Only the highest concentration of HNE was able to elicit a significant decrease in OCR over time, so the final 60 min of the OCR trace was selected to more clearly display the differential effects of the sequential injections of oligomycin (O, 1 $\mu\text{g}/\text{mL}$), FCCP (F, 1 μM), and antimycin A (A, 10 μM) due to the exposure to HNE (**Figure 3-9B**). These values were then used to calculate the parameters of mitochondrial function in response to HNE exposure.

Exposure to HNE for 4 hr resulted in a significant, concentration-dependent decrease in the basal OCR of the BAEC (**Figure 3-10A**). This decrease in basal OCR elicited by HNE exposure was preceded by a concentration-dependent decrease in the ATP linked OCR, which was significant with the treatment of concentrations of 10 μM HNE and higher (**Figure 3-10B**). While 5 μM HNE had no effect on proton leak, both 10 μM and 20 μM HNE stimulated a significant increase in proton leak (**Figure 3-10C**). Treatment with the proton ionophore FCCP yields the maximal OCR, which is constrained by the availability of respiratory substrates and the overall capacity of the electron transport chain [179, 180, 250, 252, 330]. Similar to the effect on basal OCR, HNE was able to

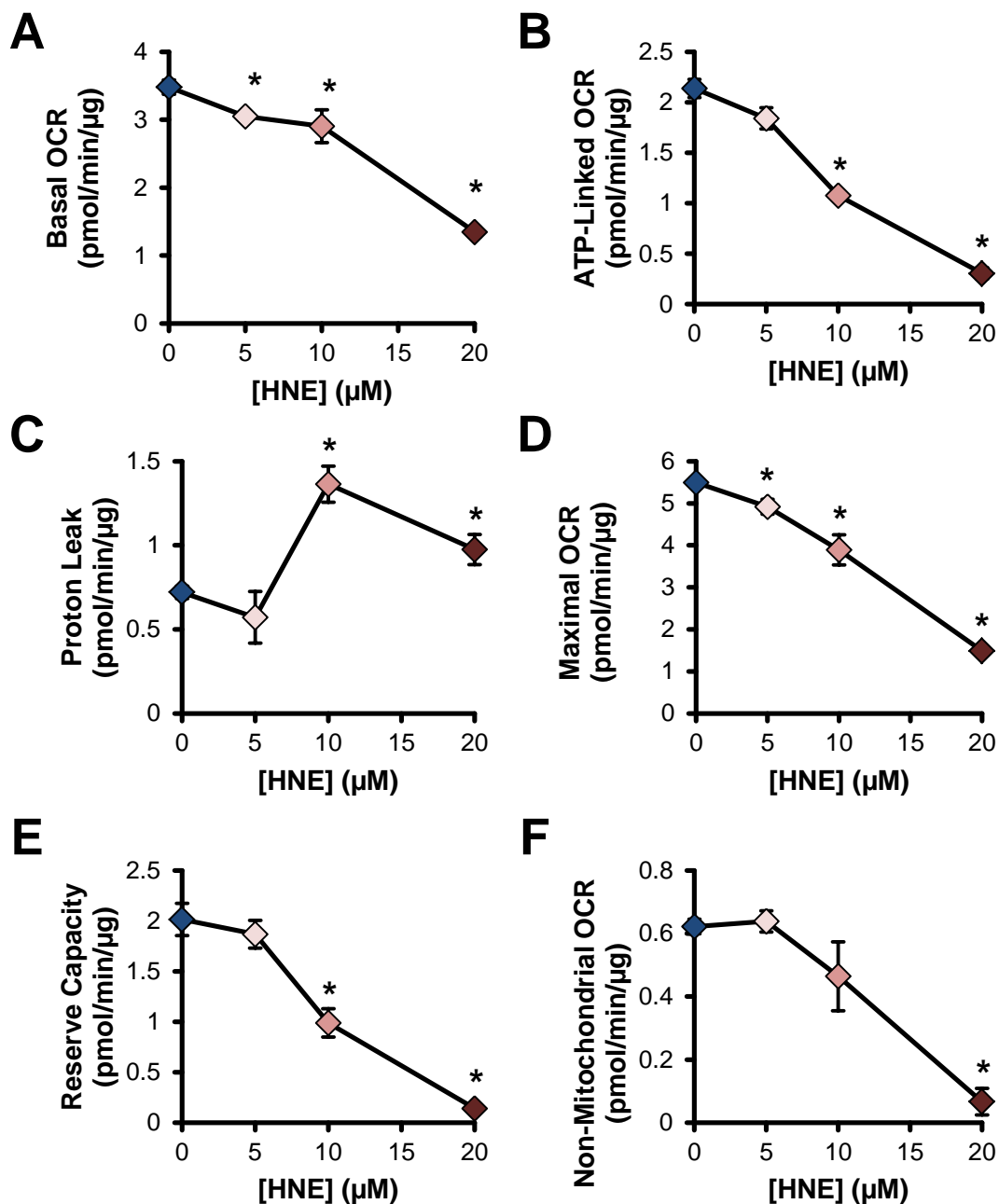


Figure 3-10. Effect of HNE on mitochondrial function in endothelial cells. Several parameters of mitochondrial function of the BAEC exposed to HNE (5-20 μM) for 4 hr were calculated from Figure 3-9B and normalized for protein (μg). (A) The basal OCR was measured prior to oligomycin injection. Oligomycin treatment allowed for the measurement of ATP-linked OCR (B) and proton leak (C). (D) Maximal OCR was determined by the injection of FCCP, and the reserve capacity was calculated as the difference between maximal and basal OCR (E). (F) The non-mitochondrial OCR is the OCR remaining after antimycin A injection. Results are mean \pm SEM. $n=5$ per group. * $p < 0.05$ compared to vehicle.

significantly diminish the maximal OCR of the endothelial cells in a concentration-dependent manner (**Figure 3-10D**). The difference between the basal and maximal OCR is termed the reserve capacity and represents the available mitochondrial function that could be utilized under conditions of increased workload or stress [179, 180, 250, 252, 330]. The reserve capacity is significantly decreased by approximately 50% following exposure to 10 μM HNE and is essentially completely diminished with 20 μM HNE (**Figure 3-10E**). These data suggest a progressive perturbation of mitochondrial function with increasing concentrations of HNE.

HNE also caused a decrease in the non-mitochondrial OCR of the BAEC, which became significant after the treatment with 20 μM HNE (**Figure 3-10F**). HNE may be eliciting the decreased non-mitochondrial OCR by either inducing cell death or by inhibiting the function of proteins other than CcOX which consume O_2 , such as xanthine oxidase or NADPH oxidase. However, because both xanthine oxidase and NADPH oxidase have been shown to be activated by HNE [336-339], this affect is likely due to the induction of cell death [340-345]. The unreactive lipid analog of HNE (nonanal) was used to verify that the effect of HNE on these parameters of mitochondrial function is due to its reactivity with nucleophiles and indeed caused no significant alterations in the O_2 consumption profile of these cells (data not shown).

Oxygen-Dependence of Endothelial Cell Bioenergetic Alterations Induced by HNE.

BAEC were next exposed to HNE (0-20 μM) while subjected to hypoxia (45 μM O_2) using the capability of the XF24 to inject compounds into the wells during the course of an experiment. The OCR of the cells were then monitored for 4 hr following HNE ex-

posure (**Figure 3-11A**). Exposure to HNE in hypoxia resulted in a concentration-dependent decrease of the OCR, with even the lowest concentration of HNE (5 μM) resulting in the slight but significant inhibition of respiration 24 min after treatment. However, after 60 min exposure to HNE, the O_2 concentration had fallen to the level where it limited OCR in the control and, after a further period of 60 min, the rates of OCR in all samples became identical.

To test the possibility that the inhibitory effects of HNE on the parameters of mitochondrial function were altered by decreasing the O_2 concentration, the mitochondrial functionality test was performed at 384 min, corresponding to the O_2 concentration of 16 μM (**Figure 3-11B**). The responsiveness to the mitochondrial inhibitors showed a similar OCR profile in hypoxia as was obtained in room air (**Figure 3-2,3-9B**). Interestingly, the exposure of BAEC to HNE (0-20 μM) in hypoxia resulted in no changes in the basal OCR of the cells after 4 hr (**Figure 3-12A**). This was due to the significant decrease in the ATP-linked OCR with 10 and 20 μM HNE treatment (**Figure 3-12B**) and the simultaneous increase in the proton leak of the BAEC at the same HNE concentrations (**Figure 3-12C**). These higher concentrations of HNE also caused a significant decrease in maximal OCR and reserve capacity (**Figure 3-12D,E**), suggesting that although HNE did not affect the basal OCR of the cells, it was causing them to be more susceptible to damage from increased ATP demand or stress, such as would occur upon reoxygenation. Furthermore, only 20 μM HNE treatment in hypoxia was able to slightly decrease the non-mitochondrial OCR compared to vehicle control, while the lower concentrations of HNE were not significantly different (**Figure 3-12F**), contrasting with the effects in room air, where HNE caused a large decrease in the non-mitochondrial OCR.

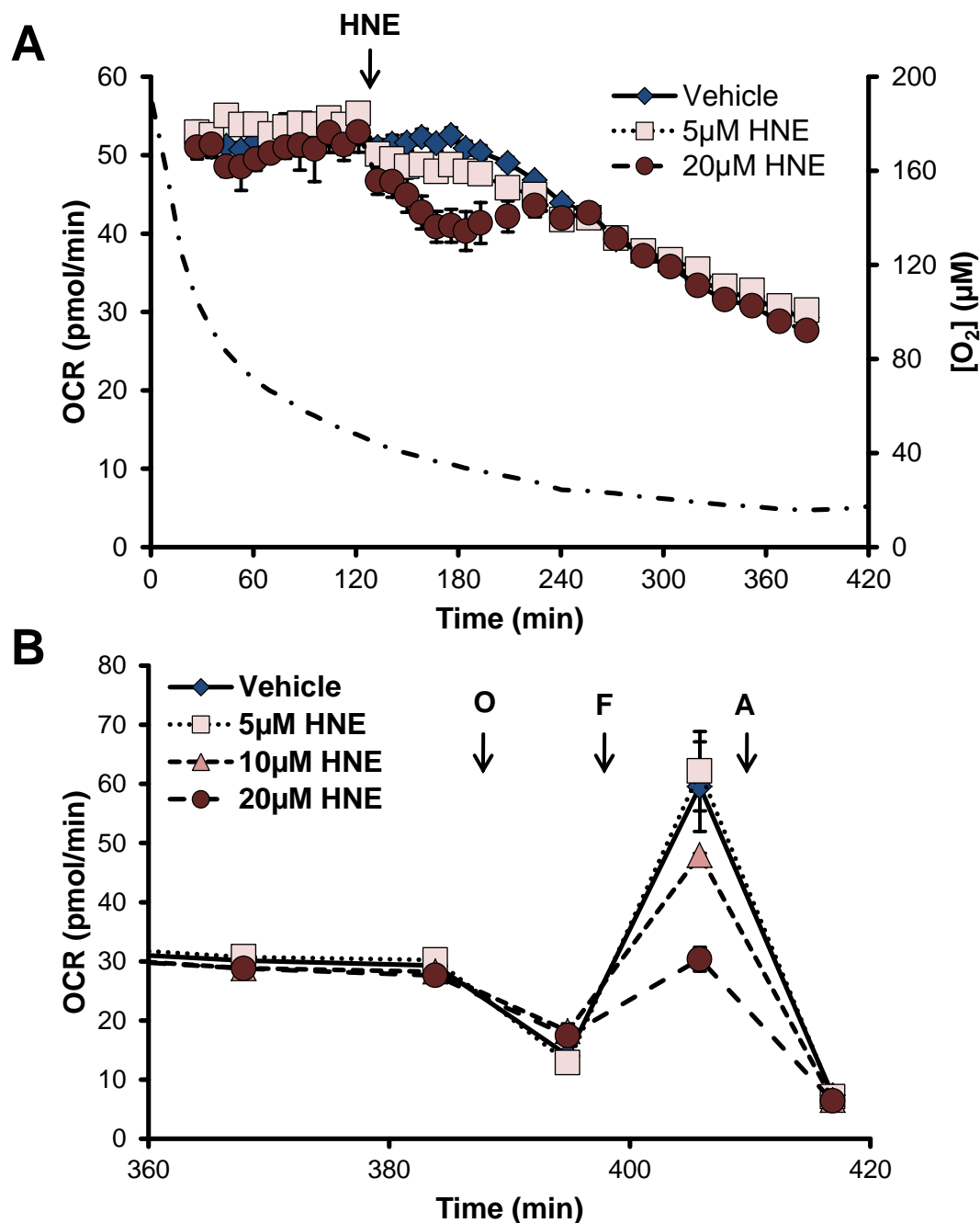


Figure 3-11. Bioenergetic response of endothelial cells to HNE exposure in hypoxia. (A) BAEC seeded at 40,000 cells/well were exposed to hypoxia with HNE treatment (5-20 µM) after 2 hr with continued OCR measurement for 4 hr. The dotted line represents the [O₂] of the media. (B) Parameters of mitochondrial function were examined after the 4 hr exposure of the BAEC to HNE in hypoxia using sequential injections of oligomycin (O, 1 µg/mL), FCCP (F, 1 µM), and antimycin A (A, 10 µM). The graph is zoomed in to show the last five OCR measurements resulting from the injections of these compounds. Results are mean ± SEM. n≥3 per group.

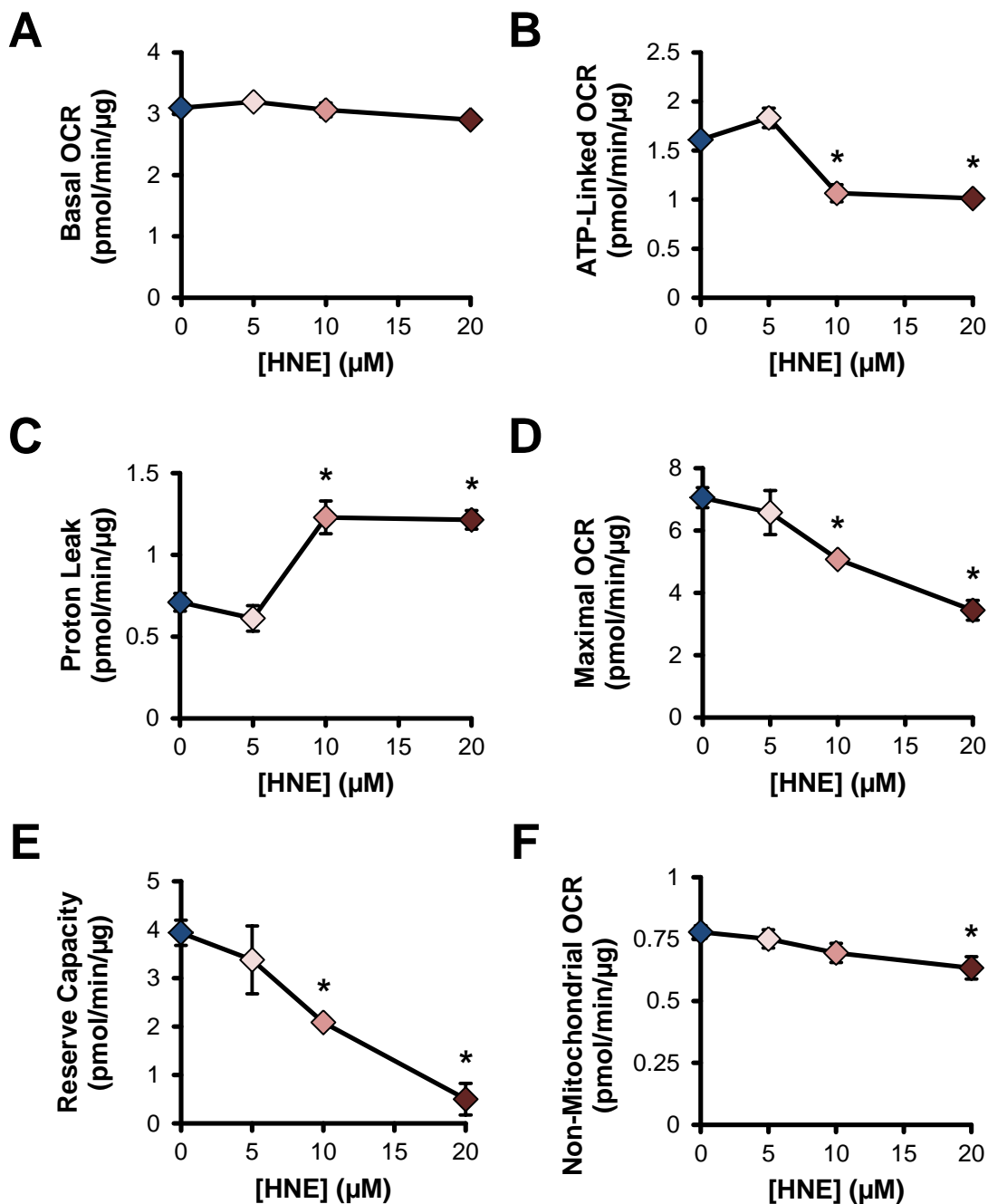


Figure 3-12. Effects of HNE exposure in hypoxia on mitochondrial function. Parameters of mitochondrial function were calculated using the OCR traces in Figure 3-11B normalized to total protein (μg). (A) The basal OCR was measured prior to oligomycin injection. Oligomycin allows for the measurement of ATP-linked OCR (B) and proton leak (C). (D) Maximal OCR was determined by the injection of FCCP, and the reserve capacity was calculated as the difference between maximal and basal OCR (E). (F) The non-mitochondrial OCR is the OCR remaining after antimycin A injection. Results are mean ± SEM. n ≥ 3 per group. *p > 0.05 compared to vehicle.

To verify that the differences in the alteration of mitochondrial function by HNE in room air and hypoxia were not due to different levels of protein-HNE adduct formation, the total cell lysates were taken at the conclusion of the experiment and were analyzed for protein-HNE adducts by Western blotting (**Figure 3-13A**). Treatment with increasing concentrations of HNE resulted in a significant increases in protein-HNE adducts in BAEC in both room air and hypoxia (**Figure 3-13B**). Interestingly, the differential effects of HNE on the mitochondrial function of the BAEC in room air and hypoxia was independent of protein-HNE adduct formation, as there was no difference in the adduct formation between the different groups.

Exacerbation of Reoxygenation-Induced Loss of Mitochondrial Function by HNE

Ischemia/reperfusion injury is known to induce an increase in oxidative stress and lipid peroxidation [31, 37, 202, 271, 272, 285, 298, 299, 311, 346-348]. This results in the exposure of the endothelium to lipid peroxidation products, such as HNE. In order to determine the effect that HNE has on the mitochondrial function in the endothelium, BAEC were exposed to 4.5 hr of hypoxia followed by 3.5 hr of reoxygenation in the XF24 analyzer. The OCR of the BAEC remained stable as the media became hypoxic (as seen before in **Figure 3-7B**); however, when reoxygenated the BAEC exhibited a progressive decrease in their OCR (**Figure 3-14**). This decrease in OCR is representative of the progressive development of mitochondrial dysfunction, since the majority of this OCR is attributed to the mitochondria and is inhibitable by antimycin A.

Furthermore, when the BAEC were exposed to HNE (20 μ M) under hypoxia for 2.5 hr followed by 3.5 hr of reoxygenation, the cells exhibited a more rapid decrease in

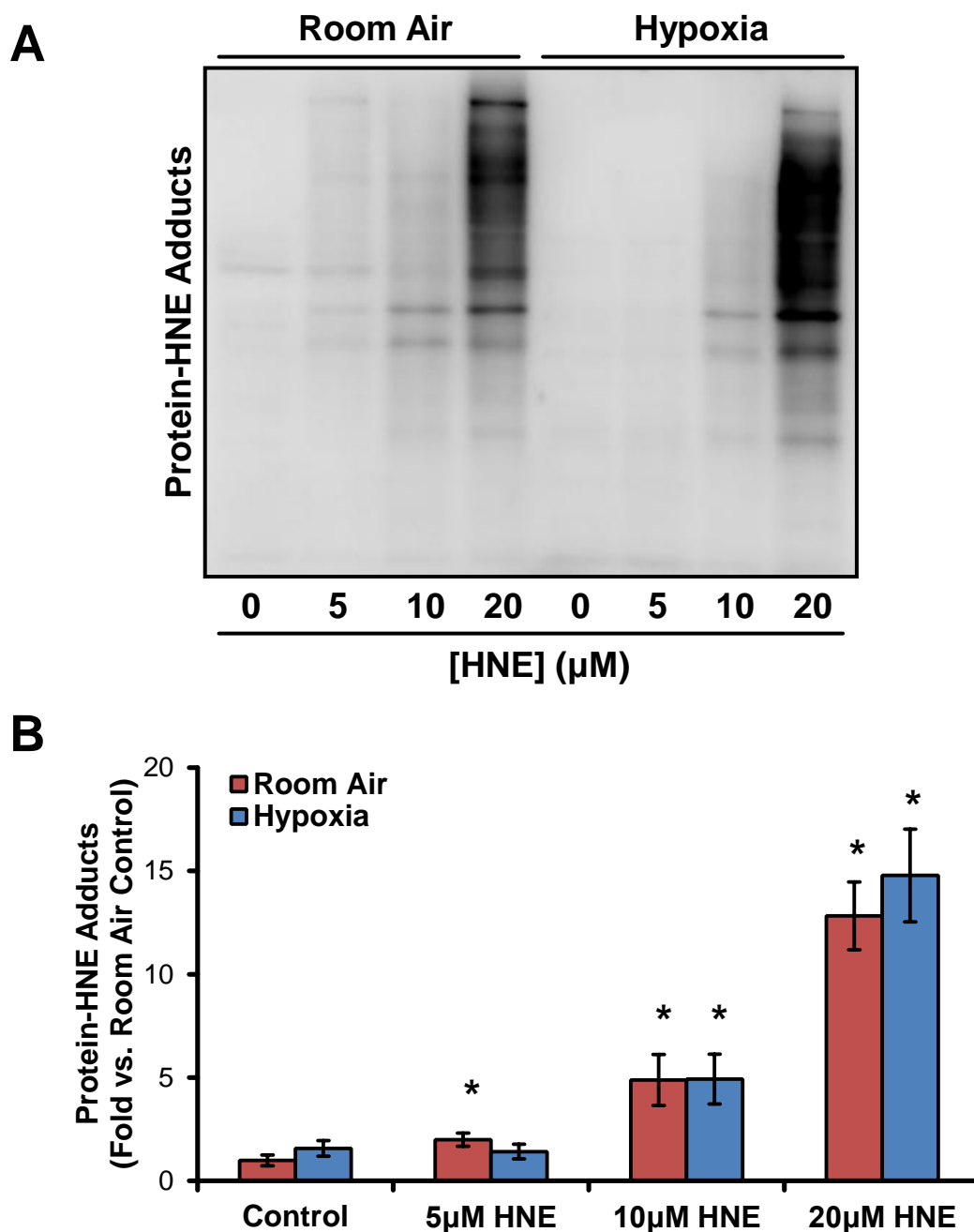


Figure 3-13. Protein-HNE adduct formation after exposure to HNE in both hypoxia and room air. (A) BAEC were exposed to HNE (5-20 μM) in both room air and hypoxia for 4 hr. The resulting lysates were then separated by SDS-PAGE, transferred to PVDF, and probed using an anti-protein-HNE adduct antibody. (B) Quantification of protein-HNE adduct densitometry normalized to room air control. Results are mean \pm SEM. $n=5$ per group. * $p>0.05$ compared to room air control.

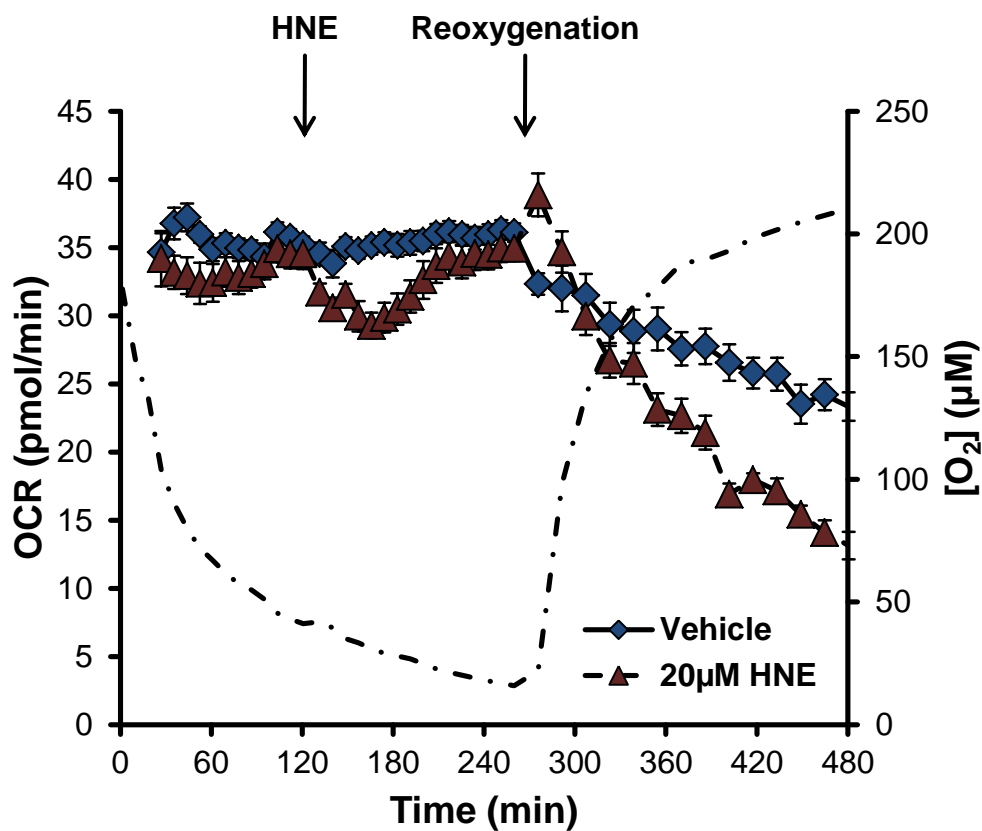


Figure 3-14. HNE exacerbates reoxygenation injury in endothelial cells. The change in OCR over time of BAEC seeded at 40,000 cells/well in response to exposure to HNE (20 µM) or vehicle in hypoxia for 2 hr, followed by re-equilibration to room air for 4 hr. The change in O₂ concentration over time is designated by the dotted line. Results are mean ± SEM. n≥3 per group.

their OCR compared to the vehicle control. Taken together, these data suggest that even though HNE does not seem to significantly alter the basal OCR of the BAEC under hypoxia, when the cells are reoxygenated, the protein-HNE adducts which were formed during hypoxia result in the exacerbated loss of mitochondrial function compared to BAEC exposed to HNE in room air (**Figure 3-9**).

Assuming that the progressive loss of OCR seen in response to reoxygenation and HNE is attributable to the loss of bioenergetic function, calculating the derivative of the decreasing OCR allows for a quantitative measurement of the development of mitochondrial damage (**Figure 3-15**). Exposure to 20 μM HNE in room air resulted in an approximately 3-fold increase of bioenergetic dysfunction as compared to the room air control, while HNE treatment in hypoxia induced a slight, yet significant, increase in this parameter as compared to the hypoxia control. Moreover, BAEC exposed to hypoxia exhibited a significantly increased loss of OCR compared to cells in room air, due to the decreasing OCR as the O_2 concentration became limiting. Furthermore, endothelial cells exposed to hypoxia/reoxygenation displayed a further exacerbation of the loss of mitochondrial function. This result is likely due to reoxygenation injury, which is associated with the increased formation of ROS, RNS, and RLS leading to mitochondrial damage. Finally, the exposure of 20 μM HNE to BAEC in hypoxia followed by reoxygenation resulted in a substantial induction of bioenergetic dysfunction.

The extensive loss of mitochondrial function which is exhibited by BAEC with the combination of HNE and reoxygenation supports the “two-hit hypothesis” in which the first “hit” is HNE, which lowers the reserve capacity of the cells, rendering the BAEC more susceptible to further stress [258]. The reoxygenation-induced damage then acts as

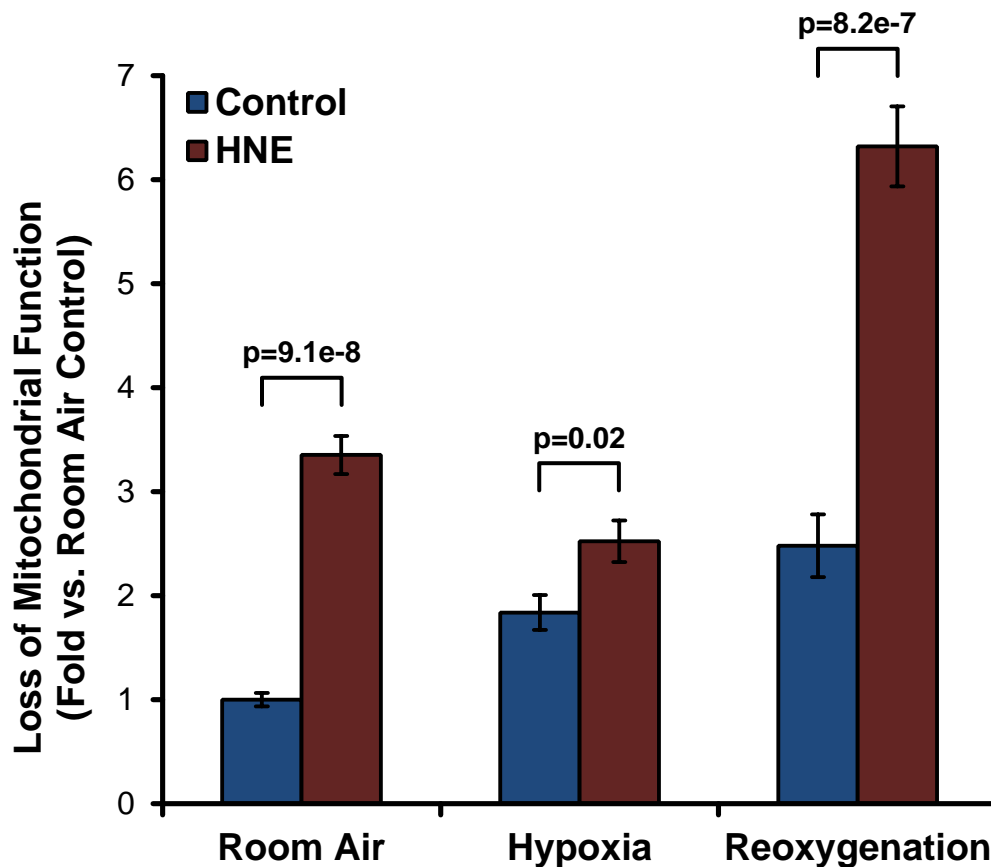


Figure 3-15. Mitochondrial damage in endothelial cells induced by changing oxygen concentrations and HNE exposure. The decrease in OCR of BAEC over time following exposure to HNE (20 μ M) or vehicle control in room air, hypoxia, and hypoxia/reoxygenation was calculated from Figures 3-9, 3-11, and 3-14, respectively. Mitochondrial damage was determined by calculating the derivative of the slope of the change of OCR from each group and normalizing by the room air control. Results are mean \pm SEM. $n \geq 3$ per group.

the second “hit,” resulting in the development of mitochondrial dysfunction that would lead to cell and potentially organ failure *in vivo*.

DISCUSSION

The data presented in this chapter demonstrate that BAEC were able to maintain consistent and stable respiration over several hours while in room air (**Figure 3-4**); however, upon exposure to hypoxia, the BAEC exhibited an O₂ concentration-dependent decrease in mitochondrial function, which conformed to saturation enzyme kinetics, with an apparent J_{max} of 55 pmoles O₂/min and a P₅₀ of 9.27 μM O₂. (**Figure 3-5,3-6**). Furthermore, BAEC subjected to 4.5 hr of hypoxia followed by reoxygenation exhibited a progressive loss of mitochondrial function over time, likely mimicking the phenomenon of reperfusion injury which involves the generation of ROS and the development of mitochondrial dysfunction [31, 204, 207, 213, 215, 299].

HNE is a reactive lipid peroxidation product which is formed in high concentrations in response to increased oxidative stress due to ischemia/reperfusion and other pathologies associated with oxidative stress [324, 341, 344]. The effect of HNE on endothelial cell bioenergetics was then examined under conditions of varying O₂ tensions. Exposure to HNE in media equilibrated to room air for 4 hr resulted in a significant, concentration-dependent decrease in the basal OCR of the BAEC (**Figure 3-10A**). Interestingly, this result differs from the HNE-induced effects of HNE on neonatal rat ventricular myocytes (NRVM), in which their OCR is stimulated by HNE [179]. While the mechanism underlying these unique bioenergetic responses to HNE exposure is not yet clear, it is likely mediated by the fact that cardiomyocytes have a much higher maximal

OCR and reserve capacity than BAEC [179, 180, 330, 349], possess higher levels of creatine kinase [84, 86, 350, 351], and contain myoglobin [352-354], all of which have been shown to be modulated by the exposure to HNE and other reactive lipid species [179, 322, 355-364]. Furthermore, HNE exposure resulted in a concentration-dependent progressive loss in all parameters of mitochondrial function, with the exception that the higher concentrations of HNE significantly induced proton leak (**Figure 3-8,3-9**).

Exposure of BAEC to HNE in decreasing O₂ tensions caused a transient HNE concentration-dependent loss of OCR that persisted until the O₂ concentration decreased to 24 μM, at which point there were no further differences in OCR between vehicle- and HNE-treated BAEC (**Figure 3-11**). Interestingly, HNE treatment in hypoxia elicited similar changes in the parameters of mitochondrial function as in room air, with a significant decrease in ATP-linked OCR, maximal OCR, and reserve capacity and an increase in proton leak; however, HNE treatment in hypoxia elicited no change in basal OCR after 4 hr (**Figure 3-12**). These differences are not due to alterations in the formation of protein-HNE adducts, as there was no significant difference in the levels of adducts formed (**Figure 3-13**).

Importantly, FCCP was able to stimulate an increased OCR in the vehicle control endothelial cells in hypoxia, indicating that the progressively decreasing OCR was not due solely to the limited availability of O₂ to CcOX. FCCP uncouples the mitochondria by diminishing the proton gradient across the mitochondrial inner membrane. This electrochemical proton gradient is a major source of control over the activity of CcOX, and now that it has been decreased by FCCP, CcOX doesn't have a strong electrochemical gradient against which it must pump protons. This thereby increases CcOX activity to a

rate that is then limited by the availability of O₂ and electrons from cytochrome *c* [365-372].

Because 20 μM HNE was shown to decrease the reserve capacity in both room air and hypoxia, it was predicted that HNE would exacerbate the reoxygenation damage seen in BAEC. Indeed, BAEC treated with HNE in hypoxia again only saw a transient change in OCR; however, when the cells were reoxygenated, the BAEC treated with HNE exhibited a significantly higher rate of loss of OCR, signifying the loss of mitochondrial function (**Figure 3-13, 3-14**).

Taken together, the data discussed in this chapter evaluate the dependence of the OCR of endothelial cells on the O₂ concentration of the media, as well as the ability to measure the effects of reoxygenation injury on bioenergetic function in real time. The development of this model can be used to further elucidate the mechanisms by which hypoxia/reoxygenation can alter cellular bioenergetics, and can also be applied to the studies of other pathologies which are associated with changes in O₂ availability such as ALD or myocardial infarction.

CHAPTER 4

MITOCHONDRIAL HAPLOTYPE DETERMINES SUSCEPTIBILITY TO CARDIOMYOCYTE DYSFUNCTION RESULTING FROM CARDIAC VOLUME OVERLOAD

INTRODUCTION

Cardiovascular diseases are the leading cause of mortality in the United States, resulting in over 800,000 deaths per year; moreover, approximately 7% of these deaths are attributed to heart failure [52, 53]. A major cause of heart failure is left ventricular volume overload caused by mitral regurgitation (MR), which progresses to heart failure through three stages: acute, chronic compensated, and chronic decompensated [373-375] (**Figure 4-1**). In patients with acute MR, the LV develops volume overload because with each contraction it must pump the volume of blood that goes into the aorta in addition to the blood that leaks back into the left atrium [216, 376, 377]. This increase in stroke volume causes the progressive increase in LV volume, resulting in LV dysfunction and heart failure.

Effects of Volume Overload on Cardiomyocyte Mitochondria

During the progression to heart failure, alterations occur in mitochondrial bioenergetics through several mechanisms. [17, 27, 46, 47, 217, 221, 378-386]. Volume overload is associated with an increased workload on the myocardium, resulting in a greater utilization of ATP and yielding increased levels of AMP and ADP [387-391].

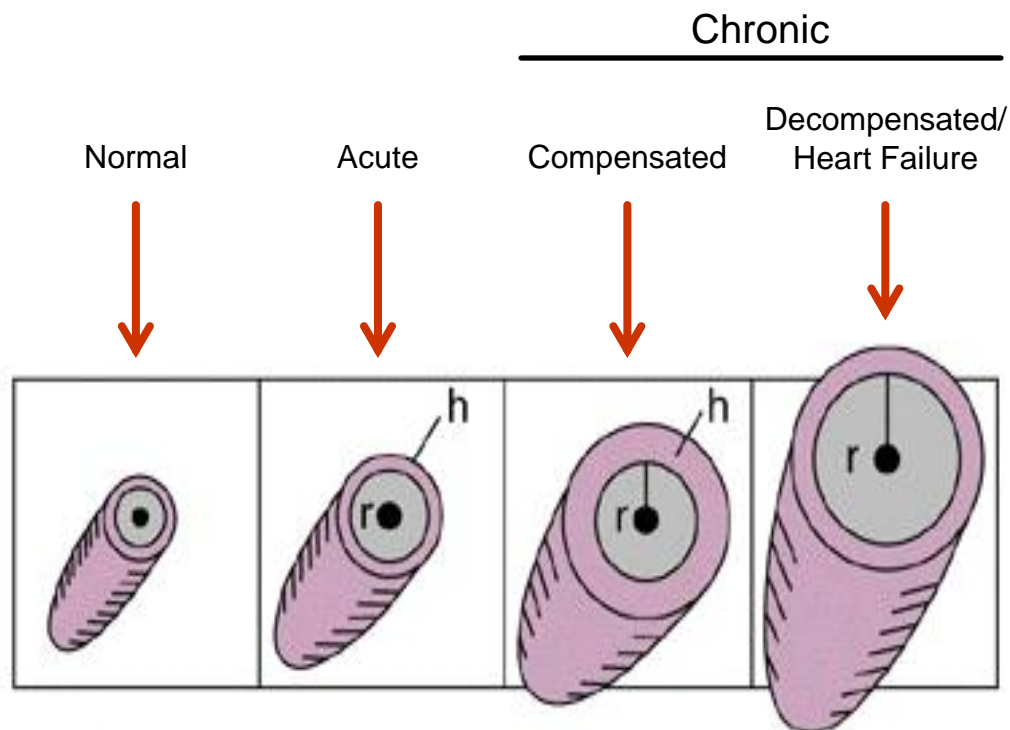


Figure 4-1. The disease progression of volume overload leading to the development of heart failure. Volume overload occurs as the left ventricular preload increases due to mitral valve insufficiency. This disease progression occurs through three stages: acute, compensated, and heart failure. During the acute stage of volume overload there is an increase in LV volume, which is accompanied by the stretching of the LV wall and the moderate loss of cardiac function. As the volume of the LV continues to increase over time, the LV wall thickens to compensate, improving cardiac function. Eventually the LV can no longer compensate for the still increasing LV volume, at which point there is cardiomyocyte dysfunction and the loss of cardiac function, resulting in heart failure.

These can be degraded through purine catabolism to form xanthine and hypoxanthine, which act as substrates for xanthine oxidase to produce superoxide and hydrogen peroxide [220-222, 387, 388]. These ROS, alone or in combination with $\cdot\text{NO}$ to produce RNS, lead to the oxidative damage of cellular proteins, particularly those in the mitochondria which are known to be a target of ROS [87, 374]. This causes mitochondrial dysfunction, which manifests as a decrease in ATP production along with an increase in the production of ROS by the mitochondria. The increase in mitochondrial ROS and the decrease in the ATP/ADP ratio result in the further induction of bioenergetic and myocyte dysfunction, because there is insufficient ATP to meet the demand of the cell [27, 384].

Another mechanism by which volume overload leads to alterations in mitochondrial bioenergetics is through the disruption of the desmin cytoskeleton [223, 224]. Desmin is known to play a role in the maintenance of cardiomyocyte organization and has also been shown to regulate mitochondrial bioenergetics [49, 50, 392, 393]. In addition to the alterations in mitochondrial function induced by the loss of desmin in the progression towards heart failure, bioenergetic dysfunction has also been shown to occur due to the disruption of energy transfer pathways between the mitochondria, the sarcoplasmic reticulum, and the sarcomeres [49, 350, 351, 380, 393-397]. The maintenance of cardiomyocyte contraction and relaxation is dependent upon efficient myofibrillar function and the sarcoplasmic reticulum calcium ATPases, both of which require high ATP/ADP ratios to function properly [84, 398].

It has become increasingly apparent through the last few decades that alterations in mitochondrial and cellular bioenergetics play a central role in the progression towards heart failure. The studies of the mechanisms by which this occurs most often focus on

the increased energetic demands, increased oxidative stress, loss of cytoskeletal regulation, and the disruption of energy transfer pathways. However, recent studies have shown that differences in mitochondrial efficiency and ROS formation caused by distinct mtDNA haplotypes can alter the susceptibility to several pathologies associated with mitochondrial dysfunction [54-56, 58-60]. The relationship between mtDNA and volume overload have not been studied. Therefore, the focus of this chapter is to determine if different mtDNA haplotypes can influence the susceptibility to bioenergetic dysfunction induced by volume overload.

Elucidating Role of mtDNA Haplotype on Susceptibility to Volume Overload

Mammalian mtDNA is a circular double-stranded DNA molecule of approximately 16,000 base pairs which encodes for 13 peptide subunits of different complexes of the mitochondrial electron transport chain, as well as 2 rRNAs and 22 tRNAs [20, 139, 143, 399-403]. Using recent advances in DNA sequencing over the last 30 years, phylogenetic trees have been developed tracing the ancestry of populations of inbred mouse strains based on polymorphisms in their mtDNA sequence [399-402, 404-406]. These different populations with common mtDNA polymorphisms are grouped into mtDNA haplogroups. Many mtDNA haplogroups are known to have different susceptibilities to pathologies associated with alterations in mitochondrial function, which has been suggested to be mediated by their distinct bioenergetic efficiencies and mitochondrial ROS formation [54-56, 58-60].

In order to test the hypothesis that mtDNA haplotype plays a role in the susceptibility to volume overload-induced bioenergetic dysfunction, C57BL/6 and C3H/HeN

mouse strains were selected due to their different mtDNA haplotypes and known susceptibilities to several pathologies [407-419] (**Figure 4-2**). C57BL/6 mice are known to be susceptible to models of cardiovascular diseases, inflammation, obesity, and diabetes, while C3H/HeN mice have been shown to be very resistant to models of these diseases [409, 414-416, 418]. The studies which have elucidated these differences in disease susceptibilities have focused primarily on inter-strain nuclear DNA (nDNA) polymorphisms with the goal of describing the gene or genes that mediate this altered susceptibility, particularly in the context of atherosclerosis [415-419]. For example, many investigators have used the C3H/HeJ strain for studies of atherosclerosis, which, unlike C3H/HeN mice, are Toll-like receptor-4 (Tlr4) deficient due to a missense mutation in the third exon of the Tlr4 gene [420-423]. Because Tlr4 is known to play a critical role in the innate immune response and inflammation, in part through modulating the release of tumor necrosis factor- α (TNF- α) and interleukin-1 β (IL-1 β), the deficiency of Tlr4 can readily modulate the development of atherosclerosis and other inflammatory diseases [424-426]. Importantly, using C3H/HeN mice allows for the elimination of the lack of Tlr4 as a potential variable which likely alters disease susceptibility.

A mechanism which could likely mediate these observed differences in disease susceptibility that has been largely overlooked in the literature is the potential role of differences in mtDNA sequences, which are known to modulate mitochondrial bioenergetics [54, 56, 59, 60, 406, 427]. Importantly, the two mouse strains studied in this chapter have different mtDNA haplotypes due to the presence of a single-nucleotide polymorphism (SNP) in the genes which encode for CcOX subunit III (CcOX-III), Complex I subunit III (NDIII), and the mitochondrial tRNA for arginine (mt-tRNA^{Arg}) [400, 401].

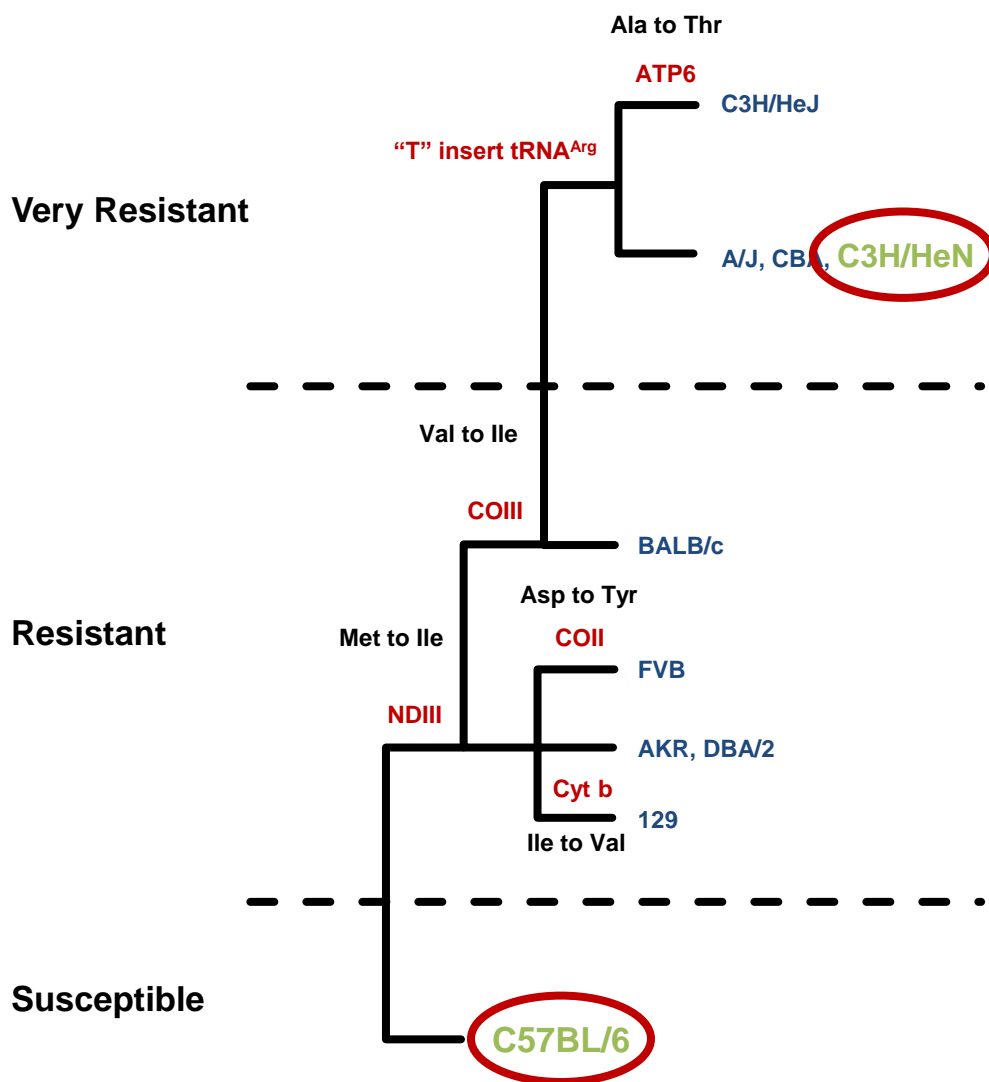


Figure 4-2. Differences in mtDNA haplotype between different strains of mice. Different strains of mice possess different mtDNA haplotypes as shown above. Moreover, the mice strains cluster both based upon their differences in mtDNA and their relative susceptibilities to atherosclerosis, hypertension, ischemia/reperfusion, and diabetes. The strains of mice used in this dissertation are the C57BL/6, which are the most susceptible, and C3H/HeN mice, which are the most resistant.

The mitochondrial genotypic difference in CcOX-III likely alters the bioenergetic efficiency and ROS production of the mitochondria because CcOX-III is part of the catalytic core of CcOX, where it mediates electron transfer to O₂ and proton pumping from the matrix to the intermembrane space [428]. The SNP in the gene which codes for the mt-tRNA^{Arg} may also mediate any differences in phenotype, as previous studies have shown that mutations in this gene can induce mitochondrial defects [429-431].

In order to separate the role of the mtDNA haplotype from the effects of the nuclear genome, mitochondria-nuclear exchange (MNX) mice were developed. These MNX mice express the nDNA of one strain and the mtDNA of the other. The utilization of the MNX mice allows for the segregation of effects with either the nDNA or mtDNA.

MATERIALS AND METHODS

Reagents

All chemicals were purchased from Sigma-Aldrich (St.-Louis, MO) unless stated otherwise and were of the highest grade available.

Generation of Mitochondria:Nuclear Exchange (MNX) Mice

C57BL/6 and C3H/HeN mice were used to create mitochondria:nuclear exchange (MNX) mice, in which the resulting MNX mice have the nDNA of one strain and the mtDNA of the other strain (**Figure 4-3**). This was achieved by enucleating the embryos of both strains leaving embryos with the mitochondria, and thus mtDNA, of the parent strain but with no nucleus. A removed nucleus from one strain was then transferred into

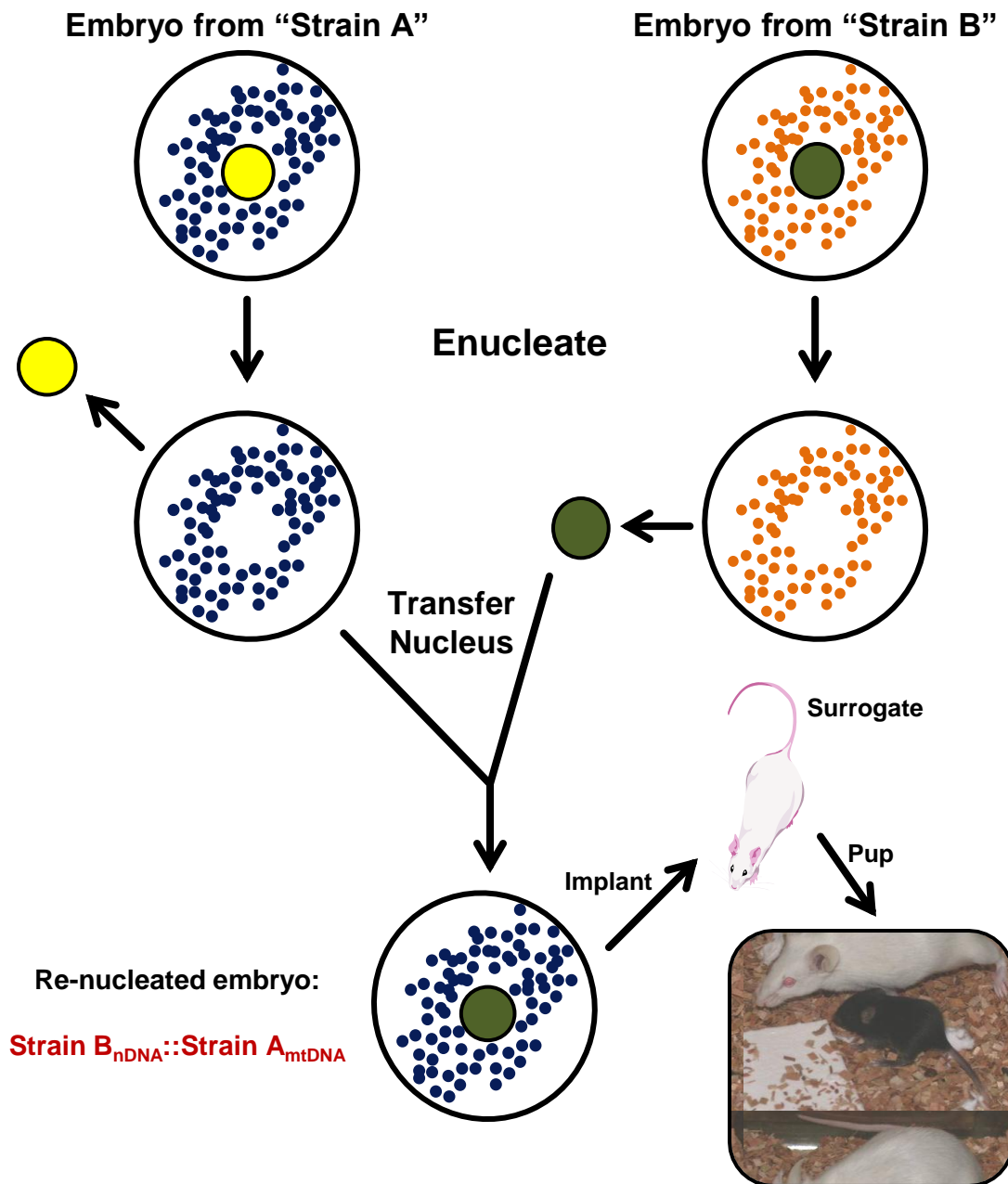


Figure 4-3. Generation of mitochondria:nuclear exchange (MNX) mice. MNX mice were created by enucleating an embryo from "Strain A" and replacing the removed nucleus with a nucleus from an embryo from "Strain B." The re-nucleated embryo still contains the mitochondria, and thus the mtDNA, from "Strain A" while now having the nucleus and nDNA from "Strain B." This new MNX mouse strain is therefore denoted as Strain B_{nDNA}::Strain A_{mtDNA}. The opposite MNX mouse strain is also made, which would be Strain A_{nDNA}::Strain B_{mtDNA}. The two strains utilized to produce the MNX mice used in this study were C57BL/6 and C3H/HeN mice, but this method could be applied to other strains of mice as well.

an enucleated embryo of the other strain, resulting in the formation of an embryo with the mtDNA of one strain and the nDNA of the other strain (**Table 4-1**).

Strain	nDNA	mtDNA
C57BL/6	C57BL/6	C57BL/6
C3H/HeN	C3H/HeN	C3H/HeN
C57 _n ::C3H _{mt}	C57BL/6	C3H/HeN
C3H _n ::C57 _{mt}	C3H/HeN	C57BL/6

Table 4-1. Mouse strains utilized for studies of susceptibility to volume overload. C57BL/6 and C3H/HeN mice were used for all studies. In addition, two novel strains of MNX mice were generated and used herein. C57_n::C3H_{mt} mice contain the nDNA of a C57BL/6 mouse and the mtDNA of a C3H/HeN mouse. C3H_n::C57_{mt} mice contain the nDNA of a C3H/HeN mouse and the mtDNA of a C57BL/6 mouse. MNX mice were developed by S.W. Ballinger.

Aortocaval Fistula Surgery

C57BL/6, C3H/HeN, C57_n::C3H_{mt} MNX, and C3H_n::C57_{mt} MNX male mice (18-24 weeks) were used for volume overload studies. An aortocaval fistula (ACF) was surgically created as described previously [432-434] (**Figure 4-4**). Briefly, ACF and sham operations were performed under sterile conditions on all three strains of mice at 18 to 24 weeks of age. With mice under isoflurane anesthesia, the abdominal cavity was opened via a midline incision, and a fistula was created between the abdominal aorta and the inferior vena cava. Induced sham and ACF mice were sacrificed 3 days after surgery, at which point the hearts were excised and used for the isolation of cardiomyocytes for bioenergetic measurements, Western blot, and mitochondrial enzyme activity assays or for LV sections for transmission electron microscopy, *in situ* zymography, and immunohistochemistry.

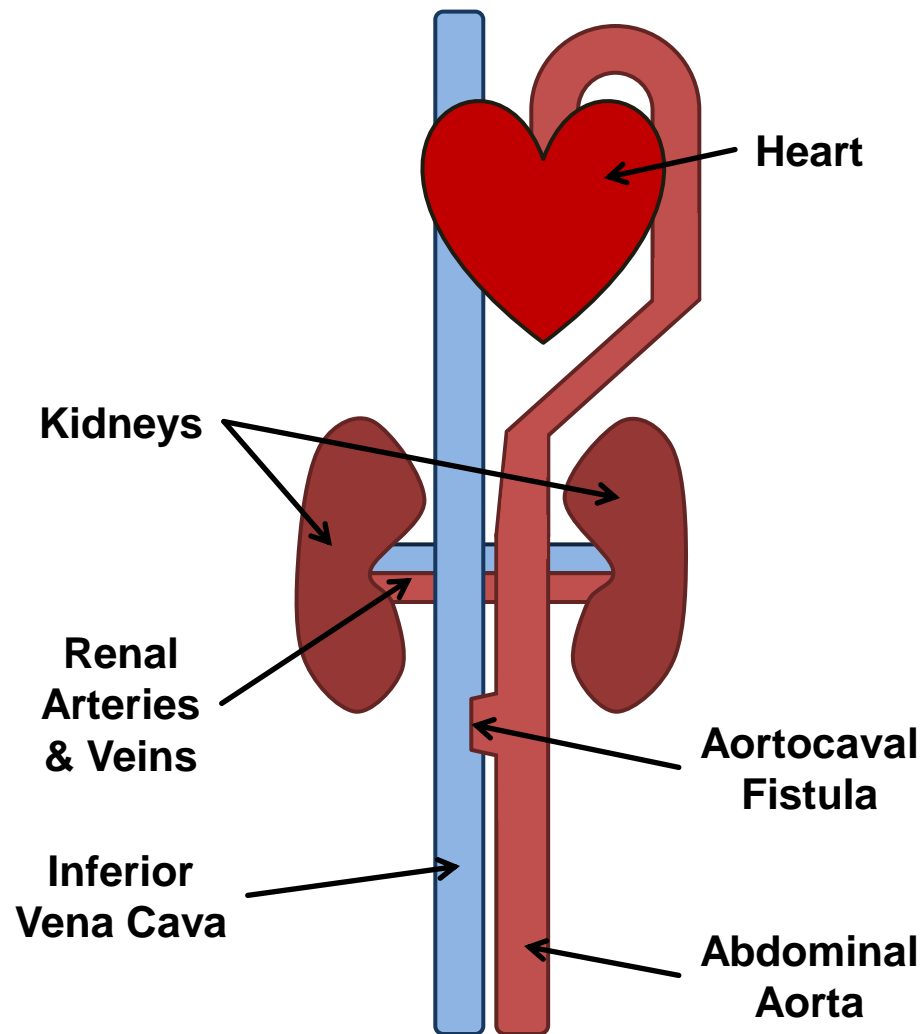


Figure 4-4. Induction of left ventricular volume overload by surgically creating an aortocaval fistula. Left ventricular volume overload was induced surgically by creating an aortocaval fistula. A 30-gauge needle was used to create a hole in both the inferior vena cava and abdominal aorta, and the two were attached by suturing the holes together. This causes an increased venous return to the heart, resulting in an increased ventricular preload, leading to the development of left ventricular volume overload.

Cardiomyocyte Isolation

Primary adult cardiac myocytes (AMCM) were isolated from sham and ACF mice from each of the different strains, as described previously by our laboratory [27, 218]. Briefly, hearts were perfused with perfusion buffer (120 mM NaCl, 15 mM KCl, 0.5 mM KH₂PO₄, 5 M NaHCO₃, 10 mM HEPES, and 5 mM glucose, pH 7.0) for 5 min and digested with perfusion buffer containing 2% collagenase II (Invitrogen, Carlsbad, CA) for 30 min at 37°C. The right ventricle, atria and apex were removed before the perfused-heart was minced. The digestion was filtered and washed, and the cells were pelleted. Only samples with purity > 95% and viability (rod-shaped) > 80% were used.

Mitochondrial Enzyme Activities

Citrate synthase and CcOX were measured using primary AMCM isolated from both C57BL/6 and C3H/HeN mice and lysed in PBS containing 0.2% lauryl maltoside, as previously described [242, 249, 250]. Briefly, CcOX activity was measured by using a spectrophotometer to monitor the oxidation of cytochrome *c* over time by the hepatocyte lysates at 550 nm [249]. Citrate synthase activity was measured by monitoring the conversion of oxaloacetate and acetyl-CoA into citrate and CoA. CoA formation was detected by adding DTNB (5,5'-dithiobis-(2-nitrobenzoic acid)), which is converted to TNB (2-nitro-5-thiobezoic acid) by CoA and can be measured spectrophotometrically at 412 nm.

Immunoblot Analysis

AMCM homogenates (10 μ g total protein) were separated by SDS/PAGE and Western blot and were probed for MnSOD (Assay Designs, Plymouth Meeting, PA), CcOX subunit I (CcOXsI; Invitrogen), VDAC (Invitrogen), ATP Synthase β subunit (Invitrogen), and oligomycin sensitivity conferring protein (Invitrogen) followed by the HRP-conjugated anti-rabbit or anti-mouse secondary antibodies (GE Healthcare, Piscataway, NJ). The intensities of protein bands were quantified prior to saturation using AlphaEaseFC software (Alpha Innotech, Santa Clara, CA).

Cellular Bioenergetics

To determine the effects of mitochondrial haplotype on cellular bioenergetics, an XF24 analyzer (Seahorse Bioscience, Billerica, MA) was used to measure O_2 consumption by live cells in culture [177, 178]. This instrument allows for high throughput, real-time, non-invasive measurements of O_2 consumption by using fluorescent probes adhered to disposable assay cartridges. These measurements can then be used to correlate O_2 consumption rate (OCR) to mitochondrial function. AMCM were attached to specialized V28 plates (Seahorse Bioscience, Billerica, MA) coated with laminin at 7,500 cells/well. The cells were then allowed to attach for 2 hr, after which time the culture media was changed to unbuffered DMEM supplemented with 1% FBS (Atlanta Biologicals, Lawrenceville, GA) and 4 mM L-glutamine (Invitrogen) for the XF24 assays.

Various parameters of mitochondrial function were measured utilizing the ability of the XF24 to inject compounds into the wells through an assay as described previously [179, 180, 250, 252, 330, 349]. Briefly, basal O_2 consumption of the AMCM was deter-

mined by measuring the OCR of the cells over time without any treatment (**Figure 4-5**). Next, FCCP (1 μ M) was injected to stimulate the maximal OCR of the cells. This maximal OCR also allows for the calculation of the reserve capacity, which is the difference between the maximal and basal OCR, and represents the cells spare mitochondrial function that is available to be utilized during an increased work load or stress. Finally, antimycin A (10 μ M) and rotenone (1 μ M) were injected simultaneously to completely inhibit the mitochondrial electron transport chain, thus yielding the non-mitochondrial OCR of the myocytes.

For most cell types, oligomycin would be injected prior to FCCP. This typically causes a decrease in the OCR, which is due to the ATP-linked OCR with the remaining mitochondrial OCR being attributed to proton leak. However, the OCR of AMCM is not inhibitable by oligomycin (**Figure 4-6**), as has been shown previously [435]. This is likely due to the high energy buffering capacity of the creatine shuttle and the low ATP demand within the myocytes *ex vivo*. The amount of AMCM plated per well and the concentrations of these compounds in these experiments were determined by titrating for their maximal effect (data not shown). The OCR was normalized to the total protein for each well, as measured by the DC protein assay (BioRad, Hercules, CA).

Echocardiography and Hemodynamic Measurements

Echocardiography and hemodynamics were performed on the sham and ACF mice prior to sacrifice using the Visualsonics imaging system (Toronto, Canada) with the animals under light isoflurane anesthesia. LV dimension and wall thickness can be matched to simultaneous high-fidelity LV pressure throughout the cardiac cycle to obtain

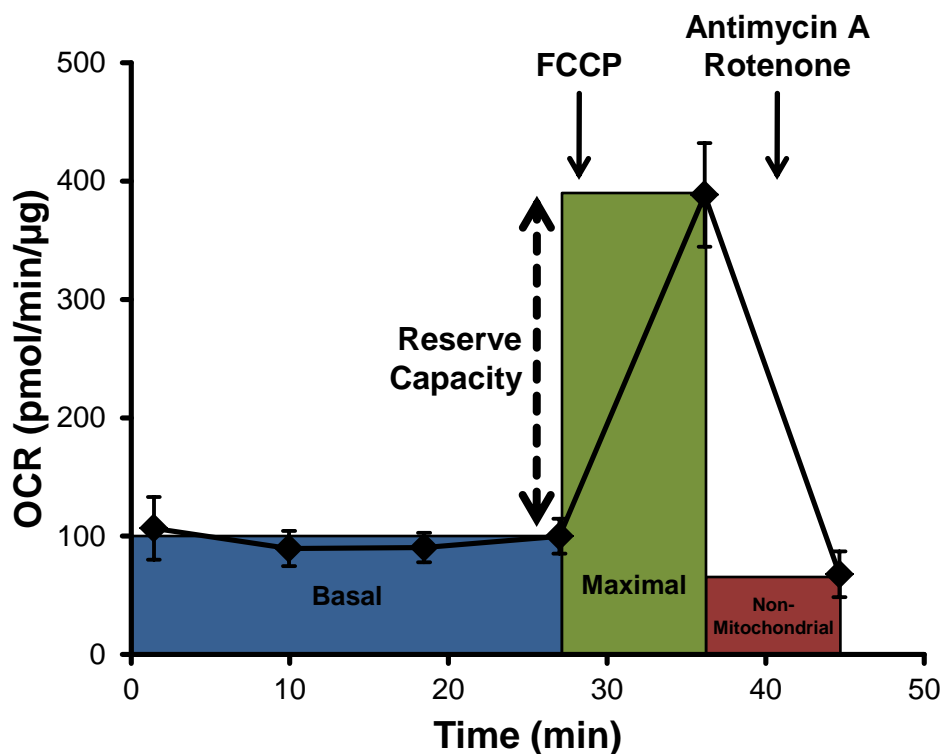


Figure 4-5. Measurement of mitochondrial function of cardiomyocytes using an XF24 analyzer. Mitochondrial function of AMCM, seeded at 7,500 cells/well, was measured over time. Basal oxygen consumption was determined by measuring the OCR of AMCM prior to any treatments. The maximal OCR was then determined by injecting FCCP (1 μ M), followed by the injection of antimycin A (10 μ M) and rotenone (1 μ M) to fully inhibit the mitochondrial electron transport chain, yielding the non-mitochondrial OCR.

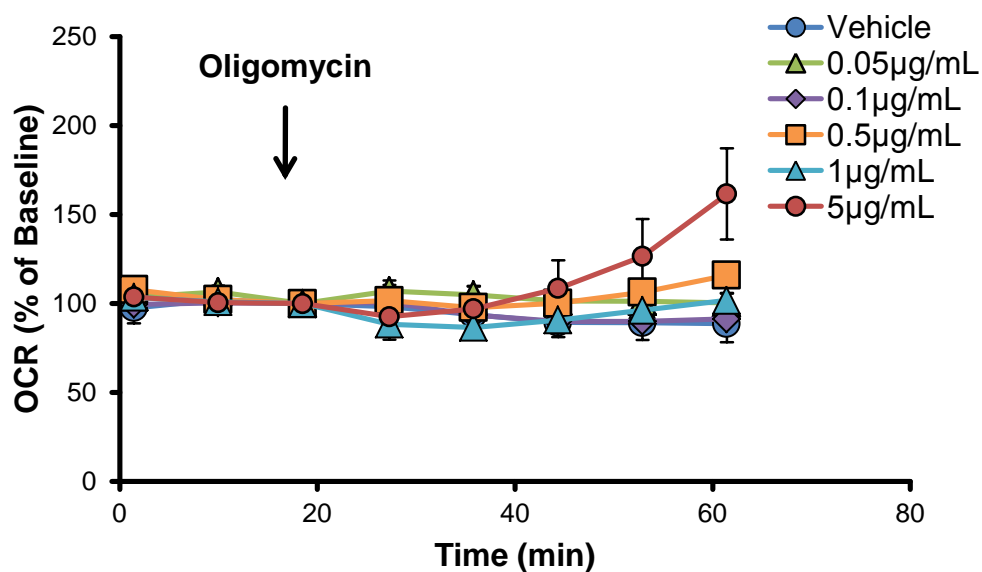


Figure 4-6. Oligomycin does not decrease cardiomyocyte oxygen consumption. AMCM were plated at 7,500 cells/well and their oxygen consumption rate (OCR) was measured over time. A range of concentrations of oligomycin was then injected into the wells (0.05-5 µg/mL) and the OCR was measured over time. No concentrations of oligomycin were able to decrease the OCR of the AMCM to allow for the calculations of ATP-linked OCR and proton leak. However, 5 µg/mL oligomycin was able to cause uncoupling of the mitochondria, resulting in the increase in OCR which is seen. Results are mean ± SEM. n=3-4 per group.

echo-derived volumes calculated from the Teicholz formula with matching pressures [27, 436, 437] (**Figure 4-7**).

Immunohistochemistry

Mouse hearts were immersion-fixed in 10% neutral buffered formalin and paraffin-embedded. 5 μm sections were mounted on slides, deparaffinized in xylene and rehydrated in a graded series of ethanol. After blocking with 5% goat serum (in 1% bovine serum/PBS), followed by 1 hr room temperature incubation with desmin antibody (Abcam #ab15200, Cambridge, MA, 1:200), the sections were treated with AlexaFluor 488-conjugated secondary antibody (Molecular Probes, Eugene, OR; 1:500) to visualize desmin (green) in the tissue. Nuclei were stained (blue) with DAPI (1.5 $\mu\text{g}/\text{ml}$; Vector Laboratories, Burlingame, CA). Image acquisition (100x objective) was performed on a Leica DM6000 epifluorescence microscope with SimplePCI software (Compix, Inc., Cranberry Township, PA). Images were adjusted appropriately to remove background fluorescence.

Transmission Electron Microscopy

Heart LV tissue samples were fixed with Karnovsky's solution (2% paraformaldehyde/2.5% glutaraldehyde in 0.1 M phosphate buffer) overnight. After fixation, the specimens were rinsed several times with PBS followed by post fixation with 1% OsO_4 solution in PBS for one hour. Then the tissue samples were dehydrated through a series of graded ethyl alcohols from 50 to 100%. After dehydration, the infiltration was performed in intermediate solvent, 2 changes of 100% propylene oxide (PO) for 15 min

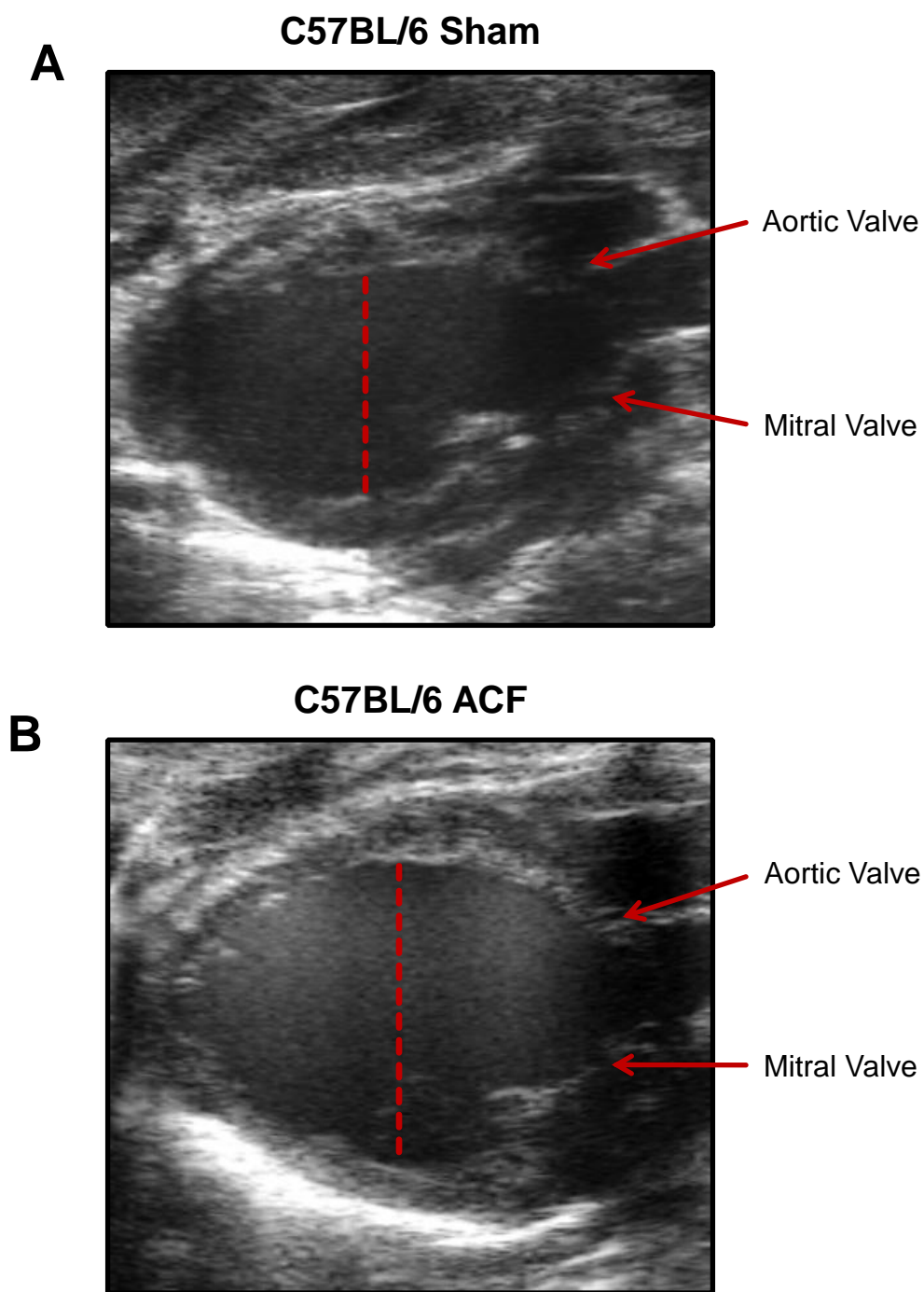


Figure 4-7. Using echocardiography to measure cardiac function *in vivo*. Echocardiography was used to measure the cardiac function of the mice following 3 days of exposure to ACF or sham surgeries. Cross-section of the left ventricle (LV) of the heart in a sham (A) and ACF (B) C57BL/6 mouse. The LV end diastolic dimension (EDD) is the cross section of the LV during diastole. Echocardiography performed by W.E. Bradley.

each, and then immersed into a 1:1 mixture of PO and the embedding resin (Embed 812, Electron Microscopy Sciences, Fort Washington, PA) for 12-18 hr. Samples were then transferred to fresh 100% embedding media, tissue blocks were polymerized for 12-18 hr at 60°C, sectioned at 70-100 nm and then placed on nickel mesh grids. After drying, the sections were stained with the heavy metals uranyl acetate and lead citrate and were viewed on a Tecnai Twin 120kv TE microscope (FEI, Hillsboro, OR). Digital images were taken with an AMT CCD camera, transferred onto a personal computer, and analyzed.

Statistics

Transmission electron microscopy and immunohistochemistry images are qualitative and are representative images from their respective groups. Mitochondrial function, cardiac function, Western blot, and mitochondrial enzyme activity data were compared using a student's *T*-test or a two-way ANOVA with Student-Newman-Keuls post hoc analysis. A $p < 0.05$ between groups was considered statistically significant.

RESULTS

Comparison of C57BL/6 and C3H/HeN Mitochondrial Phenotypes

Isolated primary AMCM from C57BL/6 and C3H/HeN mice were used to elucidate any differences in mitochondrial protein levels or enzymatic activities between the two strains. Proteins representative of different mitochondrial compartments were probed to assess any potential differences between the strains. Manganese superoxide dismutase (MnSOD) is expressed in the mitochondrial matrix, and was found not to

change between C57BL/6 and C3H/HeN mice (**Figure 4-8A,B**). CcOX subunit I (CcOXsI), ATP synthase β , and oligomycin sensitivity conferring protein (OSCP) are expressed in the mitochondrial inner membrane and were also found not to change between the strains (**Figure 4-8A,B**). Voltage dependent anion channel (VDAC) is expressed in the mitochondrial outer membrane and did not exhibit different levels between the C57BL/6 and C3H/HeN mice (**Figure 4-8A,B**).

The relative activities of CcOX and citrate synthase were measured in isolated AMCM from the two strains to determine if there was any difference in mitochondrial amount or activity. CcOX activity is of particular interest because, as discussed earlier, there is a single-nucleotide polymorphism in the mtDNA that codes for CcOX subunit 3 which could alter the activity of the complex. Furthermore, citrate synthase (CS) activity was measured as a normalization factor, since citrate synthase activity and levels are known to be similar within mitochondria from the same cell populations [438, 439]. Interestingly, there was no difference between the CcOX, nor was there a change when normalized by CS activity, which was also the same between strains (**Figure 4-8C**).

Even though there was no difference between mitochondrial protein levels or activities between AMCM isolated from C57BL/6 and C3H/HeN mice, we next wanted to determine if there was a difference in the bioenergetic function in the AMCM of the two strains. Therefore, AMCM from C57BL/6 and C3H/HeN mice were isolated and plated in V28 plates to assay their O₂ consumption *ex vivo* using the XF24 analyzer. There was no significant difference between the basal OCR of the C57BL/6 and C3H/HeN myocytes; however, the AMCM isolated from C57BL/6 mice exhibited an approximately 50% increase in their FCCP-stimulated maximal OCR as compared to the C3H/HeN

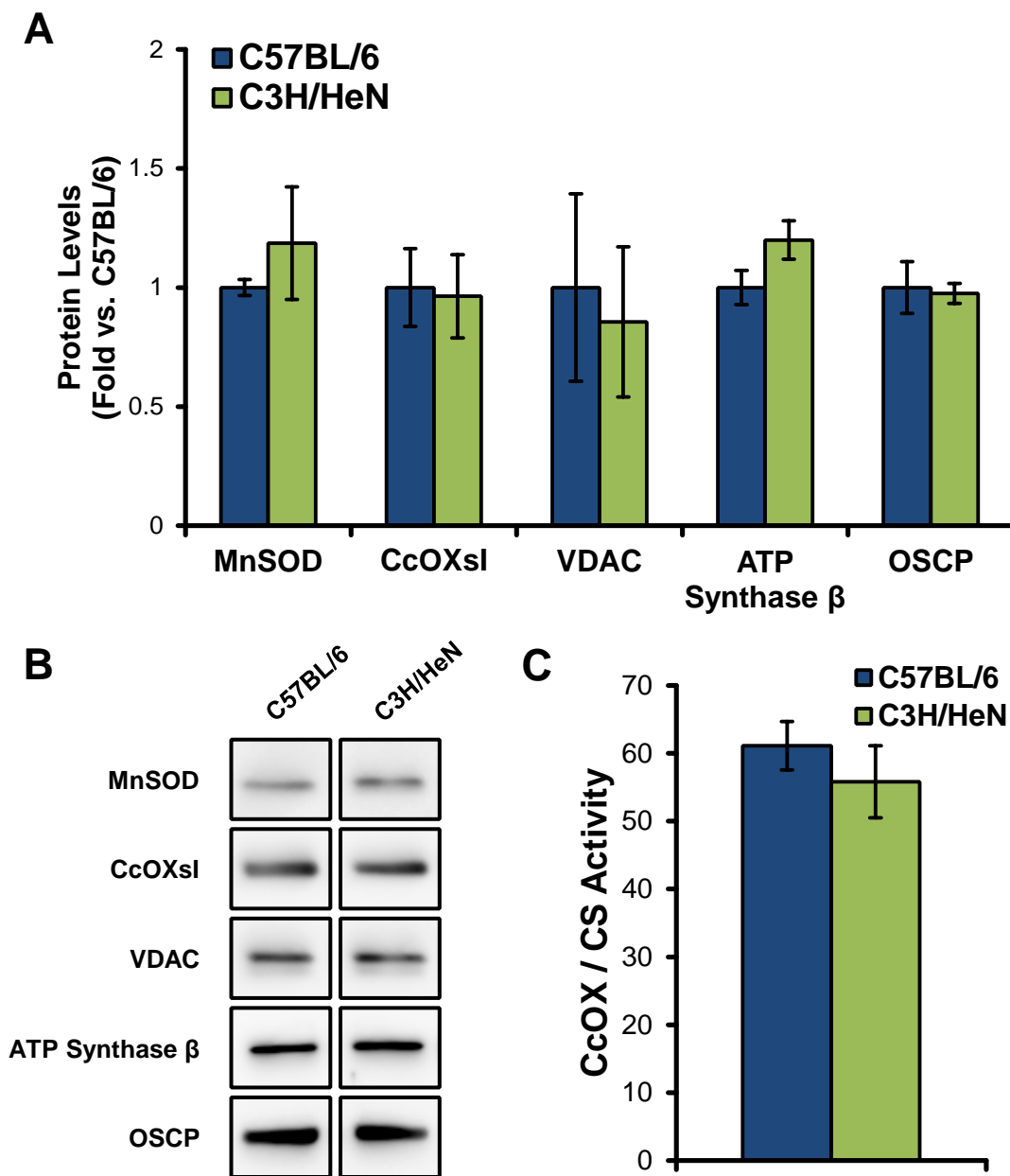


Figure 4-8. Comparison of mitochondrial protein levels and activity from cardiomyocytes isolated from C57BL/6 and C3H/HeN mice. (A) The levels of various mitochondrial proteins from isolated AMCM were determined by separating lysates via SDS-PAGE and Western blotting for the respective proteins. Representative protein bands are shown in (B). (C) The activity of cytochrome *c* oxidase (CcOX) was assayed from AMCM lysates and normalized to citrate synthase (CS) activity. Results are mean \pm SEM. $n=4$ per group for panels A and B, and $n=7-8$ per group for panel C. MnSOD = manganese superoxide dismutase. CcOXsI = cytochrome *c* oxidase subunit I. VDAC = voltage dependent anion channel. OSCP = oligomycin sensitivity conferring protein.

myocytes (**Figure 4-9**). Furthermore, the non-mitochondrial OCR of the AMCM isolated from both strains of mice were found to be not significantly different.

Bioenergetic Response of C57BL/6 and C3H/HeN Mice to Volume Overload

The susceptibility to alterations in mitochondrial bioenergetics in response to acute volume overload induced by ACF was then tested by measuring the mitochondrial function of AMCM from both strains following 3 d of exposure to sham or ACF surgery. The sham myocytes from C57BL/6 mice once again exhibited a 6-fold increase in their maximal OCR over their basal respiration rate, indicating that these cells have a very large reserve capacity which they can utilize in conditions of increased ATP demand (**Figure 4-10A**). However, AMCM isolated from C57BL/6 mice subjected to 3 d of ACF had a significantly lower maximal OCR, which also manifests as a decreased reserve capacity. This data suggests that not only does the ACF induce the loss of bioenergetic function in C57BL/6 cardiomyocytes, but it also renders them more susceptible to damage in response to increased ATP demand. This becomes particularly important when taking into account the fact that volume overload increases the workload of the heart in order to pump the increased volume of blood to the rest of the body, which increases ATP utilization and demand within the AMCM *in vivo*.

Cardiomyocytes from adult C3H/HeN mice were also isolated following sham surgery, and as discussed previously, they exhibit a 4-fold increase in maximal OCR over basal when stimulated by FCCP (**Figure 4-10B**). Interestingly, despite the fact that the C3H/HeN cardiomyocytes exhibit a lower maximal OCR than C57BL/6 myocytes, they were protected from the loss of maximal mitochondrial function in response to 3 d of

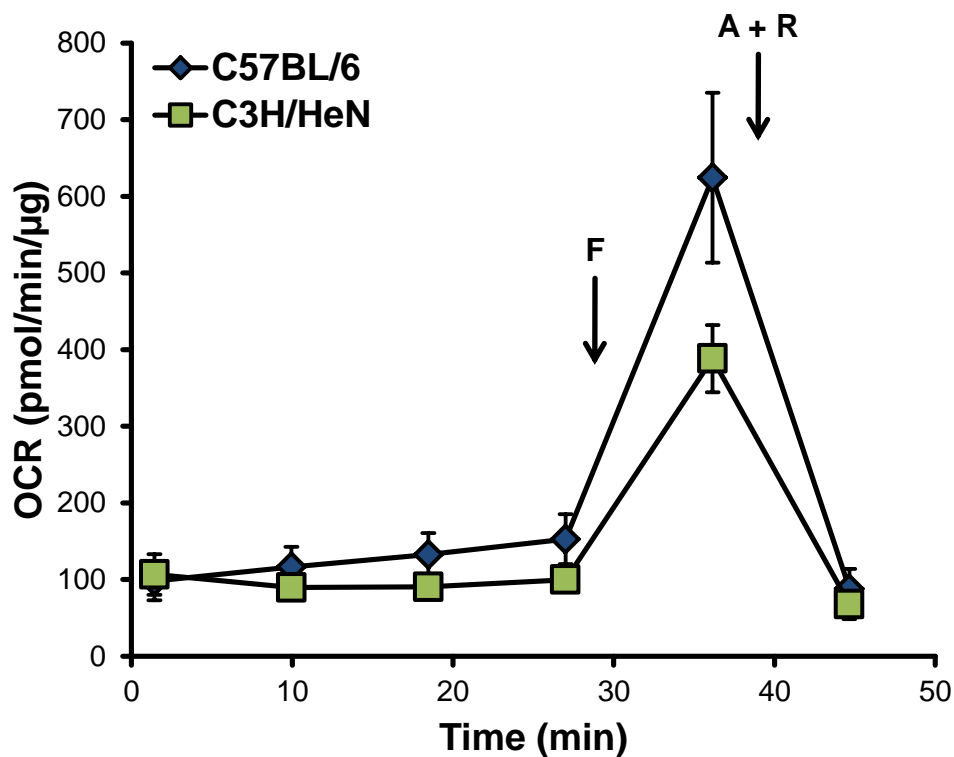


Figure 4-9. Cardiomyocytes isolated from C57BL/6 and C3H/HeN mice exhibit differences in mitochondrial function. The oxygen consumption rate (OCR) of AMCM from the two strains of mice, seeded at 7,500 cells/well, was measured over time and in response to sequential injections of 1 μ M FCCP (F) and 10 μ M antimycin A plus rotenone 1 μ M rotenone (A + R). Results are mean \pm SEM. n=7-8 mice per group.

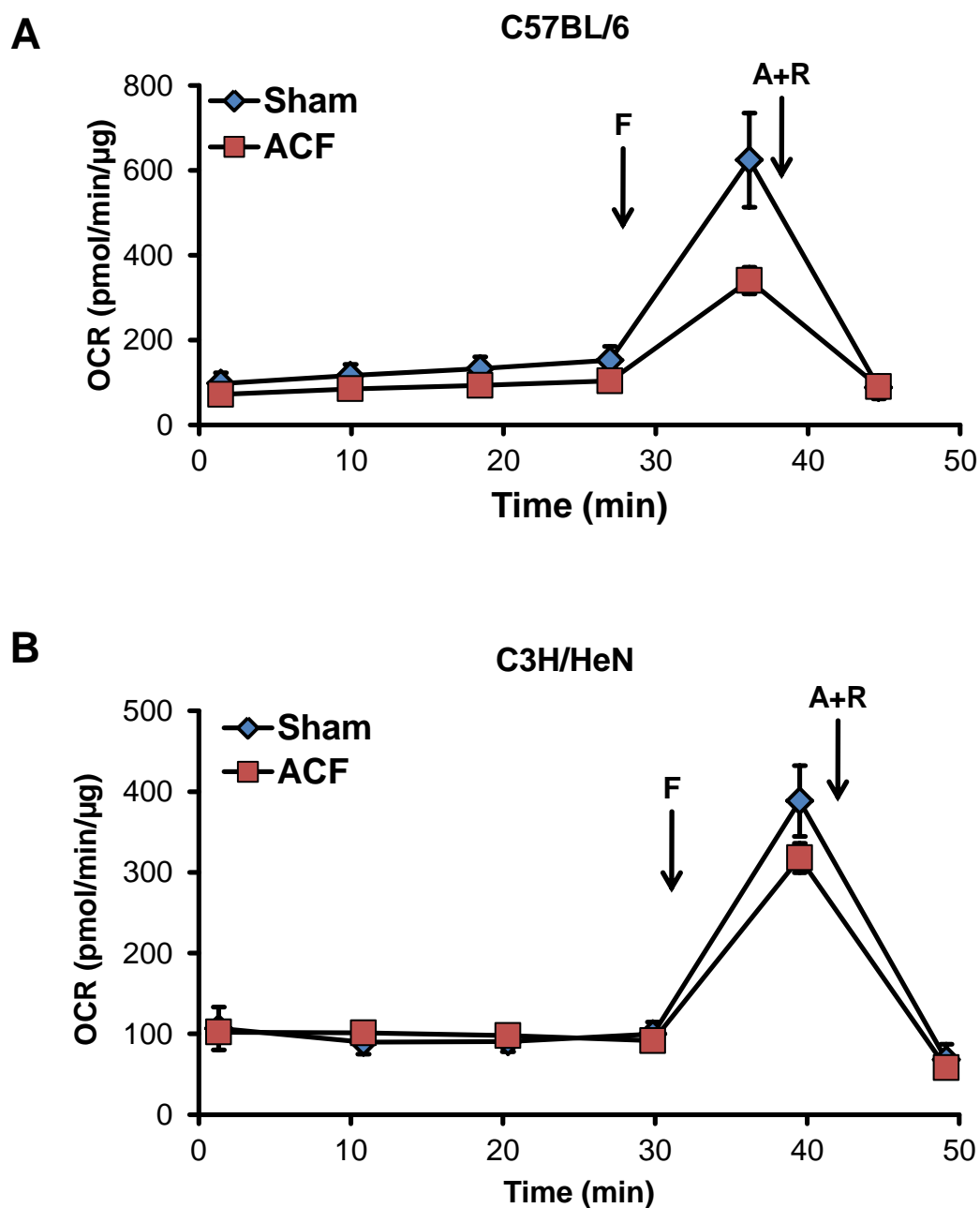


Figure 4-10. Cardiomyocytes isolated from C57BL/6 and C3H/HeN mice exhibit different bioenergetic responses to volume overload. The oxygen consumption rate (OCR) of AMCM from the two strains of mice 3 d following a sham (A) or ACF (B) surgery was measured over time. The mitochondrial function of the sham and ACF AMCM was assessed using sequential injections of 1 μ M FCCP (F) and 10 μ M antimycin A plus rotenone 1 μ M rotenone (A + R). Results are mean \pm SEM. $n \geq 5$ mice per group.

ACF. Taken together, these data suggest that even though C57BL/6 and C3H/HeN mice have similar mitochondrial protein levels and enzyme activities, they have different mitochondrial function and bioenergetic efficiencies. Furthermore, the C3H/HeN AMCM seem to be protected from ACF-induced alterations in mitochondrial bioenergetics.

Morphometry and Left Ventricular Function of Mice after Volume Overload

To test whether the susceptibility of the C57BL/6 mice to ACF-induced loss of mitochondrial function is dependent on the C57 mtDNA haplotype, C57_n::C3H_{mt} MNX mice were subjected to ACF or sham surgery along with C57BL/6 and C3H/HeN mice. In order to determine any baseline differences between the strains and any differential effects of the ACF surgery on the mice, various parameters of cardiac morphometry and LV function were assessed using echocardiography and hemodynamic measurements prior to sacrifice. The ACF did not alter the body weight in any of the strains as compared to the sham; however, the body weights of the C57_n::C3H_{mt} mice were slightly higher than those of the C57BL/6 and C3H/HeN mice (**Table 4-2**). The heart rate was also not significantly altered by the three days of ACF. However, because the ACF causes ejection into the low pressure venous system, there was a significant decrease in the mean arterial pressure (MAP) as was expected. The posterior wall thickness (PWT) of the mice was measured in the three strains of mice exposed to sham or ACF surgeries, and there was no difference between the sham mice from the different strains. However, the C57_n::C3H_{mt} mice with an induced ACF exhibited a significant increase in PWT during systole, indicating that there was greater thickening of the ventricular wall at the end of systole.

	C3H/HeN		C57BL/6		C57 _n ::C3H _{mt}	
	Sham	ACF	Sham	ACF	Sham	ACF
Body Weight (g)	26 ± 1	26 ± 1	24 ± 1	25 ± 1	32 ± 2 [#]	29 ± 1 [#]
MAP (mm Hg)	87 ± 2 [#]	73 ± 5*	77 ± 1	64 ± 5*	79 ± 1	59 ± 2*
Heart Rate (bpm)	523 ± 23	491 ± 13	523 ± 21	549 ± 22	469 ± 44	536 ± 46
LV PWT – Syst. (mm)	0.99 ± 0.08	1.05 ± 0.07	0.97 ± 0.08	1.05 ± 0.14	1.11 ± 0.03	1.24 ± 0.04*
LV PWT – Diast. (mm)	0.62 ± 0.05	0.75 ± 0.05	0.72 ± 0.06	0.62 ± 0.07	0.75 ± 0.03	0.69 ± 0.02
n	7	5	5	5	4	4

*p < 0.05 vs. respective sham, [#]p < 0.05 vs. C57BL/6

Table 4-2. Acute hemodynamic and echocardiography data. C3H/HeN, C57BL/6, and C57_n::C3H_{mt} mice were subjected to ACF or sham surgery 3 d prior to hemodynamic and echocardiography measurements. Results are mean ± SEM. *p < 0.05 compared to its respective sham. [#]p < 0.05 compared to C57BL/6 sham. MAP = mean arterial pressure. PWT = posterior wall thickness. Data obtained by W.E. Bradley.

The LV end-diastolic dimension (LVEDD) represents the cross-sectional diameter of the LV at the end of diastolic filling. The C57BL/6 mice exhibited a small but significant increase in LVEDD following ACF, indicating that they have a greater dilatation in response to the ACF (**Figure 4-11A**). The C3H/HeN mice had no change in LVEDD, and the C57_n::C3H_{mt} mice were also protected from developing any LV dilatation. The next parameter of cardiac function that was measured was the relative wall thickness (RWT), which is calculated using the posterior wall thickness to the LVEDD, which as this ratio decreases is an index of adverse LV remodeling. The RWT was measured in all three strains and was found to not be significantly different either between the strains or between sham and ACF mice (**Figure 4-11B**).

The fractional shortening is the extent of LV shortening from end-diastole to end-systole. Increased fractional shortening indicates better cardiac function, or a

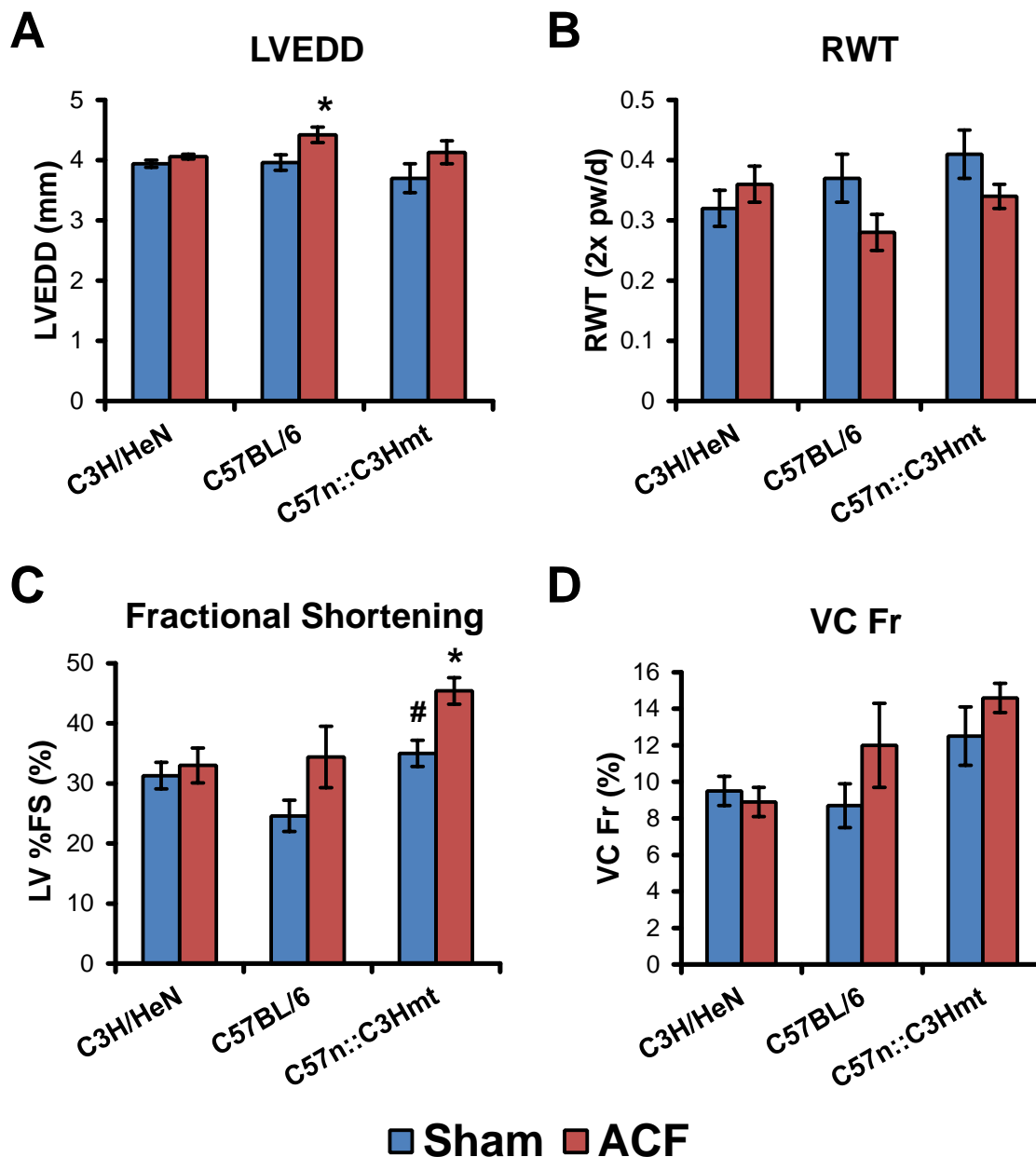


Figure 4-11. Changes in left ventricular dimension and volume in response to volume overload. C3H/HeN, C57BL/6, and C57_n::C3H_{mt} mice were subjected to ACF or sham surgery for 3 days prior to echocardiography measurements. (A) LV end-diastolic dimension (EDD) was determined by measuring the diameter of the left ventricle during diastole. (B) Relative wall thickness (RWT) was determined by dividing the LV diastolic posterior wall thickness by the LV EDD. (C) Fractional shortening represents the percentage of the LV EDD that is lost in systole. (D) The velocity of circumferential shortening (VC Fr) represents the Results are mean \pm SEM. $n \geq 4$ for all groups. * $p > 0.05$ compared to its respective sham. Data obtained by W.E. Bradley.

more complete ventricular output. Interestingly, the sham C57_n::C3H_{mt} mice had a significantly higher fractional shortening than the C57BL/6 or C3H/HeN mice, which was even further increased in response to three days of ACF (**Figure 4-11C**). The increase in fractional shortening suggests a better compensatory response to the increase in preload created by the ACF. The final parameter of cardiac function tested in the mice following sham or ACF surgeries was the velocity of circumferential shortening (VC Fr), which represents the speed in which the LV contracts from end-diastole to end-systole. The C57_n::C3H_{mt} mice exhibited a trend towards a higher VC Fr than the C57BL/6 and C3H/HeN mice although it did not reach significance (**Figure 4-11D**). There were no significant differences in VC Fr between the sham and ACF mice of any of the strains. In summary, such minor changes in LV shortening and rate of shortening are not significant at such an early stage in ACF.

Volume Overload-Induced Alterations in Bioenergetic Function

The mitochondrial function of AMCM from the C57BL/6, C3H/HeN, C57_n::C3H_{mt}, and C3H_n::C57_{mt} mice exposed to either sham or ACF surgeries was assessed using an XF24 analyzer. Primary AMCM were isolated and seeded into V28 plates at 7,500 cells/well, and parameters of mitochondrial function were determined as described in **Figure 4-5**. As seen in **Figure 4-12A**, the basal OCR between the sham and ACF mice for each strain were not significantly different. Although the basal OCR of the C57BL/6 AMCM was moderately higher than the C3H/HeN AMCM, the difference was not statistically significant; however, the basal OCR of the C57BL/6 mice was significantly higher than that of both MNX mouse strains.

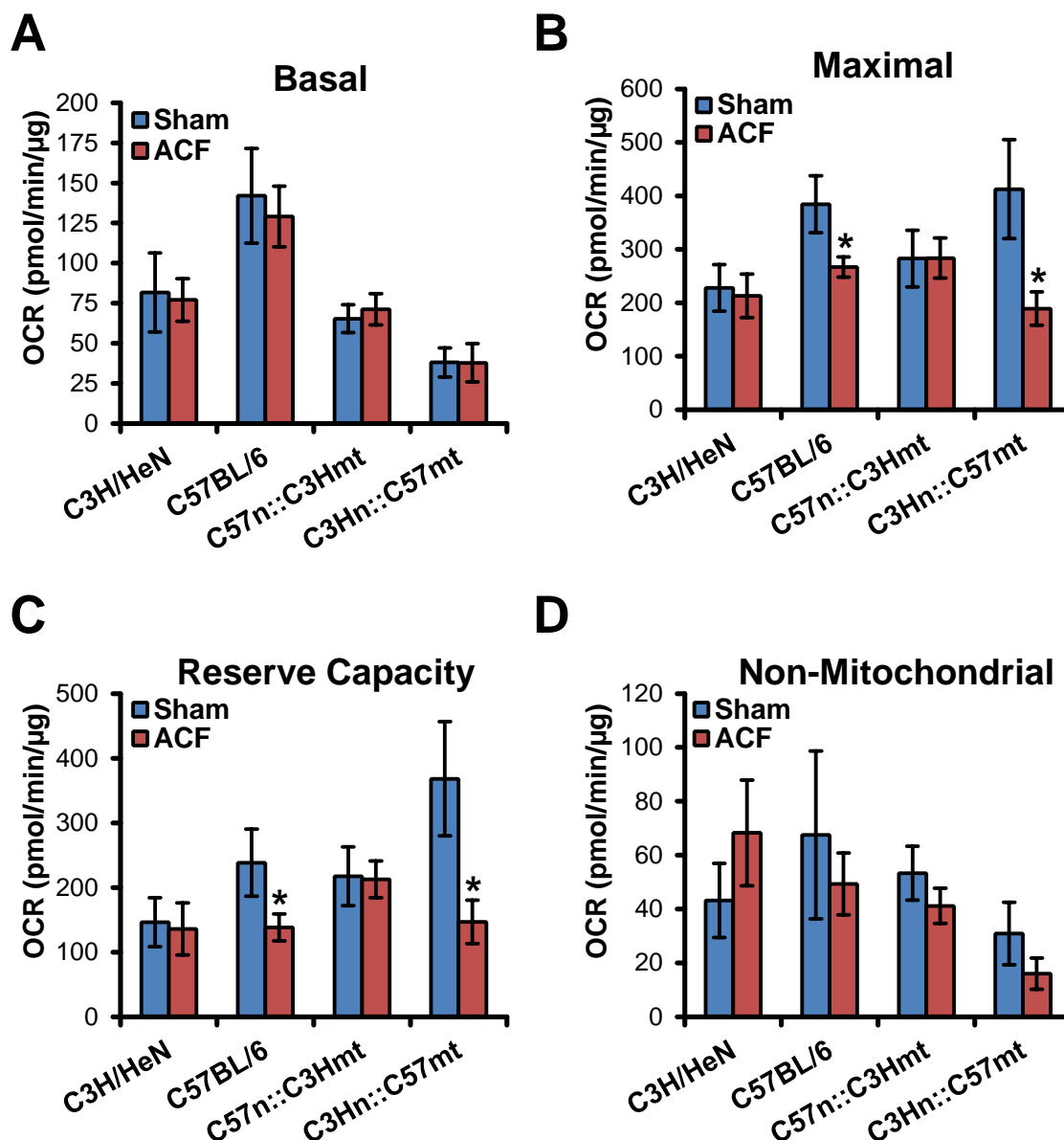


Figure 4-12. Changes in mitochondrial parameters of oxygen consumption of cardiomyocytes in response to volume overload. AMCM were isolated from sham and ACF C57/BL6, C3H/HeN, C57_n::C3H_{mt}, and C3H_n::C57_{mt} mice and were plated in V28 plates at 7,500 cells/well. Parameters of oxygen consumption were calculated from the OCR traces from each animal as described in Figure 4-5. (A) Basal OCR represents the respiration of the myocytes under basal conditions. (B) Maximal OCR was determined by injection of FCCP (1 μM). (C) The reserve capacity was determined by calculating the difference between the maximal and basal OCR. (D) Non-mitochondrial OCR was measured following antimycin A (10 μM) and rotenone (1 μM) treatment. Results are mean ± SEM. n≥3 for each group. *p>0.05 compared to sham of the same strain.

The maximal OCR of the AMCM from the different strains after sham or ACF surgeries was measured following the injection of FCCP (1 μ M) in the XF24. FCCP is a proton ionophore which stimulates maximal O₂ consumption of the cells by uncoupling the mitochondria and diminishing membrane potential. This leads to the rapid consumption of O₂ without the production of ATP. The AMCM from C57BL/6 and C3H_n::C57_{mt} mice subjected to three days of ACF exhibited a decrease in maximal OCR as compared to the shams, while the AMCM from the C3H/HeN and C57_n::C3H_{mt} mice showed no difference in maximal OCR between the sham and ACF groups (**Figure 4-12B**). This data supports the concept that while the C57BL/6 C3H_n::C57_{mt} mice are susceptible to ACF-induced damage, the C3H/HeN and C57_n::C3H_{mt} mice were resistant to any apparent damage resulting from volume overload.

The reserve capacity of the AMCM from the four strains *ex vivo* was determined by calculating the difference between the maximal and basal OCR, and again represents the spare respiratory capacity of the cells. The AMCM from the C57BL/6 and C3H_n::C57_{mt} mice exposed to ACF displayed a significant decrease in their available reserve capacity as compared to the sham controls, while the C3H/HeN and C57_n::C3H_{mt} mice showed no difference in their reserve capacities between the sham and ACF groups (**Figure 4-12C**). This data further supports the notion that the mice with C57BL/6 mtDNA are susceptible to ACF-induced injury while mice with C3H/HeN mtDNA are resistant to damage.

Finally, in order to measure the non-mitochondrial OCR of the AMCM, antimycin A (10 μ M) and rotenone (1 μ M) were injected onto the myocytes simultaneously to fully inhibit the mitochondrial electron transport chain, resulting in a substantial decrease

in OCR. The remaining non-mitochondrial OCR can be attributed to extra-mitochondrial sources of O₂ consumption, such as xanthine oxidase and the NAPDH oxidases. As shown in **Figure 4-12D**, the non-mitochondrial OCR of the four strains of mice were not significantly different from each other, and ACF did not alter the non-mitochondrial OCR in any of the groups.

Alterations in Desmin Organization in Cardiomyocytes after Volume Overload

Desmin is an intermediate filament protein expressed in high levels in cardiomyocytes, and is known to be important in myocyte architecture and function [49, 50, 223, 224, 228]. The loss of desmin in the cardiomyocytes has been observed in dilated cardiomyopathies, and has been linked to the loss of contractile and mitochondrial function [49, 50, 223, 224, 227, 228, 351, 393, 440]. In **Figure 4-13**, we used immunohistochemistry to observe the distribution of desmin left ventricular sections from the different mouse strains exposed to ACF or sham surgeries. The sham C57BL/6 mice exhibited a normal desmin organization, which was clearly distributed along the Z-lines of the myofibrils and along the intercalated discs. However, in the LV sections of C57BL/6 mice exposed to ACF for three days, there is the clear loss of desmin protein along the Z-lines within the myocytes. Moreover, the desmin expression in the intercalated discs did not change between the sham and ACF C57BL/6 mice, showing that the loss of desmin due to volume overload was specific to the Z-line, where it plays an important role in connecting the sarcomeres to each other, as well as to the mitochondria.

In the LV sections of C3H/HeN mice given the sham surgery, there is the normal distribution of desmin along the Z-lines and intercalated discs, as also seen in the sham

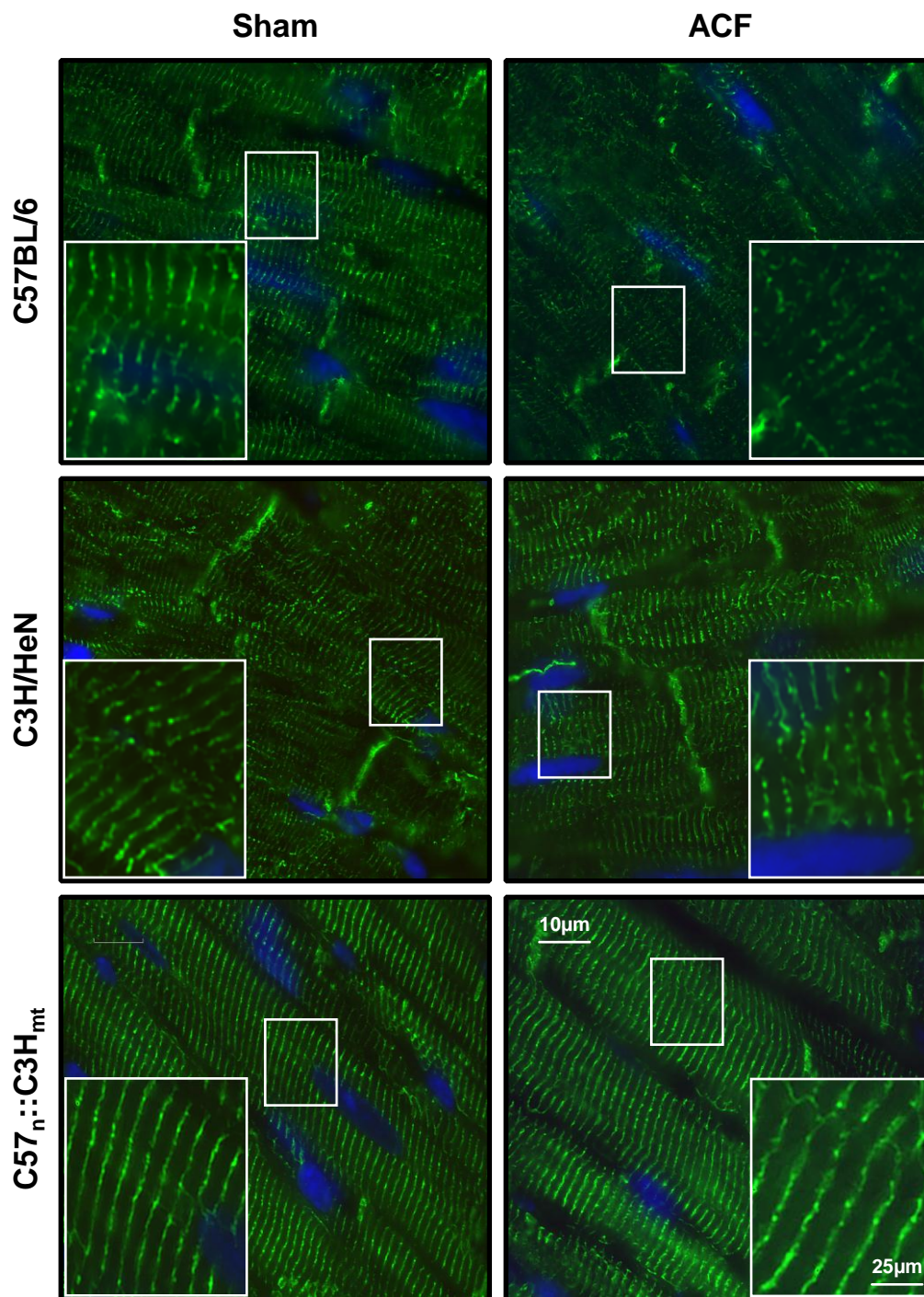


Figure 4-13. Volume overload alters desmin expression in left ventricular myocytes in C57BL/6 mice. C57BL/6, C3H/HeN, and C57_n::C3H_{mt} mice were given an ACF for 3 d prior to left ventricular isolation and immunohistochemical staining for desmin (green) and nuclei (blue). Fluorescence was measured using fluorescence microscopy. The white boxes represent the areas of the 2.5x zoomed-in images. Results are representative images from each group. Magnification = 100x. $n \geq 4$ for each group. Data obtained by P.C. Powell.

C57BL/6 mice. Interestingly, the C3H/HeN mice exposed to 3 d of ACF did not exhibit any significant alterations in desmin organization as compared to the shams. We next probed for desmin in LV sections from sham and ACF C57_n::C3H_{mt} mice. The sham mice also exhibited normal desmin organization, which was not altered after exposure to 3 d of ACF. This suggests that the C3H mtDNA was able to attenuate the ACF-induced loss of desmin cytoskeleton in the C57_n::C3H_{mt} mice that is seen in the C57BL/6 mice.

Effect of Volume Overload on Mitochondrial Morphology

Transmission electron microscopy of LV sections from the different strains of mice after ACF or sham surgery was performed to examine the effects of ACF on cardiomyocyte morphology. Sham C57BL/6 mice exhibited intact myofibrils and large, round mitochondria. Moreover, the intermyofibrillar mitochondria line up along the myofibrils between the Z-lines, often with one mitochondrion per sarcomere (**Figure 4-14**). However, in C57BL/6 mice given an ACF, there were distinct alterations in intracellular morphology, with apparent mitochondrial fission and myofibrillar degradation along with the loss of extracellular matrix. These morphological alterations were made more apparent by using a higher magnification (**Figure 4-15**).

The C3H/HeN sham mice have a mitochondrial and myofibrillar organization similar to the C57BL/6 mice, although the mitochondria appear to be slightly smaller in size. However, the LV from the C3H/HeN ACF mice did not exhibit any changes in mitochondrial or myofibrillar morphology from the shams, suggesting that the C3H/HeN mice are resistant to the ACF-induced loss of mitochondrial and myofibrillar structure and organization.

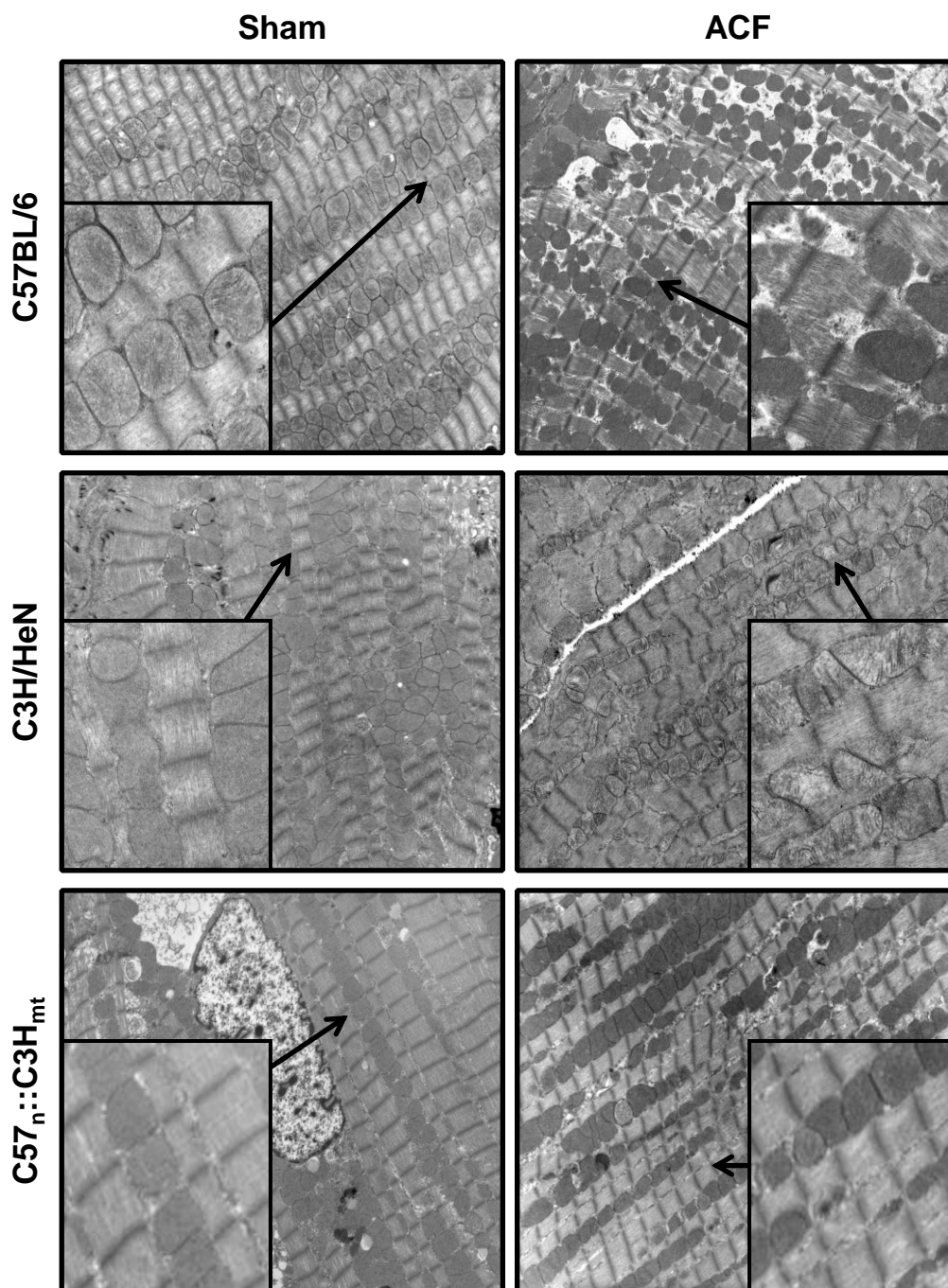


Figure 4-14. Transmission electron microscopy of left ventricle in mice subjected to volume overload. C57BL/6, C3H/HeN, and C57_n::C3H_{mt} mice were subjected to ACF or sham surgery 3 d prior to tissue collection. Left ventricular sections of C57BL/6, C3H/HeN, and C57_n::C3H_{mt} mice were collected and prepared for transmission electron microscopy. Results are representative images from each group. Magnification = 4,500x. Imaging by Emlabs, Inc., Birmingham, AL.

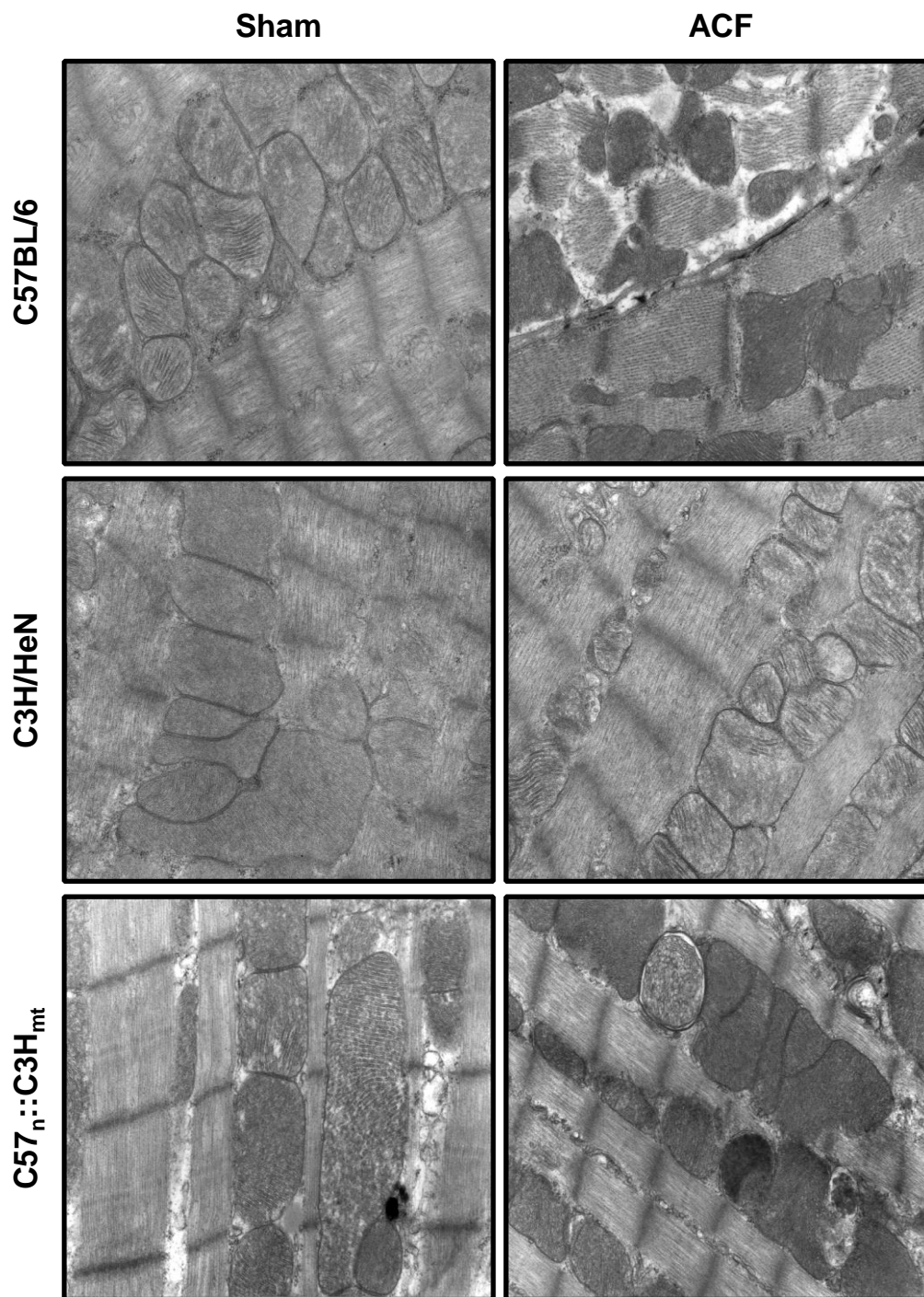


Figure 4-15. Further magnification of transmission electron microscopy of left ventricle in mice subjected to volume overload. C57BL/6, C3H/HeN, and C57_n::C3H_{mt} mice were subjected to ACF or sham surgery 3 d prior to tissue collection. Left ventricular sections of C57BL/6, C3H/HeN, and C57_n::C3H_{mt} mice were collected and prepared for transmission electron microscopy. Results are representative images from each group. Magnification = 17,000x. Imaging by Emlabs, Inc., Birmingham, AL.

In order to separate the effects of the different nDNA and mtDNA haplotypes of the C57BL/6 and C3H/HeN mice on the susceptibility to ACF-induced cardiomyocyte damage, C57_n::C3H_{mt} MNX mice were used. The C57_n::C3H_{mt} mice, which possess the nDNA of the C57BL/6 mice and the mtDNA of the C3H/HeN mice, which were subjected to sham surgeries also had a similar morphology as the sham C57BL/6 and C3H/HeN mice. Interestingly, the C57_n::C3H_{mt} mice subjected to three days of ACF maintained their morphology, exhibiting no major differences from the sham mice.

Taken together, these data show that C57BL/6 mice are susceptible to the ACF-induced loss of mitochondrial and myofibrillar organization, while the C3H/HeN mice are resistant to the morphological changes seen in the C57BL/6 mice subjected to ACF. Moreover, the fact that the C57_n::C3H_{mt} mice were resistant to ACF-induced morphological damage shows that the mtDNA of the resistant C3H/HeN was able to render the mice with the otherwise normal C57BL/6 phenotype resistant to ACF-induced injury.

DISCUSSION

The progression to heart failure induced by volume overload is characterized by cardiomyocyte remodeling and alterations in cellular bioenergetic function [27, 217, 218, 221-224, 387-389, 436, 437]. Previous studies have also shown that volume overload causes an increased energy demand on the myocytes and is also associated with the production of ROS [27, 46, 47, 221]. This chapter examines the role of the mitochondria in the progression of volume overload towards cardiomyocyte dysfunction. Furthermore, the role of mtDNA haplotype in determining the susceptibility to volume overload-related pathology is also a major focus of the data discussed herein.

In order to study the effect of mtDNA haplotype on the predisposition to volume overload-induced cardiomyocyte dysfunction, C57BL/6 and C3H/HeN mice were selected due to their known differences in mtDNA haplotype and disease susceptibilities [400, 409, 414-416, 418]. Because these two strains have a single-nucleotide polymorphism in the gene encoding for CcOX subunit III, the levels and activities of mitochondrial proteins were measured between the strains [400]. C57BL/6 and C3H/HeN AMCM exhibited no differences in the levels of proteins from different mitochondrial compartments or the activities of CcOX or citrate synthase (**Figure 4-8**). Importantly, the CcOX activity assay used measures maximal enzymatic activity using lysates; therefore, any differences in the regulation of CcOX or the proton pumping ability would likely not be detected using this approach. Next, the mitochondrial function of the AMCM isolated from both strains was then compared using the XF24 analyzer. The AMCM from the C57BL/6 mice had a significantly higher maximal OCR than the C3H/HeN cardiomyocytes (**Figure 4-9**). Moreover, because the basal OCR was not significantly different between the strains, the C57BL/6 AMCM had a higher reserve capacity. The higher reserve capacity seen in the C57BL/6 suggests that these mice should be more resistant to increased energy demand or stress than the C3H/HeN mice.

Interestingly, when the two strains were subjected to ACF surgeries for three days, the C57BL/6 mice exhibited a loss in their maximal mitochondrial function, while the C3H/HeN AMCM showed no significant changes in their mitochondrial function (**Figure 4-10**). The differential bioenergetic response of the C57BL/6 and C3H/HeN mice supports previously published work showing disparate susceptibilities to pathology using other models of cardiovascular diseases [415, 416, 418]. These differences are

likely due to differences in bioenergetic efficiency, substrate handling, or mitochondrial regulation.

In order to further elucidate the role of mtDNA haplotype in the proclivity for the development of disease, MNX mice were also subjected to sham and ACF surgeries to determine their susceptibilities to volume overload-induced pathologies. Following three days of exposure to ACF, the cardiac function of the mice was assessed using echocardiography and catheterization. C57BL/6 mice showed a significant increase in LVEDD compared to the sham mice, while there was no difference between the sham and ACF C3H/HeN mice (**Figure 4-11A**). Interestingly, there was also no difference in LVEDD between the sham and ACF C57_n::C3H_{mt} mice, showing that the C3H/HeN mtDNA was able to render the mice with C57BL/6 nDNA resistant to ACF-induced volume overload. The C57_n::C3H_{mt} mice also exhibited an increased fractional shortening as compared to the C57BL/6 mice, showing that the C3H/HeN mtDNA improved the LV function of the mice (**Figure 4-11C**).

Several parameters of mitochondrial function of myocytes isolated from C57BL/6, C3H/HeN, and both MNX mice subjected to sham or ACF surgeries for three days was then assessed. The basal OCR of all four strains of mice were not altered in response to ACF induction (**Figure 4-12A**); however, the C57BL/6 and C3H_n::C57_{mt} mice subjected to ACF exhibited a significantly decreased maximal OCR, while the C3H/HeN and C57_n::C3H_{mt} mice were resistant to any change in maximal OCR in response to ACF induction (**Figure 4-12B**). The decrease in maximal OCR in the C57BL/6 mice subjected to ACF represents the diminishing of maximal mitochondrial function at CcOX (analogous to state 3 respiration in isolated mitochondria) as has been

shown before in rats [27]. The fact that there was no change in basal OCR in the C57BL/6 or C3H_n::C57_{mt} AMCM exposed to ACF suggests that even though their basal mitochondrial function *ex vivo* was sufficient to support cellular function, there was less total mitochondrial function available should the cell need it due to an increase in workload or a secondary stress. Moreover, the AMCM were no longer contracting after isolation as they would have been *in vivo*, suggesting that they would have had a significantly higher ATP demand and may have needed a higher percent of their maximal mitochondrial function to support their basal function. This would result in even less reserve capacity in the AMCM subjected to ACF that the myocytes could call upon in the event of increased workload or stress, which could lead to cardiomyocyte dysfunction if there is not enough available mitochondrial function to fulfill the energy requirements of the cell.

Because the disruption of the desmin cytoskeleton has been implicated in both the development of heart failure and the regulation of mitochondrial bioenergetics [49, 50, 223, 224], the effects of ACF on the desmin organization was examined in LV sections from C57BL/6, C3H/HeN, and C57_n::C3H_{mt} mice. As can be seen in the desmin images from the sham mice from all of the strains, desmin is organized along the Z-lines of the myofibrils, maintaining the structure of the myocyte (**Figure 4-13**). Desmin also attaches to the mitochondria, both maintaining their organization along the myocytes and regulating their function [49, 50]. In the C57BL/6 mice subjected to ACF, there is an apparent loss of desmin staining along the Z-lines within the myocytes, indicating the loss of desmin cytoskeletal organization. Interestingly, the C3H/HeN and C57_n::C3H_{mt} mice were resistant to ACF-induced alterations in their desmin localization. Taken together, this

data provides a likely explanation as to why the mitochondrial function was altered in the C57BL/6 mice but not the C3H/HeN and C57_n::C3H_{mt} mice.

Next, transmission electron microscopy was used to examine the morphology of the myocytes from the three strains following sham or ACF surgeries (**Figure 4-14, 4-15**). As can be seen in the C57BL/6 sham sections, the intermyofibrillar mitochondria are organized along the myofibrils at the Z-lines with one mitochondrion per sarcomere [441]. This arrangement allows for efficient energy transfer from the mitochondria to the sarcomeres, supporting proper bioenergetic function *in vivo* while the heart is beating [86, 351, 393]. However, in C57BL/6 mice subjected to ACF, the mitochondrial organization is lost, most likely due to the disruption of the desmin cytoskeleton which holds them in place [49, 223, 224, 228]. Interestingly, the mitochondria also appear to be smaller and more electron dense, suggesting that they may also be undergoing mitochondrial fission [442, 443]. This induction of mitochondrial fission can mediate the initiation of mitophagy, which leads to the turnover of dysfunctional mitochondria [444-446].

The C3H/HeN sham mice exhibit the same mitochondrial and myofibrillar organization as the C57BL/6 shams; however, when subjected to ACF for three days, the C3H/HeN mice did not display the same loss of mitochondrial and myofibrillar organization as the C57BL/6 ACF mice. Upon closer inspection, it is evident that rather than condensing like the mitochondria in the C57BL/6 ACF mice, there is mitochondrial swelling and the apparent disruption of the cristae structure within the mitochondria [223]. These data suggest that without the loss of desmin, the mitochondrial organization is kept intact; however, there are still ACF-induced alterations to the mitochondria, even though these changes have yet to alter mitochondrial function.

Finally, LV sections from C57_n::C3H_{mt} mice subjected to either sham or ACF surgery were examined using transmission electron microscopy. The sham mice displayed the same mitochondrial organization as the C57BL/6 and C3H/HeN mice, and this organization was maintained in the animals subjected to ACF. Interestingly, the sections from the ACF C57_n::C3H_{mt} mice show a combination of the phenotypes of the C57BL/6 and C3H/HeN mice subjected to ACF. Similar to the C3H/HeN mice, the mitochondrial organization was maintained, likely due to the maintenance of the cytoskeleton. Moreover, even though the mitochondrial organization was maintained, the mitochondria appear to be smaller and more condensed, indicating that they are undergoing mitochondrial fission.

Taken together, these data suggest that the induction of mitochondrial fission and the loss of cytoskeletal organization leading to the loss of mitochondrial organization and function in response to ACF track with the mtDNA of the C57BL/6 mice. Furthermore, the C3H/HeN mtDNA seems to confer the protection of the mitochondrial organization and function by maintaining the desmin cytoskeleton in response to ACF. The differences in the cytoskeletal response to ACF likely play a role in the increased susceptibility to alterations in cardiac morphometry and function to ACF seen in the C57BL/6 mice as compared to the C3H/HeN mice. These effects may be mediated by the differential bioenergetic efficiencies between the strains, but further experiments would be required to prove a causal relationship. Moreover, the majority of the datasets discussed in this chapter need to be completed with the C3H_n::C57_{mt} mice to further strengthen our conclusion that the susceptibility to ACF-induced damage is mediated by the mtDNA haplotype.

Importantly, the differential susceptibilities of the two mtDNA haplotypes to volume overload-induced pathology can be related to differential population-based susceptibility to diseases in humans. Using the same methods that allowed for the development of mouse mtDNA phylogenetic trees, DNA sequencing has allowed for the tracing of the ancestry of populations of humans based on polymorphisms in their mtDNA sequence [403-405, 447]. Populations with similar mtDNA polymorphisms were then grouped into several different mtDNA haplogroups [20, 139-144, 448, 449]. Interestingly, the C57BL/6 mtDNA haplotype is similar to the African L haplogroup in humans, with increased mitochondrial efficiency and higher rates of ROS production while the C3H/HeN mtDNA haplotype is similar to the European H haplogroup, with decreased mitochondrial efficiency and lower rates of ROS production [140, 144]. Furthermore, it has been shown that a higher percent of people of African descent suffer from various forms of cardiovascular diseases than those of European descent, which supports the theory that increased ROS production due to the African mtDNA haplotype plays a role in the increased disease susceptibility [52, 53, 450, 451]. Therefore, the utilization of mouse models to examine the role of mtDNA haplotypes in susceptibility to pathologies will lead to the further understanding of the mechanisms by which the mtDNA can alter bioenergetic efficiency and disease progression, with obvious implications in the elucidation of human susceptibility and pathogenesis.

CHAPTER 5
DISCUSSION
INTRODUCTION

The data presented in this thesis illustrates the bioenergetic responses to stress induced by three pathologies in which mitochondrial dysfunction is a common feature. This was achieved by utilizing extracellular flux technology to measure alterations in the bioenergetics of intact primary cells induced by chronic EtOH consumption, hypoxia/reoxygenation, and cardiac volume overload. In Chapter 2 of this dissertation, the effects of chronic EtOH consumption on the mitochondrial bioenergetics within hepatocytes were examined using primary hepatocytes isolated from EtOH-fed rats. Next, the alterations of mitochondrial function in primary aortic endothelial cells in response to the stress of hypoxia/reoxygenation were assessed in Chapter 3. Finally, the bioenergetic response to volume overload was studied in Chapter 4 using primary cardiomyocytes isolated from adult mice with different mtDNA haplotypes, which further illuminates the role of mtDNA in modulating mitochondrial function and disease susceptibility.

While these studies focus on the examination of the alterations in mitochondrial bioenergetics induced by these three specific pathologies, the data discussed herein are potentially applicable to the study of any other disease state associated with inflammation, increased energy demand, and/or mitochondrial dysfunction. The pathogenesis of ALD [28-30, 34, 160, 161, 257], hypoxia/reoxygenation [39, 40, 271, 272, 285], and car-

diac volume overload [27, 46, 47, 221] are all associated with the progression towards bioenergetic dysfunction and cell death mediated by the loss of mitochondrial function. A critical factor in this development of cellular dysfunction is the loss of the bioenergetic reserve capacity, which represents the cells' spare mitochondrial function which is not used under basal conditions but can be utilized in response to increased ATP demand or pathological stress [179, 180, 330, 349]. In this chapter, implications of the data illustrated in this dissertation will be discussed, focusing in particular on the importance of the bioenergetic reserve capacity in the three disease models described. Furthermore, the possible future directions of these projects and the potential application of this work to other pathologies will also be discussed.

Reserve Capacity and the Cellular Response to Pathological Stress

Mitochondria play a vital role in the maintenance of bioenergetic function in part through the production of ATP during normal physiological conditions. The rate of ATP production by mitochondria is exquisitely regulated and highly dependent upon the ATP demand of the cell. Because of this, mitochondria in most cell types operate well below their maximal capacity of ATP production under basal conditions, leaving a bioenergetic reserve capacity of additional mitochondrial function which the cells can utilize under increased ATP demand for the detoxification of reactive species, the repair of damaged proteins, and the preservation of cellular and organ function. Although the physiological importance of the reserve capacity has only recently become appreciated, the concept of reserve capacity has existed in the literature for a few decades. The first quantitative measurements of reserve capacity were achieved using O₂ measurements in conjunction

with ^{31}P -NMR to measure the synthesis of phosphocreatine and ATP in myocytes [181, 182]. These studies showed that with increased exercise or treatment with an uncoupler, there was an increase in O_2 consumption and ATP/phosphocreatine synthesis beyond the basal rate, suggesting that there is “spare” mitochondrial function which can be utilized upon increased ATP demand. These discoveries have been expanded upon in several different disease models associated with increased ATP demand along with the loss of mitochondrial reserve capacity, leading to bioenergetic failure.

In addition to inducing an increase in ATP demand, the pathologies studied in this dissertation are also associated with oxidative and nitrative stress, which can damage the mitochondria and thus lower their maximal functional capacity. The data described in this dissertation examine the effects of chronic EtOH consumption, hypoxia/reoxygenation, and cardiac volume overload on the bioenergetic function in primary hepatocytes, endothelial cells, and cardiomyocytes, respectively. All three of these pathologies resulted in a diminished reserve capacity, leaving the cells more susceptible to stress-induced bioenergetic dysfunction.

ALCOHOL-INDUCED LOSS OF MITOCHONDRIAL FUNCTION

In Chapter 2, the bioenergetic response of hepatocytes to chronic EtOH consumption, as well as their susceptibility to bioenergetic dysfunction in response to NO and hypoxia, was examined. The data presented in Chapter 2 show that chronic EtOH consumption resulted in the inhibition of the maximal OCR of the hepatocytes. Furthermore, hepatocytes isolated from control and EtOH-fed rats exhibited the same basal OCR. Taken together, these data demonstrate that EtOH-induced hepatotoxicity causes a de-

crease in the reserve capacity of the hepatocytes, which we hypothesized would render them more susceptible to bioenergetic dysfunction induced by stress.

Role of Nitric Oxide in Alcohol-Dependent Hepatotoxicity

Importantly, chronic EtOH consumption is well known to cause an increase in iNOS expression in the liver, leading to the increased production of $\cdot\text{NO}$ [33, 34, 36]. $\cdot\text{NO}$ can reversibly inhibit respiration by competing for O_2 at CcOX and irreversibly inhibit respiration by reacting with superoxide to produce peroxynitrite, which can oxidatively damage mitochondrial proteins [189-192, 452-457]. To test the hypothesis that the decreased reserve capacity of primary hepatocytes isolated from EtOH-fed rats renders them more susceptible to bioenergetic dysfunction in response to an additional insult, the hepatocytes were then treated with the $\cdot\text{NO}$ donor DetaNO [180, 254]. Indeed, the hepatocytes isolated from EtOH-fed rats that were treated with $\cdot\text{NO}$ developed bioenergetic dysfunction, as seen by the decrease in both basal and maximal OCR and the almost complete loss of reserve capacity. These effects are likely mediated by both the ability of $\cdot\text{NO}$ to reversibly inhibit respiration and the formation of reactive nitrogen species upon reacting with ROS (**Figure 5-1**). Importantly, chronic EtOH consumption has been shown to cause increased levels of ROS production in the liver, which supports this concept [29, 30, 160, 263, 458].

Alcohol Consumption Alters Hepatocellular Response to Hypoxia

The next set of experiments in Chapter 2 examines the effects of $\cdot\text{NO}$ treatment to control and EtOH hepatocytes in the context of hypoxia. ALD is also associated with the

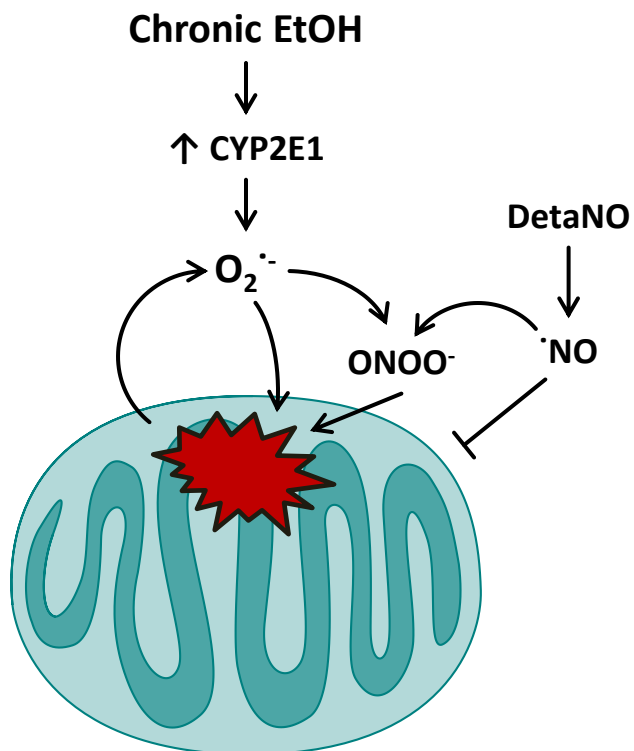


Figure 5-1. Peroxynitrite formation is a likely mediator of bioenergetic dysfunction in alcohol-induced hepatotoxicity. Primary hepatocytes isolated from EtOH-fed rats have increased expression of CYP2E1, which can produce superoxide. Superoxide can react with $\cdot NO$ produced from DetaNO to form peroxynitrite ($ONOO^-$). $ONOO^-$ itself, and the radical products of its reaction, with CO_2 can damage mitochondrial proteins, lipids, and DNA and cause bioenergetic dysfunction.

development of hypoxia in the liver, which has been implicated in mediating the development of mitochondrial damage [35, 36, 161, 187, 188, 253, 263, 264]. Primary hepatocytes isolated from control animals exhibited a progressive decrease in OCR over time as the concentration of O₂ dropped. Interestingly, hepatocytes from EtOH-fed animals were less sensitive to the decreasing O₂ concentrations compared to the control hepatocytes. This differential response to hypoxia is likely a result of the prolonged *in vivo* exposure to hypoxia that the EtOH hepatocytes were subjected to prior to isolation. The hepatocytes isolated from the EtOH-fed animals have had increased HIF-1 α signaling for the duration of the development of hypoxia associated with the chronic EtOH feeding, and HIF-1 α signaling has been shown to regulate mitochondrial metabolism and protect from a subsequent hypoxic insults [199, 244, 459-462]. Furthermore, when treated with increasing concentrations of DetaNO during the exposure to hypoxia, control hepatocytes exhibited a slight inhibition of respiration at low O₂ concentrations. However, EtOH hepatocytes were much more sensitive to \cdot NO-dependent inhibition of respiration than the control hepatocytes. This data corroborates previous findings which show a similar effect in isolated liver mitochondria following chronic EtOH consumption [33].

The increased susceptibility to bioenergetic dysfunction which is evident in the hepatocytes isolated from EtOH-fed animals is likely mediated by the diminished reserve capacity. This supports previous findings which show that chronic EtOH consumption induces decreased mitochondrial respiratory protein levels [159, 463]. These alterations have been suggested to be a result of EtOH-induced mtDNA damage [464, 465] and decrease in functional mitochondrial ribosomes [466, 467]. However, these changes in mi-

tochondrial protein levels induced by chronic EtOH consumption could also be at least partially explained by the associated liver hypoxia as discussed below.

Hypoxic Signaling as a Mediator of Alcohol-Induced Bioenergetic Alterations

Stabilization of HIF-1 α during hypoxia and the resulting induction of hypoxic signaling have been shown to mediate the adaptation to hypoxia by down-regulating mitochondrial O₂ consumption [459-461, 468]. This occurs through the induction of pyruvate dehydrogenase kinase, which inhibits pyruvate dehydrogenase from utilizing pyruvate to fuel the Krebs cycle to make reducing equivalents for the electron transport chain [468]. Furthermore, HIF-1 α signaling induces the increased expression of lactate dehydrogenase A, which converts pyruvate to lactate, leaving less pyruvate as substrate for pyruvate dehydrogenase [460]. Recent studies have also shown that hypoxic signaling induces CcOX subunit IV isoform switching, mitophagy, and the expression of microRNA-210, which inhibits the production of Fe/S clusters that are required for oxidative phosphorylation [459, 461, 462, 469-471].

These responses to hypoxic signaling decrease mitochondrial O₂ consumption, while also making the electron transport chain more efficient [461]. Taken together with the fact that the production of reducing equivalents is diminished by the increased expression of pyruvate dehydrogenase kinase and lactate dehydrogenase A in hypoxia, these mitochondrial phenotypic alterations are predicted to decrease the formation of ROS by the mitochondria during hypoxia and likely evolved as a protective mechanism to decrease oxidative damage in response to further hypoxia. However, in the context of chronic EtOH consumption, there is also the increased production of \cdot NO, which further

inhibits respiration, particularly in hypoxia. Therefore, the diminished mitochondrial function and reserve capacity render the hepatocytes more susceptible to bioenergetic dysfunction induced by the stress of hypoxia and NO . These effects, in combination with the documented increases in mtDNA damage induced by chronic EtOH, may provide a more complete understanding of the development of bioenergetic dysfunction in ALD. Future studies into the role of HIF-1 α signaling in the development of EtOH-dependent hepatotoxicity should be performed to more thoroughly elucidate the exact mechanisms which are involved in the disease progression.

EFFECT OF HYPOXIA/REOXYGENATION ON BIOENERGETIC FUNCTION

In Chapter 3, the bioenergetic response of primary bovine aortic endothelial cells (BAEC) to the exposure of hypoxia and reoxygenation was examined. Moreover, the effect of the reactive lipid HNE, which is formed *in vivo* during ischemia and reperfusion, on the mitochondrial function of BAEC in hypoxia and reoxygenation was investigated. The data presented in Chapter 3 show that endothelial cells exposed to HNE exhibit a diminished maximal mitochondrial function and reserve capacity. This decrease in mitochondrial reserve capacity led to the development of bioenergetic dysfunction when the cells were exposed to hypoxia/reoxygenation.

Endothelial Cell Mitochondrial Function is Altered in Hypoxia

The effect of changing O_2 concentrations on the bioenergetic function of endothelial cells was examined using an XF24 analyzer in a hypoxia chamber set at 1% O_2 . Upon the exposure to hypoxia, BAEC exhibited the progressive loss of O_2 consumption

at O_2 concentrations of $35 \mu\text{M}$ and below. The dependence of OCR on the O_2 concentration conformed to saturation kinetics, with apparent J_{max} of $55 \text{ pmol } O_2/\text{min}$ and an apparent P_{50} of $9.27 \mu\text{M } O_2$. Interestingly, treatment with FCCP during the progressively decreasing OCR, presumably due to the O_2 concentration limiting CcOX activity, resulted in the stimulation of O_2 consumption. This result can be explained by exploring the regulation of CcOX activity.

CcOX activity is subject to four means of regulation: the supply of O_2 as an electron acceptor, the supply of electrons from reducing equivalents and reduced cytochrome *c*, the electrochemical gradient against which it must pump protons, and its intrinsic maximal rate of enzyme turnover [229, 365, 366, 368-370, 428, 472-480] (**Figure 5-2**). Using pure enzyme or lysates with the excess supply of O_2 and an electron donor, and with no electrochemical gradient to pump protons against, allows for the measurement of the maximal intrinsic activity of CcOX. However, in a cell under normal physiological conditions, CcOX activity is typically regulated by the electrochemical gradient. When cells are uncoupled using compounds such as FCCP, the electrochemical gradient is diminished resulting in the increased activity of CcOX. This increased activity of CcOX is then largely regulated by the supply of electrons from reducing equivalents and cytochrome *c*. Under conditions of severe hypoxia, the supply of O_2 becomes limiting, decreasing the activity of CcOX.

These methods of regulation also help to explain the differences that are seen in the kinetic analysis of CcOX activity over changing O_2 concentrations (**Figure 5-3**). Pure enzyme or lysates with excess substrates and no electrochemical gradient to pump protons against exhibit the highest rate (V_{max}) of CcOX activity. The activity of CcOX in

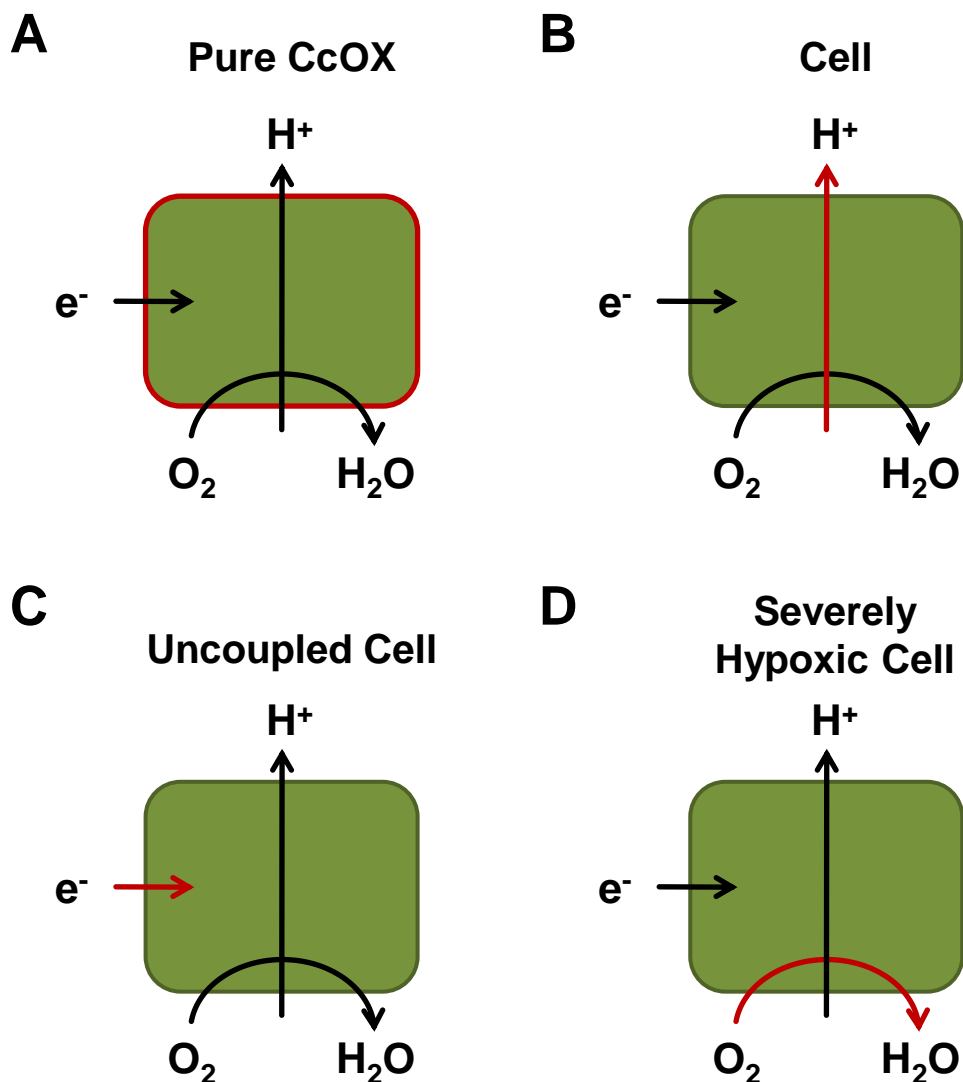


Figure 5-2. Regulation of cytochrome *c* oxidase activity in different systems. (A) In kinetic studies with pure CcOX enzyme or in lysates, electron sources (e^-) and O_2 are in excess and there is no proton gradient; therefore, the only thing limiting the reaction rate is the enzyme itself. (B) In a cell under physiological conditions, O_2 and e^- are in excess; however, there is a proton gradient, which is the limiting factor for the rate of enzyme turnover. This is why an uncoupler, which diminishes the proton gradient, is able to stimulate CcOX activity such that the supply of e^- (in normoxia) becomes limiting (C). (D) Severe hypoxia is caused by a decrease in O_2 supply, making the O_2 the rate limiting factor of CcOX activity. The red line represents the rate-limiting factor in the activity of CcOX.

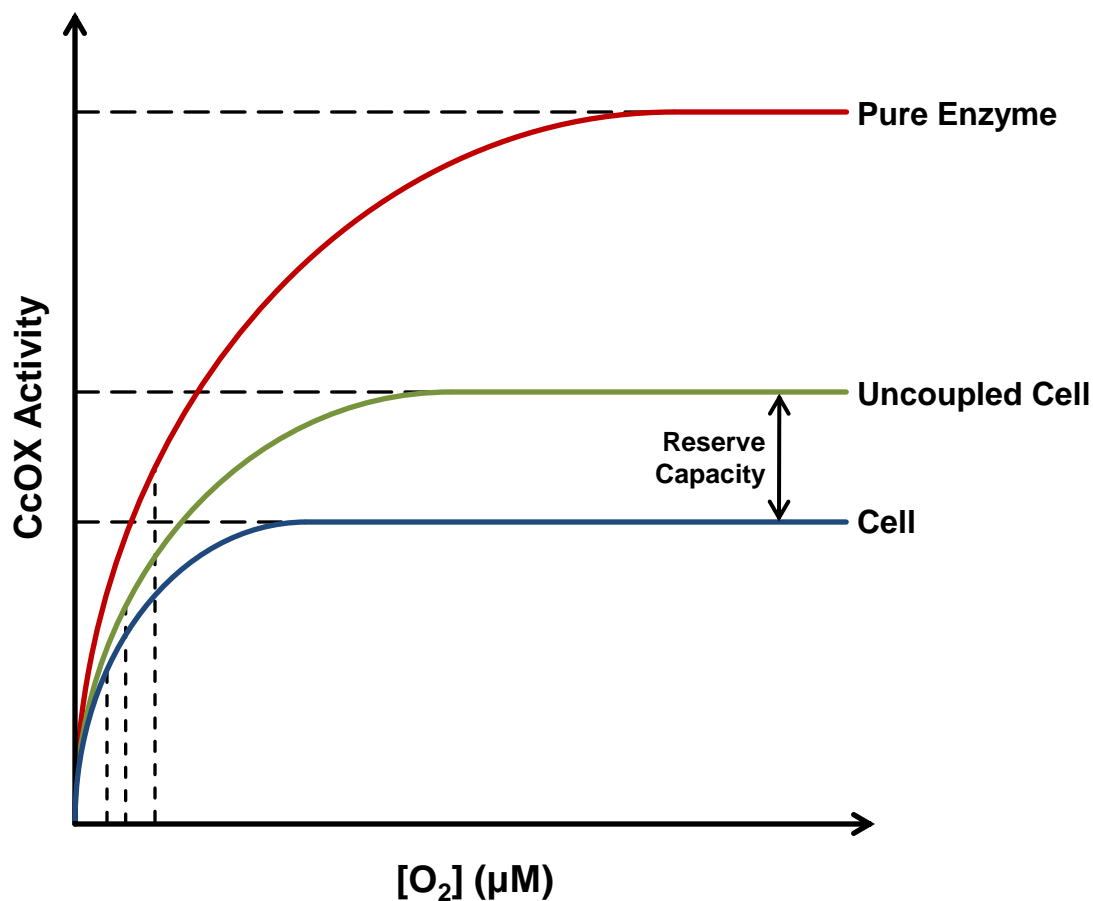


Figure 5-3. Kinetics of cytochrome *c* oxidase activity in different systems. The kinetic profile of CcOX activity as a function of O_2 concentration ($[O_2]$) varies depending on the specific system in which it's measured. In kinetic assays using pure enzyme or lysates with the excess supply of electron donors (**red line**), the V_{\max} of CcoX is dependent only on its maximal intrinsic activity and the K_m is dependent CcOX's inherent affinity for O_2 . The J_{\max} of CcOX in a cellular context (**blue line**) is limited by the electrochemical gradient against which it pumps H^+ . The J_{\max} of CcOX in uncoupled cells (**green line**) is often higher than in coupled cells due to the shift of control from the electrochemical gradient (which is now lost) to the supply of reducing equivalents. This increase in J_{\max} due to uncoupling is the biochemical basis of the reserve capacity measured in the XF24. The V_{\max} or J_{\max} is represented by the horizontal dashed lines, and the K_m or P_{50} is represented by the vertical dashed lines.

cells (J_{\max}) is much lower, as it is subject to regulation by the integrated pathway of substrate supply and the electron transport chain and most importantly the electrochemical gradient, and is representative of the basal OCR which is measured by the XF24 analyzer. Uncoupling the cells results in the stimulation of the J_{\max} of CcOX due to the loss of the membrane potential, and represents the maximal OCR as measured in the XF24. Furthermore, because the apparent K_m or P_{50} of CcOX is dependent on enzyme turnover, lysates and pure enzyme will have a higher apparent K_m compared to cells [477]. Because all of the CcOX is actively binding O_2 and converting it to H_2O in lysates, the activity of CcOX is more sensitive to the loss of O_2 . On the other hand, cells have a lower apparent P_{50} for CcOX because although all of the CcOX is binding O_2 , only a proportion of the available enzyme is active due to the regulatory constraints discussed previously. Therefore, cellular CcOX is less sensitive to decreasing O_2 concentrations due to their reserve capacity of CcOX activity.

Reoxygenation Induces Progressive Loss of Mitochondrial Function

To investigate the effects of hypoxia/reoxygenation on endothelial cells, BAEC were exposed to decreasing O_2 concentrations as described previously; however, they were reoxygenated prior to reaching the O_2 concentration shown to induce a decrease in OCR of greater than 10%. Interestingly, the exposure of BAEC to hypoxia/reoxygenation elicited a progressive decrease in the OCR of the cells. This decrease in the OCR of BAEC in response to hypoxia/reoxygenation can be related to the loss of mitochondrial function, as the majority of the OCR of endothelial cells is attributable to mitochondrial function and can be inhibited by antimycin A. The loss of mitochondrial

function in response to hypoxia/reoxygenation was then quantified by calculating the derivative of the decreasing OCR, showing that reoxygenation resulted in the significant loss of mitochondrial function.

Oxygen-Dependent Effects of HNE on Mitochondrial Function

The reactive lipid peroxidation product HNE has been shown to be produced in ischemia/reperfusion [323, 324], and is well known to modify mitochondrial proteins and alter their functions [179, 323, 330, 331, 341, 344, 349]. Another focus of Chapter 3 was to investigate whether the HNE-induced modulation of mitochondrial function in endothelial cells is dependent on the O₂ concentration. When BAEC were exposed to HNE in room air, they exhibited a concentration-dependent loss of basal, maximal, and ATP-linked OCR together with an increase in proton leak. Furthermore, HNE treatment also caused the progressive loss of reserve capacity, as has been shown previously [179]. However, when BAEC were treated with HNE in hypoxia, HNE induced a transient decrease in OCR which returned to level of vehicle-treated endothelial cells after 60 min. Interestingly, once the basal OCR of the endothelial cells began to decrease due to decreasing O₂ concentrations, HNE had no additional effects on the basal OCR. This data suggests that HNE modifies and inhibits proteins which are responsible for the control of CcOX activity, but as the O₂ concentration began to decrease the OCR, the control of CcOX was altered such that the inhibition of HNE-modified proteins no longer affected O₂ consumption at CcOX. In support of this hypothesis, when the endothelial cells treated with HNE were reoxygenated, there was a significant increase in the progressive

loss of mitochondrial function compared to vehicle-treated as well as HNE-treated BAEC in room air.

Taken together, these data show that the mitochondrial dysfunction which occurs in ischemia/reperfusion can be recapitulated *in vitro* using this model of hypoxia/reoxygenation (**Figure 5-4**). Furthermore, the fact that the combination of stress from HNE exposure and reoxygenation caused the greater loss of mitochondrial function supports the hypothesis that the loss of reserve capacity renders cells more susceptible to bioenergetic dysfunction, as seen with HNE-treatment in room air and hypoxia leading to the cumulative loss of mitochondrial function upon reoxygenation. Future studies will investigate the effects of different lengths of exposure to hypoxia and reoxygenation on mitochondrial function. In addition, the effects of HNE exposure in hypoxia will be further examined.

SUSCEPTIBILITY TO BIOENERGETIC ALTERATIONS IS MEDIATED BY mtDNA HAPLOTYPE

In Chapter 4, the role of mtDNA haplotype in determining the susceptibility to volume overload-induced alterations in mitochondrial bioenergetics was assessed. In order to examine the effects of different mtDNA haplotypes, two strains of mice (C57BL/6 and C3H/HeN) with known differences in mtDNA haplotype were used [400]. Although there were no differences in the mitochondrial protein levels or enzyme activities from isolated cardiomyocytes between the two strains, they each exhibited a distinct mitochondrial profile. C57BL/6 cardiomyocytes have a significantly higher maximal OCR than the C3H/HeN, and taken together with the similar basal rates, the C57BL/6 cardiomyocytes also have a significantly higher reserve capacity.

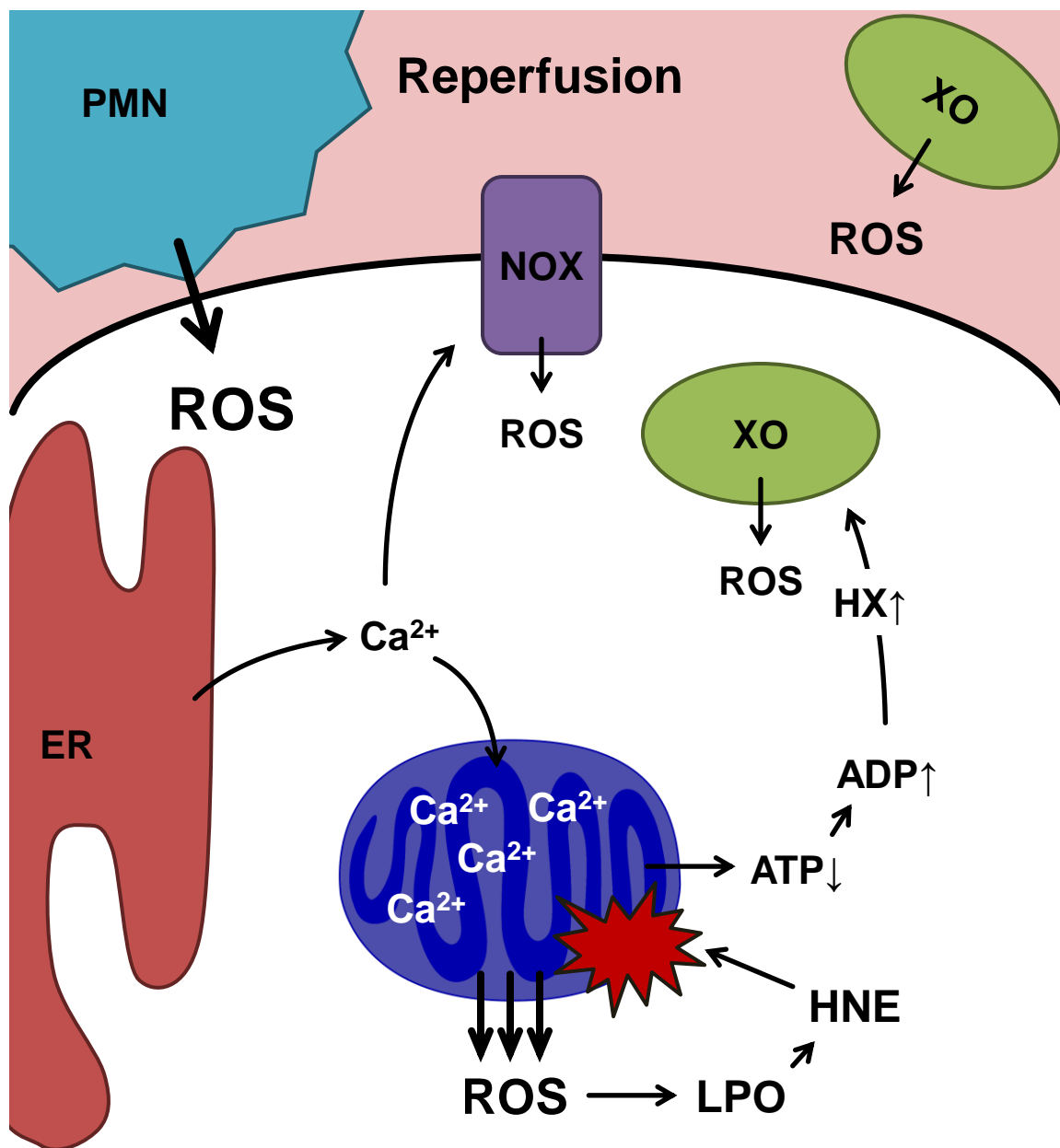


Figure 5-4. Reperfusion exacerbates bioenergetic and cellular dysfunction. Reperfusion causes damage by stimulating mitochondrial ROS formation due to reductive stress and mitochondrial damage incurred during ischemia. This loss of mitochondrial function results in increased hypoxanthine (HX) production, which is the substrate for xanthine oxidase (XO), by the breakdown of ADP. Calcium (Ca²⁺) release from the endoplasmic reticulum (ER) continues, causing further Ca²⁺ overload. NADPH oxidase (NOX) and XO are activated in reperfusion, producing high levels of ROS. Reperfusion is also associated with circulating XO, as well as recruited polymorphonuclear cells (PMNs) due to tissue damage during ischemia, inducing inflammation and further oxidative stress. The ROS formed during ischemia and reperfusion induce lipid peroxidation (LPO), resulting in the production of 4-hydroxynonenal (HNE) leading to the progression of mitochondrial dysfunction.

Bioenergetic Responses to Volume Overload in C57BL/6 and C3H/HeN Mice

Possessing a higher reserve capacity implies that the C57BL/6 cardiomyocytes have more mitochondrial function which they can utilize under conditions of increased energy demand or stress, which typically suggests that they would be more protected from stress [180]. However, when subjected to three days of ACF, the C57BL/6 mice exhibited a significant decrease in maximal OCR, while C3H/HeN mice displayed no alterations in their maximal OCR in response to ACF. When looking at the C57BL/6 strain alone, inducing the ACF did indeed induce a decrease in reserve capacity, suggesting that the myocytes would be more susceptible to further stress. However, when comparing across different haplotypes and strains, a lower reserve capacity is not a sufficient predictor of pathological outcomes. Because there are many other factors which play a role in cellular bioenergetics in cardiomyocytes, a broader examination of different pathways involved in the maintenance of bioenergetic function must be undertaken. For example, the different strains may exhibit differences in their expressions or activities of the isoforms of creatine kinase or have different levels of phosphocreatine as an energy buffer [84, 86, 351, 393, 394, 481]. Furthermore, they may have distinct reliances on fatty acid oxidation or glycolysis, or they may have mitochondria with different efficiencies [59, 400, 407, 409, 416]. All of these factors can play critical roles in the bioenergetic function of the cardiomyocytes, and elucidating the functions of these pathways in the different strains is a potential future direction for these studies.

Effect of mtDNA on Changes in Morphometry and Function by Volume Overload

In order to control for the various phenotypic differences which exist between the C57BL/6 and C3H/HeN mice due to their different nuclear genomes, MNX mice were utilized with the nDNA of one strain and the mtDNA of the other strain. Using this novel mouse model, any differences which are observed can be traced to the nDNA or the mtDNA, and therefore allow for the elucidation of the role of mtDNA haplotype in the determination of disease susceptibility. In the first set of experiments using MNX mice, echocardiography and catheterization were used to measure different parameters of left ventricular morphometry and function following three days after sham or ACF surgeries. C57BL/6 mice exposed to ACF surgery exhibited a significant increase in the LVEDD as compared to the shams, while the C3H/HeN mice showed no difference between the groups. Interestingly, the C57_n::C3H_{mt} mice subjected to ACF did not show a significant increase in LVEDD as compared to sham, suggesting that the susceptibility to ACF-induced volume overload was due to the C57BL/6 mtDNA because the switching the C57BL/6 nDNA mouse to the C3H/HeN mtDNA reversed this susceptibility.

Volume Overload-Induced Alterations in Mitochondrial Function in MNX Mice

Volume overload and heart failure have been shown to be associated with the induction of alterations in mitochondrial function and cellular bioenergetics [17, 27, 221, 384, 385, 389, 482]. AMCM were isolated from C57BL/6, C3H/HeN, C57_n::C3H_{mt}, and C3H_n::C57_{mt} mice three days after the induction of an ACF or the sham surgery to assess their mitochondrial function. The C57BL/6 mice had higher basal OCR than the sham mice from the other three strains, but the AMCM isolated from ACF mice were not dif-

ferent than the sham mice from the same strains. This data supports previous findings which have shown that volume overload increases the vulnerability of heart mitochondria without affecting their function in the absence of stress [389]. Interestingly, treating the AMCM with FCCP to stimulate their maximal OCR revealed that ACF caused a decrease in maximal mitochondrial function in C57BL/6 and C3H_n::C57_{mt} mice as compared to their respective shams. Moreover, the maximal OCR of the AMCM was found to not be affected by ACF in the C3H/HeN and C57_n::C3H_{mt} mice. Because there were no differences between the basal OCR within each strain, the reserve capacity of the AMCM in response to ACF followed the same trend as the maximal OCR. Additionally, there were no significant differences in the non-mitochondrial OCR between the strains or between sham and ACF within the same strain. Taken together, these data support the concept that mtDNA haplotype can determine the susceptibility to volume overload-induced bioenergetic dysfunction.

Loss of Desmin Mediates Bioenergetic Alterations Induced by Volume Overload

The desmin cytoskeleton has been implicated in maintaining cardiomyocyte structure and regulating its bioenergetic function, and has been shown to be altered during the progression to heart failure [27, 49, 50, 223, 224, 228, 351, 394]. Using immunohistochemistry, the desmin organization was examined in sham and ACF C57BL/6, C3H/HeN, and C57_n::C3H_{mt} mice. As can be seen in the LV sections from the sham mice of all three strains, the desmin cytoskeleton runs along the Z-lines of the myofibrils to maintain the cardiomyocyte structure, as well as to preserve the mitochondrial organization along the myofibrils [49, 50]. Interestingly, C57BL/6 mice subjected to ACF ex-

hibited a decrease in desmin staining, showing a loss or disruption of the desmin cytoskeleton. However, the C3H/HeN and C57_n::C3H_{mt} mice subjected to ACF were resistant to alterations in their desmin cytoskeleton. This data further supports the concept of mtDNA haplotype regulating the disease susceptibility, and also provides a likely mechanism to explain the alterations in mitochondrial function seen in the C57BL/6 mice.

Volume Overload-Induced Changes in Cardiomyocyte Morphology

Finally, transmission electron microscopy was used to examine any gross morphological effects of ACF on the LV tissue in each strain. In the sham mice, normal cardiomyocyte morphology can be seen, with myofibrils running in parallel and the mitochondria organized along the myofibrils, often with one mitochondrion per sarcomere. Interestingly, in the C57BL/6 mice subjected to ACF, there is the loss of mitochondrial organization, which is likely mediated by the disruption of the desmin cytoskeleton. Furthermore, the mitochondria are smaller and more condensed, suggesting that they are undergoing mitochondrial fission, which has recently been identified as a mechanism of initiation for mitophagy [374, 443-446, 483]. In C3H/HeN mice, the mitochondrial organization was maintained upon induction of ACF. However, the mitochondria appear to be swelling, which suggests that even though there were no apparent changes in mitochondrial bioenergetics or organization, the mitochondria may be progressing towards dysfunction through different mechanisms. The C57_n::C3H_{mt} mice subjected to ACF were also protected from the loss of mitochondrial organization; however, they also exhibit smaller and more electron-dense mitochondria which appear to be undergoing fission.

The completion of these data sets with the C3H_n::C57_{mt} MNX mice is needed to more fully understand the phenomena discussed in this Chapter 4. However, these data suggest that the C57BL/6 mtDNA haplotype renders the mice susceptible to the ACF-induced disruption of the desmin cytoskeleton, which may be mediated by increased MMP activity, leading to the loss of mitochondrial organization and subsequent alterations in bioenergetic function. Furthermore, the C3H/HeN mtDNA haplotype was resistant to these ACF-induced changes, and was able to rescue the MNX mice with C57BL/6 nDNA and C3H/HeN mtDNA. Moreover, the C57BL/6 mtDNA rendered the MNX mice with C3H/HeN nDNA susceptible to ACF-induced bioenergetic dysfunction, although further studies will be necessary to confirm this induced susceptibility with other endpoints.

Relating Mouse mtDNA Haplotypes to Human mtDNA Haplogroups

The determination of mtDNA haplogroups/haplotypes was made possible by the sequencing of the mtDNA of both humans and mice [143, 399-401, 403, 404]. Human mtDNA haplogroups were grouped based on similar sequences, which allowed for the determination of the human mtDNA phylogenetic tree, which allows insight into the evolution of select populations of humans during early global migrations [20, 139, 140, 142, 143, 427, 448, 484, 485]. Importantly, different mtDNA haplotypes exhibit varying mitochondrial phenotypes; moreover, the evolution of distinct mtDNA haplogroups has been postulated to have been selected for based on the different environments of each population [20, 139, 140, 142, 144, 447-449, 484, 485]. These unique mitochondrial phenotypes, which once may have been beneficial, are now credited with different haplo-

groups' altered susceptibilities to various diseases associated with mitochondrial pathology [54, 56, 57, 60, 143, 406, 450, 484].

The phenotypes of the C57BL/6 and C3H/HeN mouse mtDNA haplotypes are similar to the African (L) and European (H) human mtDNA haplogroups, respectively. Both the C57BL/6 haplotype and the L haplogroup are characterized by high bioenergetic efficiency and high levels of ROS production, as well as being more susceptible to cardiovascular diseases. In contrast, the C3H/HeN haplotype and H haplogroup are associated with being less bioenergetically efficient while producing lower levels of mitochondrial ROS, and they are both typically more resistant to cardiovascular diseases [52, 53]. These different mitochondrial phenotypes are due to the different polymorphisms which separate the strains (**Figure 5-5**) [143, 401]. Importantly, while the C57BL/6 and C3H/HeN haplotypes mimic the phenotypes of the L and H haplogroups, the SNPs which separate these groups are different in the mice and humans. Therefore, investigations which utilize this mouse model of C57BL/6 and C3H/HeN mice as different mtDNA haplotypes, while showing the efficacy of these types of studies, may only elucidate the effects of the specific alterations in the CcOX-III, NDIII, and mt-tRNA^{Arg} genes; however, selecting mice haplotypes which share the same SNPs as specific human haplogroups, or inducing alterations in the mtDNA of mice to match differences between human haplogroups, would allow for the examination of the phenotypic changes which occur with specific human mtDNA haplogroups. Using the knowledge gained from studies comparing different mtDNA haplotypes, the role of distinct polymorphisms in the susceptibility to or initiation of specific diseases may be elucidated, which would have tremendous potential for the development of therapeutics to treat the diseases.

mtDNA SNPs between C57BL/6 and C3H/HeN:

NADH Dehydrogenase subunit III
 Cytochrome c Oxidase subunit III
 tRNA^{Arg}

mtDNA SNPs between L and H:

NADH Dehydrogenase subunit II
 NADH Dehydrogenase subunit III
 2x – NADH Dehydrogenase subunit V
 Cytochrome *b*
 Cytochrome c Oxidase subunit I
 ATP Synthase F0 subunit VI
 tRNA^{Asp}
 tRNA^{Ile}
 4x – 12S ribosomal RNA
 3x – 16S ribosomal RNA

Figure 5-5. mtDNA single nucleotide polymorphisms between C57BL/6 and C3H/HeN mouse haplotypes and between L and H human haplogroups. Single nucleotide polymorphisms (SNPs) which result in non-synonymous mutations in the mtDNA gene products between the two haplotypes/haplogroups [111, 401].

CONCLUSIONS

In this dissertation, the mechanisms of pathogenesis mediated by alterations in mitochondrial bioenergetic function of three disease models have been investigated by monitoring the alterations of mitochondrial function in response to stress. While a great deal is already known about the diseases of interest, recent advances in technology were utilized to elucidate stress-induced changes in mitochondrial bioenergetics while still within the context of intact cells. Examining alterations in mitochondrial function within primary cells is of critical importance because the mitochondria are still subjected to their endogenous regulation, which is extremely difficult to mimic in studies of isolated mitochondria or enzymes.

In Chapter 2, chronic EtOH consumption was shown to decrease the reserve capacity of isolated primary hepatocytes, rendering them more susceptible to bioenergetic dysfunction induced by the EtOH-associated mitochondrial stresses of $\cdot\text{NO}$ and hypoxia. Data discussed in Chapter 3 exhibited that exposure of endothelial cells to hypoxia/reoxygenation resulted in the progressive loss of mitochondrial function. Furthermore, Chapter 3 examined the O_2 -dependence of the HNE-induced alterations in mitochondrial function, showing that although HNE has only transient effects on the basal OCR in hypoxia, upon reoxygenation HNE induced a significant exacerbation of the loss of mitochondrial function. Chapter 4 investigated the effects of volume overload on mitochondrial bioenergetics and cellular morphology, and revealed that the susceptibility to these volume overload-induced changes in physiology is controlled by the mtDNA haplotype.

Taken together, the data presented in this dissertation further elucidate the central role of the mitochondrion in the development and progression of ALD, vascular ische-

mia/reperfusion, and cardiac volume overload. Importantly, these studies support the hypothesis that bioenergetic dysfunction develops in response to the mitochondrial stresses which are associated with these diseases discussed herein. Moreover, the techniques which were developed to accomplish these studies and the knowledge gained in their accomplishment can be applied to the investigations of other pathological conditions associated with the development of bioenergetic dysfunction, such as diabetes and neurodegenerative disorders.

REFERENCES

1. Lehninger, A.L., *The enzymic and morphologic organization of the mitochondria*. Pediatrics, 1960. **26**: p. 466-75.
2. Lardy, H.A. and S.M. Ferguson, *Oxidative phosphorylation in mitochondria*. Annu Rev Biochem, 1969. **38**: p. 991-1034.
3. Rizzuto, R., P. Bernardi, and T. Pozzan, *Mitochondria as all-round players of the calcium game*. J Physiol, 2000. **529 Pt 1**: p. 37-47.
4. Crompton, M., *The mitochondrial permeability transition pore and its role in cell death*. Biochem J, 1999. **341 (Pt 2)**: p. 233-49.
5. Duchen, M.R., *Mitochondria and Ca(2+) in cell physiology and pathophysiology*. Cell Calcium, 2000. **28(5-6)**: p. 339-48.
6. Duchen, M.R., *Mitochondria and calcium: from cell signalling to cell death*. J Physiol, 2000. **529 Pt 1**: p. 57-68.
7. Nicholls, D.G. and R.M. Locke, *Thermogenic mechanisms in brown fat*. Physiol Rev, 1984. **64(1)**: p. 1-64.
8. Silva, J.E. and R. Rabelo, *Regulation of the uncoupling protein gene expression*. Eur J Endocrinol, 1997. **136(3)**: p. 251-64.
9. Cannon, B. and J. Nedergaard, *Brown adipose tissue: function and physiological significance*. Physiol Rev, 2004. **84(1)**: p. 277-359.
10. Quintero, M., et al., *Mitochondria as signaling organelles in the vascular endothelium*. Proc Natl Acad Sci U S A, 2006. **103(14)**: p. 5379-84.

11. Liu, X., et al., *Induction of apoptotic program in cell-free extracts: requirement for dATP and cytochrome c*. Cell, 1996. **86**(1): p. 147-57.
12. Garrido, C., et al., *Mechanisms of cytochrome c release from mitochondria*. Cell Death Differ, 2006. **13**(9): p. 1423-33.
13. Ow, Y.P., et al., *Cytochrome c: functions beyond respiration*. Nat Rev Mol Cell Biol, 2008. **9**(7): p. 532-42.
14. Cowan, K.J., *The Mitochondria: Powerhouse of the Cell*, in *Functional Metabolism: Regulation and Adaptation*, K.B. Storey, Editor 2004, John Wiley and Sons: Hoboken, NJ. p. 211-241.
15. Racker, E. and H. L.L., *Mechanism and Control of Oxidative Phosphorylation*, in *Energy Metabolism and the Regulation of Metabolic Processes in Mitochondria*, M.A. Mehlman and R.W. Hanson, Editors. 1972, Academic Press: New York. p. 1-25.
16. RANDLE, P.J., et al., *The glucose fatty-acid cycle. Its role in insulin sensitivity and the metabolic disturbances of diabetes mellitus*. Lancet, 1963. **1**(7285): p. 785-9.
17. Marín-García, J., *Mitochondria and the Heart* 2005, New York: Springer. 400.
18. Hopkins, T.A., J.R. Dyck, and G.D. Lopaschuk, *AMP-activated protein kinase regulation of fatty acid oxidation in the ischaemic heart*. Biochem Soc Trans, 2003. **31**(Pt 1): p. 207-12.
19. Wallace, D.C., *Diseases of the mitochondrial DNA*. Annu Rev Biochem, 1992. **61**: p. 1175-212.
20. Wallace, D.C., *Mitochondrial DNA sequence variation in human evolution and disease*. Proc Natl Acad Sci U S A, 1994. **91**(19): p. 8739-46.
21. Wallace, D.C., *Mitochondrial diseases in man and mouse*. Science, 1999. **283**(5407): p. 1482-8.

22. Wallace, D.C., *A mitochondrial paradigm of metabolic and degenerative diseases, aging, and cancer: a dawn for evolutionary medicine*. *Annu Rev Genet*, 2005. **39**: p. 359-407.
23. Ballinger, S.W., *Mitochondrial dysfunction in cardiovascular disease*. *Free Radic Biol Med*, 2005. **38**(10): p. 1278-95.
24. Lemasters, J.J., et al., *Mitochondrial dysfunction in the pathogenesis of necrotic and apoptotic cell death*. *J Bioenerg Biomembr*, 1999. **31**(4): p. 305-19.
25. Lemasters, J.J., *V. Necrapoptosis and the mitochondrial permeability transition: shared pathways to necrosis and apoptosis*. *Am J Physiol*, 1999. **276**(1 Pt 1): p. G1-6.
26. Lemasters, J.J., et al., *Role of mitochondrial inner membrane permeabilization in necrotic cell death, apoptosis, and autophagy*. *Antioxid Redox Signal*, 2002. **4**(5): p. 769-81.
27. Ulasova, E., et al., *Loss of interstitial collagen causes structural and functional alterations of cardiomyocyte subsarcolemmal mitochondria in acute volume overload*. *J Mol Cell Cardiol*, 2011. **50**(1): p. 147-56.
28. Cunningham, C.C. and S.M. Bailey, *Ethanol consumption and liver mitochondria function*. *Biol Signals Recept*, 2001. **10**(3-4): p. 271-82.
29. Bailey, S.M. and C.C. Cunningham, *Contribution of mitochondria to oxidative stress associated with alcoholic liver disease*. *Free Radic Biol Med*, 2002. **32**(1): p. 11-6.
30. Cahill, A., et al., *Effects of alcohol and oxidative stress on liver pathology: the role of the mitochondrion*. *Alcohol Clin Exp Res*, 2002. **26**(6): p. 907-15.
31. Li, C. and R.M. Jackson, *Reactive species mechanisms of cellular hypoxia-reoxygenation injury*. *Am J Physiol Cell Physiol*, 2002. **282**(2): p. C227-41.
32. Hoek, J.B., A. Cahill, and J.G. Pastorino, *Alcohol and mitochondria: a dysfunctional relationship*. *Gastroenterology*, 2002. **122**(7): p. 2049-63.

33. Venkatraman, A., et al., *Chronic alcohol consumption increases the sensitivity of rat liver mitochondrial respiration to inhibition by nitric oxide*. Hepatology, 2003. **38**(1): p. 141-7.
34. Venkatraman, A., et al., *The role of iNOS in alcohol-dependent hepatotoxicity and mitochondrial dysfunction in mice*. Hepatology, 2004. **40**(3): p. 565-73.
35. Arteel, G.E., et al., *Chronic enteral ethanol treatment causes hypoxia in rat liver tissue in vivo*. Hepatology, 1997. **25**(4): p. 920-6.
36. McKim, S.E., et al., *Inducible nitric oxide synthase is required in alcohol-induced liver injury: studies with knockout mice*. Gastroenterology, 2003. **125**(6): p. 1834-44.
37. Poyton, R.O., K.A. Ball, and P.R. Castello, *Mitochondrial generation of free radicals and hypoxic signaling*. Trends Endocrinol Metab, 2009. **20**(7): p. 332-40.
38. McCord, J.M., *Oxygen-derived free radicals in postischemic tissue injury*. N Engl J Med, 1985. **312**(3): p. 159-63.
39. Halestrap, A.P., *A pore way to die: the role of mitochondria in reperfusion injury and cardioprotection*. Biochem Soc Trans, 2010. **38**(4): p. 841-60.
40. Ladilov, Y., et al., *Mechanism of Ca²⁺ overload in endothelial cells exposed to simulated ischemia*. Cardiovasc Res, 2000. **47**(2): p. 394-403.
41. Peters, S.C. and H.M. Piper, *Reoxygenation-induced Ca²⁺ rise is mediated via Ca²⁺ influx and Ca²⁺ release from the endoplasmic reticulum in cardiac endothelial cells*. Cardiovasc Res, 2007. **73**(1): p. 164-71.
42. Lounsbury, K.M., Q. Hu, and R.C. Ziegelstein, *Calcium signaling and oxidant stress in the vasculature*. Free Radic Biol Med, 2000. **28**(9): p. 1362-9.
43. Zhang, D.X. and D.D. Gutterman, *Mitochondrial reactive oxygen species-mediated signaling in endothelial cells*. Am J Physiol Heart Circ Physiol, 2007. **292**(5): p. H2023-31.

44. Atkeson, A., et al., *Endothelial function in obstructive sleep apnea*. Prog Cardiovasc Dis, 2009. **51**(5): p. 351-62.
45. Faller, D.V., *Endothelial cell responses to hypoxic stress*. Clin Exp Pharmacol Physiol, 1999. **26**(1): p. 74-84.
46. Abel, E.D. and T. Doenst, *Mitochondrial adaptations to physiological vs. pathological cardiac hypertrophy*. Cardiovasc Res, 2011. **90**(2): p. 234-42.
47. Doenst, T. and E.D. Abel, *Spotlight on metabolic remodelling in heart failure*. Cardiovasc Res, 2011. **90**(2): p. 191-3.
48. Ahmed, M.I., et al., *Mitral regurgitation*. Curr Probl Cardiol, 2009. **34**(3): p. 93-136.
49. Appaix, F., et al., *Possible role of cytoskeleton in intracellular arrangement and regulation of mitochondria*. Exp Physiol, 2003. **88**(1): p. 175-90.
50. Capetanaki, Y., *Desmin cytoskeleton: a potential regulator of muscle mitochondrial behavior and function*. Trends Cardiovasc Med, 2002. **12**(8): p. 339-48.
51. Dhalla, N.S., et al., *Pathophysiology of cardiac dysfunction in congestive heart failure*. Can J Cardiol, 1993. **9**(10): p. 873-87.
52. Lloyd-Jones, D., et al., *Heart disease and stroke statistics--2010 update: a report from the American Heart Association*. Circulation, 2010. **121**(7): p. e46-e215.
53. Roger, V.L., et al., *Heart disease and stroke statistics--2011 update: a report from the American Heart Association*, in *Circulation* 2011: United States. p. e18-e209.
54. Marcuello, A., et al., *Human mitochondrial variants influence on oxygen consumption*. Mitochondrion, 2009. **9**(1): p. 27-30.
55. Martínez-Redondo, D., et al., *Human mitochondrial haplogroup H: the highest VO₂max consumer--is it a paradox?* Mitochondrion, 2010. **10**(2): p. 102-7.

56. Gallardo, M.E., et al., *m.6267G>A: a recurrent mutation in the human mitochondrial DNA that reduces cytochrome c oxidase activity and is associated with tumors*. Hum Mutat, 2006. **27**(6): p. 575-82.
57. Gómez-Durán, A., et al., *Unmasking the causes of multifactorial disorders: OXPHOS differences between mitochondrial haplogroups*. Hum Mol Genet, 2010. **19**(17): p. 3343-53.
58. Moreno-Loshuertos, R., et al., *Differences in reactive oxygen species production explain the phenotypes associated with common mouse mitochondrial DNA variants*. Nat Genet, 2006. **38**(11): p. 1261-8.
59. Battersby, B.J. and E.A. Shoubridge, *Reactive oxygen species and the segregation of mtDNA sequence variants*. Nat Genet, 2007. **39**(5): p. 571-2; author reply 572.
60. Domínguez-Garrido, E., et al., *Association of mitochondrial haplogroup J and mtDNA oxidative damage in two different North Spain elderly populations*. Biogerontology, 2009. **10**(4): p. 435-42.
61. Lardy, H.A. and S.M. Ferguson, *Oxidative phosphorylation in mitochondria*. Annu Rev Biochem, 1969. **38**: p. 991-1034.
62. Scheffler, I.E., *Mitochondria*. 2nd Ed. ed2008, Hoboken, NJ: John Wiley & Sons.
63. Srere, P.A., B. Sumegi, and A.D. Sherry, *Organizational aspects of the citric acid cycle*. Biochem Soc Symp, 1987. **54**: p. 173-8.
64. Saraste, M., *Oxidative phosphorylation at the fin de siècle*. Science, 1999. **283**(5407): p. 1488-93.
65. Nicholls, D.G. and S.J. Ferguson, *Bioenergetics 32002*, San Diego: Academic Press. 297.
66. Hägerhäll, C., *Succinate: quinone oxidoreductases. Variations on a conserved theme*. Biochim Biophys Acta, 1997. **1320**(2): p. 107-41.
67. Hirst, J., et al., *The nuclear encoded subunits of complex I from bovine heart mitochondria*. Biochim Biophys Acta, 2003. **1604**(3): p. 135-50.

68. Sazanov, L.A., *Respiratory complex I: mechanistic and structural insights provided by the crystal structure of the hydrophilic domain*. *Biochemistry*, 2007. **46**(9): p. 2275-88.
69. Iwata, S., et al., *Complete structure of the 11-subunit bovine mitochondrial cytochrome bc₁ complex*. *Science*, 1998. **281**(5373): p. 64-71.
70. Babcock, G.T. and M. Wikström, *Oxygen activation and the conservation of energy in cell respiration*. *Nature*, 1992. **356**(6367): p. 301-9.
71. Tsukihara, T., et al., *The Whole Structure of the 13-Subunit Oxidized Cytochrome c Oxidase at 2.8 Å*. *Science*, 1996. **272**(5265): p. 1136-1144.
72. Yoshikawa, S., et al., *Redox-coupled crystal structural changes in bovine heart cytochrome c oxidase*. *Science*, 1998. **280**(5370): p. 1723-9.
73. MITCHELL, P., *Coupling of phosphorylation to electron and hydrogen transfer by a chemi-osmotic type of mechanism*. *Nature*, 1961. **191**: p. 144-8.
74. Mitchell, P., *Chemiosmotic coupling in oxidative and photosynthetic phosphorylation*. *Biol Rev Camb Philos Soc*, 1966. **41**(3): p. 445-502.
75. Lutter, R., et al., *F₁F₀-ATP synthase from bovine heart mitochondria: development of the purification of a monodisperse oligomycin-sensitive ATPase*. *Biochem J*, 1993. **295** (Pt 3): p. 799-806.
76. Thomson, D.M. and W.W. Winder, *AMP-activated protein kinase control of fat metabolism in skeletal muscle*. *Acta Physiol (Oxf)*, 2009. **196**(1): p. 147-54.
77. Viollet, B., et al., *AMP-activated protein kinase in the regulation of hepatic energy metabolism: from physiology to therapeutic perspectives*. *Acta Physiol (Oxf)*, 2009. **196**(1): p. 81-98.
78. Canto, C., et al., *AMPK regulates energy expenditure by modulating NAD⁺ metabolism and SIRT1 activity*. *Nature*, 2009. **458**(7241): p. 1056-60.

79. Canto, C. and J. Auwerx, *PGC-1alpha, SIRT1 and AMPK, an energy sensing network that controls energy expenditure*. *Curr Opin Lipidol*, 2009. **20**(2): p. 98-105.
80. Miranda, N., et al., [*AMPK as a cellular energy sensor and its function in the organism*]. *Rev Invest Clin*, 2007. **59**(6): p. 458-69.
81. Klingenberg, M., E. Winkler, and S. Huang, *ADP/ATP carrier and uncoupling protein*. *Methods Enzymol*, 1995. **260**: p. 369-89.
82. Wohlrab, H., *The human mitochondrial transport protein family: identification and protein regions significant for transport function and substrate specificity*. *Biochim Biophys Acta*, 2005. **1709**(2): p. 157-68.
83. Ciapaite, J., et al., *Metabolic control of mitochondrial properties by adenine nucleotide translocator determines palmitoyl-CoA effects. Implications for a mechanism linking obesity and type 2 diabetes*. *FEBS J*, 2006. **273**(23): p. 5288-302.
84. Dzeja, P.P. and A. Terzic, *Phosphotransfer networks and cellular energetics*. *J Exp Biol*, 2003. **206**(Pt 12): p. 2039-47.
85. Jacobus, W.E., *Theoretical support for the heart phosphocreatine energy transport shuttle based on the intracellular diffusion limited mobility of ADP*. *Biochem Biophys Res Commun*, 1985. **133**(3): p. 1035-41.
86. Saks, V.A., et al., *Creatine kinase of rat heart mitochondria. The demonstration of functional coupling to oxidative phosphorylation in an inner membrane-matrix preparation*. *J Biol Chem*, 1985. **260**(12): p. 7757-64.
87. Kowaltowski, A.J., et al., *Mitochondria and reactive oxygen species*. *Free Radic Biol Med*, 2009. **47**(4): p. 333-43.
88. Balaban, R.S., S. Nemoto, and T. Finkel, *Mitochondria, oxidants, and aging*. *Cell*, 2005. **120**(4): p. 483-95.
89. Dröge, W., *Free radicals in the physiological control of cell function*. *Physiol Rev*, 2002. **82**(1): p. 47-95.

90. Jensen, P.K., *Antimycin-insensitive oxidation of succinate and reduced nicotinamide-adenine dinucleotide in electron-transport particles. I. pH dependency and hydrogen peroxide formation.* Biochim Biophys Acta, 1966. **122**(2): p. 157-66.
91. Chance, B., H. Sies, and A. Boveris, *Hydroperoxide metabolism in mammalian organs.* Physiol Rev, 1979. **59**(3): p. 527-605.
92. Loschen, G., L. Flohé, and B. Chance, *Respiratory chain linked H₂O₂ production in pigeon heart mitochondria.* FEBS Lett, 1971. **18**(2): p. 261-264.
93. Boveris, A. and B. Chance, *The mitochondrial generation of hydrogen peroxide. General properties and effect of hyperbaric oxygen.* Biochem J, 1973. **134**(3): p. 707-16.
94. Andreyev, A.Y., Y.E. Kushnareva, and A.A. Starkov, *Mitochondrial metabolism of reactive oxygen species.* Biochemistry (Mosc), 2005. **70**(2): p. 200-14.
95. D.T., S. and V. J.S., *How super is superoxide?* Acc. Chem. Res., 1981. **14**(12): p. 393-400.
96. Murphy, M.P., *How mitochondria produce reactive oxygen species.* Biochem J, 2009. **417**(1): p. 1-13.
97. Hinkle, P.C., et al., *Partial resolution of the enzymes catalyzing oxidative phosphorylation. XV. Reverse electron transfer in the flavin-cytochrome beta region of the respiratory chain of beef heart submitochondrial particles.* J Biol Chem, 1967. **242**(22): p. 5169-73.
98. Cadenas, E., et al., *Production of superoxide radicals and hydrogen peroxide by NADH-ubiquinone reductase and ubiquinol-cytochrome c reductase from beef-heart mitochondria.* Arch Biochem Biophys, 1977. **180**(2): p. 248-57.
99. Hirst, J., M.S. King, and K.R. Pryde, *The production of reactive oxygen species by complex I.* Biochem Soc Trans, 2008. **36**(Pt 5): p. 976-80.
100. Kussmaul, L. and J. Hirst, *The mechanism of superoxide production by NADH:ubiquinone oxidoreductase (complex I) from bovine heart mitochondria.* Proc Natl Acad Sci U S A, 2006. **103**(20): p. 7607-12.

101. Adam-Vizi, V. and C. Chinopoulos, *Bioenergetics and the formation of mitochondrial reactive oxygen species*. Trends Pharmacol Sci, 2006. **27**(12): p. 639-45.
102. Kudin, A.P., et al., *Characterization of superoxide-producing sites in isolated brain mitochondria*. J Biol Chem, 2004. **279**(6): p. 4127-35.
103. Votyakova, T.V. and I.J. Reynolds, *DeltaPsi(m)-Dependent and -independent production of reactive oxygen species by rat brain mitochondria*. J Neurochem, 2001. **79**(2): p. 266-77.
104. Liu, Y., G. Fiskum, and D. Schubert, *Generation of reactive oxygen species by the mitochondrial electron transport chain*. J Neurochem, 2002. **80**(5): p. 780-7.
105. Krishnamoorthy, G. and P.C. Hinkle, *Studies on the electron transfer pathway, topography of iron-sulfur centers, and site of coupling in NADH-Q oxidoreductase*. J Biol Chem, 1988. **263**(33): p. 17566-75.
106. Chance, B. and G. Hollunger, *The interaction of energy and electron transfer reactions in mitochondria. I. General properties and nature of the products of succinate-linked reduction of pyridine nucleotide*. J Biol Chem, 1961. **236**: p. 1534-43.
107. St-Pierre, J., et al., *Topology of superoxide production from different sites in the mitochondrial electron transport chain*. J Biol Chem, 2002. **277**(47): p. 44784-90.
108. Lambert, A.J. and M.D. Brand, *Inhibitors of the quinone-binding site allow rapid superoxide production from mitochondrial NADH:ubiquinone oxidoreductase (complex I)*. J Biol Chem, 2004. **279**(38): p. 39414-20.
109. Lambert, A.J. and M.D. Brand, *Superoxide production by NADH:ubiquinone oxidoreductase (complex I) depends on the pH gradient across the mitochondrial inner membrane*. Biochem J, 2004. **382**(Pt 2): p. 511-7.
110. Hurd, T.R., et al., *Detection of reactive oxygen species-sensitive thiol proteins by redox difference gel electrophoresis: implications for mitochondrial redox signaling*. J Biol Chem, 2007. **282**(30): p. 22040-51.

111. Forman, H.J. and A. Azzi, *On the virtual existence of superoxide anions in mitochondria: thoughts regarding its role in pathophysiology*. FASEB J, 1997. **11**(5): p. 374-5.
112. Turrens, J.F., A. Alexandre, and A.L. Lehninger, *Ubisemiquinone is the electron donor for superoxide formation by complex III of heart mitochondria*. Arch Biochem Biophys, 1985. **237**(2): p. 408-14.
113. Zhang, L., L. Yu, and C.A. Yu, *Generation of superoxide anion by succinate-cytochrome c reductase from bovine heart mitochondria*. J Biol Chem, 1998. **273**(51): p. 33972-6.
114. Rich, P.R. and W.D. Bonner, *The sites of superoxide anion generation in higher plant mitochondria*. Arch Biochem Biophys, 1978. **188**(1): p. 206-13.
115. Grigolava, I.V., et al., [*Tiron as a spin-trap for superoxide radicals produced by the respiratory chain of submitochondrial particles*]. Biokhimiia, 1980. **45**(1): p. 75-82.
116. Han, D., et al., *Voltage-dependent anion channels control the release of the superoxide anion from mitochondria to cytosol*. J Biol Chem, 2003. **278**(8): p. 5557-63.
117. Muller, F.L., Y. Liu, and H. Van Remmen, *Complex III releases superoxide to both sides of the inner mitochondrial membrane*. J Biol Chem, 2004. **279**(47): p. 49064-73.
118. Weisiger, R.A. and I. Fridovich, *Mitochondrial superoxide simutase. Site of synthesis and intramitochondrial localization*. J Biol Chem, 1973. **248**(13): p. 4793-6.
119. Weisiger, R.A. and I. Fridovich, *Superoxide dismutase. Organelle specificity*. J Biol Chem, 1973. **248**(10): p. 3582-92.
120. Okado-Matsumoto, A. and I. Fridovich, *Subcellular distribution of superoxide dismutases (SOD) in rat liver: Cu,Zn-SOD in mitochondria*. J Biol Chem, 2001. **276**(42): p. 38388-93.

121. Sturtz, L.A., et al., *A fraction of yeast Cu,Zn-superoxide dismutase and its metallochaperone, CCS, localize to the intermembrane space of mitochondria. A physiological role for SOD1 in guarding against mitochondrial oxidative damage.* J Biol Chem, 2001. **276**(41): p. 38084-9.
122. Holmgren, A., *Antioxidant function of thioredoxin and glutaredoxin systems.* Antioxid Redox Signal, 2000. **2**(4): p. 811-20.
123. Nordberg, J. and E.S. Arnér, *Reactive oxygen species, antioxidants, and the mammalian thioredoxin system.* Free Radic Biol Med, 2001. **31**(11): p. 1287-312.
124. Loschen, G., A. Azzi, and L. Flohé, *Mitochondrial H₂O₂ formation: relationship with energy conservation.* FEBS Lett, 1973. **33**(1): p. 84-7.
125. Facundo, H.T., J.G. de Paula, and A.J. Kowaltowski, *Mitochondrial ATP-sensitive K⁺ channels are redox-sensitive pathways that control reactive oxygen species production.* Free Radic Biol Med, 2007. **42**(7): p. 1039-48.
126. Tahara, E.B., F.D. Navarete, and A.J. Kowaltowski, *Tissue-, substrate-, and site-specific characteristics of mitochondrial reactive oxygen species generation.* Free Radic Biol Med, 2009. **46**(9): p. 1283-97.
127. Brookes, P.S., *Mitochondrial H(+) leak and ROS generation: an odd couple.* Free Radic Biol Med, 2005. **38**(1): p. 12-23.
128. Caldeira da Silva, C.C., et al., *Mild mitochondrial uncoupling in mice affects energy metabolism, redox balance and longevity.* Aging Cell, 2008. **7**(4): p. 552-60.
129. Korshunov, S.S., V.P. Skulachev, and A.A. Starkov, *High protonic potential actuates a mechanism of production of reactive oxygen species in mitochondria.* FEBS Lett, 1997. **416**(1): p. 15-8.
130. Kowaltowski, A.J., A.D. Costa, and A.E. Vercesi, *Activation of the potato plant uncoupling mitochondrial protein inhibits reactive oxygen species generation by the respiratory chain.* FEBS Lett, 1998. **425**(2): p. 213-6.
131. Skulachev, V.P., *Uncoupling: new approaches to an old problem of bioenergetics.* Biochim Biophys Acta, 1998. **1363**(2): p. 100-24.

132. Czarna, M. and W. Jarmuszkiewicz, *Activation of alternative oxidase and uncoupling protein lowers hydrogen peroxide formation in amoeba Acanthamoeba castellanii mitochondria*. FEBS Lett, 2005. **579**(14): p. 3136-40.
133. Ferranti, R., M.M. da Silva, and A.J. Kowaltowski, *Mitochondrial ATP-sensitive K⁺ channel opening decreases reactive oxygen species generation*. FEBS Lett, 2003. **536**(1-3): p. 51-5.
134. Nègre-Salvayre, A., et al., *A role for uncoupling protein-2 as a regulator of mitochondrial hydrogen peroxide generation*. FASEB J, 1997. **11**(10): p. 809-15.
135. Costford, S.R., et al., *Long-term high-fat feeding induces greater fat storage in mice lacking UCP3*. Am J Physiol Endocrinol Metab, 2008. **295**(5): p. E1018-24.
136. Samec, S., J. Seydoux, and A.G. Dulloo, *Interorgan signaling between adipose tissue metabolism and skeletal muscle uncoupling protein homologs: is there a role for circulating free fatty acids?* Diabetes, 1998. **47**(11): p. 1693-8.
137. Samec, S., J. Seydoux, and A.G. Dulloo, *Role of UCP homologues in skeletal muscles and brown adipose tissue: mediators of thermogenesis or regulators of lipids as fuel substrate?* FASEB J, 1998. **12**(9): p. 715-24.
138. Wallace, D.C., *Mitochondrial genetics: a paradigm for aging and degenerative diseases?* Science, 1992. **256**(5057): p. 628-32.
139. Wallace, D.C., *Why do we still have a maternally inherited mitochondrial DNA? Insights from evolutionary medicine*. Annu Rev Biochem, 2007. **76**: p. 781-821.
140. Mishmar, D., et al., *Natural selection shaped regional mtDNA variation in humans*. Proc Natl Acad Sci U S A, 2003. **100**(1): p. 171-6.
141. Balloux, F., *The worm in the fruit of the mitochondrial DNA tree*. Heredity, 2010. **104**(5): p. 419-20.
142. Balloux, F., et al., *Climate shaped the worldwide distribution of human mitochondrial DNA sequence variation*. Proc Biol Sci, 2009. **276**(1672): p. 3447-55.

143. Ruiz-Pesini, E., et al., *An enhanced MITOMAP with a global mtDNA mutational phylogeny*. Nucleic Acids Res, 2007. **35**(Database issue): p. D823-8.
144. Ruiz-Pesini, E., et al., *Effects of purifying and adaptive selection on regional variation in human mtDNA*. Science, 2004. **303**(5655): p. 223-6.
145. Denaro, M., et al., *Ethnic variation in Hpa I endonuclease cleavage patterns of human mitochondrial DNA*. Proc Natl Acad Sci U S A, 1981. **78**(9): p. 5768-72.
146. Wallace, D.C. and W. Fan, *The pathophysiology of mitochondrial disease as modeled in the mouse*. Genes Dev, 2009. **23**(15): p. 1714-36.
147. Wallace, D.C., et al., *Mitochondrial DNA mutation associated with Leber's hereditary optic neuropathy*. Science, 1988. **242**(4884): p. 1427-30.
148. Holt, I.J., A.E. Harding, and J.A. Morgan-Hughes, *Deletions of muscle mitochondrial DNA in patients with mitochondrial myopathies*. Nature, 1988. **331**(6158): p. 717-9.
149. Chamberlain, S., et al., *Mapping of mutation causing Friedreich's ataxia to human chromosome 9*. Nature, 1988. **334**(6179): p. 248-50.
150. Fujita, R., et al., *Confirmation of linkage of Friedreich ataxia to chromosome 9 and identification of a new closely linked marker*. Genomics, 1989. **4**(1): p. 110-1.
151. Hanauer, A., et al., *The Friedreich ataxia gene is assigned to chromosome 9q13-q21 by mapping of tightly linked markers and shows linkage disequilibrium with D9S15*. Am J Hum Genet, 1990. **46**(1): p. 133-7.
152. Mulder, H. and C. Ling, *Mitochondrial dysfunction in pancreatic beta-cells in Type 2 diabetes*. Mol Cell Endocrinol, 2009. **297**(1-2): p. 34-40.
153. Forbes, J.M., M.T. Coughlan, and M.E. Cooper, *Oxidative stress as a major culprit in kidney disease in diabetes*. Diabetes, 2008. **57**(6): p. 1446-54.
154. Ramachandran, A., et al., *Mitochondria, nitric oxide, and cardiovascular dysfunction*. Free Radic Biol Med, 2002. **33**(11): p. 1465-74.

155. Ferrari, R., *The role of mitochondria in ischemic heart disease*. J Cardiovasc Pharmacol, 1996. **28 Suppl 1**: p. S1-10.
156. Madamanchi, N.R. and M.S. Runge, *Mitochondrial dysfunction in atherosclerosis*. Circ Res, 2007. **100**(4): p. 460-73.
157. Gutierrez, J., et al., *Free Radicals, Mitochondria, and Oxidized Lipids: The Emerging Role in Signal Transduction in Vascular Cells*. Circ Res, 2006. **99**(9): p. 924-932.
158. Mantena, S.K., et al., *High fat diet induces dysregulation of hepatic oxygen gradients and mitochondrial function in vivo*. Biochem J, 2009. **417**(1): p. 183-93.
159. Venkatraman, A., et al., *Modification of the mitochondrial proteome in response to the stress of ethanol-dependent hepatotoxicity*. J Biol Chem, 2004. **279**(21): p. 22092-101.
160. Venkatraman, A., et al., *Oxidative modification of hepatic mitochondria protein thiols: effect of chronic alcohol consumption*. Am J Physiol Gastrointest Liver Physiol, 2004. **286**(4): p. G521-7.
161. Young, T.A., et al., *Chronic ethanol consumption decreases mitochondrial and glycolytic production of ATP in liver*. Alcohol Alcohol, 2006. **41**(3): p. 254-60.
162. Rosenstock, T.R., A.I. Duarte, and A.C. Rego, *Mitochondrial-associated metabolic changes and neurodegeneration in Huntington's disease - from clinical features to the bench*. Curr Drug Targets, 2010. **11**(10): p. 1218-36.
163. Ferreira, I.L., et al., *Multiple defects in energy metabolism in Alzheimer's disease*. Curr Drug Targets, 2010. **11**(10): p. 1193-206.
164. Burbulla, L.F., G. Krebiehl, and R. Krüger, *Balance is the challenge--the impact of mitochondrial dynamics in Parkinson's disease*. Eur J Clin Invest, 2010. **40**(11): p. 1048-60.
165. Levonen, A., et al., *Cellular mechanisms of redox cell signalling: role of cysteine modification in controlling antioxidant defences in response to electrophilic lipid oxidation products*. Biochem J, 2004. **378**(Pt 2): p. 373-82.

166. Gardner, P.R. and I. Fridovich, *Superoxide sensitivity of the Escherichia coli aconitase*. J Biol Chem, 1991. **266**(29): p. 19328-33.
167. Gardner, P.R. and I. Fridovich, *Inactivation-reactivation of aconitase in Escherichia coli. A sensitive measure of superoxide radical*. J Biol Chem, 1992. **267**(13): p. 8757-63.
168. Hausladen, A. and I. Fridovich, *Superoxide and peroxynitrite inactivate aconitases, but nitric oxide does not*. J Biol Chem, 1994. **269**(47): p. 29405-8.
169. Murakami, K. and M. Yoshino, *Inactivation of aconitase in yeast exposed to oxidative stress*. Biochem Mol Biol Int, 1997. **41**(3): p. 481-6.
170. Andersson, U., et al., *Inactivation of aconitase and oxoglutarate dehydrogenase in skeletal muscle in vitro by superoxide anions and/or nitric oxide*. Biochem Biophys Res Commun, 1998. **249**(2): p. 512-6.
171. Duan, J. and M. Karmazyn, *Relationship between oxidative phosphorylation and adenine nucleotide translocase activity of two populations of cardiac mitochondria and mechanical recovery of ischemic hearts following reperfusion*. Can J Physiol Pharmacol, 1989. **67**(7): p. 704-9.
172. Halestrap, A.P., K.Y. Woodfield, and C.P. Connern, *Oxidative stress, thiol reagents, and membrane potential modulate the mitochondrial permeability transition by affecting nucleotide binding to the adenine nucleotide translocase*. J Biol Chem, 1997. **272**(6): p. 3346-54.
173. Murphy, M., *How understanding the control of energy metabolism can help investigation of mitochondrial dysfunction, regulation and pharmacology*. Biochim Biophys Acta, 2001. **1504**(1): p. 1-11.
174. Garrido, C., et al., *Mechanisms of cytochrome c release from mitochondria*. Cell Death Differ, 2006. **13**(9): p. 1423-33.
175. Ow, Y.P., et al., *Cytochrome c: functions beyond respiration*. Nat Rev Mol Cell Biol, 2008. **9**(7): p. 532-42.
176. Brand, M.D. and D.G. Nicholls, *Assessing mitochondrial dysfunction in cells*. Biochem. J., 2011. **435**(2): p. 297-312.

177. Wu, M., et al., *Multiparameter metabolic analysis reveals a close link between attenuated mitochondrial bioenergetic function and enhanced glycolysis dependency in human tumor cells*. *Am J Physiol Cell Physiol*, 2007. **292**(1): p. C125-36.
178. Ferrick, D.A., A. Neilson, and C. Beeson, *Advances in measuring cellular bioenergetics using extracellular flux*. *Drug Discov Today*, 2008. **13**(5-6): p. 268-74.
179. Hill, B.G., et al., *Importance of the bioenergetic reserve capacity in response to cardiomyocyte stress induced by 4-hydroxynonenal*. *Biochem J*, 2009. **424**(1): p. 99-107.
180. Dranka, B.P., B.G. Hill, and V.M. Darley-Usmar, *Mitochondrial reserve capacity in endothelial cells: The impact of nitric oxide and reactive oxygen species*. *Free Radic Biol Med*, 2010. **48**(7): p. 905-14.
181. Kingsley-Hickman, P.B., et al., *31P NMR measurement of mitochondrial uncoupling in isolated rat hearts*. *J Biol Chem*, 1990. **265**(3): p. 1545-50.
182. Sako, E.Y., et al., *ATP synthesis kinetics and mitochondrial function in the postischemic myocardium as studied by 31P NMR*. *J Biol Chem*, 1988. **263**(22): p. 10600-7.
183. Gong, G., et al., *Oxidative capacity in failing hearts*. *Am J Physiol Heart Circ Physiol*, 2003. **285**(2): p. H541-8.
184. Almsherqi, Z.A., et al., *Reduced cardiac output is associated with decreased mitochondrial efficiency in the non-ischemic ventricular wall of the acute myocardial-infarcted dog*. *Cell Res*, 2006. **16**(3): p. 297-305.
185. Bird, G.L. and R. Williams, *Factors determining cirrhosis in alcoholic liver disease*. *Mol Aspects Med*, 1988. **10**(2): p. 97-105.
186. Jones-Webb, R., *Drinking patterns and problems among African-Americans: recent findings*. *Alcohol Health Res World*, 1998. **22**(4): p. 260-4.

187. Ivester, P., M.J. Lide, and C.C. Cunningham, *Effect of chronic ethanol consumption on the energy state and structural stability of periportal and perivenous hepatocytes*. Arch Biochem Biophys, 1995. **322**(1): p. 14-21.
188. Baio, D.L., et al., *Effect of chronic ethanol consumption on respiratory and glycolytic activities of rat periportal and perivenous hepatocytes*. Arch Biochem Biophys, 1998. **350**(2): p. 193-200.
189. Shiva, S., et al., *Nitric oxide partitioning into mitochondrial membranes and the control of respiration at cytochrome c oxidase*. PNAS, 2001. **98**(13): p. 7212-7217.
190. Brookes, P.S., et al., *Measurement of mitochondrial respiratory thresholds and the control of respiration by nitric oxide*. Methods Enzymol, 2002. **359**: p. 305-19.
191. Brookes, P.S., et al., *Control of mitochondrial respiration by NO*, effects of low oxygen and respiratory state*. J Biol Chem, 2003. **278**(34): p. 31603-9.
192. Shiva, S., et al., *Nitroxia: The pathological consequence of dysfunction in the nitric oxide-cytochrome c oxidase signaling pathway*. Free Radical Biology and Medicine, 2005. **38**(3): p. 297-306.
193. Landar, A. and V.M. Darley-Usmar, *Nitric oxide and cell signaling: modulation of redox tone and protein modification*. Amino Acids, 2003. **25**(3-4): p. 313-21.
194. Hill, B.G., et al., *What part of NO don't you understand? Some answers to the cardinal questions in nitric oxide biology*. J Biol Chem, 2010. **285**(26): p. 19699-704.
195. Murphy, B.J., et al., *Hypoxic coordinate regulation of mitochondrial enzymes in mammalian cells*. Science, 1984. **223**(4637): p. 707-9.
196. Robin, E.D., B.J. Murphy, and J. Theodore, *Coordinate regulation of glycolysis by hypoxia in mammalian cells*. J Cell Physiol, 1984. **118**(3): p. 287-90.
197. Melillo, G., et al., *A hypoxia-responsive element mediates a novel pathway of activation of the inducible nitric oxide synthase promoter*. J Exp Med, 1995. **182**(6): p. 1683-93.

198. Chandel, N.S., et al., *Mitochondrial reactive oxygen species trigger hypoxia-induced transcription*. Proc Natl Acad Sci U S A, 1998. **95**(20): p. 11715-20.
199. Semenza, G., *Signal transduction to hypoxia-inducible factor 1*. Biochem Pharmacol, 2002. **64**(5-6): p. 993-8.
200. Sridharan, V., et al., *O(2)-sensing signal cascade: clamping of O(2) respiration, reduced ATP utilization, and inducible fumarate respiration*. Am J Physiol Cell Physiol, 2008. **295**(1): p. C29-37.
201. Taylor, C.T. and S. Moncada, *Nitric Oxide, Cytochrome C Oxidase, and the Cellular Response to Hypoxia*. Arterioscler Thromb Vasc Biol, 2009.
202. Kang, S. and Y. Yang, *Coronary microvascular reperfusion injury and no-reflow in acute myocardial infarction*. Clin Invest Med, 2007. **30**(3): p. E133-45.
203. Niccoli, G., et al., *Myocardial no-reflow in humans*. J Am Coll Cardiol, 2009. **54**(4): p. 281-92.
204. de Groot, H. and M. Brecht, *Reoxygenation injury in rat hepatocytes: mediation by O₂/H₂O₂ liberated by sources other than xanthine oxidase*. Biol Chem Hoppe Seyler, 1991. **372**(1): p. 35-41.
205. Semenza, G.L., *Cellular and molecular dissection of reperfusion injury: ROS within and without*. Circ Res, 2000. **86**(2): p. 117-8.
206. Irani, K., *Oxidant signaling in vascular cell growth, death, and survival : a review of the roles of reactive oxygen species in smooth muscle and endothelial cell mitogenic and apoptotic signaling*. Circ Res, 2000. **87**(3): p. 179-83.
207. Saikumar, P., et al., *Role of hypoxia-induced Bax translocation and cytochrome c release in reoxygenation injury*. Oncogene, 1998. **17**(26): p. 3401-15.
208. Simon, L.M., et al., *Enzymatic basis for bioenergetic differences of alveolar versus peritoneal macrophages and enzyme regulation by molecular O₂*. J Clin Invest, 1977. **59**(3): p. 443-8.

209. Kayyali, U.S., et al., *Phosphorylation of xanthine dehydrogenase/oxidase in hypoxia*. J Biol Chem, 2001. **276**(17): p. 14359-65.
210. Killilea, D.W., et al., *Free radical production in hypoxic pulmonary artery smooth muscle cells*. Am J Physiol Lung Cell Mol Physiol, 2000. **279**(2): p. L408-12.
211. Yao, Z., et al., *Role of reactive oxygen species in acetylcholine-induced preconditioning in cardiomyocytes*. Am J Physiol, 1999. **277**(6 Pt 2): p. H2504-9.
212. Tan, S., et al., *Increased injury following intermittent fetal hypoxia-reoxygenation is associated with increased free radical production in fetal rabbit brain*. J Neuropathol Exp Neurol, 1999. **58**(9): p. 972-81.
213. Zweier, J.L., et al., *Measurement and characterization of free radical generation in reoxygenated human endothelial cells*. Am J Physiol, 1994. **266**(3 Pt 1): p. C700-8.
214. Ratych, R.E., R.S. Chuknyiska, and G.B. Bulkley, *The primary localization of free radical generation after anoxia/reoxygenation in isolated endothelial cells*. Surgery, 1987. **102**(2): p. 122-31.
215. de Groot, H., I. Anundi, and A. Littauer, *Hypoxia-reoxygenation injury and the generation of reactive oxygen in isolated hepatocytes*. Biomed Biochim Acta, 1989. **48**(2-3): p. S11-5.
216. Boudoulas, H., *Mitral valve prolapse: etiology, clinical presentation and neuroendocrine function*. J Heart Valve Dis, 1992. **1**(2): p. 175-88.
217. Dell'Italia, L.J., G.L. Freeman, and W.H. Gaasch, *Cardiac function and functional capacity: implications for the failing heart*. Curr Probl Cardiol, 1993. **18**(12): p. 705-58.
218. Pat, B., et al., *Dissociation between cardiomyocyte function and remodeling with beta-adrenergic receptor blockade in isolated canine mitral regurgitation*. Am J Physiol Heart Circ Physiol, 2008. **295**(6): p. H2321-7.

219. Krenitsky, T.A., et al., *A comparison of the distribution and electron acceptor specificities of xanthine oxidase and aldehyde oxidase*. Comp Biochem Physiol B, 1974. **49**(4): p. 687-703.
220. Parks, D.A. and D.N. Granger, *Xanthine oxidase: biochemistry, distribution and physiology*. Acta Physiol Scand Suppl, 1986. **548**: p. 87-99.
221. Ahmed, M.I., et al., *Increased oxidative stress and cardiomyocyte myofibrillar degeneration in patients with chronic isolated mitral regurgitation and ejection fraction >60%*. J Am Coll Cardiol, 2010. **55**(7): p. 671-9.
222. Ekundayo, O.J., et al., *Association between hyperuricemia and incident heart failure among older adults: a propensity-matched study*. Int J Cardiol, 2010. **142**(3): p. 279-87.
223. Gupta, A., et al., *Impairment of ultrastructure and cytoskeleton during progression of cardiac hypertrophy to heart failure*. Lab Invest, 2010. **90**(4): p. 520-30.
224. Schaper, J., et al., *Impairment of the myocardial ultrastructure and changes of the cytoskeleton in dilated cardiomyopathy*. Circulation, 1991. **83**(2): p. 504-14.
225. Rude, M.K., et al., *Aldosterone stimulates matrix metalloproteinases and reactive oxygen species in adult rat ventricular cardiomyocytes*. Hypertension, 2005. **46**(3): p. 555-61.
226. Winter, L., C. Abrahamsberg, and G. Wiche, *Plectin isoform 1b mediates mitochondrion-intermediate filament network linkage and controls organelle shape*. J Cell Biol, 2008. **181**(6): p. 903-11.
227. Schröder, R., et al., *Association of plectin with Z-discs is a prerequisite for the formation of the intermyofibrillar desmin cytoskeleton*. Lab Invest, 2000. **80**(4): p. 455-64.
228. Schröder, R., et al., *Disorganization of the desmin cytoskeleton and mitochondrial dysfunction in plectin-related epidermolysis bullosa simplex with muscular dystrophy*. J Neuropathol Exp Neurol, 2002. **61**(6): p. 520-30.

229. Torres, J., V. Darley-USmar, and M.T. Wilson, *Inhibition of cytochrome c oxidase in turnover by nitric oxide: mechanism and implications for control of respiration*. Biochem J, 1995. **312 (Pt 1)**: p. 169-73.
230. Beltran, B., et al., *The effect of nitric oxide on cell respiration: A key to understanding its role in cell survival or death*. Proc Natl Acad Sci U S A, 2000. **97(26)**: p. 14602-7.
231. Cleeter, M.W., et al., *Reversible inhibition of cytochrome c oxidase, the terminal enzyme of the mitochondrial respiratory chain, by nitric oxide. Implications for neurodegenerative diseases*. FEBS Lett, 1994. **345(1)**: p. 50-4.
232. Clementi, E., et al., *Persistent inhibition of cell respiration by nitric oxide: crucial role of S-nitrosylation of mitochondrial complex I and protective action of glutathione*. Proc Natl Acad Sci U S A, 1998. **95(13)**: p. 7631-6.
233. Mateo, J., et al., *Regulation of hypoxia-inducible factor-1alpha by nitric oxide through mitochondria-dependent and -independent pathways*. Biochem J, 2003. **376(Pt 2)**: p. 537-44.
234. Nisoli, E., et al., *Mitochondrial biogenesis in mammals: the role of endogenous nitric oxide*. Science, 2003. **299(5608)**: p. 896-9.
235. Brookes, P.S., et al., *Mitochondria: regulators of signal transduction by reactive oxygen and nitrogen species*. Free Radic Biol Med, 2002. **33(6)**: p. 755-64.
236. Cadenas, E., *Mitochondrial free radical production and cell signaling*. Mol Aspects Med, 2004. **25(1-2)**: p. 17-26.
237. Brown, G.C., *Nitric oxide regulates mitochondrial respiration and cell functions by inhibiting cytochrome oxidase*. FEBS Lett, 1995. **369(2-3)**: p. 136-9.
238. Liu, X., et al., *Accelerated reaction of nitric oxide with O₂ within the hydrophobic interior of biological membranes*. Proc Natl Acad Sci U S A, 1998. **95(5)**: p. 2175-9.
239. Brookes, P.S., et al., *Control of mitochondrial respiration by NO*, effects of low oxygen and respiratory state*. J Biol Chem, 2003. **278(34)**: p. 31603-9.

240. Chacko, B.K., et al., *The mitochondria-targeted ubiquinone MitoQ decreases ethanol-dependent micro and macro hepatosteatosis*. Hepatology, 2011.
241. Brookes, P.S., et al., *Increased sensitivity of mitochondrial respiration to inhibition by nitric oxide in cardiac hypertrophy*. J Mol Cell Cardiol, 2001. **33**(1): p. 69-82.
242. Venkatraman, A., et al., *Chronic alcohol consumption increases the sensitivity of rat liver mitochondrial respiration to inhibition by nitric oxide*. Hepatology, 2003. **38**(1): p. 141-7.
243. Venkatraman, A., et al., *The role of iNOS in alcohol-dependent hepatotoxicity and mitochondrial dysfunction in mice*. Hepatology, 2004. **40**(3): p. 565-73.
244. Wang, G.L., et al., *Hypoxia-inducible factor 1 is a basic-helix-loop-helix-PAS heterodimer regulated by cellular O₂ tension*. Proc Natl Acad Sci U S A, 1995. **92**(12): p. 5510-4.
245. Kallio, P.J., et al., *Regulation of the hypoxia-inducible transcription factor 1alpha by the ubiquitin-proteasome pathway*. J Biol Chem, 1999. **274**(10): p. 6519-25.
246. Palmer, L.A., et al., *Hypoxia induces type II NOS gene expression in pulmonary artery endothelial cells via HIF-1*. Am J Physiol, 1998. **274**(2 Pt 1): p. L212-9.
247. Lieber, C.S. and L.M. DeCarli, *The feeding of alcohol in liquid diets: two decades of applications and 1982 update*. Alcohol Clin Exp Res, 1982. **6**(4): p. 523-31.
248. Lindros, K.O. and K.E. Penttilä, *Digitonin-collagenase perfusion for efficient separation of periportal or perivenous hepatocytes*. Biochem J, 1985. **228**(3): p. 757-60.
249. Wharton, D.C. and A. Tzagoloff, *Cytochrome oxidase from beef heart mitochondria*. Methods Enzymol, 1967. **10**: p. 245-50.
250. Perez, J., et al., *Role of cellular bioenergetics in smooth muscle cell proliferation induced by platelet-derived growth factor*. Biochem J, 2010. **428**(2): p. 255-67.

251. Sridharan, V., et al., *O(2)-sensing signal cascade: clamping of O(2) respiration, reduced ATP utilization, and inducible fumarate respiration*. Am J Physiol Cell Physiol, 2008. **295**(1): p. C29-37.
252. Hill, B.G., et al., *Regulation of vascular smooth muscle cell bioenergetic function by protein glutathiolation*. Biochim Biophys Acta, 2010. **1797**(2): p. 285-95.
253. Arteel, G.E., et al., *Acute alcohol produces hypoxia directly in rat liver tissue in vivo: role of Kupffer cells*. Am J Physiol, 1996. **271**(3 Pt 1): p. G494-500.
254. Keefer, L.K., et al., *"NONOates" (1-substituted diazen-1-ium-1,2-diolates) as nitric oxide donors: convenient nitric oxide dosage forms*. Methods Enzymol, 1996. **268**: p. 281-93.
255. Tsutsumi, M., et al., *The intralobular distribution of ethanol-inducible P450IIE1 in rat and human liver*. Hepatology, 1989. **10**(4): p. 437-46.
256. Yamazaki, H., et al., *Intralobular distribution of rat liver aldehyde dehydrogenase and alcohol dehydrogenase*. Int J Biochem, 1988. **20**(4): p. 435-7.
257. Mantena, S.K., et al., *Mitochondrial dysfunction and oxidative stress in the pathogenesis of alcohol- and obesity-induced fatty liver diseases*. Free Radic Biol Med, 2008. **44**(7): p. 1259-72.
258. Bailey, S.M., et al., *Ethanol and tobacco smoke increase hepatic steatosis and hypoxia in the hypercholesterolemic apoE(-/-) mouse: implications for a "multihit" hypothesis of fatty liver disease*. Free Radic Biol Med, 2009. **46**(7): p. 928-38.
259. Eccleston, H.B., et al., *Chronic Exposure to a High-Fat Diet Induces Hepatic Steatosis, Impairs Nitric Oxide Bioavailability, and Modifies the Mitochondrial Proteome in Mice*. Antioxid Redox Signal, 2011.
260. Hagen, T., et al., *Redistribution of intracellular oxygen in hypoxia by nitric oxide: effect on HIF1alpha*. Science, 2003. **302**(5652): p. 1975-8.
261. Shiva, S., et al., *Nitric oxide partitioning into mitochondrial membranes and the control of respiration at cytochrome c oxidase*. Proc Natl Acad Sci U S A, 2001. **98**(13): p. 7212-7.

262. Sastre, J., et al., *Mitochondrial function in liver disease*. Front Biosci, 2007. **12**: p. 1200-9.
263. Arteel, G.E., et al., *Oxidative stress occurs in perfused rat liver at low oxygen tension by mechanisms involving peroxynitrite*. Mol Pharmacol, 1999. **55**(4): p. 708-15.
264. Thurman, R.G., et al., *Mechanisms of alcohol-induced hepatotoxicity: studies in rats*. Front Biosci, 1999. **4**: p. e42-6.
265. Baraona, E., et al., *Ethanol consumption increases nitric oxide production in rats, and its peroxynitrite-mediated toxicity is attenuated by polyenylphosphatidylcholine*. Alcohol Clin Exp Res, 2002. **26**(6): p. 883-9.
266. Martinez, R.R., et al., *Nitric oxide contributes to right coronary vasodilation during systemic hypoxia*. Am J Physiol Heart Circ Physiol, 2005. **288**(3): p. H1139-46.
267. Sies, H., *Oxygen gradients during hypoxic steady states in liver. Urate oxidase and cytochrome oxidase as intracellular O₂ indicators*. Hoppe Seylers Z Physiol Chem, 1977. **358**(8): p. 1021-32.
268. Chandel, N.S., et al., *Reactive oxygen species generated at mitochondrial complex III stabilize hypoxia-inducible factor-1alpha during hypoxia: a mechanism of O₂ sensing*. J Biol Chem, 2000. **275**(33): p. 25130-8.
269. Duranteau, J., et al., *Intracellular signaling by reactive oxygen species during hypoxia in cardiomyocytes*. J Biol Chem, 1998. **273**(19): p. 11619-24.
270. Schroedl, C., et al., *Hypoxic but not anoxic stabilization of HIF-1alpha requires mitochondrial reactive oxygen species*. Am J Physiol Lung Cell Mol Physiol, 2002. **283**(5): p. L922-31.
271. Eltzschig, H.K. and C.D. Collard, *Vascular ischaemia and reperfusion injury*. Br Med Bull, 2004. **70**: p. 71-86.
272. Gourdin, M.J., B. Bree, and M. De Kock, *The impact of ischaemia-reperfusion on the blood vessel*. Eur J Anaesthesiol, 2009. **26**(7): p. 537-47.

273. Dawson, T.L., et al., *Mitochondria as a source of reactive oxygen species during reductive stress in rat hepatocytes*. Am J Physiol, 1993. **264**(4 Pt 1): p. C961-7.
274. Lemasters, J.J. and A.L. Nieminen, *Mitochondrial oxygen radical formation during reductive and oxidative stress to intact hepatocytes*. Biosci Rep, 1997. **17**(3): p. 281-91.
275. Niknahad, H., S. Khan, and P.J. O'Brien, *Hepatocyte injury resulting from the inhibition of mitochondrial respiration at low oxygen concentrations involves reductive stress and oxygen activation*. Chem Biol Interact, 1995. **98**(1): p. 27-44.
276. Becker, L.B., et al., *Generation of superoxide in cardiomyocytes during ischemia before reperfusion*. Am J Physiol, 1999. **277**(6 Pt 2): p. H2240-6.
277. Höhler, B., et al., *Hypoxic upregulation of tyrosine hydroxylase gene expression is paralleled, but not induced, by increased generation of reactive oxygen species in PC12 cells*. FEBS Lett, 1999. **457**(1): p. 53-6.
278. Dirmeier, R., et al., *Exposure of yeast cells to anoxia induces transient oxidative stress. Implications for the induction of hypoxic genes*. J Biol Chem, 2002. **277**(38): p. 34773-84.
279. Kwast, K.E., et al., *Oxygen sensing in yeast: evidence for the involvement of the respiratory chain in regulating the transcription of a subset of hypoxic genes*. Proc Natl Acad Sci U S A, 1999. **96**(10): p. 5446-51.
280. Bell, E.L., et al., *The Qo site of the mitochondrial complex III is required for the transduction of hypoxic signaling via reactive oxygen species production*. J Cell Biol, 2007. **177**(6): p. 1029-36.
281. Chandel, N.S. and G.R. Budinger, *The cellular basis for diverse responses to oxygen*. Free Radic Biol Med, 2007. **42**(2): p. 165-74.
282. Klimova, T. and N.S. Chandel, *Mitochondrial complex III regulates hypoxic activation of HIF*. Cell Death Differ, 2008. **15**(4): p. 660-6.
283. Parks, D.A. and D.N. Granger, *Ischemia-induced vascular changes: role of xanthine oxidase and hydroxyl radicals*. Am J Physiol, 1983. **245**(2): p. G285-9.

284. Wei, Z., et al., *Simulated ischemia in flow-adapted endothelial cells leads to generation of reactive oxygen species and cell signaling*. *Circ Res*, 1999. **85**(8): p. 682-9.
285. Hoffman, D.L., J.D. Salter, and P.S. Brookes, *Response of mitochondrial reactive oxygen species generation to steady-state oxygen tension: implications for hypoxic cell signaling*. *Am J Physiol Heart Circ Physiol*, 2007. **292**(1): p. H101-8.
286. Guzy, R.D. and P.T. Schumacker, *Oxygen sensing by mitochondria at complex III: the paradox of increased reactive oxygen species during hypoxia*. *Exp Physiol*, 2006. **91**(5): p. 807-19.
287. Cadenas, S., J. Aragonés, and M.O. Landázuri, *Mitochondrial reprogramming through cardiac oxygen sensors in ischaemic heart disease*. *Cardiovasc Res*, 2010. **88**(2): p. 219-28.
288. Aley, P.K., et al., *Hypoxic modulation of Ca²⁺ signaling in human venous endothelial cells. Multiple roles for reactive oxygen species*. *J Biol Chem*, 2005. **280**(14): p. 13349-54.
289. Aley, P.K., et al., *Hypoxia stimulates Ca²⁺ release from intracellular stores in astrocytes via cyclic ADP ribose-mediated activation of ryanodine receptors*. *Cell Calcium*, 2006. **39**(1): p. 95-100.
290. Ziegelstein, R.C., et al., *Modulation of calcium homeostasis in cultured rat aortic endothelial cells by intracellular acidification*. *Am J Physiol*, 1993. **265**(4 Pt 2): p. H1424-33.
291. Hu, Q. and R.C. Ziegelstein, *Hypoxia/reoxygenation stimulates intracellular calcium oscillations in human aortic endothelial cells*. *Circulation*, 2000. **102**(20): p. 2541-7.
292. Levraut, J., et al., *Cell death during ischemia: relationship to mitochondrial depolarization and ROS generation*. *Am J Physiol Heart Circ Physiol*, 2003. **284**(2): p. H549-58.
293. Halestrap, A.P., S.J. Clarke, and S.A. Javadov, *Mitochondrial permeability transition pore opening during myocardial reperfusion--a target for cardioprotection*. *Cardiovasc Res*, 2004. **61**(3): p. 372-85.

294. Solaini, G. and D.A. Harris, *Biochemical dysfunction in heart mitochondria exposed to ischaemia and reperfusion*. *Biochem J*, 2005. **390**(Pt 2): p. 377-94.
295. Silverman, H.S. and M.D. Stern, *Ionic basis of ischaemic cardiac injury: insights from cellular studies*. *Cardiovasc Res*, 1994. **28**(5): p. 581-97.
296. Dong, Z., et al., *Intracellular Ca²⁺ thresholds that determine survival or death of energy-deprived cells*. *Am J Pathol*, 1998. **152**(1): p. 231-40.
297. Saikumar, P., et al., *Mechanisms of cell death in hypoxia/reoxygenation injury*. *Oncogene*, 1998. **17**(25): p. 3341-9.
298. Millar, T.M., V. Phan, and L.A. Tibbles, *ROS generation in endothelial hypoxia and reoxygenation stimulates MAP kinase signaling and kinase-dependent neutrophil recruitment*. *Free Radic Biol Med*, 2007. **42**(8): p. 1165-77.
299. Therade-Matharan, S., et al., *Reactive oxygen species production by mitochondria in endothelial cells exposed to reoxygenation after hypoxia and glucose depletion is mediated by ceramide*. *Am J Physiol Regul Integr Comp Physiol*, 2005. **289**(6): p. R1756-62.
300. Honda, H., P. Korge, and J. Weiss, *Mitochondria and ischemia/reperfusion injury*. *Ann N Y Acad Sci*, 2005. **1047**: p. 248-58.
301. Piper, H.M., K. Meuter, and C. Schafer, *Cellular mechanisms of ischemia-reperfusion injury*. *Ann Thorac Surg*, 2003. **75**(2): p. S644-8.
302. Schaefer, C.A., et al., *Statins inhibit hypoxia-induced endothelial proliferation by preventing calcium-induced ROS formation*. *Atherosclerosis*, 2006. **185**(2): p. 290-6.
303. Holland, J.A., et al., *Endothelial cell oxidant production: effect of NADPH oxidase inhibitors*. *Endothelium*, 2000. **7**(2): p. 109-19.
304. Du, G., A. Mouithys-Mickalad, and F.E. Sluse, *Generation of superoxide anion by mitochondria and impairment of their functions during anoxia and reoxygenation in vitro*. *Free Radic Biol Med*, 1998. **25**(9): p. 1066-74.

305. Kowaltowski, A.J. and A.E. Vercesi, *Mitochondrial damage induced by conditions of oxidative stress*. Free Radic Biol Med, 1999. **26**(3-4): p. 463-71.
306. Shlafer, M., C.L. Myers, and S. Adkins, *Mitochondrial hydrogen peroxide generation and activities of glutathione peroxidase and superoxide dismutase following global ischemia*. J Mol Cell Cardiol, 1987. **19**(12): p. 1195-206.
307. Weinberg, J.M., et al., *Mitochondrial dysfunction during hypoxia/reoxygenation and its correction by anaerobic metabolism of citric acid cycle intermediates*. Proc Natl Acad Sci U S A, 2000. **97**(6): p. 2826-31.
308. Russell, W.J., S. Matalon, and R.M. Jackson, *Manganese superoxide dismutase expression in alveolar type II epithelial cells from nonventilated and hypoperfused lungs*. Am J Respir Cell Mol Biol, 1994. **11**(3): p. 366-71.
309. Boyle, E.M., et al., *Endothelial cell injury in cardiovascular surgery: ischemia-reperfusion*. Ann Thorac Surg, 1996. **62**(6): p. 1868-75.
310. Forman, M.B., D.W. Puett, and R. Virmani, *Endothelial and myocardial injury during ischemia and reperfusion: pathogenesis and therapeutic implications*. J Am Coll Cardiol, 1989. **13**(2): p. 450-9.
311. Sener, G., A. Sakarcan, and B.C. Yegen, *Role of garlic in the prevention of ischemia-reperfusion injury*. Mol Nutr Food Res, 2007. **51**(11): p. 1345-52.
312. Li, C., M.M. Wright, and R.M. Jackson, *Reactive species mediated injury of human lung epithelial cells after hypoxia-reoxygenation*. Exp Lung Res, 2002. **28**(5): p. 373-89.
313. Dong, Z., et al., *Serine protease inhibitors suppress cytochrome c-mediated caspase-9 activation and apoptosis during hypoxia-reoxygenation*. Biochem J, 2000. **347 Pt 3**: p. 669-77.
314. Cai, J. and D.P. Jones, *Superoxide in apoptosis. Mitochondrial generation triggered by cytochrome c loss*. J Biol Chem, 1998. **273**(19): p. 11401-4.
315. Brunelle, J.K. and N.S. Chandel, *Oxygen deprivation induced cell death: an update*. Apoptosis, 2002. **7**(6): p. 475-82.

316. Dong, Y.Y., et al., *Effect of hypoxia-reoxygenation on endothelial function in porcine cardiac microveins*. Ann Thorac Surg, 2006. **81**(5): p. 1708-14.
317. Vrints, C.J., *Pathophysiology of the no-reflow phenomenon*. Acute Card Care, 2009. **11**(2): p. 69-76.
318. Leonarduzzi, G., et al., *Lipid oxidation products in cell signaling*. Free Radic Biol Med, 2000. **28**(9): p. 1370-8.
319. Carini, M., G. Aldini, and R. Facino, *Mass spectrometry for detection of 4-hydroxy-trans-2-nonenal (HNE) adducts with peptides and proteins*. Mass Spectrom Rev. **23**(4): p. 281-305.
320. Doorn, J.A. and D.R. Petersen, *Covalent modification of amino acid nucleophiles by the lipid peroxidation products 4-hydroxy-2-nonenal and 4-oxo-2-nonenal*. Chem Res Toxicol, 2002. **15**(11): p. 1445-50.
321. Isom, A.L., et al., *Modification of Cytochrome c by 4-hydroxy- 2-nonenal: evidence for histidine, lysine, and arginine-aldehyde adducts*. J Am Soc Mass Spectrom, 2004. **15**(8): p. 1136-47.
322. Alderton, A.L., et al., *Induction of redox instability of bovine myoglobin by adduction with 4-hydroxy-2-nonenal*. Biochemistry, 2003. **42**(15): p. 4398-405.
323. Poli, G., et al., *4-hydroxynonenal: a membrane lipid oxidation product of medicinal interest*. Med Res Rev, 2008. **28**(4): p. 569-631.
324. Uchida, K., *4-Hydroxy-2-nonenal: a product and mediator of oxidative stress*. Prog Lipid Res, 2003. **42**(4): p. 318-43.
325. Eaton, P., et al., *Formation of 4-hydroxy-2-nonenal-modified proteins in ischemic rat heart*. Am J Physiol, 1999. **276**(3 Pt 2): p. H935-43.
326. Hill, B.G., et al., *Myocardial ischaemia inhibits mitochondrial metabolism of 4-hydroxy-trans-2-nonenal*. Biochem J, 2009. **417**(2): p. 513-24.
327. Echtay, K.S., et al., *A signalling role for 4-hydroxy-2-nonenal in regulation of mitochondrial uncoupling*. Embo J, 2003. **22**(16): p. 4103-10.

328. Humphries, K.M., Y. Yoo, and L.I. Szweda, *Inhibition of NADH-linked mitochondrial respiration by 4-hydroxy-2-nonenal*. *Biochemistry*, 1998. **37**(2): p. 552-7.
329. Humphries, K.M. and L.I. Szweda, *Selective inactivation of alpha-ketoglutarate dehydrogenase and pyruvate dehydrogenase: reaction of lipoic acid with 4-hydroxy-2-nonenal*. *Biochemistry*, 1998. **37**(45): p. 15835-41.
330. Sansbury, B.E., et al., *Bioenergetic function in cardiovascular cells: The importance of the reserve capacity and its biological regulation*. Chem Biol Interact, 2010.
331. Chen, J., et al., *Inhibition of cytochrome c oxidase activity by 4-hydroxynonenal (HNE). Role of HNE adduct formation with the enzyme subunits*. *Biochim Biophys Acta*, 1998. **1380**(3): p. 336-44.
332. Raza, H., et al., *Alterations in mitochondrial respiratory functions, redox metabolism and apoptosis by oxidant 4-hydroxynonenal and antioxidants curcumin and melatonin in PC12 cells*. *Toxicol Appl Pharmacol*, 2008. **226**(2): p. 161-8.
333. Gerencser, A.A., et al., *Quantitative microplate-based respirometry with correction for oxygen diffusion*. *Anal Chem*, 2009. **81**(16): p. 6868-78.
334. Leonarduzzi, G., et al., *4-Hydroxynonenal and cholesterol oxidation products in atherosclerosis*. *Mol Nutr Food Res*, 2005. **49**(11): p. 1044-9.
335. Uchida, K., *Role of reactive aldehyde in cardiovascular diseases*. *Free Radic Biol Med*, 2000. **28**(12): p. 1685-96.
336. Cighetti, G., et al., *Mechanisms of action of malondialdehyde and 4-hydroxynonenal on xanthine oxidoreductase*. *Arch Biochem Biophys*, 2001. **389**(2): p. 195-200.
337. Haberland, A., A.K. Schütz, and I. Schimke, *The influence of lipid peroxidation products (malondialdehyde, 4-hydroxynonenal) on xanthine oxidoreductase prepared from rat liver*. *Biochem Pharmacol*, 1992. **43**(10): p. 2117-20.

338. Jang, Y.J., et al., *Kaempferol attenuates 4-hydroxynonenal-induced apoptosis in PC12 cells by directly inhibiting NADPH oxidase*. J Pharmacol Exp Ther, 2011. **337**(3): p. 747-54.
339. Yun, M.R., et al., *5-Lipoxygenase plays an essential role in 4-HNE-enhanced ROS production in murine macrophages via activation of NADPH oxidase*. Free Radic Res, 2010. **44**(7): p. 742-50.
340. de Villiers, W.J., et al., *4-Hydroxynonenal-induced apoptosis in rat hepatic stellate cells: mechanistic approach*. J Gastroenterol Hepatol, 2007. **22**(3): p. 414-22.
341. Xu, J., et al., *Effects of 4-hydroxy-2-nonenal on cultured human aortic endothelial cells and myocardial cell*. Conf Proc IEEE Eng Med Biol Soc, 2005. **6**: p. 5598-602.
342. Awasthi, Y., et al., *Role of 4-hydroxynonenal in stress-mediated apoptosis signaling*. Mol Aspects Med. **24**(4-5): p. 219-30.
343. Liu, W., et al., *4-hydroxynonenal induces a cellular redox status-related activation of the caspase cascade for apoptotic cell death*. J Cell Sci, 2000. **113** (Pt 4): p. 635-41.
344. Raza, H. and A. John, *4-hydroxynonenal induces mitochondrial oxidative stress, apoptosis and expression of glutathione S-transferase A4-4 and cytochrome P450 2E1 in PC12 cells*. Toxicol Appl Pharmacol, 2006. **216**(2): p. 309-18.
345. Vaillancourt, F., et al., *4-Hydroxynonenal induces apoptosis in human osteoarthritic chondrocytes: the protective role of glutathione-S-transferase*. Arthritis Res Ther, 2008. **10**(5): p. R107.
346. Jung, H.J., et al., *Terpestacin inhibits tumor angiogenesis by targeting UQCRB of mitochondrial complex III and suppressing hypoxia-induced reactive oxygen species production and cellular oxygen sensing*. J Biol Chem, 2010. **285**(15): p. 11584-95.
347. Kang, P.M., et al., *Morphological and molecular characterization of adult cardiomyocyte apoptosis during hypoxia and reoxygenation*. Circ Res, 2000. **87**(2): p. 118-25.

348. Li, G., et al., *Catalase-overexpressing transgenic mouse heart is resistant to ischemia-reperfusion injury*. Am J Physiol, 1997. **273**(3 Pt 2): p. H1090-5.
349. Sansbury, B.E., et al., *Responses of hypertrophied myocytes to reactive species: implications for glycolysis and electrophile metabolism*. Biochem J, 2011.
350. Kaasik, A., et al., *Energetic crosstalk between organelles: architectural integration of energy production and utilization*. Circ Res, 2001. **89**(2): p. 153-9.
351. Saks, V., et al., *Structure-function relationships in feedback regulation of energy fluxes in vivo in health and disease: mitochondrial interactosome*. Biochim Biophys Acta, 2010. **1797**(6-7): p. 678-97.
352. Marcinek, D.J., et al., *Mitochondrial coupling in vivo in mouse skeletal muscle*. Am J Physiol Cell Physiol, 2004. **286**(2): p. C457-63.
353. Zobi, F., et al., *CO releasing properties and cytoprotective effect of cis-trans-[Re(II)(CO)2Br2L2]n complexes*. Inorg Chem, 2010. **49**(16): p. 7313-22.
354. Kanatous, S.B. and P.P. Mammen, *Regulation of myoglobin expression*. J Exp Biol, 2010. **213**(Pt 16): p. 2741-7.
355. Horáková, E., et al., *Mechanisms of iron-induced oxidative modifications of creatine kinase in rat brain in vitro. possible involvement of HNE*. Gen Physiol Biophys, 2002. **21**(3): p. 327-36.
356. Hussain, S.N., et al., *Modifications of proteins by 4-hydroxy-2-nonenal in the ventilatory muscles of rats*. Am J Physiol Lung Cell Mol Physiol, 2006. **290**(5): p. L996-1003.
357. Lynch, M.P. and C. Faustman, *Effect of aldehyde lipid oxidation products on myoglobin*. J Agric Food Chem, 2000. **48**(3): p. 600-4.
358. Faustman, C., et al., *alpha,beta-unsaturated aldehydes accelerate oxymyoglobin oxidation*. J Agric Food Chem, 1999. **47**(8): p. 3140-4.
359. Suman, S.P., R.A. Mancini, and C. Faustman, *Lipid-oxidation-induced carboxymyoglobin oxidation*. J Agric Food Chem, 2006. **54**(24): p. 9248-53.

360. Suman, S.P., et al., *Redox instability induced by 4-hydroxy-2-nonenal in porcine and bovine myoglobins at pH 5.6 and 4 degrees C*. J Agric Food Chem, 2006. **54**(9): p. 3402-8.
361. Suman, S.P., et al., *Proteomics of lipid oxidation-induced oxidation of porcine and bovine oxymyoglobins*. Proteomics, 2007. **7**(4): p. 628-40.
362. Joseph, P., et al., *Mass spectrometric evidence for aldehyde adduction in carboxymyoglobin*. Meat Sci, 2009.
363. Walsh, D.M., et al., *Vitamin E and selenium deficiencies increase indices of lipid peroxidation in muscle tissue of ruminant calves*. Int J Vitam Nutr Res, 1993. **63**(3): p. 188-94.
364. Barnes, S., et al., *High-resolution mass spectrometry analysis of protein oxidations and resultant loss of function*. Biochem Soc Trans, 2008. **36**(Pt 5): p. 1037-44.
365. Gnaiger, E., *Oxygen conformance of cellular respiration. A perspective of mitochondrial physiology*. Adv Exp Med Biol, 2003. **543**: p. 39-55.
366. Steinlechner-Maran, R., et al., *Oxygen dependence of respiration in coupled and uncoupled endothelial cells*. Am J Physiol, 1996. **271**(6 Pt 1): p. C2053-61.
367. Aw, T.Y., B.S. Andersson, and D.P. Jones, *Suppression of mitochondrial respiratory function after short-term anoxia*. Am J Physiol, 1987. **252**(4 Pt 1): p. C362-8.
368. Petersen, L.C., P. Nicholls, and H. Degn, *The effect of energization on the apparent Michaelis-Mentne constant for oxygen in mitochondrial respiration*. Biochem J, 1974. **142**(2): p. 247-52.
369. Gnaiger, E., et al., *Mitochondrial oxygen affinity, respiratory flux control and excess capacity of cytochrome c oxidase*. J Exp Biol, 1998. **201**(Pt 8): p. 1129-39.
370. Gnaiger, E., et al., *Mitochondrial respiration in the low oxygen environment of the cell. Effect of ADP on oxygen kinetics*. Biochim Biophys Acta, 1998. **1365**(1-2): p. 249-54.

371. Wilson, D.F. and W.L. Rumsey, *Factors modulating the oxygen dependence of mitochondrial oxidative phosphorylation*. Adv Exp Med Biol, 1988. **222**: p. 121-31.
372. Wilson, D.F., et al., *The oxygen dependence of mitochondrial oxidative phosphorylation measured by a new optical method for measuring oxygen concentration*. J Biol Chem, 1988. **263**(6): p. 2712-8.
373. Abassi, Z., et al., *Aortocaval fistula in rat: a unique model of volume-overload congestive heart failure and cardiac hypertrophy*. J Biomed Biotechnol, 2011. **2011**: p. 729497.
374. Palaniyandi, S.S., et al., *Regulation of mitochondrial processes: a target for heart failure*. Drug Discov Today Dis Mech, 2010. **7**(2): p. e95-e102.
375. Wang, X., et al., *Characterization of cardiac hypertrophy and heart failure due to volume overload in the rat*. J Appl Physiol, 2003. **94**(2): p. 752-63.
376. Ray, S., *The echocardiographic assessment of functional mitral regurgitation*. Eur J Echocardiogr, 2010. **11**(10): p. i11-17.
377. Boudoulas, H., E.E. Sparks, and C.F. Wooley, *Mitral valvular regurgitation : etiology, pathophysiologic mechanisms, clinical manifestations*. Herz, 2006. **31**(1): p. 6-13.
378. Rimbaud, S., A. Garnier, and R. Ventura-Clapier, *Mitochondrial biogenesis in cardiac pathophysiology*. Pharmacol Rep, 2009. **61**(1): p. 131-8.
379. Rimbaud, S., et al., *Stimulus specific changes of energy metabolism in hypertrophied heart*. J Mol Cell Cardiol, 2009. **46**(6): p. 952-9.
380. De Sousa, E., et al., *Subcellular creatine kinase alterations. Implications in heart failure*. Circ Res, 1999. **85**(1): p. 68-76.
381. Garnier, A., et al., *Depressed mitochondrial transcription factors and oxidative capacity in rat failing cardiac and skeletal muscles*. J Physiol, 2003. **551**(Pt 2): p. 491-501.

382. Javadov, S., et al., *NHE-1 inhibition improves impaired mitochondrial permeability transition and respiratory function during postinfarction remodelling in the rat*. J Mol Cell Cardiol, 2005. **38**(1): p. 135-43.
383. Jüllig, M., et al., *Is the failing heart out of fuel or a worn engine running rich? A study of mitochondria in old spontaneously hypertensive rats*. Proteomics, 2008. **8**(12): p. 2556-72.
384. Sheeran, F.L. and S. Pepe, *Energy deficiency in the failing heart: linking increased reactive oxygen species and disruption of oxidative phosphorylation rate*. Biochim Biophys Acta, 2006. **1757**(5-6): p. 543-52.
385. Marín-García, J., et al., *Regional Distribution of Mitochondrial Dysfunction and Apoptotic Remodeling in Pacing-Induced Heart Failure*. Journal of Cardiac Failure, 2009. **15**(8): p. 700-708.
386. Schultz, D., et al., *Selective induction of the creatine kinase-B gene in chronic volume overload hypertrophy is not affected by ACE-inhibitor therapy*. J Mol Cell Cardiol, 1997. **29**(10): p. 2665-73.
387. Ekelund, U.E., et al., *Intravenous allopurinol decreases myocardial oxygen consumption and increases mechanical efficiency in dogs with pacing-induced heart failure*. Circ Res, 1999. **85**(5): p. 437-45.
388. Cappola, T.P., et al., *Allopurinol improves myocardial efficiency in patients with idiopathic dilated cardiomyopathy*. Circulation, 2001. **104**(20): p. 2407-11.
389. Marcil, M., et al., *Compensated volume overload increases the vulnerability of heart mitochondria without affecting their functions in the absence of stress*. J Mol Cell Cardiol, 2006. **41**(6): p. 998-1009.
390. Vogt, A.M. and W. Kübler, *Heart failure: is there an energy deficit contributing to contractile dysfunction?* Basic Res Cardiol, 1998. **93**(1): p. 1-10.
391. Jameel, M.N. and J. Zhang, *Myocardial energetics in left ventricular hypertrophy*. Curr Cardiol Rev, 2009. **5**(3): p. 243-50.
392. Milner, D.J., et al., *Desmin cytoskeleton linked to muscle mitochondrial distribution and respiratory function*. J Cell Biol, 2000. **150**(6): p. 1283-98.

393. Andrienko, T., et al., *Metabolic consequences of functional complexes of mitochondria, myofibrils and sarcoplasmic reticulum in muscle cells*. J Exp Biol, 2003. **206**(Pt 12): p. 2059-72.
394. Seppet, E.K., et al., *Structure-function relationships in the regulation of energy transfer between mitochondria and ATPases in cardiac cells*. Exp Clin Cardiol, 2006. **11**(3): p. 189-94.
395. Wilding, J.R., et al., *Altered energy transfer from mitochondria to sarcoplasmic reticulum after cytoarchitectural perturbations in mice hearts*. J Physiol, 2006. **575**(Pt 1): p. 191-200.
396. Saks, V.A., et al., *Functional coupling as a basic mechanism of feedback regulation of cardiac energy metabolism*. Mol Cell Biochem, 2004. **256-257**(1-2): p. 185-99.
397. Vendelin, M., et al., *Intracellular diffusion of adenosine phosphates is locally restricted in cardiac muscle*. Mol Cell Biochem, 2004. **256-257**(1-2): p. 229-41.
398. Dzeja, P.P., et al., *Failing energetics in failing hearts*. Curr Cardiol Rep, 2000. **2**(3): p. 212-7.
399. Ferris, S.D., et al., *Mitochondrial DNA evolution in mice*. Genetics, 1983. **105**(3): p. 681-721.
400. Goios, A., et al., *mtDNA phylogeny and evolution of laboratory mouse strains*. Genome Res, 2007. **17**(3): p. 293-8.
401. Bayona-Bafaluy, M.P., et al., *Revisiting the mouse mitochondrial DNA sequence*. Nucleic Acids Res, 2003. **31**(18): p. 5349-55.
402. Bibb, M.J., et al., *Sequence and gene organization of mouse mitochondrial DNA*. Cell, 1981. **26**(2 Pt 2): p. 167-80.
403. Anderson, S., et al., *Sequence and organization of the human mitochondrial genome*. Nature, 1981. **290**(5806): p. 457-65.

404. Brown, W.M., *Polymorphism in mitochondrial DNA of humans as revealed by restriction endonuclease analysis*. Proc Natl Acad Sci U S A, 1980. **77**(6): p. 3605-9.
405. Cann, R.L., M. Stoneking, and A.C. Wilson, *Mitochondrial DNA and human evolution*. Nature, 1987. **325**(6099): p. 31-6.
406. Yu, X., et al., *Dissecting the effects of mtDNA variations on complex traits using mouse conplastic strains*. Genome Res, 2009. **19**(1): p. 159-65.
407. Yoshiki, A. and K. Moriwaki, *Mouse phenome research: implications of genetic background*. ILAR J, 2006. **47**(2): p. 94-102.
408. Butler, E.G., P.J. England, and G.M. Williams, *Genetic differences in enzymes associated with peroxisome proliferation and hydrogen peroxide metabolism in inbred mouse strains*. Carcinogenesis, 1988. **9**(8): p. 1459-63.
409. Nishina, P.M., et al., *Atherosclerosis and plasma and liver lipids in nine inbred strains of mice*. Lipids, 1993. **28**(7): p. 599-605.
410. Tabata, S., et al., *Effect of streptozotocin-induced diabetes mellitus on type 1 deiodinase (D1) in inherited D1-deficient mice*. Endocr J, 1999. **46**(4): p. 497-504.
411. Iwai, S., et al., *High sensitivity of fatty liver Shionogi (FLS) mice to diethylnitrosamine hepatocarcinogenesis: comparison to C3H and C57 mice*. Cancer Lett, 2007. **246**(1-2): p. 115-21.
412. Lee, G.H., et al., *Strain specific sensitivity to diethylnitrosamine-induced carcinogenesis is maintained in hepatocytes of C3H/HeN in equilibrium with C57BL/6N chimeric mice*. Cancer Res, 1991. **51**(12): p. 3257-60.
413. Van Lenten, B.J., et al., *Lipid-induced changes in intracellular iron homeostasis in vitro and in vivo*. J Clin Invest, 1995. **95**(5): p. 2104-10.
414. Nishina, P.M., J. Verstuyft, and B. Paigen, *Synthetic low and high fat diets for the study of atherosclerosis in the mouse*. J Lipid Res, 1990. **31**(5): p. 859-69.

415. Ishida, B.Y., et al., *Effects of atherogenic diet consumption on lipoproteins in mouse strains C57BL/6 and C3H*. J Lipid Res, 1991. **32**(4): p. 559-68.
416. Paigen, B., et al., *Atherosclerosis susceptibility differences among progenitors of recombinant inbred strains of mice*. Arteriosclerosis, 1990. **10**(2): p. 316-23.
417. Paigen, B., et al., *Ath-1, a gene determining atherosclerosis susceptibility and high density lipoprotein levels in mice*. Proc Natl Acad Sci U S A, 1987. **84**(11): p. 3763-7.
418. Paigen, B., et al., *Comparison of atherosclerotic lesions and HDL-lipid levels in male, female, and testosterone-treated female mice from strains C57BL/6, BALB/c, and C3H*. Atherosclerosis, 1987. **64**(2-3): p. 215-21.
419. Paigen, B., et al., *Genetic analysis of murine strains C57BL/6J and C3H/HeJ to confirm the map position of Ath-1, a gene determining atherosclerosis susceptibility*. Biochem Genet, 1987. **25**(7-8): p. 501-11.
420. Poltorak, A., et al., *Defective LPS signaling in C3H/HeJ and C57BL/10ScCr mice: mutations in Tlr4 gene*. Science, 1998. **282**(5396): p. 2085-8.
421. Poltorak, A., et al., *Genetic and physical mapping of the Lps locus: identification of the toll-4 receptor as a candidate gene in the critical region*. Blood Cells Mol Dis, 1998. **24**(3): p. 340-55.
422. Qureshi, S.T., et al., *Endotoxin-tolerant mice have mutations in Toll-like receptor 4 (Tlr4)*. J Exp Med, 1999. **189**(4): p. 615-25.
423. Töttemeyer, S., et al., *Toll-like receptor expression in C3H/HeN and C3H/HeJ mice during Salmonella enterica serovar Typhimurium infection*. Infect Immun, 2003. **71**(11): p. 6653-7.
424. Devaraj, S., P. Tobias, and I. Jialal, *Knockout of toll-like receptor-4 attenuates the pro-inflammatory state of diabetes*. Cytokine, 2011.
425. Loppnow, H., K. Werdan, and M. Buerke, *Vascular cells contribute to atherosclerosis by cytokine- and innate-immunity-related inflammatory mechanisms*. Innate Immun, 2008. **14**(2): p. 63-87.

426. Hritz, I., et al., *The critical role of toll-like receptor (TLR) 4 in alcoholic liver disease is independent of the common TLR adapter MyD88*. *Hepatology*, 2008. **48**(4): p. 1224-31.
427. Amo, T. and M.D. Brand, *Were inefficient mitochondrial haplogroups selected during migrations of modern humans? A test using modular kinetic analysis of coupling in mitochondria from cybrid cell lines*. *Biochem J*, 2007. **404**(2): p. 345-51.
428. Cooper, C.E., P. Nicholls, and J.A. Freedman, *Cytochrome c oxidase: structure, function, and membrane topology of the polypeptide subunits*. *Biochemistry and Cell Biology*, 1991. **69**(9): p. 586-607.
429. Smits, P., et al., *Functional consequences of mitochondrial tRNA Trp and tRNA Arg mutations causing combined OXPHOS defects*. *Eur J Hum Genet*, 2010. **18**(3): p. 324-9.
430. Uusimaa, J., et al., *Molecular epidemiology of childhood mitochondrial encephalomyopathies in a Finnish population: sequence analysis of entire mtDNA of 17 children reveals heteroplasmic mutations in tRNAArg, tRNAGlu, and tRNALeu(UUR) genes*. *Pediatrics*, 2004. **114**(2): p. 443-50.
431. Hayashi, J., et al., *Functional and morphological abnormalities of mitochondria in human cells containing mitochondrial DNA with pathogenic point mutations in tRNA genes*. *J Biol Chem*, 1994. **269**(29): p. 19060-6.
432. Karram, T., et al., *Induction of cardiac hypertrophy by a controlled reproducible sutureless aortocaval shunt in the mouse*. *J Invest Surg*, 2005. **18**(6): p. 325-34.
433. Perry, G.J., et al., *Genetic variation in angiotensin-converting enzyme does not prevent development of cardiac hypertrophy or upregulation of angiotensin II in response to aortocaval fistula*. *Circulation*, 2001. **103**(7): p. 1012-6.
434. Scheuermann-Freestone, M., et al., *A new model of congestive heart failure in the mouse due to chronic volume overload*. *Eur J Heart Fail*, 2001. **3**(5): p. 535-43.
435. Smith, D.R., D. Stone, and V.M. Darley-Usmar, *Stimulation of mitochondrial oxygen consumption in isolated cardiomyocytes after hypoxia-reoxygenation*. *Free Radic Res*, 1996. **24**(3): p. 159-66.

436. Wei, C.C., et al., *Cardiac interstitial bradykinin and mast cells modulate pattern of LV remodeling in volume overload in rats*. Am J Physiol Heart Circ Physiol, 2003. **285**(2): p. H784-92.
437. Wei, C.C., et al., *Mast cell chymase limits the cardiac efficacy of Ang I-converting enzyme inhibitor therapy in rodents*. J Clin Invest, 2010. **120**(4): p. 1229-39.
438. Souza-Pinto, N.C., et al., *Age-associated increase in 8-oxo-deoxyguanosine glycosylase/AP lyase activity in rat mitochondria*. Nucleic Acids Res, 1999. **27**(8): p. 1935-42.
439. Robinson, J.B. and P.A. Srere, *Organization of Krebs tricarboxylic acid cycle enzymes in mitochondria*. J Biol Chem, 1985. **260**(19): p. 10800-5.
440. Reipert, S., et al., *Association of mitochondria with plectin and desmin intermediate filaments in striated muscle*. Exp Cell Res, 1999. **252**(2): p. 479-91.
441. Hom, J. and S.S. Sheu, *Morphological dynamics of mitochondria--a special emphasis on cardiac muscle cells*. J Mol Cell Cardiol, 2009. **46**(6): p. 811-20.
442. Ong, S.B., et al., *Inhibiting mitochondrial fission protects the heart against ischemia/reperfusion injury*. Circulation, 2010. **121**(18): p. 2012-22.
443. Okamoto, K. and J.M. Shaw, *Mitochondrial morphology and dynamics in yeast and multicellular eukaryotes*. Annu Rev Genet, 2005. **39**: p. 503-36.
444. Twig, G., et al., *Fission and selective fusion govern mitochondrial segregation and elimination by autophagy*. EMBO J, 2008. **27**(2): p. 433-46.
445. Twig, G., B. Hyde, and O.S. Shirihai, *Mitochondrial fusion, fission and autophagy as a quality control axis: the bioenergetic view*. Biochim Biophys Acta, 2008. **1777**(9): p. 1092-7.
446. Dagda, R.K., et al., *Loss of PINK1 function promotes mitophagy through effects on oxidative stress and mitochondrial fission*. J Biol Chem, 2009. **284**(20): p. 13843-55.

447. Excoffier, L. and A. Langaney, *Origin and differentiation of human mitochondrial DNA*. Am J Hum Genet, 1989. **44**(1): p. 73-85.
448. Pakendorf, B. and M. Stoneking, *Mitochondrial DNA and human evolution*. Annu Rev Genomics Hum Genet, 2005. **6**: p. 165-83.
449. Underhill, P.A. and T. Kivisild, *Use of y chromosome and mitochondrial DNA population structure in tracing human migrations*. Annu Rev Genet, 2007. **41**: p. 539-64.
450. Wallace, D.C., *The mitochondrial genome in human adaptive radiation and disease: on the road to therapeutics and performance enhancement*. Gene, 2005. **354**: p. 169-80.
451. Amo, T., et al., *Experimental assessment of bioenergetic differences caused by the common European mitochondrial DNA haplogroups H and T*. Gene, 2008. **411**(1-2): p. 69-76.
452. Shiva, S. and V.M. Darley-Usmar, *Control of the nitric oxide-cytochrome c oxidase signaling pathway under pathological and physiological conditions*. IUBMB Life, 2003. **55**(10-11): p. 585-90.
453. Blough, N.V. and O.C. Zafiriou, *1.Reaction of superoxide with nitric oxide to form peroxynitrite in alkaline aqueous solution*. Inorganic Chemistry, 1985. **24**(22): p. 3502-3504.
454. Beckman, J.S., et al., *Apparent hydroxyl radical production by peroxynitrite: implications for endothelial injury from nitric oxide and superoxide*. Proc Natl Acad Sci U S A, 1990. **87**(4): p. 1620-4.
455. Beckman, J.S. and W.H. Koppenol, *Nitric oxide, superoxide, and peroxynitrite: the good, the bad, and ugly*. Am J Physiol Cell Physiol, 1996. **271**(5): p. C1424-1437.
456. Pryor, W.A. and G.L. Squadrito, *The chemistry of peroxynitrite: a product from the reaction of nitric oxide with superoxide*. Am J Physiol, 1995. **268**(5 Pt 1): p. L699-722.

457. Squadrito, G.L. and W.A. Pryor, *The formation of peroxynitrite in vivo from nitric oxide and superoxide*. Chem Biol Interact, 1995. **96**(2): p. 203-6.
458. Bailey, S.M. and C.C. Cunningham, *Effect of dietary fat on chronic ethanol-induced oxidative stress in hepatocytes*. Alcohol Clin Exp Res, 1999. **23**(7): p. 1210-8.
459. Fukuda, R., et al., *HIF-1 regulates cytochrome oxidase subunits to optimize efficiency of respiration in hypoxic cells*. Cell, 2007. **129**(1): p. 111-22.
460. Semenza, G.L., *Oxygen-dependent regulation of mitochondrial respiration by hypoxia-inducible factor 1*. Biochem J, 2007. **405**(1): p. 1-9.
461. Semenza, G.L., *Hypoxia-inducible factor 1: Regulator of mitochondrial metabolism and mediator of ischemic preconditioning*. Biochim Biophys Acta, 2010.
462. Zhang, H., et al., *Mitochondrial autophagy is an HIF-1-dependent adaptive metabolic response to hypoxia*. J Biol Chem, 2008. **283**(16): p. 10892-903.
463. Andringa, K.K., et al., *Analysis of the liver mitochondrial proteome in response to ethanol and S-adenosylmethionine treatments: novel molecular targets of disease and hepatoprotection*. Am J Physiol Gastrointest Liver Physiol, 2010. **298**(5): p. G732-45.
464. Cahill, A., X. Wang, and J.B. Hoek, *Increased oxidative damage to mitochondrial DNA following chronic ethanol consumption*. Biochem Biophys Res Commun, 1997. **235**(2): p. 286-90.
465. Cahill, A., et al., *Chronic ethanol consumption causes alterations in the structural integrity of mitochondrial DNA in aged rats*. Hepatology, 1999. **30**(4): p. 881-8.
466. Cahill, A., et al., *Differential effects of chronic ethanol consumption on hepatic mitochondrial and cytoplasmic ribosomes*. Alcohol Clin Exp Res, 1996. **20**(8): p. 1362-7.
467. Patel, V.B. and C.C. Cunningham, *Altered hepatic mitochondrial ribosome structure following chronic ethanol consumption*. Arch Biochem Biophys, 2002. **398**(1): p. 41-50.

468. Papandreou, I., et al., *HIF-1 mediates adaptation to hypoxia by actively downregulating mitochondrial oxygen consumption*. Cell Metab, 2006. **3**(3): p. 187-97.
469. Kulshreshtha, R., et al., *A microRNA signature of hypoxia*. Mol Cell Biol, 2007. **27**(5): p. 1859-67.
470. Corn, P.G., *Hypoxic regulation of miR-210: shrinking targets expand HIF-1's influence*. Cancer Biol Ther, 2008. **7**(2): p. 265-7.
471. Chan, S.Y., et al., *MicroRNA-210 controls mitochondrial metabolism during hypoxia by repressing the iron-sulfur cluster assembly proteins ISCU1/2*. Cell Metab, 2009. **10**(4): p. 273-84.
472. Ludwig, B., et al., *Cytochrome c Oxidase and the Regulation of Oxidative Phosphorylation*. ChemBioChem, 2001. **2**(6): p. 392-403.
473. Cooper, C.E., *The steady-state kinetics of cytochrome c oxidation by cytochrome oxidase*. Biochimica et Biophysica Acta, 1990. **1017**(3): p. 187-203.
474. Gnaiger, E. and A.V. Kuznetsov, *Mitochondrial respiration at low levels of oxygen and cytochrome c*. Biochem Soc Trans, 2002. **30**(2): p. 252-8.
475. Kadenbach, B., et al., *Isozymes of cytochrome c oxidase: characterization and isolation from different tissues*. Methods in Enzymology, 1986. **126**: p. 32-45.
476. Kadenbach, B., et al., *Mitochondrial energy metabolism is regulated via nuclear-coded subunits of cytochrome c oxidase*. Free Radical Biology and Medicine, 2000. **29**(3-4): p. 211-221.
477. Verkhovskiy, M.I., et al., *Kinetic trapping of oxygen in cell respiration*. Nature, 1996. **380**(6571): p. 268-70.
478. Scandurra, F.M. and E. Gnaiger, *Cell respiration under hypoxia: facts and artefacts in mitochondrial oxygen kinetics*. Adv Exp Med Biol, 2010. **662**: p. 7-25.

479. Wiedemann, F.R. and W.S. Kunz, *Oxygen dependence of flux control of cytochrome c oxidase -- implications for mitochondrial diseases*. FEBS Lett, 1998. **422**(1): p. 33-5.
480. Brand, M.D., B.P. Vallis, and A. Kessler, *The sum of flux control coefficients in the electron-transport chain of mitochondria*. Eur J Biochem, 1994. **226**(3): p. 819-29.
481. Ingwall, J.S., *Energy metabolism in heart failure and remodelling*. Cardiovasc Res, 2009. **81**(3): p. 412-9.
482. Tsutsui, H., S. Kinugawa, and S. Matsushima, *Mitochondrial oxidative stress and dysfunction in myocardial remodelling*. Cardiovasc Res, 2009. **81**(3): p. 449-56.
483. Gottlieb, R.A. and A.B. Gustafsson, *Mitochondrial turnover in the heart* ☆. Biochim Biophys Acta, 2010.
484. Coskun, P.E., E. Ruiz-Pesini, and D.C. Wallace, *Control region mtDNA variants: longevity, climatic adaptation, and a forensic conundrum*. Proc Natl Acad Sci U S A, 2003. **100**(5): p. 2174-6.
485. Elson, J.L., D.M. Turnbull, and R.W. Taylor, *Testing the adaptive selection of human mtDNA haplogroups: an experimental bioenergetics approach*. Biochem J, 2007. **404**(2): p. e3-5.

APPENDIX A
IACUC APPROVAL FORMS



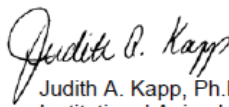
THE UNIVERSITY OF ALABAMA AT BIRMINGHAM

Institutional Animal Care and Use Committee (IACUC)

NOTICE OF RENEWAL

DATE: January 4, 2011

TO: SHANNON M BAILEY, Ph.D.
RPHB-623 0022
FAX: (205) 975-6341

FROM: 
Judith A. Kapp, Ph.D., Chair
Institutional Animal Care and Use Committee (IACUC)

SUBJECT: Title: Redox Modification of Thiols in Alcohol Hepatotoxicity
Sponsor: NIH
Animal Project Number: 110107077

As of January 21, 2011, the animal use proposed in the above referenced application is renewed. The University of Alabama at Birmingham Institutional Animal Care and Use Committee (IACUC) approves the use of the following species and numbers of animals:

Species	Use Category	Number in Category
Rats	A	20
Rats	B	48

Animal use must be renewed by January 20, 2012. Approval from the IACUC must be obtained before implementing any changes or modifications in the approved animal use.

Please keep this record for your files, and forward the attached letter to the appropriate granting agency.

Refer to Animal Protocol Number (APN) 110107077 when ordering animals or in any correspondence with the IACUC or Animal Resources Program (ARP) offices regarding this study. If you have concerns or questions regarding this notice, please call the IACUC office at (205) 934-7692.

Institutional Animal Care and Use Committee
CH19 Suite 403
933 19th Street South
205.934.7692
FAX 205.934.1188

Mailing Address:
CH19 Suite 403
1530 3RD AVE S
BIRMINGHAM AL 35294-0019



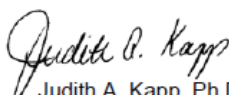
THE UNIVERSITY OF ALABAMA AT BIRMINGHAM

Institutional Animal Care and Use Committee (IACUC)

NOTICE OF APPROVAL

DATE: November 19, 2010

TO: LOUIS J DELL'ITALIA, M.D.
BMR2-432 2180
FAX: (205) 996-2586

FROM: 
Judith A. Kapp, Ph.D., Chair
Institutional Animal Care and Use Committee (IACUC)

SUBJECT: Title: Role of Mitochondrial Haplotype in Heart Failure
Sponsor: Internal
Animal Project Number: 101109302

As of November 19, 2010, the animal use proposed in the above referenced application is approved. The University of Alabama at Birmingham Institutional Animal Care and Use Committee (IACUC) approves the use of the following species and numbers of animals:

Species	Use Category	Number in Category
Mice	B	600

Animal use must be renewed by November 18, 2011. Approval from the IACUC must be obtained before implementing any changes or modifications in the approved animal use.

Please keep this record for your files, and forward the attached letter to the appropriate granting agency.

Refer to Animal Protocol Number (APN) 101109302 when ordering animals or in any correspondence with the IACUC or Animal Resources Program (ARP) offices regarding this study. If you have concerns or questions regarding this notice, please call the IACUC office at (205) 934-7692.

Institutional Animal Care and Use Committee
CH19 Suite 403
933 19th Street South
205.934.7692
FAX 205.934.1188

Mailing Address:
CH19 Suite 403
1530 3RD AVE S
BIRMINGHAM AL 35294-0019